NCHRP
REPORT 516

NATIONAL COOPERATIVE HIGHWAY RESEARCH PROGRAM

Pier and Contraction Scour in Cohesive Soils

TRANSPORTATION RESEARCH BOARD
OF THE NATIONAL ACADEMIES

NATIONAL COOPERATIVE HIGHWAY RESEARCH PROGRAM

NCHRP REPORT 516

Pier and Contraction Scour in Cohesive Soils

J.-L. BRIAUD
H.-C. CHEN
Y. LI
P. NURTJAHYO
AND
J. WANG
Texas A&M University
College Station, TX

SUBJECT AREAS
Highway and Facility Design • Bridges, Other Structures, and Hydraulics and Hydrology • Soils, Geology, and Foundations • Materials and Construction

Research Sponsored by the American Association of State Highway and Transportation Officials in Cooperation with the Federal Highway Administration

TRANSPORTATION RESEARCH BOARD

WASHINGTON, D.C.
2004
www.TRB.org

NATIONAL COOPERATIVE HIGHWAY RESEARCH PROGRAM

Systematic, well-designed research provides the most effective approach to the solution of many problems facing highway administrators and engineers. Often, highway problems are of local interest and can best be studied by highway departments individually or in cooperation with their state universities and others. However, the accelerating growth of highway transportation develops increasingly complex problems of wide interest to highway authorities. These problems are best studied through a coordinated program of cooperative research.

In recognition of these needs, the highway administrators of the American Association of State Highway and Transportation Officials initiated in 1962 an objective national highway research program employing modern scientific techniques. This program is supported on a continuing basis by funds from participating member states of the Association and it receives the full cooperation and support of the Federal Highway Administration, United States Department of Transportation.

The Transportation Research Board of the National Academies was requested by the Association to administer the research program because of the Board's recognized objectivity and understanding of modern research practices. The Board is uniquely suited for this purpose as it maintains an extensive committee structure from which authorities on any highway transportation subject may be drawn; it possesses avenues of communications and cooperation with federal, state and local governmental agencies, universities, and industry; its relationship to the National Research Council is an insurance of objectivity; it maintains a full-time research correlation staff of specialists in highway transportation matters to bring the findings of research directly to those who are in a position to use them.

The program is developed on the basis of research needs identified by chief administrators of the highway and transportation departments and by committees of AASHTO. Each year, specific areas of research needs to be included in the program are proposed to the National Research Council and the Board by the American Association of State Highway and Transportation Officials. Research projects to fulfill these needs are defined by the Board, and qualified research agencies are selected from those that have submitted proposals. Administration and surveillance of research contracts are the responsibilities of the National Research Council and the Transportation Research Board.

The needs for highway research are many, and the National Cooperative Highway Research Program can make significant contributions to the solution of highway transportation problems of mutual concern to many responsible groups. The program, however, is intended to complement rather than to substitute for or duplicate other highway research programs.

Note: The Transportation Research Board of the National Academies, the National Research Council, the Federal Highway Administration, the American Association of State Highway and Transportation Officials, and the individual states participating in the National Cooperative Highway Research Program do not endorse products or manufacturers. Trade or manufacturers' names appear herein solely because they are considered essential to the object of this report.

NCHRP REPORT 516

Project E24-15 FY'98

ISSN 0077-5614

ISBN 0-309-088062

Library of Congress Control Number 2004096313

Price $22.00

NOTICE

The project that is the subject of this report was a part of the National Cooperative Highway Research Program conducted by the Transportation Research Board with the approval of the Governing Board of the National Research Council. Such approval reflects the Governing Board's judgment that the program concerned is of national importance and appropriate with respect to both the purposes and resources of the National Research Council.

The members of the technical committee selected to monitor this project and to review this report were chosen for recognized scholarly competence and with due consideration for the balance of disciplines appropriate to the project. The opinions and conclusions expressed or implied are those of the research agency that performed the research, and, while they have been accepted as appropriate by the technical committee, they are not necessarily those of the Transportation Research Board, the National Research Council, the American Association of State Highway and Transportation Officials, or the Federal Highway Administration, U.S. Department of Transportation.

Each report is reviewed and accepted for publication by the technical committee according to procedures established and monitored by the Transportation Research Board Executive Committee and the Governing Board of the National Research Council.

Published reports of the

NATIONAL COOPERATIVE HIGHWAY RESEARCH PROGRAM

are available from:

Transportation Research Board
Business Office
500 Fifth Street, NW
Washington, DC 20001

and can be ordered through the Internet at:

http://www.national-academies.org/trb/bookstore

Printed in the United States of America

THE NATIONAL ACADEMIES

Advisers to the Nation on Science, Engineering, and Medicine

The **National Academy of Sciences** is a private, nonprofit, self-perpetuating society of distinguished scholars engaged in scientific and engineering research, dedicated to the furtherance of science and technology and to their use for the general welfare. On the authority of the charter granted to it by the Congress in 1863, the Academy has a mandate that requires it to advise the federal government on scientific and technical matters. Dr. Bruce M. Alberts is president of the National Academy of Sciences.

The **National Academy of Engineering** was established in 1964, under the charter of the National Academy of Sciences, as a parallel organization of outstanding engineers. It is autonomous in its administration and in the selection of its members, sharing with the National Academy of Sciences the responsibility for advising the federal government. The National Academy of Engineering also sponsors engineering programs aimed at meeting national needs, encourages education and research, and recognizes the superior achievements of engineers. Dr. William A. Wulf is president of the National Academy of Engineering.

The **Institute of Medicine** was established in 1970 by the National Academy of Sciences to secure the services of eminent members of appropriate professions in the examination of policy matters pertaining to the health of the public. The Institute acts under the responsibility given to the National Academy of Sciences by its congressional charter to be an adviser to the federal government and, on its own initiative, to identify issues of medical care, research, and education. Dr. Harvey V. Fineberg is president of the Institute of Medicine.

The **National Research Council** was organized by the National Academy of Sciences in 1916 to associate the broad community of science and technology with the Academy's purposes of furthering knowledge and advising the federal government. Functioning in accordance with general policies determined by the Academy, the Council has become the principal operating agency of both the National Academy of Sciences and the National Academy of Engineering in providing services to the government, the public, and the scientific and engineering communities. The Council is administered jointly by both the Academies and the Institute of Medicine. Dr. Bruce M. Alberts and Dr. William A. Wulf are chair and vice chair, respectively, of the National Research Council.

The **Transportation Research Board** is a division of the National Research Council, which serves the National Academy of Sciences and the National Academy of Engineering. The Board's mission is to promote innovation and progress in transportation through research. In an objective and interdisciplinary setting, the Board facilitates the sharing of information on transportation practice and policy by researchers and practitioners; stimulates research and offers research management services that promote technical excellence; provides expert advice on transportation policy and programs; and disseminates research results broadly and encourages their implementation. The Board's varied activities annually engage more than 5,000 engineers, scientists, and other transportation researchers and practitioners from the public and private sectors and academia, all of whom contribute their expertise in the public interest. The program is supported by state transportation departments, federal agencies including the component administrations of the U.S. Department of Transportation, and other organizations and individuals interested in the development of transportation. **www.TRB.org**

www.national-academies.org

AUTHOR ACKNOWLEDGMENTS

Special thanks go to the NCHRP group associated with this project for their advice and comments throughout the study: the NCHRP Project Panel and NCHRP staff.

Special thanks also go to our consultants: Peter Lagasse, Ayres Associates; Peter Smith, Parsons Brinckerhoff Quade & Douglas, Inc.; and Art Parola, Jr., University of Louisville.

We also wish to acknowledge the help from people at Texas A&M University, including John Reed, Bob Randall, Andrew Fawcett, Mike Linger, Richard Gehle, and Josh Reinbolt.

FOREWORD

By Timothy G. Hess
Staff Officer
Transportation Research Board

This report discusses the findings of a research project undertaken to investigate bridge scour in cohesive soils. The report presents a recommended method for predicting the extent of complex pier and contraction scour in cohesive soils. This report will be of immediate interest to engineers with responsibility for predicting the extent of scour at bridge foundations and to engineers with responsibility for designing bridge foundations and bridge scour countermeasures.

Scour at bridges founded in or on cohesive soil is a complex phenomenon that is not completely understood. Conventional approaches to scour prediction were developed from laboratory experiments in cohesionless materials and are generally regarded as overly conservative when applied to cohesive soils. Accurate and accepted methods for predicting scour depths in cohesive soils that account for the soil's greater scour resistance are not yet available to practicing engineers. The lack of an accurate predictive method often results in an overly conservative and sometimes unnecessarily costly bridge foundation. Research investigating the relationship between properties of cohesive material and the erosive power of flowing water is needed to improve the prediction of scour in cohesive soils.

Under NCHRP Project 24-15, the Texas Transportation Institute developed a method for predicting pier and contraction scour in cohesive soil. The research team first reviewed the literature to identify existing knowledge in the subject area. The design of an erosion function apparatus (EFA) developed in earlier research was enhanced, and a new EFA was constructed and used in the development of erosion curves for specific soils. Laboratory flume tests were conducted, followed by numerical simulations; and finally prediction equations were developed.

The prediction method developed, termed SRICOS (Scour Rate In Cohesive Soils), was applied to several contraction and complex-pier configurations typically encountered by state highway agencies. An evaluation of the accuracy and precision of the SRICOS Method was conducted by comparing predicted and measured data. Example problems using the SRICOS Method were developed to assist practitioners in applying the method. A computer program, termed SRICOS-EFA was developed to automate the calculations used in the SRICOS Method and to assist in the implementation of the research results.

NCHRP Report 516 includes a discussion of existing knowledge and practice, a description of the erosion function apparatus, a discussion of laboratory tests and numerical simulations conducted, presentation of the SRICOS-EFA method, and one appendix, Appendix A: Photographs from the Flume Tests. Compilations of flume test data and case history data were provided by the Texas Transportation Institute but are not included in this publication; however, they are available on request from NCHRP. Subsequent to completion of NCHRP Project 24-15, the Texas Transportation Institute updated the SRICOS-EFA computer program and added other enhancements. The SRICOS-EFA computer program and User's Manual are available from the Texas Transportation Institute via the internet at http://ceprofs.tamu.edu/briaud/sricos-efa.htm.

CONTENTS

PIER AND CONTRACTION SCOUR IN COHESIVE SOILS

SUMMARY

SCOUR TYPES

Bridge scour is the loss of soil by erosion due to water flowing around bridge supports. Bridge scour includes general scour and local scour. General scour is the aggradation or degradation of the riverbed not related to the presence of local obstacles. Aggradation is the gradual and general accumulation of sediments on the river bottom. Degradation is the gradual and general removal of sediments from the riverbed. Local scour is the scour around obstacles to the water flow. Local scour includes pier scour, abutment scour, and contraction scour. Pier scour is the removal of the soil around the foundation of a pier; abutment scour is the removal of soil around an abutment at the junction between a bridge and embankment; and contraction scour is the removal of soil from the bottom of the river due to a narrowing of the river channel created by the approach embankments for a bridge.

SOILS: A DEFINITION

Soils can be defined as loosely bound to unbound, naturally occurring materials that cover the top few hundred meters of the Earth. By opposition, rock is a strongly bound, naturally occurring material found within similar depths or deeper. Intermediate geomaterials occur at the boundary between soils and rocks. For soils, the classification tests consist of grain size analysis and Atterberg Limits. The D_{50} grain size is the grain size corresponding to 50% of the soil weight passing a sieve with an opening equal to D_{50}. The first major division in soils classification is between large-grained soils and fine-grained soils. Large-grained soils have D_{50} larger than 0.075 mm; fine-grained soils have D_{50} smaller than 0.075 mm. Large-grained soils include gravels and sands that are identified on the basis of their grain size. Fine-grained soils include silts and clays that are identified on the basis of Atterberg Limits. Gravels and sands are typically referred to as cohesionless soils; silts and clays are typically referred to as cohesive soils.

THE PROBLEM ADDRESSED

This project deals with pier scour and contraction scour in cohesive soils. A previous project performed by the same team of researchers began in 1990 and was sponsored by

the Texas Department of Transportation (TxDOT). This previous project dealt with pier scour in cohesive soils. In the TxDOT project, the piers were cylindrical and the water depth was more than two times the pier diameter (deepwater case). In the TxDOT project, a new tool called the Erosion Function Apparatus (EFA) was conceived, built, patented, and commercialized to measure the erodibility of soils. The EFA test, which gives the erosion function for a soil, became an integral part of the Scour Rate In COhesive Soils (SRICOS) Method. The SRICOS-EFA Method developed at the end of the TxDOT project predicted the scour depth as a function of time when a cylindrical pier founded in a layered soil was subjected to a long-term deepwater flow-velocity hydrograph. In this NCHRP project, the SRICOS-EFA Method was extended to the case of complex piers and contraction scour. Complex piers are piers with various shapes, flow attack angles, spacing between piers, and existing in any water depth. Contraction refers to a narrowing of the flow channel by an embankment with a given encroachment length, embankment width, and transition angle.

WHY WAS THIS PROBLEM ADDRESSED?

The reason for solving this problem was that, in the absence of a solution, calculations have been based on the solution developed for cohesionless soils. Within the bridge engineering community, there were concerns that such an approach was sometimes very conservative and, therefore, costly. Indeed, overly conservative scour depths lead to foundations that are considered deeper than necessary. The major difference between cohesionless soils and cohesive soils is the following. Floods create peak velocities that last a few days. A few days is a length of time that is usually sufficient to generate the maximum scour depth in cohesionless soils. This means that only the peak velocity needs to be used in the calculations of scour depth for cohesionless soils and that such a scour depth is the maximum scour depth for that velocity. The velocities used are typically the 100-year flood velocity and the 500-year flood velocity. In cohesive soils, scour and erosion rates can be 1,000 times slower than in cohesionless soils and a few days may generate only a small fraction of the maximum scour depth. Therefore, for cohesive soils, it becomes necessary to consider the rate of erosion and to accumulate the effect of multiple floods. This complicates the problem significantly, but is necessary in order to get an accurate prediction.

APPROACH SELECTED TO SOLVE THE PROBLEM

The approach selected to solve the problem of predicting the scour depth versus time for complex piers in a contracted channel and for a given velocity hydrograph was based on a combination of a review of existing knowledge, flume tests, numerical simulations, fundamental principles in method development, and verification of the method against available data. The review of existing knowledge avoided duplication of effort and helped to establish a solid foundation. The flume tests gave the equations for the maximum scour depth and the influence of various factors. The flume tests also gave a calibration basis for the numerical simulations. These numerical simulations were used to generate the equations for the maximum initial shear stress at the initiation of scour. The method was assembled by linking the calculated initial erosion rate (given by the numerical simulation results and the results of the EFA test) to the calculated maximum scour depth (given by the flume test results) through the use of a hyperbolic model. The multiflood hydrograph and multilayer soil were included through simple accumulation algorithms. Verification was based on comparison with

existing databases as well as performing calculations for example cases and evaluating the reasonableness of the results based on experience.

ERODIBILITY OF COHESIVE SOILS

Erodibility is not an index but a relationship or function between water velocity (or, better, the shear stress at the water-soil interface) and the erosion rate of the soil. Erodibility is represented by this erosion function. Two important parameters help describe the erosion function: the critical shear stress and the initial slope of the erosion function. Although the critical shear stress of a cohesive soil is not related to its mean grain size, the common range of critical shear stress values for cohesive soils (0.5 N/m^2 to 5 N/m^2) is comparable to the range obtained in sands. This explains why the maximum scour depth in cohesive soils is comparable to the one obtained in sands. The initial slope of the erosion function can be many times less than the one in sand (e.g., 1,000 times less) and, therefore, the scour depth can develop very slowly in some cohesive soils. Thus, it would be advantageous to develop a method that can predict scour depth as a function of time for a given hydrograph (cohesive soil) rather than a maximum depth of scour for a design flood (sands). This was the goal of this project. It also was found that the critical shear stress and the initial slope were not related to soil properties because the R^2 of the regressions were all very low. Therefore, it is recommended that Erosion Function Apparatus (EFA) be used to determine the erosion function.

EROSION FUNCTION APPARATUS (EFA)

The EFA was developed in the early 1990s to obtain the erosion function. A soil sample is retrieved from the bridge site using an ASTM-standard thin-walled steel tube (Shelby tube), placing it through a tight-fitting opening in the bottom of a rectangular cross-section conduit, pushing a small protrusion of soil into the conduit, sending flowing water over the top of the sample at a chosen velocity, and recording the corresponding erosion rate. This is repeated for several velocities and the erosion function is obtained in this fashion.

SRICOS-EFA METHOD FOR CYLINDRICAL PIERS IN DEEP WATER

SRICOS stands for Scour Rate In COhesive Soils. Since the method makes use of the erosion function measured in the EFA, the method is referred to as the SRICOS-EFA Method. For a given velocity hydrograph at a bridge, a given soil exhibiting a multilayered stratigraphy with an erosion function defined for each layer, and a given cylindrical pier in deep water (water depth larger than 1.6 times the pier diameter), the SRICOS-EFA Method (program) gives the scour depth as a function of time for the period covered by the hydrograph.

The method is based on the calculation of two basic parameters: the maximum depth of pier scour and the initial rate of scour. The maximum depth of scour is based on an equation obtained from flume tests and the initial rate is based on an equation giving the initial shear stress obtained from numerical simulations. The initial rate of scour is read on the EFA erosion function at the corresponding value of the calculated initial shear stress. A hyperbola is used to connect the initial scour rate to the maximum or asymptotic scour depth and describes the complete scour-depth–versus–time curve. Robust algorithms are used to incorporate the effect of varying velocities and multilayered soil systems. This earlier method was developed by the authors under TxDOT

sponsorship and was verified by satisfactory comparison between predicted scour and measured scour at eight bridges in Texas.

SRICOS-EFA METHOD FOR MAXIMUM SCOUR DEPTH AT COMPLEX PIERS

A set of flume experiments was conducted to study the maximum depth of scour for a pier, including the effects of shallow water depth, rectangular shapes, angle of attack on rectangular shapes, and spacing between piers positioned in a row perpendicular to the flow. The proposed equation for the maximum depth of scour is in the form of the equation for the cylindrical pier in deep water with correction factors based on the results of the flume tests:

$$Z_{\max}(\text{Pier}) \text{ in mm} = K_w K_{sp} K_{sh} \left(0.18 R_e^{0.635}\right)$$

where Z_{max}(Pier) is the maximum depth of pier scour in millimeters; R_e is the Reynolds number equal to VB'/v; V is the mean depth velocity at the location of the pier if the bridge were not there; v is the water viscosity; the K factors take the shallow water depth, spacing, and shape into account; and the angle of attack being considered through the use of the projected width B' in the calculation of the Reynolds Number.

SRICOS-EFA METHOD FOR INITIAL SCOUR RATE AT COMPLEX PIERS

A set of numerical simulations was performed to study the maximum shear stress around a pier, including the effects of shallow water depth, rectangular shapes, angle of attack on rectangular shapes, and spacing between piers positioned in a row perpendicular to the flow. The proposed equation for the maximum shear stress is in the form of the equation for the cylindrical pier in deep water with correction factors based on the results of the numerical simulations.

$$\tau_{\max}(\text{Pier}) = k_w k_{sh} k_{sp} k_a \left(0.094 \rho V^2 \left[\frac{1}{\log R_e} - \frac{1}{10}\right]\right)$$

where τ_{max}(Pier) is the maximum shear stress around the pier; R_e is the Reynolds Number equal to VB/v; V is the mean depth velocity at the location of the pier if the bridge were not there; v is the water viscosity; B is the pier diameter or pier width; and the k factors take shallow water depth, pier shape, pier spacing, and attack angle into account.

SRICOS-EFA METHOD FOR MAXIMUM CONTRACTION SCOUR DEPTH

A set of flume experiments was conducted to study the depth of scour associated with the contraction of a channel, including the effects of the ratio of the contracted channel width over the approach channel width, contracted channel length, and transition angle. The proposed equation for the maximum depth of contraction scour is

$$Z_{\max}(\text{Cont}) = K_\theta K_L \times 1.90\, H_1 \left(\frac{1.49 V_{hec}}{\sqrt{g H_1}} - \frac{\left(\frac{\tau_c}{\rho}\right)^{0.5}}{g n H_1^{1/3}} \right) \geq 0$$

where Z_{max}(Cont) is the maximum depth of contraction scour; H_1 is the water depth along the center line of the uncontracted channel after scour has occurred; V_{hec} is the mean depth water velocity at the location of the pier in the contracted channel; τ_c is the

critical shear stress of the soil; ρ is the mass density of water; *g* is the acceleration due to gravity; *n* is the Manning's Coefficient; and the *K* factors take the transition and contracted channel length into account. Note that the parentheses in the equation is a factored difference between the Froude Number and the critical Froude Number. Equations are also proposed for the uniform contraction scour depth as well as the location of the scour depths.

SRICOS-EFA METHOD FOR INITIAL CONTRACTION SCOUR RATE

A set of numerical simulations were performed to study the maximum shear stress around the contraction of a channel, including the effects of the ratio of the contracted channel width over the approach channel width, transition angle, water depth, and contracted channel length. The proposed equation for the maximum shear stress is in the form of the equation for the shear stress at the bottom of an open and uncontracted channel with correction factors based on the results of the numerical simulations.

$$\tau_{\max}(\text{Cont}) = k_{c-R}k_{c-\theta}k_{c-H}k_{c-L}\left(\gamma n^2 V^2 R_h^{-\frac{1}{3}}\right)$$

where τ_{max}(Cont) is the maximum shear stress along the centerline of the contracted channel; γ is the unit weight of water; *n* is the Manning's Coefficient; *V* is the upstream mean depth velocity; R_h is the hydraulic radius defined as the cross section area of the flow divided by the wetted perimeter; and the *k* factors take the contraction ratio, transition angle, water depth effect, and contracted length into account. Equations are also proposed for the location of the maximum shear stress.

SRICOS-EFA METHOD FOR COMPLEX PIER SCOUR AND CONTRACTION SCOUR IN COHESIVE SOILS

Once the equations were established, the SRICOS-EFA Method was assembled. Care was taken not to simply add complex pier scour and contraction scour to get total pier scour. Instead, advantage was taken of the fact that at the end of the maximum contraction scour, the velocity is at the critical velocity and the maximum pier scour should be calculated using the critical velocity of the soil and not the initial velocity in the contracted channel. In addition, the rules of accumulation due to the hydrograph and the multilayer system developed for the simple pier scour method were adapted for the complex pier and contraction scour method. The superposition and accumulation reasoning led to the following steps that enabled the SRICOS-EFA Method to predict the scour depth at a complex pier in a contracted channel. This step-by-step procedure has been automated in a computer program.

1. Collect the input data: velocity and water depth hydrograph, geometry of the pier and of the contracted channel, erosion functions of the soil layers;
2. Calculate the maximum contraction scour depth for the *i*th velocity in the hydrograph;
3. Calculate the maximum complex pier scour depth using the *i*th velocity in the hydrograph at the pier location if there is no contraction scour in Step 2, or the critical velocity for the soil if there is contraction scour in Step 2;
4. Calculate the total pier scour depth as the total of Steps 2 and 3;
5. Calculate the initial maximum shear stress for pier scour using the *i*th velocity in the hydrograph;

6. Read the initial scour rate corresponding to the initial maximum shear stress of Step 5 on the erosion function of the soil layer corresponding to the current scour depth;
7. Use the results of Steps 4 and 6 to construct the hyperbola describing the scour depth versus time curve for the pier;
8. Calculate the equivalent time for the given curve of Step 7. The equivalent time is the time required for the *i*th velocity on the hydrograph to scour the soil to a depth equal to the depth scoured by all of the velocities occurring prior to the *i*th velocity;
9. Read the additional scour generated by the *i*th velocity starting at the equivalent time and ending at the equivalent time plus the time increment; and
10. Repeat Steps 2 to 9 for the (*i*+1)th velocity and so on until the entire hydrograph is consumed.

VERIFICATION OF THE SRICOS-EFA METHOD

Several full case histories were identified for verification, but none could satisfy the requirements necessary to verify the method developed. Some did not have enough details on the observed scour depth, some turned out not to be made of cohesive soil after drilling, some did not have a gage station nearby. The study team decided to compare the maximum scour depth for pier and contraction to existing databases. These databases were mostly in sand, however, and included those collected by Mueller (pier scour), Froehlich (pier scour), and Gill (contraction scour). The comparisons between the predicted and measured scour depths are very satisfactory, although it is not clear whether they should be given that the soils were not primarily cohesive. Nevertheless, these comparisons give an indication that the SRICOS-EFA Method may not be limited to cohesive soils. Indeed, the fact that the method is based on site-specific testing of the erosion function permits incorporating the soil behavior directly into the predictions.

FUTURE HYDROGRAPHS AND SCOUR RISK ANALYSIS

A novel technique is presented on generating future hydrographs. Indeed, since the SRICOS-EFA Method predicts the scour depth as a function of time, it is necessary to input the hydrograph over the design life of the bridge into the program. The proposed technique consists of using a past hydrograph (from a gage station, for example), preparing the frequency distribution plot for the floods within that hydrograph, sampling the distribution randomly, and preparing a future hydrograph. This future hydrograph is for the required period and has the same mean and standard deviation as the measured hydrograph. This process is repeated 10,000 times and, for each hydrograph, a final scour depth (the depth reached at the end of the design life of the bridge) is generated. These 10,000 final depths of scour are organized in a frequency distribution plot with a mean and standard deviation. That plot can be used to quote a scour depth with a corresponding probability of occurrence, or better, to choose a risk level and quote the corresponding final depth of scour.

EXAMPLE PROBLEMS

A set of example problems is presented to help the reader become more familiar with the SRICOS-EFA Method. Some examples are performed using hand calculations; some use the computer program.

RECOMMENDATIONS

It is recommended that

1. The proposed method be incorporated in the next version of HEC-18;
2. The SRICOS-EFA Method program be transferred to a Windows™ environment;
3. The project be continued to solve abutment scour, the last major unsolved scour problem in cohesive soils; and
4. A set of short courses be offered across the country to teach the new SRICOS-EFA Method.

CHAPTER 1

INTRODUCTION

1.1 BRIDGE SCOUR

Bridge scour is the loss of soil by erosion due to water flowing around bridge supports. Bridge scour includes general scour and local scour. General scour is the aggradation or degradation of the riverbed not related to the presence of local obstacles. Aggradation is the gradual and general accumulation of sediments on the river bottom; one possible scenario is the existence of slope failures upstream leading to the formation of spoils in the river, the erosion of these spoils under higher velocities, followed by transport and deposition under lower velocities at the aggrading location. Degradation is the gradual and general removal of sediments from the riverbed; one possible scenario is the man-made straightening of a river course, a resulting increase in the water velocity, and the associated increase in erosion. Local scour is the scour around obstacles in the path of the water flow; it includes pier scour, abutment scour, and contraction scour. Pier scour is the removal of the soil around the foundation of a pier; abutment scour is the removal of the soil around an abutment at the junction between a bridge and embankment; contraction scour is the removal of soil from the bottom of the river due to a narrowing of the river channel created by the approach embankments for a bridge.

1.2 CLASSIFICATION OF SOILS

Soils can be defined as loosely bound to unbound, naturally occurring materials that cover the top few hundred meters of the Earth. By opposition, rock is a strongly bound, naturally occurring material found within similar depths or deeper. Intermediate geomaterials occur at the boundary between soils and rocks. Classification tests and mechanical properties help to distinguish between these three types of naturally occurring materials and to classify different categories of soils. For soils, the classification tests consist of grain size analysis and Atterberg Limits (Das, 2001). The D_{50} grain size is the grain size corresponding to 50% of the soil weight passing a sieve with an opening equal to D_{50}. The first major division in soils classification is between large-grained soils and fine-grained soils; large-grained soils have D_{50} larger than 0.075 mm while fine-grained soils have D_{50} smaller than 0.075 mm. Large-grained soils include gravels and sands that are identified on the basis of their grain size. Fine-grained soils include silts and clays that are identified on the basis of Atterberg Limits. Gravels and sands are typically referred to as cohesionless soils; silts and clays are typically referred to as cohesive soils.

1.3 THE PROBLEM ADDRESSED

This project deals with pier scour and contraction scour in cohesive soils (Figure 1.1). A previous project performed by the same team of researchers (Briaud et al., 1999, 2002a, and 2002b) began in 1990 and was sponsored by the Texas Department of Transportation (TxDOT); it dealt only with pier scour in cohesive soils. In the TxDOT project, the piers were cylindrical and the water depth was more than two times the pier diameter (deep water case). As part of the TxDOT project, a new device to measure the erodibility of soils—the Erosion Function Apparatus (EFA)—was developed. The EFA test gives the erosion function for a soil and became an integral part of the Scour Rate in Cohesive Soils (SRICOS) Method to predict the scour depth as a function of time when a cylindrical pier founded in a layered soil is subjected to long-term, deep water flow. In this NCHRP project, the SRICOS-EFA Method was extended to the case of complex piers and contraction scour. Complex piers refer to piers with various shapes, flow attack angles, spacing between piers, and any water depth. Contraction refers to a narrowing of the flow channel by an embankment with a given encroachment length, embankment width, and a given transition angle. The input to the SRICOS-EFA Method is the geometry of the piers and the contraction, the water velocity and water depth as a function of time over the life of the bridge, and the soil erosion functions for the layers involved in the soil stratigraphy. The output is the scour depth as a function of time during the life of the bridge.

1.4 WHY WAS THIS PROBLEM ADDRESSED?

Previously, the calculations for cohesive soils were based on the solution developed for cohesionless soils. Such an approach was often overly conservative. Overly conservative scour depths led to foundations that were considered to be deeper than necessary and, therefore, more costly than needed. The major difference between cohesionless soils and cohesive soils is explained in the following description. Floods create peak velocities that last a few days. This length

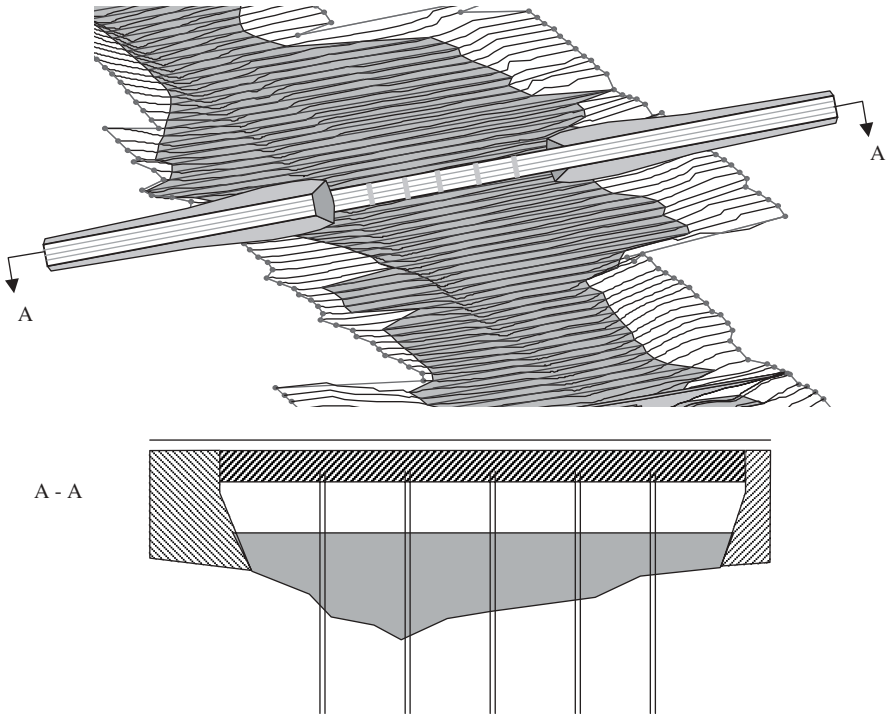

Figure 1.1. Typical bridge with potential contraction and pier scour.

of time is usually sufficient to generate the maximum scour depth in cohesionless soils. This means that only the peak velocity needs to be used in the calculations of scour depth for cohesionless soils and that such a scour depth is the maximum scour depth for that velocity. Typically, the velocities used are the 100- and 500-year flood velocities. In cohesive soils, scour and erosion rates can be 1,000 times slower than in cohesionless soils and a few days may generate only a small fraction of the maximum scour depth. Therefore, for cohesive soils it becomes necessary to consider the rate of erosion and the cumulative effect of multiple floods.

1.5 APPROACH SELECTED TO SOLVE THE PROBLEM

The approach selected to solve the problem of predicting the scour depth versus time for complex piers in a contracted channel and for a given velocity hydrograph was based on a combination of existing knowledge review, flume tests, numerical simulations, fundamental principles in method development, and verification of the method against available data. The review of existing knowledge avoided duplication of effort and helped in establishing a solid foundation. The flume tests gave the equations for the maximum scour depth and the influence of various factors. The flume tests also gave a calibration basis for the numerical simulations. These numerical simulations were used to generate the equations for the maximum initial shear stress at the initiation of scour. The method was assembled by linking the calculated initial erosion rate (given by the numerical simulation results and the results of the EFA test) to the calculated maximum scour depth (given by the flume tests results) through the use of a hyperbolic model. The multiflood hydrograph and multilayer soil were included through simple accumulation algorithms. Verification was based on comparison with existing databases as well as performing calculations for sample cases and evaluating the reasonableness of the results based on experience.

CHAPTER 2

ERODIBILITY OF COHESIVE SOILS

2.1 ERODIBILITY: A DEFINITION

Erodibility is a term used often in scour and erosion studies. Erodibility may be represented as one number that characterizes the rate at which a soil is eroded by the flowing water. With this concept, erosion-resistant soils would have a low erodibility index and erosion-sensitive soils would have a high erodibility index. This concept is not appropriate; indeed the water velocity in rivers can vary drastically from 0 m/s to 5 m/s or more. Therefore erodibility cannot be represented by a single number but is a relationship between the velocity applied and the corresponding erosion rate experienced by the soils. While this is an improved definition of erodibility, it still presents some problems because water velocity is a vector quantity that varies everywhere in the flow. It is preferable to quantify the action of the water on the soil by using the shear stress applied by the water on the soil at the water-soil interface. Erodibility is therefore defined here as the relationship between the erosion rate $\dot{z}$ and the hydraulic shear stress applied τ (Figure 2.1). This relationship is called the erosion function $\dot{z}(\tau)$. The erodibility of a soil or a rock is represented by the erosion function of that soil or rock.

2.2 EROSION PROCESS

Soils are eroded particle by particle in the case of coarse-grained soils (cohesionless soils). In the case of fine-grained soils (cohesive soils), erosion can take place particle by particle but also block of particles by block of particles. The boundaries of these blocks are formed naturally in the soil matrix by micro-fissures which result from various phenomena, such as compression and extension.

For coarse-grained soils, the resistance to erosion is influenced by the weight of the particles; for fine-grained soils, resistance to erosion is influenced by a combination of weight and electromagnetic and electrostatic interparticle forces. Slow-motion videotape observations at the soil-water interface indicate that the removal of particles or blocks of particles is by a combination of rolling and plucking actions of the water on the soil.

2.3 EXISTING KNOWLEDGE ON ERODIBILITY OF COHESIVE SOILS

A complete discussion on the erodibility of cohesive soils and a literature review on that topic can be found in Briaud et al. (1999), but is summarized below. The factors influencing the erodibility of cohesive soils according to the literature survey are listed in Table 2.1. Although conflicting findings sometimes occur, the influence of various factors on cohesive soil erodibility is shown in Table 2.1.

The critical shear stress of cohesionless soils is tied to the size of the particles and usually ranges from 0.1 N/m^2 to 5 N/m^2. The rate of erosion of cohesionless soils above the critical shear stress increases rapidly and can reach tens of thousands of millimeters per hour. The most erodible soils are fine sands and silts with mean grain sizes in the 0.1 mm range (Figure 2.2). The critical shear stress of cohesive soils is not tied to the particle size but rather to a number of factors as listed in Table 2.1. The critical shear stress of cohesive soils, however, varies within the same range as cohesionless soils (0.1 N/m^2 to 5 N/m^2 for the most common cases). Since the critical shear stress controls the maximum depth of scour, as will be seen later, it is likely that the final depth of scour will be approximately the same in sands and in clays. One major difference between cohesionless and cohesive soils is the rate of erosion beyond the critical shear stress. In cohesive soils, this rate increases slowly and is measured in millimeters per hour. This slow rate makes it advantageous to consider that scour problems are time dependent and to find ways to accumulate the effect of the complete hydrograph rather than to consider a flood design alone.

2.4 ERODIBILITY AND CORRELATION TO SOIL AND ROCK PROPERTIES

There is a critical shear stress τ_c below which no erosion occurs and above which erosion starts. This concept, while convenient, may not be theoretically simple. Indeed, as seen on Figure 2.1, there is no obvious value for the critical shear stress. In this report, the critical shear stress is arbitrarily defined as the shear stress that corresponds to an erosion rate of 1 mm/hr. The critical shear stress is associated with the critical velocity v_c. One can also define the initial slope $S_i = (d\dot{z}/d\tau)_i$ at the origin of the erosion function. Both τ_c and S_i are parameters that help describe the erosion function and, therefore, the erodibility of a material.

In cohesionless soils (sands and gravels), the critical shear stress has been empirically related to the mean grain size D_{50} (Briaud et al., 2001).

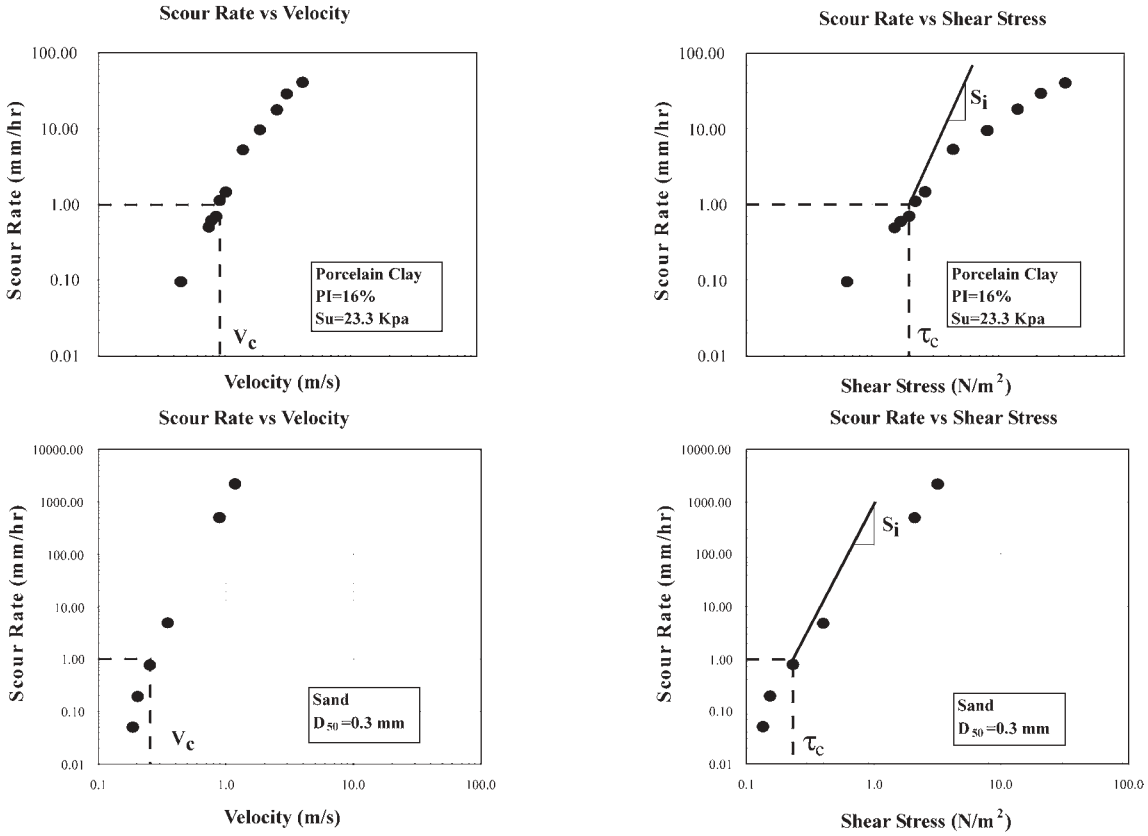

Figure 2.1. Erodibility function for a clay and a sand.

$$\tau_c\left(\mathrm{N}/m^2\right) = D_{50}(mm) \tag{2.1}$$

For such soils, the erosion rate beyond the critical shear stress is very rapid and one flood is long enough to reach the maximum scour depth. Therefore, there is a need to be able to predict the critical shear stress to know if there will be scour or no scour but there is little need to define the erosion function beyond that point because the erosion rate is not sufficiently slow to warrant a time-dependent analysis.

In cohesive soils (silts and clays) and rocks, Equation 2.1 is not applicable (Figure 2.2) and the erosion rate is sufficiently slow that a time-dependent analysis is warranted. Therefore, it is necessary to obtain the complete erosion function. An attempt was made to correlate those parameters, τ_c

TABLE 2.1 Factors influencing the erodibility of cohesive soils

When this parameter increases	Erodibility
Soil water content	*
Soil unit weight	decreases
Soil plasticity index	decreases
Soil undrained shear strength	increases
Soil void ratio	increases
Soil swell	increases
Soil mean grain size	*
Soil percent passing sieve #200	decreases
Soil clay minerals	*
Soil dispersion ratio	increases
Soil cation exchange capacity	*
Soil sodium absorption ratio	increases
Soil pH	*
Soil temperature	increases
Water temperature	increases
Water chemical composition	*

* unknown

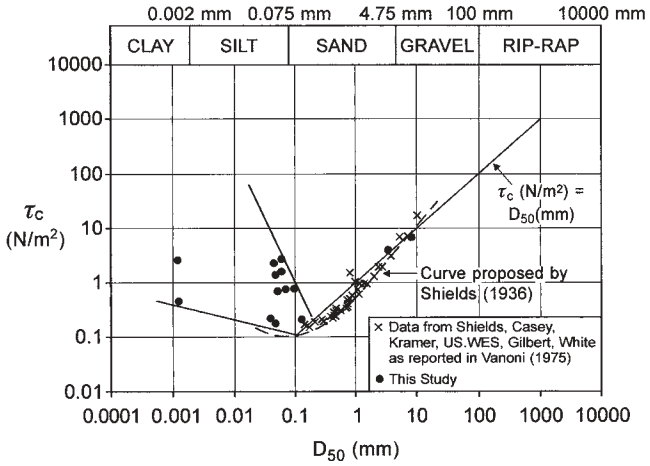

Figure 2.2. Critical shear stress versus mean soil grain diameter.

and S_i, to common soil properties in the hope that simple equations could be developed for everyday use. The process consisted of measuring the erosion function and common soil properties (i.e., water content, unit weight, plasticity index, percent passing sieve no. 200, undrained shear strength). This led to a database of 91 EFA tests (Table 2.2), which was used to perform regression analyses and obtain correlation equations (Figures 2.3 to 2.6). All attempts failed to reach a reasonable R^2 value.

The fact that in this project no relationship could be found between the critical shear stress or the initial slope of the erosion function and common soil properties seems to be at odds with the accepted idea that different cohesive soils erode at different rates. Indeed, if different clays erode at different rates, then the erosion function and therefore its parameters should be functions of the soil properties. The likely explanation is that there is a relationship between erodibility and soil properties but that this relationship is quite complicated, involves advanced soil properties, and could not be found within the budget and time of this project. Instead, it was found much easier to develop an apparatus that could measure the erosion function on any sample of cohesive soil. This device was called the Erosion Function Apparatus, or EFA.

TABLE 2.2 Database of EFA tests

Woodrow Wilson Bridge (Washington)	Tests 1 to 12
South Carolina Bridge	Tests 13 to 16
National Geotechnical Experimentation Site (Texas)	Tests 17 to 26
Arizona Bridge (NTSB)	Test 27
Indonesia samples	Tests 28 to 33
Porcelain clay (man-made)	Tests 34 to 72
Bedias Creek Bridge (Texas)	Tests 73 to 77
Sims Bayou (Texas)	Tests 78 to 80
Brazos River Bridge (Texas)	Test 81
Navasota River Bridge (Texas)	Tests 82 and 83
San Marcos River Bridge (Texas)	Tests 84 to 86
San Jacinto River Bridge (Texas)	Tests 87 to 89
Trinity River Bridge (Texas)	Tests 90 and 91

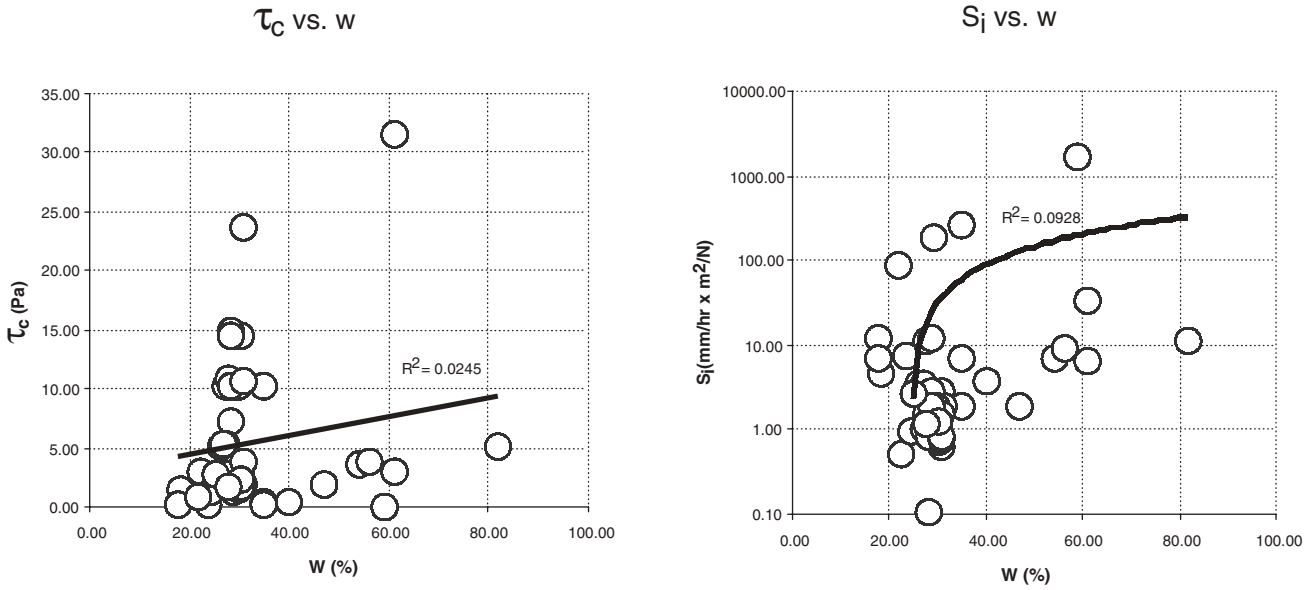

Figure 2.3. Erosion properties as a function of water content.

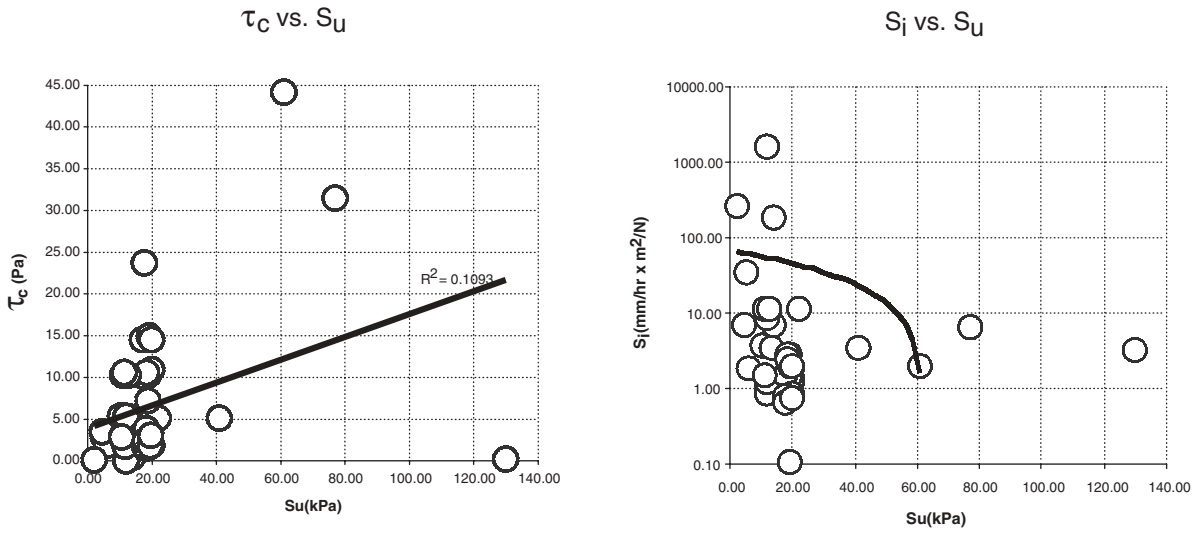

Figure 2.4. Erosion properties as a function of undrained shear strength.

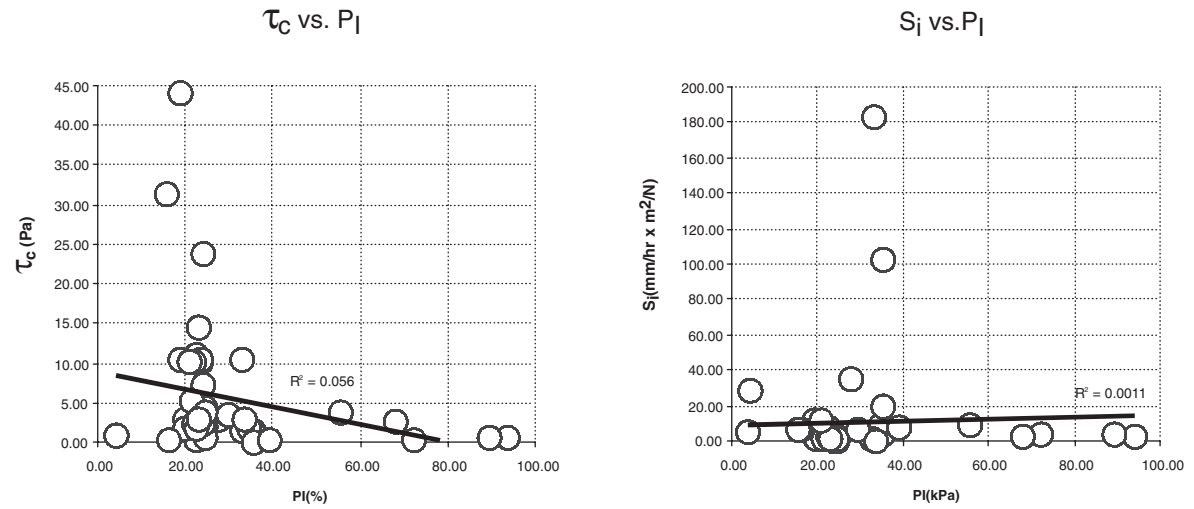

Figure 2.5. Erosion properties as a function of plasticity index.

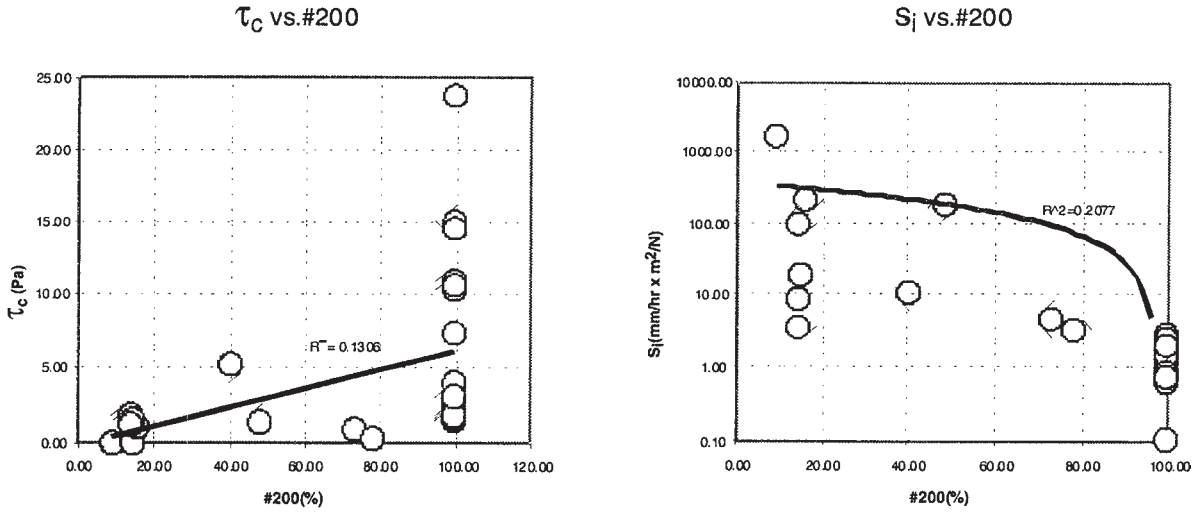

Figure 2.6. Erosion properties as a function of percent passing sieve #200.

CHAPTER 3

EROSION FUNCTION APPARATUS (EFA)

3.1 CONCEPT

The EFA shown in Figures 3.1 and 3.2 (Briaud et al. 1999, 2001, as well as http://www.humboldtmfg.com/pdf2/hm4000ds.pdf and http://tti.tamu.edu/geotech/scour) was conceived in 1991, designed in 1992, and built in 1993. A sample of soil, fine-grained or not, is taken in the field using an ASTM standard Shelby tube with a 76.2-mm outside diameter (ASTM D1587). One end of the Shelby tube full of soil is placed through a circular opening in the bottom of a rectangular cross-section conduit. A snug fit and an O-ring establish a leak-proof connection. The cross section of the rectangular conduit is 101.6 mm by 50.8 mm. The conduit is 1.22-m long and has a flow straightener at one end. The water is driven through the conduit by a pump. A valve regulates the flow and a flow meter is used to measure the flow rate. The range of mean flow velocities is 0.1 m/s to 6 m/s. The end of the Shelby tube is held flush with the bottom of the rectangular conduit. A piston at the bottom end of the sampling tube pushes the soil until it protrudes 1 mm into the rectangular conduit at the other end. This 1-mm protrusion of soil is eroded by the water flowing over it.

3.2 EFA TEST PROCEDURE

The procedure for the EFA test is as follows:

1. Place the sample in the EFA, fill the conduit with water, and wait 1 hour.
2. Set the velocity to 0.3 m/s.
3. Push the soil 1 mm into the flow.
4. Record how much time it takes for the 1 mm of soil to erode (visual inspection through Plexiglas window).
5. When the 1 mm of soil is eroded or after 1 hour of flow, whichever comes first, increase the velocity to 0.6 m/s and bring the soil back to a 1-mm protrusion.
6. Repeat Step 4.
7. Then repeat Steps 5 and 6 for velocities equal to 1 m/s, 1.5 m/s, 2 m/s, 3 m/s, 4.5 m/s, and 6 m/s.

3.3 EFA TEST DATA REDUCTION

The test result consists of the erosion rate $\dot{z}$ versus shear stress τ curve (Figure 3.1). For each flow velocity v, the erosion rate $\dot{z}$ (mm/hr) is simply obtained by dividing the length of sample eroded by the time required to do so.

$$\dot{z} = \frac{h}{t} \tag{3.1}$$

Where h is the length of soil sample eroded in a time t. The length h is 1 mm and the time t is the time required for the sample to be eroded flush with the bottom of the pipe (visual inspection through a Plexiglas window).

After several attempts at measuring the shear stress τ in the apparatus it was found that the best way to obtain τ was by using the Moody Chart (Moody, 1944) for pipe flows.

$$\tau = \frac{1}{8} f \rho v^2 \tag{3.2}$$

Where τ is the shear stress on the wall of the pipe; f is the friction factor obtained from the Moody Chart (Figure 3.3); ρ is the mass density of water (1,000 kg/m3); and v is the mean flow velocity in the pipe. The friction factor f is a function of the pipe Reynolds Number R_e and the pipe roughness ϵ/D. The Reynolds Number is vD/v where D is the pipe diameter and v is the kinematic viscosity of water (10^{-6}m^2/s at 20°C). Since the pipe in the EFA has a rectangular cross section, D is taken as the hydraulic diameter $D = 4A/P$ where A is the cross-sectional flow area, P is the wetted perimeter, and the factor 4 is used to ensure that the hydraulic diameter is equal to the diameter for a circular pipe. For a rectangular cross-section pipe:

$$D = 2ab/(a + b) \tag{3.3}$$

Where a and b are the dimensions of the sides of the rectangle. The relative roughness ϵ/D is the ratio of the average height of the roughness elements on the pipe surface over the pipe diameter D. The average height of the roughness elements ϵ is taken equal to $0.5D_{50}$ where D_{50} is the mean grain size for the soil. The factor 0.5 is used because it is assumed that the top half of the particle protrudes into the flow while the bottom half is buried in the soil mass.

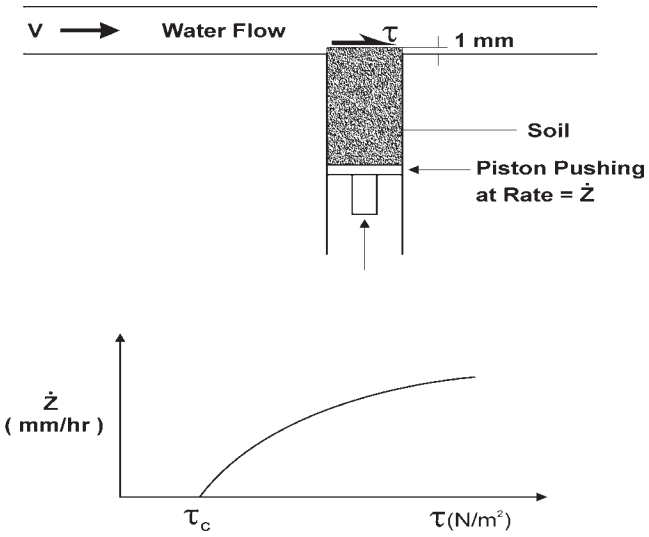

Figure 3.1. Schematic diagram and result of the Erosion Function Apparatus (EFA).

3.4 EFA PRECISION AND TYPICAL RESULTS

If the erosion rate is slow (less that 10 mm/hr), the error on $\dot{z}$ is estimated at 0.5 mm/hr. If the erosion rate is fast (more than 100 mm/hr), the error on $\dot{z}$ is estimated at 2 mm/hr. Therefore, the relative error on $\dot{z}$ is estimated to be less than 10%. Comparison between the τ_c results for the sand and the gravel tested in this study and shown on Figure 2.2 with Shields data indicates a difference of about 10%. Therefore, it is estimated that both $\dot{z}$ and τ are measured with a relative error of about 10%.

The $\dot{z}$ versus τ curve is the result of a series of tests, each of which is performed at a constant velocity. A typical series of eight velocity tests lasts one work day. Figure 2.1 and Figure 3.4 show examples of EFA test results.

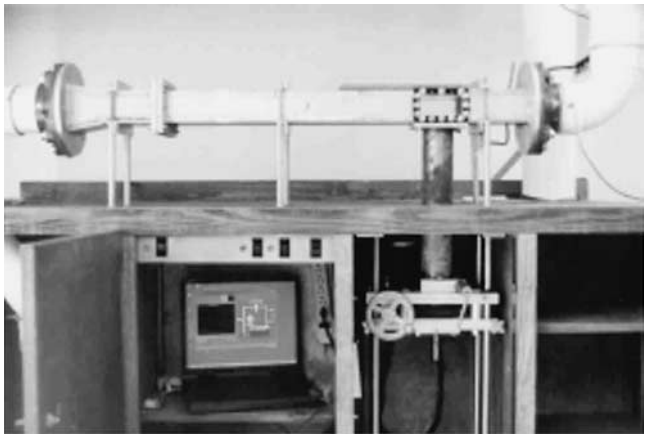

(a)

(b)

Figure 3.2. Photographs of the EFA: (a) general view, (b) close-up of the test section.

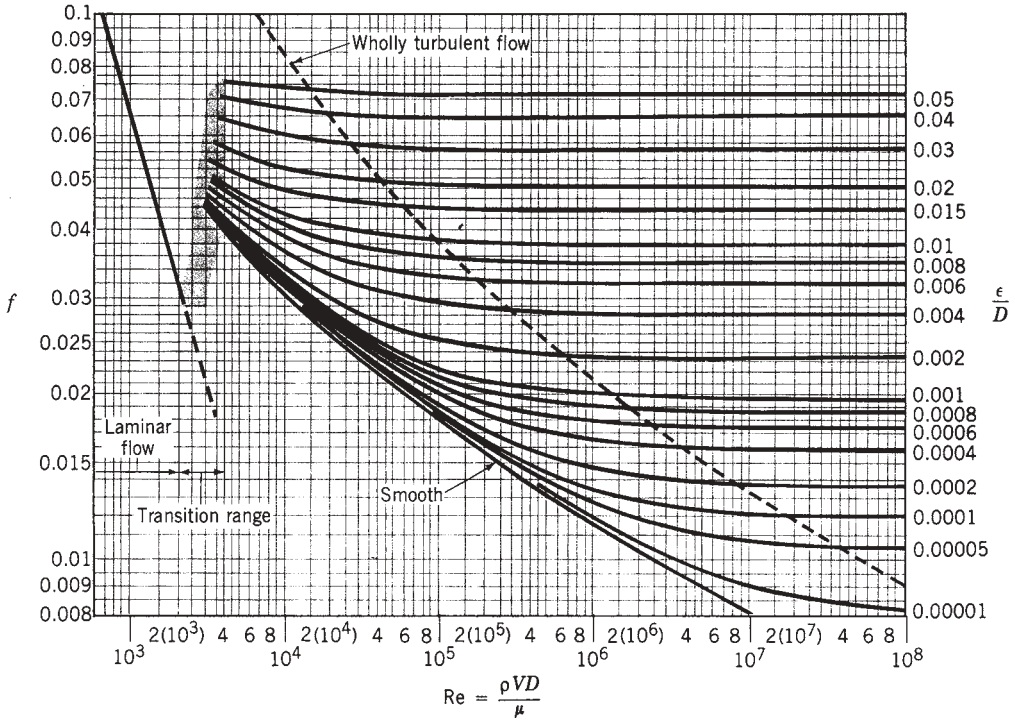

Figure 3.3. Moody Chart (reprinted with permission from Munson et al., 1990).

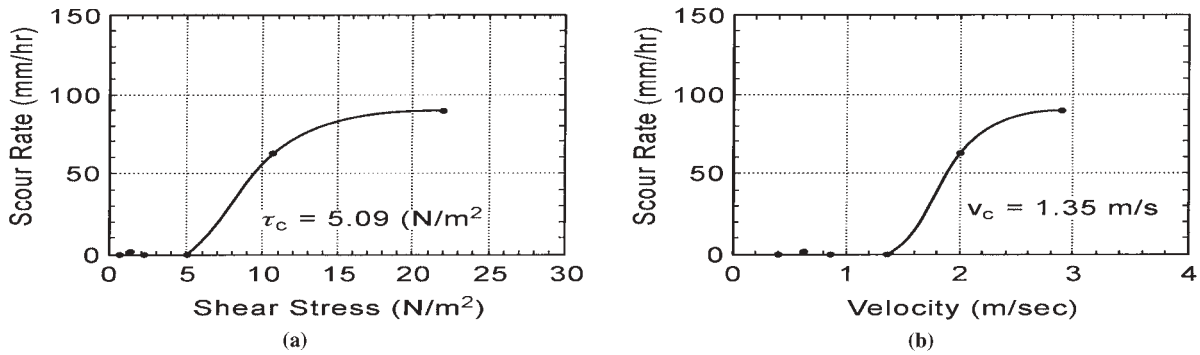

Figure 3.4. Erosion function for a soil sample taken near Pier 27E of the existing Woodrow Wilson Bridge (2.6 to 3.2 m depth): a) scour rate versus shear stress, b) scour rate versus velocity.

CHAPTER **4**

THE SRICOS-EFA METHOD FOR CYLINDRICAL PIERS IN DEEP WATER

4.1 SRICOS-EFA METHOD FOR CONSTANT VELOCITY AND UNIFORM SOIL

Because cohesive soils may scour so much more slowly than cohesionless soils, it is necessary to include the scour rate in the calculations, and the SRICOS Method was developed for this purpose. The SRICOS Method was proposed in 1999 to predict the scour depth z versus time t curve at a cylindrical bridge pier for a constant velocity flow, uniform soil, and water depth greater than two times the pier diameter. The SRICOS Method consists of the following (Briaud et al., 1999):

1. Collecting Shelby tube samples near the bridge pier,
2. Testing them in the EFA (Erosion Function Apparatus, Briaud et al., 2002) (Figure 3.1) to obtain the erosion rate $\dot{z}$ (mm/hr) versus hydraulic shear stress τ (N/m^2) curve,
3. Calculating the maximum hydraulic shear stress τ_{max} around the pier before scour starts,
4. Reading the initial erosion rate $\dot{z}_i$ (mm/hr) corresponding to τ_{max} on the $\dot{z}$ versus τ curve,
5. Calculating the maximum depth of scour z_{max},
6. Constructing the scour depth z versus time t curve using a hyperbolic model, and
7. Reading the scour depth corresponding to the duration of the flood on the z versus t curve.

The maximum hydraulic shear stress τ_{max} exerted by the water on the riverbed was obtained by performing a series of three-dimensional numerical simulations of water flowing past a cylindrical pier of diameter B on a flat river bottom and with a large water depth (water depth larger than $2B$). The results of several runs lead to the following equation (Briaud et al., 1999):

$$\tau_{max} = 0.094\,\rho v^2\left(\frac{1}{\log R_e} - \frac{1}{10}\right) \tag{4.1}$$

Where ρ is the density of water (kg/m^3); v is the depth average velocity in the river at the location of the pier if the bridge were not there (it is obtained by performing a hydrologic analysis with a computer program such as the Hydrologic Engineering Center—River Analysis System [HEC-RAS], 1997); and R_e is $\frac{vB}{\upsilon}$ where B is the pier diameter and υ the kinematic viscosity of water (10^{-6}m^2/s at 20°C). The initial rate of scour $\dot{z}_i$ is read on the $\dot{z}$ versus τ curve from the EFA test at the value of τ_{max}.

The maximum depth of scour z_{max} was obtained by performing a series of 43 model scale flume tests (36 tests on three different clays and 7 tests in sand) (Briaud et al., 1999). The results of these experiments, and a review of other work, led to the following equation, which appears to be equally valid for clays and sands:

$$z_{max}(\text{mm}) = 0.18R_e^{0.635} \tag{4.2}$$

In Equation 4.2, R_e has the same definition as in Equation 4.1. The regression coefficient for Equation 4.2 was 0.74. The equation that describes the shape of the scour depth z versus time t curve is

$$z = \frac{t}{\frac{1}{\dot{z}_i} + \frac{t}{z_{max}}} \tag{4.3}$$

Where $\dot{z}_i$ and z_{max} have been previously defined, t is time (hours). This hyperbolic equation was chosen because it fits the curves obtained in the flume tests well. Once the duration t of the flood to be simulated is known, the corresponding z value is calculated using Equation 4.3. If $\dot{z}_i$ is large, as it is in clean fine sands, then z is close to z_{max} even for small t values. But if $\dot{z}_i$ is small, as it can be in clays, then z may only be a small fraction of z_{max}. An example of the SRICOS Method is shown in Figure 4.1.

The method as described in the previous paragraphs is limited to a constant velocity hydrograph (v = constant), a uniform soil (one $\dot{z}$ versus τ curve) and a relatively deep water depth. In reality, rivers create varying velocity hydrographs and soils are layered. The following describes how SRICOS was extended to include these two features. The case of shallow water flow (water depth over pier diameter < 2), noncircular piers, and flow directions different from the pier main axis are not addressed in this chapter.

4.2 SMALL FLOOD FOLLOWED BY BIG FLOOD

For a river, the velocity versus time history over many years is very different from a constant velocity history. In

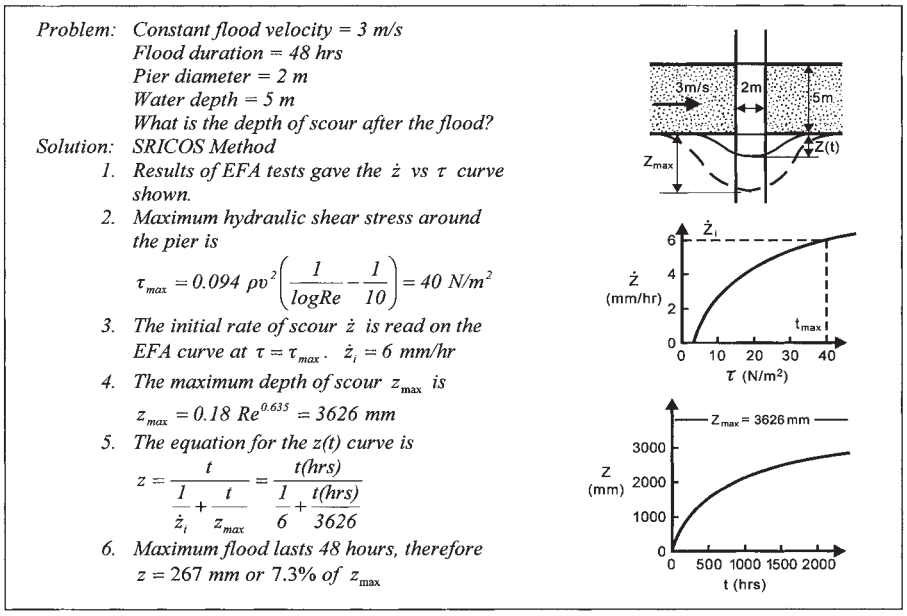

Figure 4.1. Example of the SRICOS Method for constant velocity and uniform soil.

order to investigate the influence of the difference between the two velocity histories or hydrographs on the depth of scour at a bridge pier, the case of a sequence of two different yet constant velocity floods scouring a uniform soil was first considered (Figure 4.2). Flood 1 has a velocity v_1 and lasts a time t_1 while the subsequent Flood 2 has a larger velocity v_2 and lasts a time t_2. The scour depth z versus time t curve for Flood 1 is described by:

$$z = \frac{t}{\frac{1}{\dot{z}_{i1}} + \frac{t}{z_{\max 1}}} \tag{4.4}$$

For Flood 2, the z versus t curve is:

$$z = \frac{t}{\frac{1}{\dot{z}_{i2}} + \frac{t}{z_{\max 2}}} \tag{4.5}$$

After a time t_1, Flood 1 creates a scour depth z_1 given by Equation 4.4 (Point A on Figure 4.2b). This depth z_1 would have been created in a shorter time t^* by Flood 2 because v_2 is larger than v_1 (Point B on Figure 4.2c). This time t^* can be found by setting Equation 4.4 with $z = z_1$ and $t = t_1$ equal to Equation 4.6 with $z = z_1$ and $t = t^*$.

$$t^* = \frac{t_1}{\frac{\dot{z}_{i2}}{\dot{z}_{i1}} + t_1\dot{z}_{i2}\left(\frac{1}{z_{\max 1}} - \frac{1}{z_{\max 2}}\right)} \tag{4.6}$$

When Flood 2 starts, even though the scour depth z_1 was due to Flood 1 over a time t_1, the situation is identical to having had Flood 2 for a time t^*. Therefore, when Flood 2 starts, the scour depth versus time curve proceeds from Point B on Figure 4.2c until Point C after a time t_2. The z versus t curve for the sequence of Floods 1 and 2, follows path OA on the curve for Flood 1 then switches to BC on the curve for Flood 2. This is shown as curve OAC on Figure 4.2d.

A set of two experiments was conducted to investigate this reasoning. For these experiments, a pipe with a diameter of 25 mm was placed in the middle of a flume. The pipe was pushed through a deposit of clay 150 mm thick that was made by placing prepared blocks of clay side by side in a tight arrangement. The properties of the clay are listed in Table 4.1. The water depth was 400 mm and the mean flow velocity was $v_1 = 0.3$ m/s in Flood 1 and $v_2 = 0.4$ m/s for Flood 2 (Figure 4.3a). The first of the two experiments consisted of setting the velocity equal to v_2 for 100 hours and recording the z versus t curve (Figure 4.3c). The second of the two experiments consisted of setting the velocity equal to v_1 for 115 hours (Figure 4.3b) and then switching to v_2 for 100 hours (Figure 4.3d). Also shown on Figure 4.3d is the prediction of the portion of the z versus t curve under the velocity v_2 according to the procedure described in Figure 4.3. As can be seen, the prediction is very reasonable.

4.3 BIG FLOOD FOLLOWED BY SMALL FLOOD AND GENERAL CASE

Flood 1 has a velocity v_1 and lasts t_1 (Figure 4.4a). It is followed by Flood 2, which has a velocity v_2 smaller than v_1 and lasts t_2. The scour depth z versus time t curve is given by Equation 4.4 for Flood 1 and by Equation 4.5 for Flood 2. After a time t_1, Flood 1 creates a scour depth z_1. This depth z_1 is compared with $z_{\max 2}$; if z_1 is larger than $z_{\max 2}$ then when Flood 2 starts, the scour hole is already larger than it can be

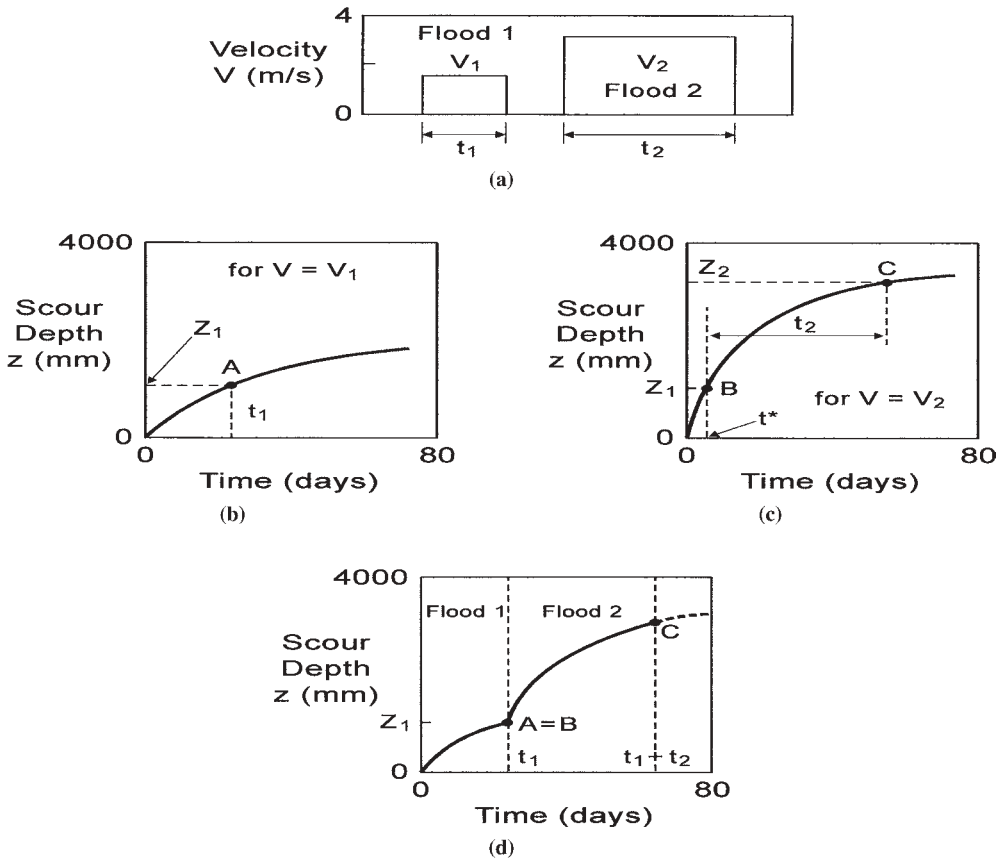

Figure 4.2. Scour due to a sequence of two flood events (small flood followed by big flood).

with Flood 2. Therefore, Flood 2 cannot create additional scour and the scour depth versus time curve remains flat during Flood 2. If z_1 is smaller than $z_{max\,2}$ then the procedure followed for the case of a small flood followed by a big flood applies, and the combined curve is as shown in Figure 4.4.

In the general case, the velocity versus time history exhibits many sequences of small floods and big floods. The calculations for scour depth are performed by choosing an increment of time Δt and breaking the complete velocity versus time history into a series of partial flood events, each lasting Δt. The first two floods in the hydrograph are handled by using the procedure shown in Figure 4.2 or Figure 4.4, depending on the case. Then the process advances by stepping into time and considering a new "Flood 2" and a new t^* at each step. The time Δt is typically one day, and a velocity versus time history can be 50 years long. The many steps of calculations are handled with a computer program called SRICOS. The output of the program is the depth of scour versus time curve over the duration of the velocity versus time history.

4.4 HARD SOIL LAYER OVER SOFT SOIL LAYER

The original SRICOS Method (Briaud et al., 1999) was developed for a uniform soil. In order to investigate the influence of the difference between a uniform soil and a more realistic layered soil on the depth of scour at a bridge pier, the case of a two-layer soil profile scoured by a constant velocity flood was considered (Figure 4.5). Layer 1 is hard and Δz_1 thick, Layer 2 underlies Layer 1 and is softer than Layer 1. The scour depth z versus time t curve for Layer 1 is given by Equation 4.4 (Figure 4.5a) and the z versus t curve for Layer 2 is given by Equation 4.5 (Figure 4.5b). If Δz_1 is larger than the maximum depth of scour in Layer 1, $z_{max\,1}$, then the scour process

TABLE 4.1 Properties of the porcelain clay for the flume experiment

Liquid Limit, %	34.4	Shear Strength, kPa(lab vane)	12.5
Plastic Limit, %	20.2	Cation Exchange Capacity, (meq/100g)	8.30
Plasticity Index, %	14.1	Sodium Adsorption Ratio	5.00
Water Content, %	28.5	Electrical Conductivity, (mmhos/cm)	1.20
Mean Diameter D_{50}, (mm)	0.0062	pH	6.00
Sand Content, %	0.0	Unit Weight (kN/m^3)	18.0
Silt Content, %	75.0	Specific Gravity	2.61
Clay Content, %	25.0		

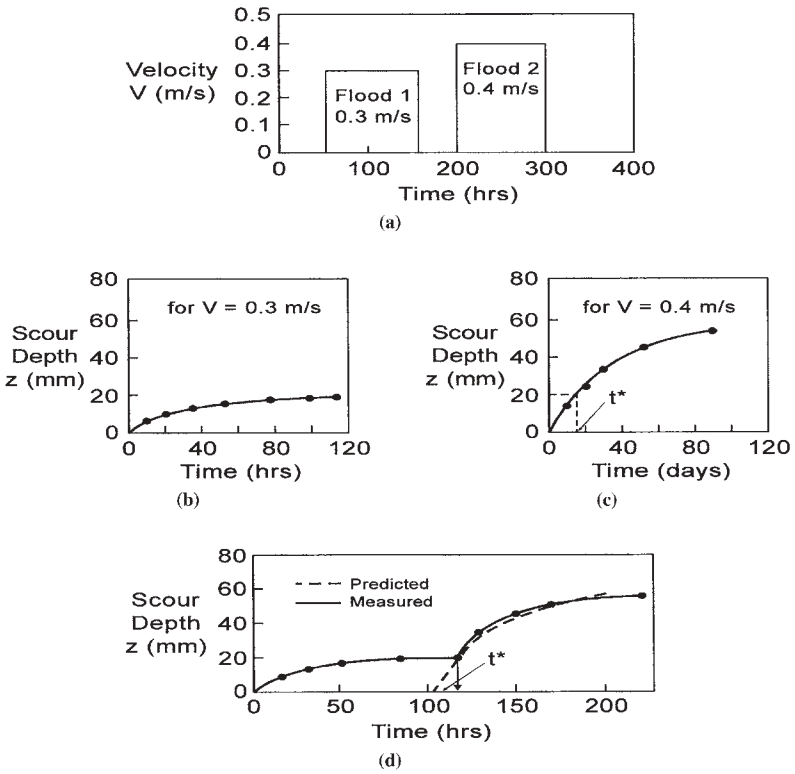

Figure 4.3. Multiflood flume experiment results: a) floods and flood sequence in the experiments, b) experiment results for Flood 1 alone, c) experiment results for Flood 2 alone, d) experiment results for Floods 1 and 2 sequence shown in a) and prediction for Flood 2.

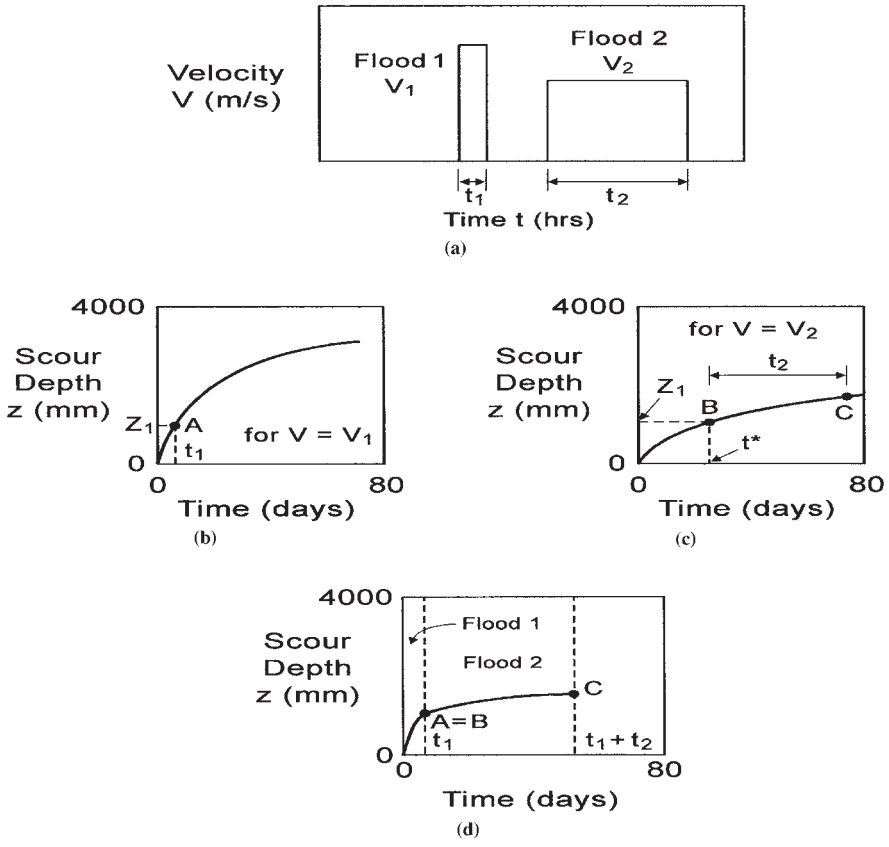

Figure 4.4. Scour due to a sequence of two flood events (big flood followed by small flood).

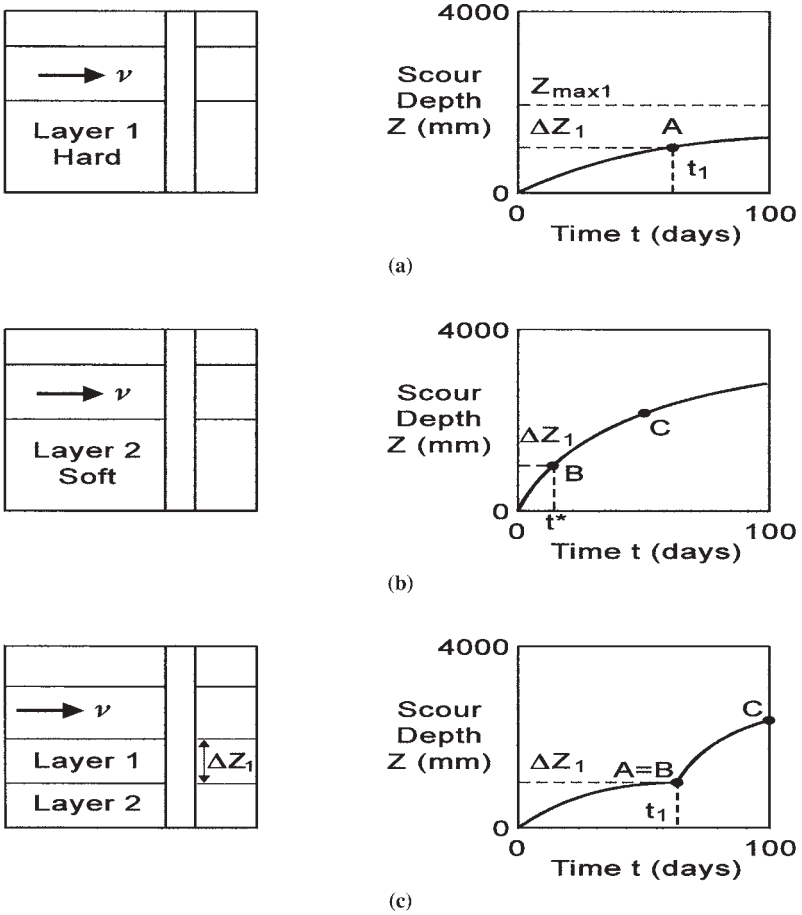

Figure 4.5. Scour of a two-layer soil (hard layer over soft layer).

is contained in Layer 1 and does not reach Layer 2. If, however, the scour depth reaches Δz_1 (Point A on Figure 4.5a), Layer 2 starts to be eroded. In this case, even though the scour depth Δz_1 was due to the scour of Layer 1 over a time t_1, at that time the situation is identical to having had Layer 2 scoured over a time t^* (Point B on Figure 4.5b). Therefore, when Layer 2 starts being eroded, the scour depth versus time curve proceeds from Point B to Point C on Figure 4.5b. The combined curve for the two-layer system is OAC on Figure 4.5c.

4.5 SOFT SOIL LAYER OVER HARD SOIL LAYER AND GENERAL CASE

Layer 1 is soft and Δz_1 thick. Layer 2 underlies Layer 1 and is harder than Layer 1. The scour depth z versus time t curve for Layer 1 is given by Equation 4.4 (Figure 4.6a), and the z versus t curve for Layer 2 is given by Equation 4.5 (Figure 4.6b). If Δz_1 is larger than the maximum depth of scour in Layer 1, $z_{\max 1}$, then the scour process is contained in Layer 1 and does not reach Layer 2. If, however, the scour depth reaches Δz_1 (Point A on Figure 4.6a), Layer 2 starts to erode. In this case, even though the scour depth Δz_1 was due to the scour of Layer 1 over a time t_1, at that time the situation is identical to having had Layer 2 scoured over an equivalent time t^* (Point B on Figure 4.6b). Therefore, when Layer 2 starts being eroded, the scour depth versus time curve proceeds from Point B to Point C on Figure 4.6b. The combined curve for the two-layer system is OAC on Figure 4.6c.

In the general case, there may be a series of soil layers with different erosion functions. The computations proceed by stepping forward in time. The time steps are Δt long, the velocity is the one for the corresponding flood event, and the erosion function ($\dot{z}$ versus t) is the one for the soil layer corresponding to the current scour depth (bottom of the scour hole). When Δt is such that the scour depth proceeds to a new soil layer, the computations follow the process described in Figures 4.5 or 4.6 depending on the case. The same SRICOS program mentioned for the velocity hydrograph also handles these calculations. The output of the program is the scour depth versus time curve for the multilayered soil system and for the complete velocity hydrograph.

4.6 EQUIVALENT TIME

The computer program SRICOS is required to predict the scour depth versus time curve as explained in the preceding

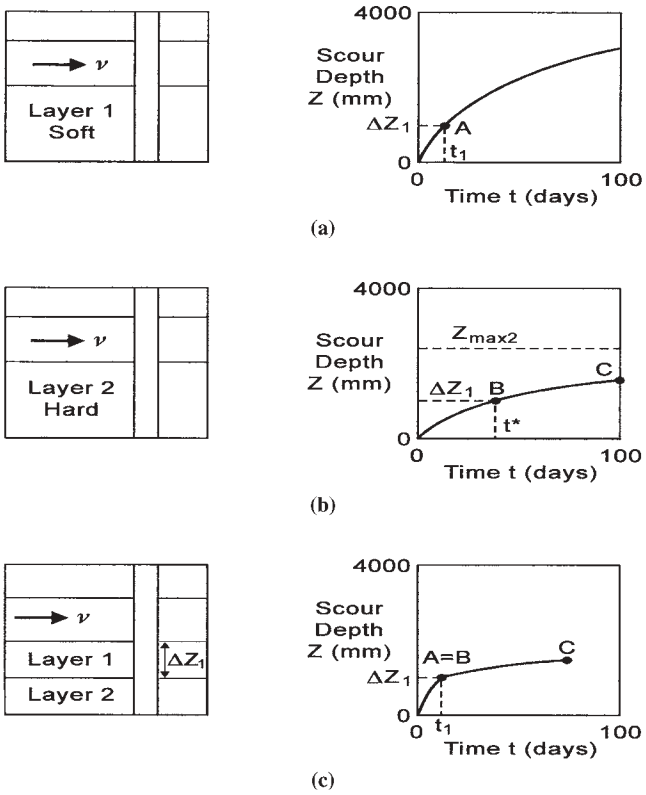

Figure 4.6. Scour of a two-layer soil (soft layer over hard layer).

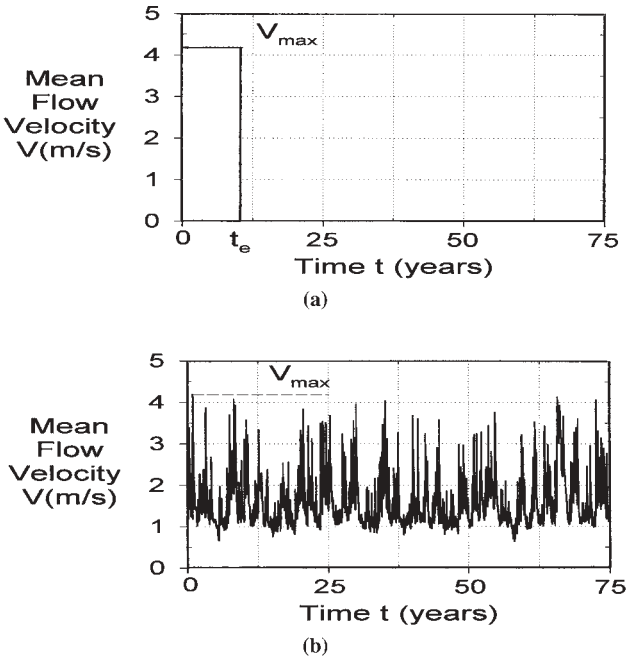

Figure 4.7. Velocity hydrographs: a) constant, b) true hydrograph. Both hydrographs would lead to the same scour depth.

section. An attempt was made to simplify the method to the point where only hand calculations would be needed. This requires the consideration of an equivalent uniform soil and an equivalent time for a constant velocity history. The equivalent uniform soil is characterized by an average $\dot{z}$ versus τ curve over the anticipated scour depth. The equivalent time t_e is the time required for the maximum velocity in the hydrograph to create the same scour depth as the one created by the complete hydrograph (Figure 4.7). The equivalent time t_e was obtained for 55 cases generated from 8 bridge sites. For each bridge site, soil samples were collected in Shelby tubes and tested in the EFA to obtain the erosion function $\dot{z}$ versus τ; then the hydrograph was collected from the nearest gage station and the SRICOS program was used to calculate the scour depth. That scour depth was entered in Equation 4.3, together with the corresponding $\dot{z}_i$ and $\dot{z}_{max}$ to get t_e. The $\dot{z}_i$ value was obtained from an average $\dot{z}$ *vs* τ curve within the final scour depth by reading the $\dot{z}$ value that corresponded to τ_{max} obtained from Equation 4.1. In Equation 4.1, the pier diameter B and the maximum velocity v_{max} found to exist in the hydrograph over the period considered were used. The z_{max} value was obtained from Equation 4.2 while using B and v_{max} for the pier Reynolds Number. The hydrograph at each bridge was also divided into shorter period hydrographs, and for each period an equivalent time t_e was calculated. This generated 55 cases (Briaud et al., 2002).

The equivalent time was then correlated to the duration of the hydrograph t_{hydro}, the maximum velocity in the hydrograph v_{max}, and the initial erosion rate $\dot{z}_i$. A multiple regression on that data gave the following relationship:

$$t_e(\text{hrs}) = 73\left(t_{hydro}(\text{years})\right)^{0.126}\left(v_{max}(\text{m/s})\right)^{1.706}\left(\dot{z}_i(\text{mm/hr})\right)^{-0.20} \quad (4.7)$$

The regression coefficient for Equation 4.7 was 0.77. This time t_e can then be used in Equation 4.3 to calculate the scour at the end of the hydrograph. A comparison between the scour depth predicted by the extended SRICOS Method using the complete hydrograph and the simple SRICOS Method using the equivalent time is shown on Figure 4.8.

4.7 EXTENDED AND SIMPLE SRICOS-EFA METHOD

For final design purposes, the extended SRICOS Method (E-SRICOS) is used to predict the scour depth z versus time t over the duration of the design hydrograph. The method proceeds as follows:

1. Calculate the maximum depth of scour z_{max} for the design velocity by using Equation 4.2.
2. Collect samples at the site within the depth z_{max}.
3. Test the samples in the EFA to obtain the erosion functions ($\dot{z}$ versus τ) for the layers involved.
4. Prepare the flow hydrograph for the bridge. This step may consist of downloading the discharge hydrograph from a United States Geological Survey (USGS) gage

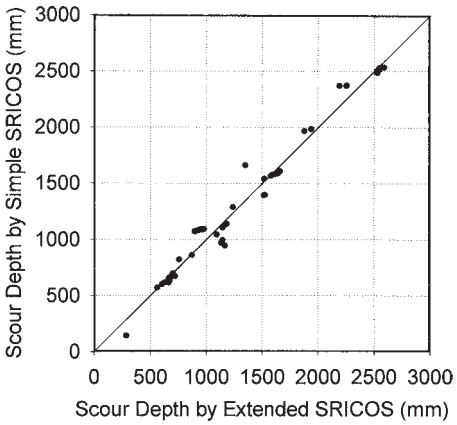

Figure 4.8. Comparison of scour depth using Extended SRICOS and Simple SRICOS Methods.

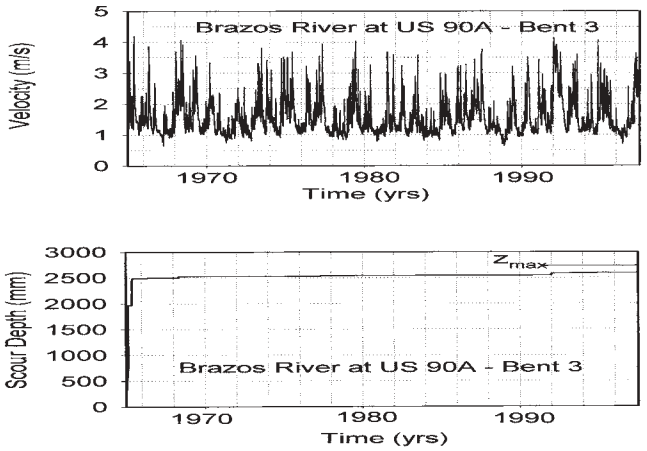

Figure 4.10. Velocity hydrograph and scour depth versus time curve for Bent 3 of the Brazos River Bridge at US 90A.

station near the bridge (Figure 4.9). These discharge hydrographs can be found on the Internet at the USGS website (www.usgs.gov). The discharge hydrograph then needs to be transformed into a velocity hydrograph (Figures 4.10, 4.11, and 4.12). This transformation is performed by using a program such as HEC-RAS (1997), which makes use of the transversed river bottom profile at the bridge site to link the discharge Q (m^3/s) to the velocity v (m/s) at the anticipated location of the bridge pier.

5. Use the SRICOS program (Kwak et al., 1999) with the following input: the $\dot{\varepsilon}$ versus τ curves for the various layers involved, the velocity hydrograph v versus t, the pier diameter B, the viscosity of the water υ, and the density of the water ρ_w. Note that the water depth y is not an input because at this time the solution is limited to a "deep water" condition. This condition is realized when $y \geq 2B$; indeed beyond this water depth the scour depth becomes independent of the water depth (Melville and Coleman, 1999, p. 197).
6. The SRICOS program proceeds by a series of time steps; it makes use of the original SRICOS Method and of the accumulation algorithms described in Figures 4.2, 4.4, 4.5, and 4.6. The usual time step Δt is 1 day because that is the usual reading frequency of the USGS gages. The duration of the hydrograph can vary from a few days to over 100 years.
7. The output of the program is the depth of scour versus time over the period covered by the hydrograph (Figures 4.10, 4.11, and 4.12).

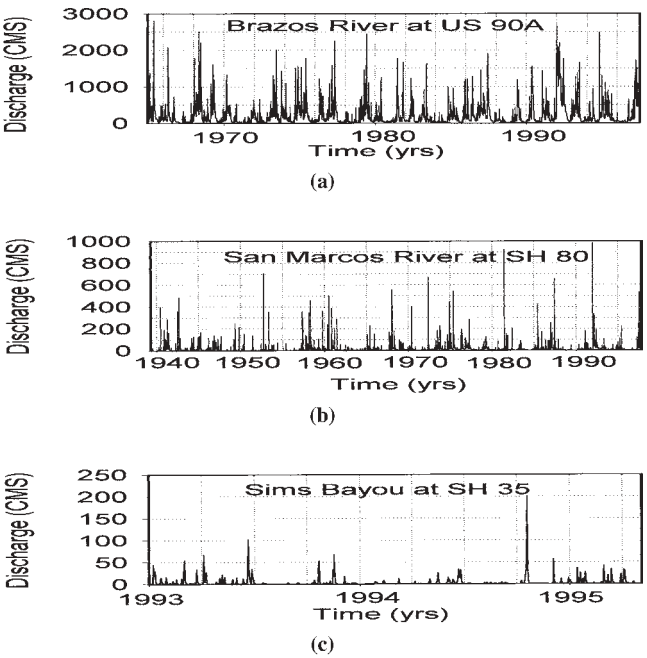

Figure 4.9. Examples of discharge hydrographs: a) Brazos River at US 90A, b) San Marcos River at SH 80, c) Sims Bayou at SH 35.

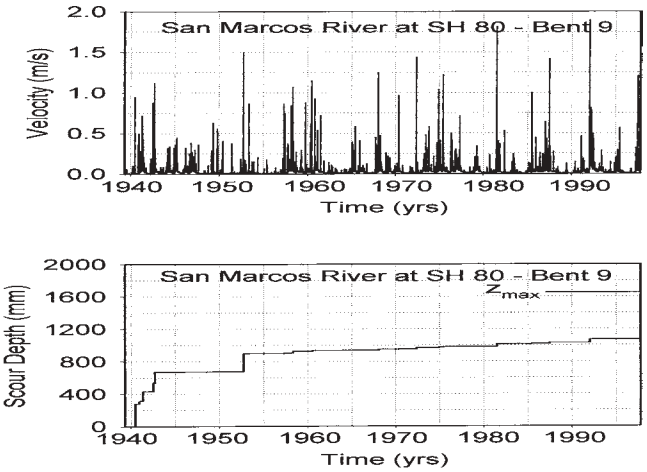

Figure 4.11. Velocity hydrograph and scour depth versus time curve for Bent 3 of the San Marcos River Bridge at SH 80.

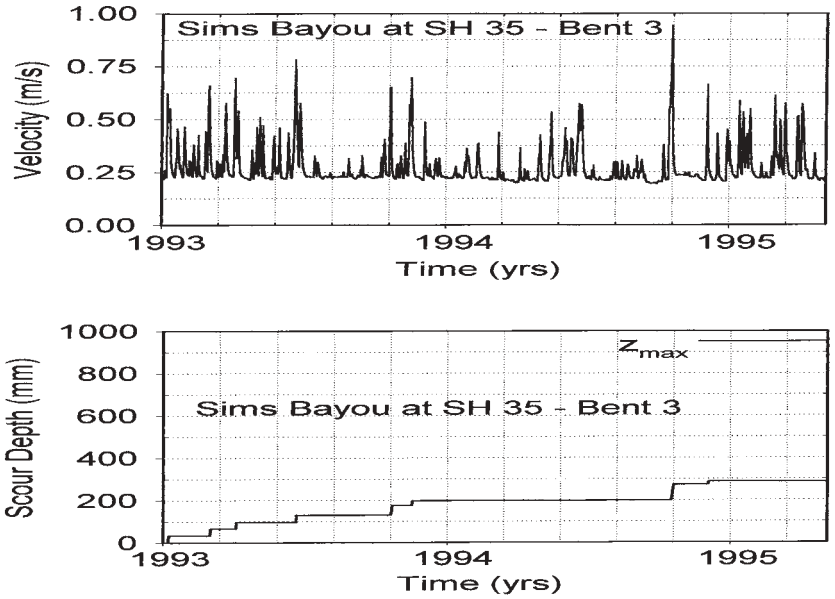

Figure 4.12. Velocity hydrograph and scour depth versus time curve for Bent 3 of the Sims Bayou River Bridge at SH 35.

For predicting the future development of a scour hole at a bridge pier over a design life t_{life}, one can either develop a synthetic hydrograph (much like is done in the case of earthquakes) or assume that the hydrograph recorded over the last period equal to t_{life} will repeat itself. The time required to perform Step 3 is about 8 hours per Shelby tube sample because it takes about eight points to properly describe the erosion function ($\dot{z}$ versus τ curve) and, for each point, the water is kept flowing for 1 hour to get a good average $\dot{z}$ value. The time required to perform all other steps, except for Step 2, is about 4 hours for someone who has done it before. In order to reduce these 4 hours to a few minutes, a simplified version of SRICOS, called S-SRICOS, was developed. Note that this simplified method is only recommended for preliminary design purposes. If S-SRICOS shows clearly that there is no need for refinement, then there is no need for E-SRICOS; if not, an E-SRICOS analysis must be performed.

For preliminary design purposes, S-SRICOS can be used. The method proceeds as follows:

1. Calculate the maximum depth of scour z_{max} for the design velocity v_{max} by using Equation 4.2. The design velocity is usually the one corresponding to the 100-year flood or the 500-year flood.
2. Collect samples at the site within the depth z_{max}.
3. Test the samples in the EFA to obtain the erosion function ($\dot{z}$ versus τ) for the layers involved.
4. Create a single equivalent erosion function by averaging the erosion functions within the anticipated depth of scour.
5. Calculate the maximum shear stress τ_{max} around the pier before scour starts by using Equation 4.1. In Equation 4.1, use the pier diameter B and the design velocity v_{max}.
6. Read the erosion rate $\dot{z}$ corresponding to τ_{max} on the equivalent erosion function.
7. Calculate the equivalent time t_e for a given design life of the bridge t_{hydro} for the design velocity v_{max} and for the $\dot{z}_i$ value of Step 6 by using Equation 4.7.
8. Knowing t_e, $\dot{z}_i$, and z_{max}, calculate the scour depth $\dot{z}$ at the end of the design life by using Equation 4.3.

An example of such scour calculations is shown in Figure 4.13.

4.8 CASE HISTORIES

In order to evaluate the E-SRICOS and S-SRICOS Methods, eight bridges were selected (Figure 4.14). These bridges all satisfied the following requirements: the predominant soil type was fine-grained soils according to existing borings; the river bottom profiles were measured at two dates separated by at least several years, these river bottom profiles indicated anywhere from 0.05 m to 4.57 m of scour; a USGS gage station existed near the bridge; and drilling access was relatively easy.

The Navasota River Bridge at SH 7 was built in 1956. The main channel bridge has an overall length of 82.8 m and consists of three continuous steel girder main spans with four concrete pan girder approach spans. The foundation type is steel piling down to 5.5 m below the channel bed, which consists of silty and sandy clay down to the bottom of the piling according to existing borings. Between 1956 and 1996 the peak flood took place in 1992 and generated a measured flow of 1,600 m^3/s, which corresponds to a HEC-RAS calculated mean approach flow velocity of 3.9 m/s at Bent 5 and 2.6 m/s at Bent 3. The pier at Bent 3 was square with a side equal to

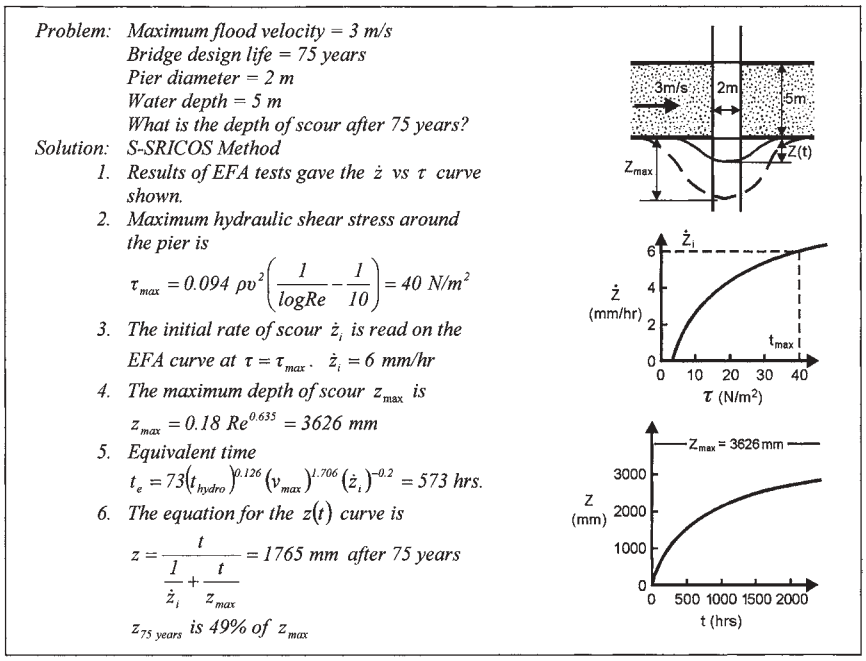

Figure 4.13. Example of scour calculations by the S-SRICOS Method.

0.36 m, while the pier at Bent 5 was 0.36 m wide and 8.53 m long and had a square nose. The angle between the flow direction and the pier main axis was 5 degrees for Bent 5. River bottom profiles exist for 1956 and 1996 and show 0.76 m of local scour at Bent 3 and 1.8 m of total scour at Bent 5. At Bent 5, the total scour was made up of 1.41 m of local scour and 0.39 m of contraction scour as explained later.

The Brazos River Bridge at US 90A was built in 1965. The bridge has an overall length of 287 m and consists of three continuous steel girder main spans with eight prestressed concrete approach spans. The foundation type is concrete piling penetrating 9.1 m below the channel bed, which consists of sandy clay, clayey sand, and sand down to the bottom of the piling according to existing borings. Between 1965 and 1998, the peak flood occurred in 1966 and generated a measured flow of 2,600 m^3/s, which corresponds to a HEC-RAS calculated mean approach velocity of 4.2 m/s at Bent 3. The pier at Bent 3 was 0.91 m wide and 8.53 m long and had a

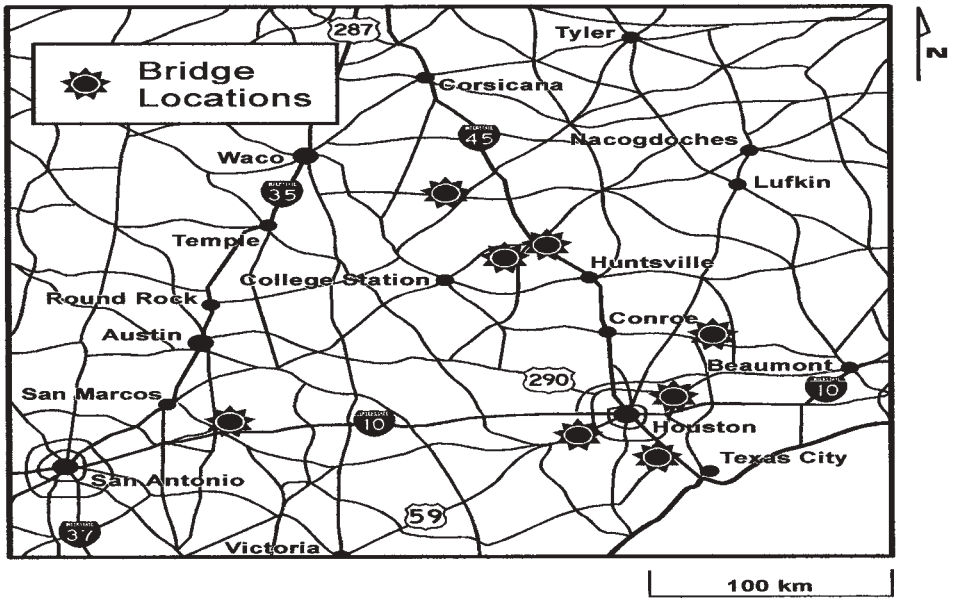

Figure 4.14. Location of case history bridges.

round nose. The pier was in line with the flow. River bottom profiles exist for 1965 and 1997 and show 4.43 m of total scour at Bent 3 made up of 2.87 m of local scour and 1.56 m of combined contraction and general scour as explained later.

The San Jacinto River Bridge at US 90 was built in 1988. The bridge is 1,472.2 m long and has 48 simple prestressed concrete beam spans and 3 continuous steel plate girder spans. The foundation type is concrete piling penetrating 24.4 m below the channel bed at Bent 43 where the soil consists of clay, silty clay, and sand down to the bottom of the piles according to existing borings. Between 1988 and 1997, the peak flood took place in 1994 and generated a measured flow of 10,000 m^3/s, which corresponds to a HEC-RAS calculated mean approach velocity of 3.1 m/s at Bent 43. The pier at Bent 43 was square with a side equal to 0.85 m. The angle between the flow direction and the pier main axis was 15 degrees. River bottom profiles exist for 1988 and 1997 and show 3.17 m of total scour at Bent 43 made up of 1.47 m of local scour and 1.70 m of combined contraction and general scour as explained later.

The Trinity River Bridge at FM 787 was built in 1976. The bridge has three main spans and three approach spans with an overall length of 165.2 m. The foundation type is timber piling and the soil is sandy clay to clayey sand. Between 1976 and 1993, the peak flood took place in 1990 and generated a measured flow of 2,950 m^3/s, which corresponds to a HEC-RAS calculated mean approach flow velocity of 2.0 m/s at Bent 3 and 4.05 m/s at Bent 4. The piers at Bent 3 and Bent 4 were 0.91 m wide and 7.3 m long, and had round noses. The angle between the flow direction and the pier main axes was 25 degrees. River bottom profiles exist for 1976 and for 1992 and show 4.57 m of total scour at both Bent 3 and Bent 4, made up of 2.17 m of local scour and 2.40 m of contraction and general scour as explained later.

The San Marcos River Bridge at SH 80 was built in 1939. This 176.2-m-long bridge has 11 prestressed concrete spans. The soil tested from the site is a low-plasticity clay. Between 1939 and 1998, the peak flood occurred in 1992 and generated a measured flow of 1,000 m^3/s, which corresponds to a HEC-RAS calculated mean approach flow velocity of 1.9 m/s at Bent 9. The pier at Bent 9 is 0.91 m wide and 14.2 m long and has a round nose. The pier is in line with the flow. River bottom profiles exist for 1939 and 1998 and show 2.66 m of total scour at Bent 9 made up of 1.27 m of local scour and 1.39 m of contraction and general scour as explained later.

The Sims Bayou Bridge at SH 35 was built in 1993. This 85.3-m-long bridge has five spans. Each bent rests on four drilled concrete shafts. Soil borings indicate mostly clay layers with a significant sand layer about 10 m thick starting at a depth of approximately 4 m. Between 1993 and 1996, the peak flood occurred in 1994 and generated a measured flow of 200 m^3/s, which corresponds to a HEC-RAS calculated mean approach flow velocity of 0.93 m/s at Bent 3. The pier at Bent 3 is circular with a 0.76 m diameter. The angle between the flow direction and the pier main axis was 5 degrees. River bottom profiles exist for 1993 and 1995 and indicate 0.05 m of local scour at Bent 3.

The Bedias Creek Bridge at US 75 was built in 1947. This 271.9-m-long bridge has 29 spans and Bent 26 is founded on a spread footing. The soil tested from the site varied from low plasticity clay to fine silty sand. Between 1947 and 1996, the peak flood occurred in 1991 and generated a measured flow of 650 m^3/s, which corresponds to a HEC-RAS calculated mean approach flow velocity of 2.15 m/s at Bent 26. The pier at Bent 26 is square with a side of 0.86 m. The pier is in line with the flow. River bottom profiles exist for 1947 and 1996 and show 2.13 m of total scour at Bent 26 made up of 1.35 m of local scour and 0.78 m of contraction and general scour as explained later.

The Bedias Creek Bridge at SH 90 was built in 1979. This 73.2-m-long bridge is founded on 8-m-long concrete piles embedded in layers of sandy clay and firm gray clay. Between 1979 and 1996, the peak flood occurred in 1991 and generated a measured flow of 650 m^3/s, which corresponds to a HEC-RAS calculated mean approach flow velocity of 1.55 m/s at Bent 6. The pier at Bent 6 was square with a side of 0.38 m. The angle between the flow direction and the pier main axis was 5 degrees. River bottom profiles exist for 1979 and 1996 and show 0.61 m of local scour at Bent 6.

4.9 PREDICTED AND MEASURED LOCAL SCOUR FOR THE EIGHT BRIDGES

The data for all bridges is listed in Tables 4.2 and 4.3. For each bridge, the E-SRICOS and S-SRICOS Methods were used to predict the local scour at the chosen bridge pier location. One pier was selected for each bridge, except for the Navasota River Bridge at SH 7 and the Trinity River Bridge at FM 787 for which two piers each were selected. Therefore, a total of 10 predictions were made for these eight bridges. These predictions are not Class A predictions since the measured values were known before the prediction process started. However, the predictions were not modified once they were obtained.

For each bridge, Shelby tube samples were taken near the bridge pier within a depth at least equal to two pier widths below the pier base. The boring location was chosen to be as close as practical to the bridge pier considered. The distance between the pier and the boring varied from 2.9 m to 146.3 m (Table 4.2). In all instances, the boring data available was studied in order to infer the relationship between the soil layers at the pier and at the sampling locations. Shelby tube samples to be tested were selected as the most probable representative samples at the bridge pier. These samples were tested in the EFA and yielded erosion functions $\dot{\varepsilon}$ versus τ. Figures 4.15 and 4.16 provide examples of the erosion functions obtained. The samples also were analyzed for common soil properties (Table 4.3).

For each bridge, the USGS gage data was obtained from the USGS Internet site. This data consisted of a record of dis-

TABLE 4.2 Full-scale bridges as case histories

Bridge	Pier Bent No.	Pier Width (m)	Pier Length (m)	Pier Shape	Skew Angle (°)	River Slope	Manning's Coefficient n	Max. Velocity (m/s)	True Duration of Hydrograph (yrs)
Navasota River at SH 7	3	0.36	0.36	Square	5	0.0010	0.035	2.54	41
Navasota River at SH 7	5	0.36	8.53	Square Nose	5	0.0010	0.035	3.82	41
Brazos River at US 90A	3	0.91	8.53	Round Nose	0	0.0011	0.035	4.20	33
San Jacinto River at US 90	43	0.85	0.85	Square	15	0.0012	0.035	3.07	10
Trinity River at FM 787	3	0.91	7.30	Round Nose	25	0.0011	0.035	2.00	17
Trinity River at FM 787	4	0.91	7.30	Round Nose	25	0.0011	0.035	4.06	17
San Marcos River at SH 80	9	0.91	14.2	Round Nose	0	0.0010	0.035	1.89	60
Sims Bayou at SH 35	3	0.76	0.76	Circular	5	0.0001	0.035	0.95	3
Bedias Creek at US 75	26	0.86	0.86	Square	0	0.0005	0.035	2.19	50
Bedias Creek at SH 90	6	0.38	0.38	Square	5	0.0010	0.035	1.54	18

Bridge	Distance between Pier and Boring (m)	Max. Shear Stress (N/m2)	Initial Erosion Rate (mm/hr)	Equivalent Time (hrs)	Predicted Local Scour (m)		Measured Local Scour (m)	Measured Total Scour (m)	Predicted Max. Local Scour (m)
					E-SRICOS	S-SRICOS			
Navasota River at SH 7	6.5	41.46	8.91	368.8	0.76	0.82	0.76	-	1.10
Navasota River at SH 7	16.1	86.53	22.39	616.0	1.24	1.29	1.41	1.80	1.42
Brazos River at US 90A	55.4	85.86	65.26	568.4	2.59	2.54	2.87	4.43	2.72
San Jacinto River at US 90	146.3	49.62	17.44	373.1	1.30	1.66	1.47	3.17	2.14
Trinity River at FM 787	37.8	22.46	50.60	155.1	1.53	1.40	2.17	4.57	1.70
Trinity River at FM 787	78.4	80.93	39.82	544.6	2.26	2.37	2.17	4.57	2.66
San Marcos River at SH 80	57.3	20.30	61.75	158.4	1.07	1.40	1.27	2.66	1.64
Sims Bayou at SH 35	20.0	26.71	2.69	63.0	0.29	0.14	0.05	-	0.95
Bedias Creek at US 75	33.0	16.31	127.44	172.5	1.66	1.61	1.35	2.13	1.74
Bedias Creek at SH 90	2.9	5.92	44.25	102.8	0.70	0.70	0.61	-	0.83

charge Q versus time t over the period of time separating the two river bottom profile observations (Figure 4.9). This discharge hydrograph was transformed into a velocity hydrograph by using the program HEC-RAS (1997) and proceeding as follows. The input to HEC-RAS is the bottom profile of the river cross section (obtained from TxDOT records), the mean longitudinal slope of the river at the bridge site (obtained from topographic maps, Table 4.2), and Manning's roughness coefficient (estimated at 0.035 for all cases after Young et al., 1997). For a given discharge Q, HEC-RAS gives the velocity distribution in the river cross section, including the mean approach velocity v at the selected pier

TABLE 4.3 Soil properties at the bridge sites

Soil Properties	Bridge	Navasota		Brazos	San Jacinto			Sims
	Layer No.	1	2	1, 2	1, 2	3	4	1
	Depth (m)	1.8–2.4	4.9–5.5	13.0–13.7	5.3-6.1	6.9-7.6	7.6-8.4	3.0-3.7
Liquid Limit (%)		27.72	26.42	24.49	22.04	-	37.50	84.16
Plastic Limit (%)		14.29	6.25	9.41	9.09	-	12.71	16.05
Plasticity Index (%)		13.43	20.17	15.08	12.95	-	24.79	68.11
Water Content (%)		19.80	26.60	17.32	151.57	26.88	27.75	25.25
Mean Diameter, D_{50} (mm)		0.125	-	0.265	-	-	-	0.0012
Shear Strength (kPa)		43.10	32.10	45.49	23.94	4.78	21.53	23.00
Unit Weight (kN/m^3)		19.20	18.80	20.20	19.60	16.70	20.80	19.60
% Passing #200 Sieve		26.20	57.70	30.09	50.36	60.71	94.50	99.07

Soil Properties	Bridge	Trinity		San Marcos		Bedias 75		Bedias 90
	Layer No.	1	2	1	2	1	2	1
	Depth (m)	10.7-11.4	13.0-13.7	6.1-6.6	7.0-7.5	6.1-6.9	6.9-7.6	1.5-2.3
Liquid Limit (%)		-	42.24	41.34	40.31	47.86	-	55.08
Plastic Limit (%)		-	8.70	16.67	19.18	13.56	-	15.79
Plasticity Index (%)		-	33.54	24.67	21.13	34.30	-	39.29
Water Content (%)		7.67	22.22	22.00	24.40	18.07	17.50	23.63
Mean Diameter, D_{50} (mm)		6.00	-	-	-	0.048	0.130	0.040
Shear Strength (kPa)		9.57	11.48	27.30	29.67	10.00	32.00	62.00
Unit Weight (kN/m^3)		22.00	22.10	19.60	20.20	20.04	21.30	19.60
% Passing #200 Sieve		11.52	68.40	78.30	73.40	86.81	35.14	91.31

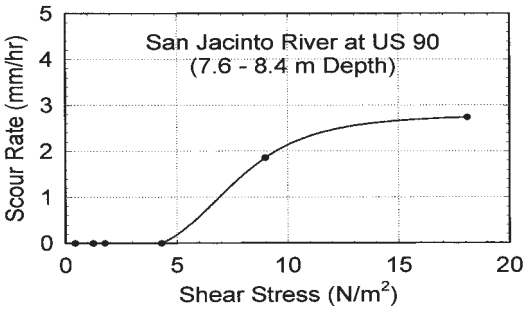

Figure 4.15. Erosion function for San Jacinto River sample (7.6 m to 8.4 m depth).

location. Many runs of HEC-RAS for different values of Q are used to develop a relationship between Q and v. The relationship (regression equation) was then used to transform the Q-t hydrograph into the v-t hydrograph at the selected pier (Figures 4.10, 4.11, and 4.12).

Then, the SRICOS program (Kwak et al., 2001) was used to predict the scour depth z versus time t curve. For each bridge, the input consisted of the $\dot{z}$ versus τ curves (erosion functions) for each layer at the bridge pier (Figures 4.15 and 4.16), the v versus t record (velocity hydrograph) (Figures 4.10, 4.11, and 4.12), the pier diameter B, the viscosity of the water υ and the density of the water ρ_w. The output of the program was the scour depth z versus time t curve for the selected bridge pier (Figures 4.10, 4.11, and 4.12) with the predicted local scour depth corresponding to the last value on the curve.

The measured local scour depth was obtained for each case history by analyzing the two bottom profiles of the river cross-section (Figures 4.17 and 4.18). This analysis was necessary to separate the scour components that added to the total scour at the selected pier. The two components were local scour and contraction/general scour. This separation was required because, at this time, SRICOS only predicts local scour. The contraction/general scour over the period of time separating the two river bottom profiles was calculated as the average scour over the width of the channel. This width was taken as the width corresponding to the mean flow level (Width AB on Figures 4.17 and 4.18). Within this width, the net area

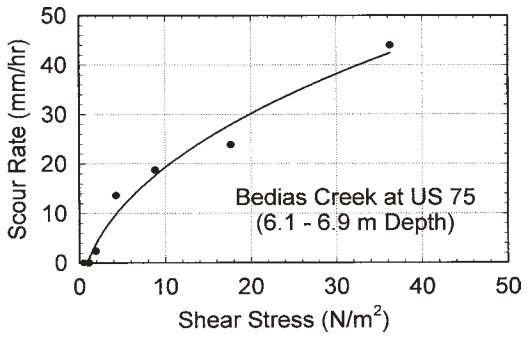

Figure 4.16. Erosion function for Bedias Creek sample (6.1 m to 6.9 m depth).

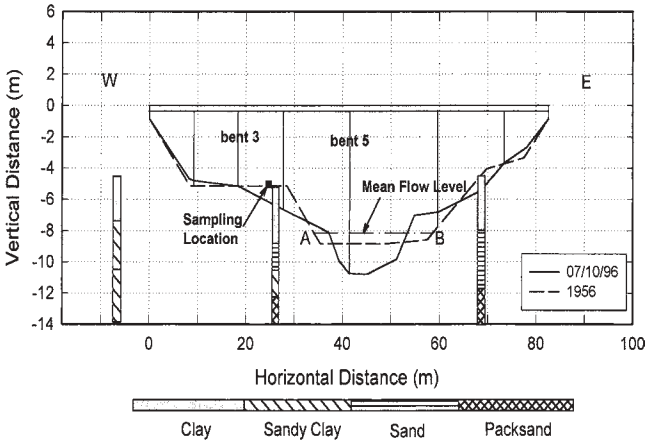

Figure 4.17. Profiles of Navasota River Bridge at SH 7.

between the two profiles was calculated with scour being positive and aggradation being negative. The net area was then divided by the Width AB to obtain an estimate of the mean contraction/general scour. Once this contraction/general scour was obtained, it was subtracted from the total scour at the bridge pier to obtain the local scour at the bridge pier. In some instances there was no need to evaluate the contraction/general scour. This was the case of Bent 3 for the Navasota Bridge (Figure 4.17). In this case, the bent was in the dry (flood plain) at the time of the field visit, and the local scour could be measured directly. Figure 4.19 shows the comparison between E-SRICOS predicted and measured values of local scour at the bridge piers. The precision and accuracy of the method appear reasonably good. Although more than 10 data points may be preferable, note that these 10 data points represent 10 full-scale, real situations.

The S-SRICOS Method was performed next. For each bridge pier, the maximum depth of scour z_{max} was calculated by using Equation 4.2. The velocity used for Equation 4.2 was the maximum velocity, which occurred during the period of time separating the two river bottom profile observations. Then, at each pier, an average erosion function ($\dot{z}$ versus τ

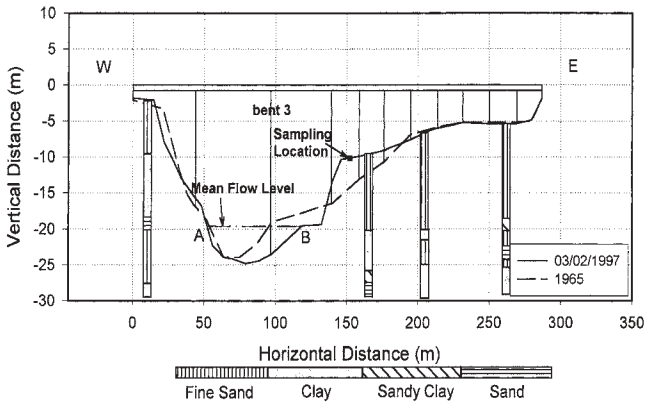

Figure 4.18. Profiles of Brazos River Bridge at US 90A.

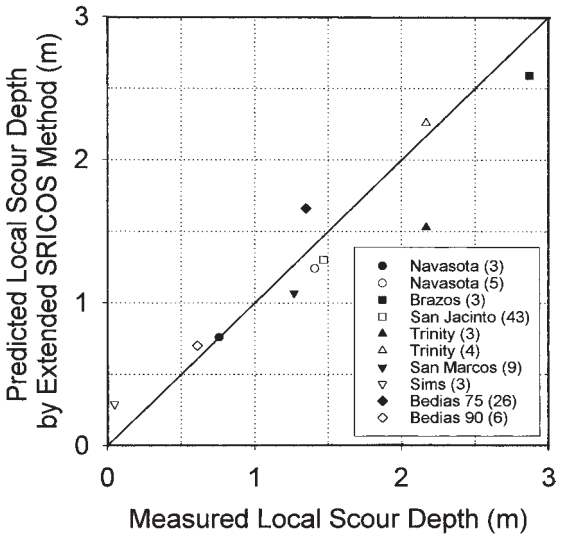

Figure 4.19. Predicted versus measured local scour for the E-SRICOS Method.

curve) within the maximum scour depth was generated. The maximum shear stress τ_{max} around the pier before scour began was calculated using Equation 4.1, assuming that the pier was circular (Table 4.2). The initial scour rate $\dot{z}_i$ was read on the average erosion function for that pier (Table 4.2). The equivalent time t_e was calculated using Equation 4.7, using t_{hydro} equal to the time separating the two river bottom profile observations, and v_{max} equal to the maximum velocity that occurred during t_{hydro} (Table 4.2). Knowing t_e, $\dot{z}_i$, and z_{max}, the scour depth accumulated during the period of t_{hydro} was calculated using Equation 4.3. Figure 4.20 is a comparison of the measured values of local scour and the predicted values using the S-SRICOS Method. The precision and accuracy of the method appear reasonably good. The 10 case histories used to evaluate the S-SRICOS Method are the same cases that were used to develop that method. Therefore, this does not represent an independent evaluation. Details of the prediction process can be found in Kwak et al. (2001).

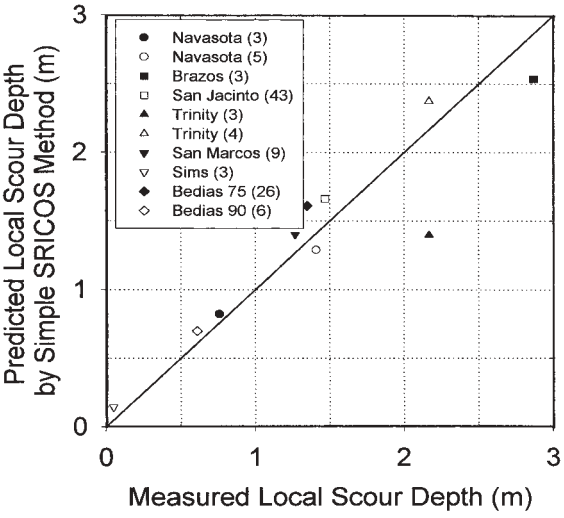

Figure 4.20. Predicted versus measured local scour for the S-SRICOS Method.

E-SRICOS and S-SRICOS described above do not include correction factors for pier shape, skew angle between the flow direction and the pier main axis, shallow water depth effects, and multiple pier effect. Chapter 5 will show how to calculate those factors.

4.10 CONCLUSIONS

The SRICOS Method predicts the depth of the local scour hole versus time curve around a bridge pier in a river for a given velocity hydrograph and for a layered soil system (Figure 4.21). The method described in this chapter is limited to cylindrical piers and water depths larger than two times the pier width. The prediction process makes use of a flood accumulation principle and a layer equivalency principle. These are incorporated in the SRICOS computer program to generate the scour versus time curve. A simplified version of this method is also described and only requires hand calculations. The simplified method can be used for preliminary design purposes. Both methods were evaluated by comparing predicted scour depths and measured scour depths for ten piers at eight full-scale bridges. The precision and accuracy of both methods appear good.

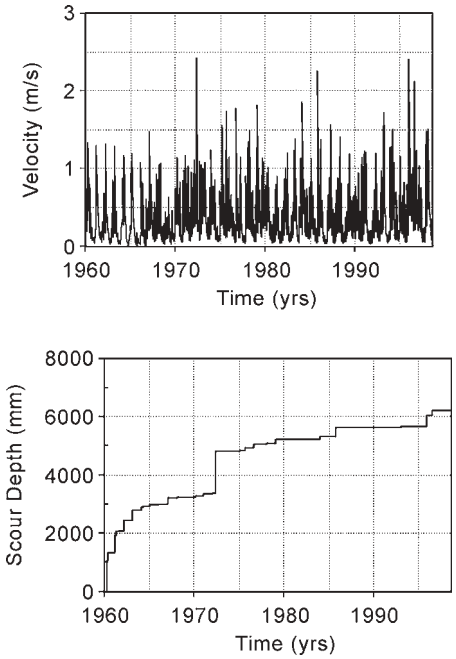

Figure 4.21. Velocity hydrograph and predicted scour depth versus time curve for pier 1E of the existing Woodrow Wilson Bridge on the Potomac River in Washington D.C.

CHAPTER 5

THE SRICOS-EFA METHOD FOR MAXIMUM SCOUR DEPTH AT COMPLEX PIERS

5.1 EXISTING KNOWLEDGE

An extensive review of the literature on the topic of pier scour in cohesive soils led to very few publications. Studies related to the maximum scour depth included those of Hosny (1995), Ivarson (1998), and Molinas et al. (1999). Hosny ran a large number of flume tests on prepared samples of clay and sand mixtures. He recommended multiplying factors to include in the HEC-18 equation for the maximum scour depth in cohesionless soils. These factors are based on simple soil properties and lead to maximum scour depths smaller than the cohesionless soil values by 10% to 40%. Ivarson (1998) developed a modification factor K_4 for the HEC-18 equation for maximum scour depth in cohesionless soils. The K_4 factor is a multiplier in the HEC-18 equation and makes use of the undrained shear strength of the cohesive soil. Molinas et al. (1999) presented a modification of the Hosny (1995) factors. Studies related to numerical simulations were more numerous.

5.2 GENERAL

Chapter 4 described the SRICOS method for cylindrical piers in deep water. This chapter deals with piers that can be rectangular, square, or cylindrical; are attacked by the flow at a non-zero angle between the flow direction and the main axis of the pier; and are in shallow water. The influence of pier spacing also is discussed. Figure 5.1 shows the definition of the parameters involved with these influencing factors. The approach consisted of using the solution for the case of the cylindrical pier in deep water:

$$Z_{max}\,(\text{mm}) = 0.18 R_e^{\,0.635} \tag{5.1}$$

and developing correction factors to include the effect of the various situations deviating from that case. Since the case of the cylindrical pier in deep water was developed on the basis of two fundamental equations (i.e., maximum scour depth and initial maximum shear stress), two sets of correction factors had to be developed. The correction factors for the maximum scour depth were developed on the basis of flume tests; the correction factors for the initial maximum shear stress were developed on the basis of numerical simulations.

5.3 FLUMES AND SCOUR MODELS

The in-floor concrete flume, which is 1.5 m wide, 30.48 m long, and 3.48 m deep, was used to conduct the complex pier scour tests. The wooden flume, which is 0.45 m wide, 36 m long, and 1.22 m deep, was used for the contraction scour tests. These two flumes form a closed system (Figure 5.2) in which the water is recirculated without any fresh water being added.

False bottoms were designed to make sure that the start and end transitions would not affect the velocity distribution in the test area. For the 1.5-m-wide flume, the slopes of the ramps at the two ends of the false bottom are 1:3 (vertical to horizontal) to guarantee a smooth transition. The distance between the two soil tanks is 7.6 m to make sure there is no interaction between them. Trial tests were conducted before starting the scour tests, and the velocity distributions were measured along the centerline of the channel to confirm the validity of the design. In the 1.5-m-wide flume, the soil tank is 0.6 m deep and 1.5 m long for the front tank and 0.6 m deep and 1.2 m long for the rear tank. The false bottom is built with plastic plates and supported by aluminum frames.

The false bottom in the 0.45-m-wide flume was designed for the contraction scour tests. A smooth transition between the uncontracted and contracted channels was constructed. The soil tank is 2.0 m long and 0.3 m deep to provide enough space for both the long contraction flow and the contraction scour hole. This false bottom is made of plywood.

Two types of pier models were used in the complex pier scour tests as shown in Figure 5.3. The cylindrical piers were cut from PVC pipes with three different diameters: 273 mm, 160 mm, and 61 mm. The rectangular piers were made of plywood with the same width (61 mm) and different lengths: 61 mm, 122 mm, 244 mm, and so on. For piers with projection Width B' larger than 160 mm, strutted frames were needed to fix the piers so they would neither sway nor be flushed away during scouring. The abutment models were all made of plywood and are shown in Figure 5.4, which also shows the transition inlets for the contraction scour tests.

5.4 MEASURING EQUIPMENT

The Acoustic Doppler Velocimeter (ADV), as shown in Figure 5.5, uses acoustic techniques to measure the velocity in a remotely sensed volume so that the measured flow is

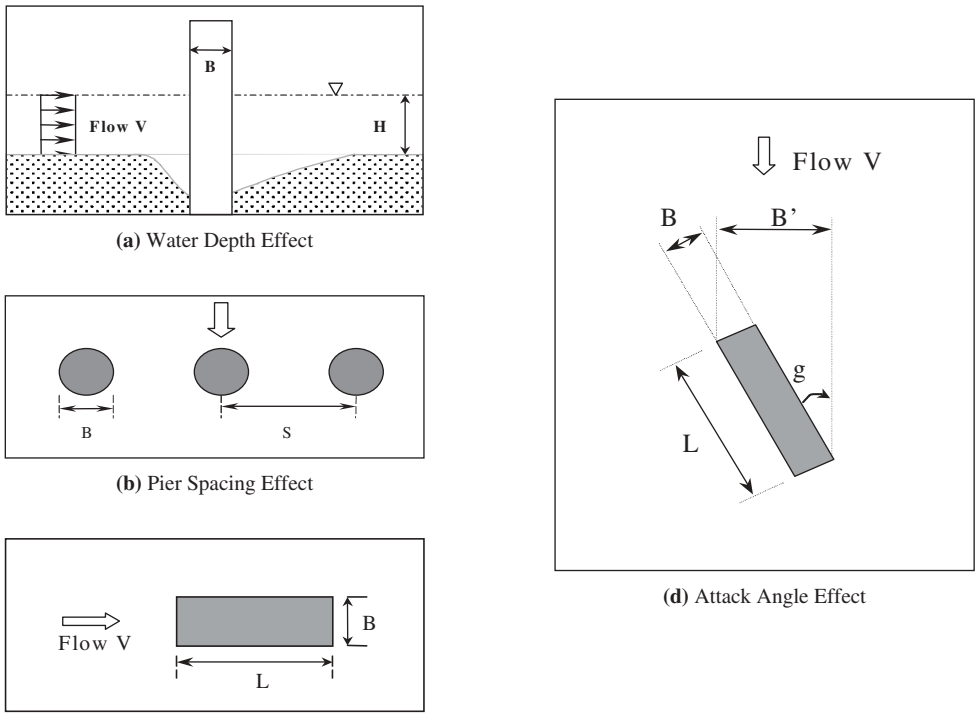

(a) Water Depth Effect

(b) Pier Spacing Effect

(c) Pier Shape Effect

(d) Attack Angle Effect

Figure 5.1. Parameter definition for complex pier scour.

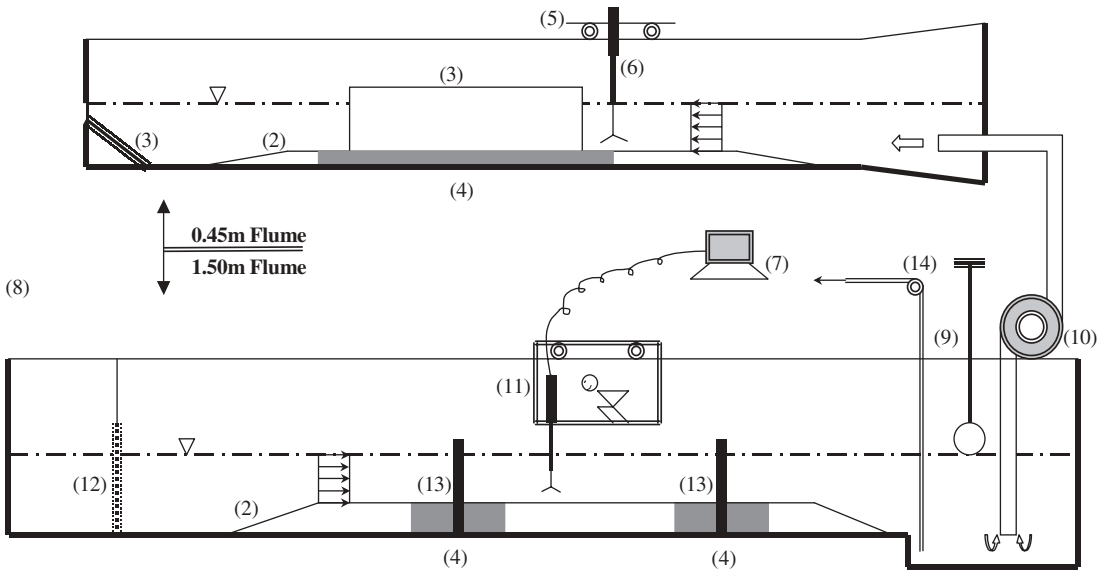

(1) Tail Gate	(4) Soil Tank	(7) Computer	(10) Pumps	(13) Piers
(2) False Bottom	(5) Carriage	(8) Water Fall	(11) Measuring Cage	(14) Mini Pump
(3) Contraction Abutments	(6) ADV and Point Gage	(9) Switch	(12) Screen Wire	

Figure 5.2. Diagram of the flume system (not to scale).

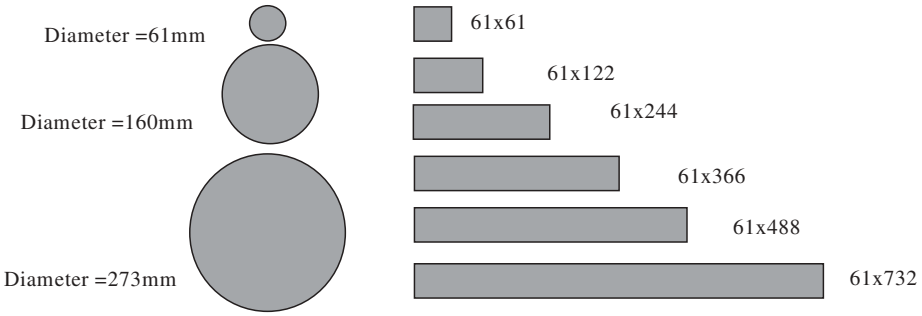

Figure 5.3. Pier models used in the complex pier scour tests.

undisturbed by the presence of the probe. An ADV with a velocity range of ±2.5 m/s and a resolution of 0.1 mm/s was used to measure the velocity during the tests. The primary use of the ADV was to measure the vertical velocity profile along the water depth around piers and contractions. The upstream mean depth velocity was the basic velocity recorded for the pier tests. For the contraction tests, the ADV was used to measure the velocity distribution along the centerline of the contracted channel at certain water depths before the scour started and after the scour stopped. In some tests, more extensive velocity measurements were conducted at specific locations. These included the corners of contraction abutments and rectangular piers.

A point gage with a new design was used in this study. Without interrupting the experiments, it was used to measure the water surface elevation, the water depth, and the change in scour depth. The point gage is designed based on the fact that air, water, and soil have different electrical conductivity. The point gage system forms a closed circuit with one node in the soil or water and the other one in the air. Once the point gage, which contains a needle attached to a vertical ruler, touches the interface between water and air or water and soil, there is a sudden conductivity change that can be read easily on a voltmeter. When the water is dirty, the maximum scour location can be searched point by point using the point gage.

As shown in Figure 5.2, the point gage and ADV are installed in a hanging measurement cage riding on a carriage that moves along the longitudinal direction of the flume. In the flume tests, it was found that the presence of piers or contraction abutments had almost no influence on the flow at a distance of one channel width upstream of the obstacle. Therefore, the velocity and water depth were determined at this location for each test. In addition, a digital camera was used to record important phenomena during the tests.

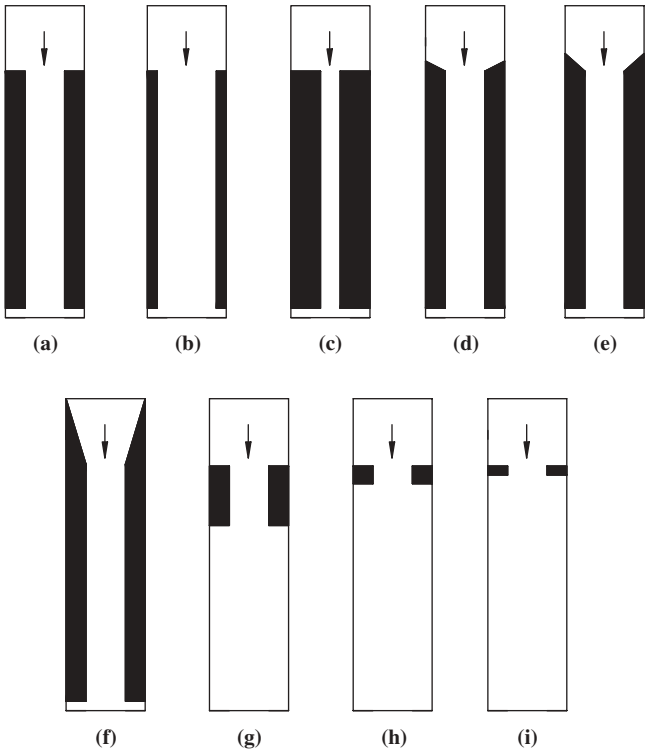

(a, b, c-Contraction Width; a, d, e, f-transition angle, a, g, h, i-contraction length)

Figure 5.4. Abutment models for contraction scour tests.

5.5 SOILS AND SOIL BED PREPARATION

A Porcelain clay was used as the primary soil; for comparison purposes, sands also were used in several tests. The predominant mineral of this commercially available Porcelain clay is Kaolinite. Geotechnical tests were conducted according to ASTM standards. The geotechnical properties of the Porcelain clay determined at two different times are summarized in Table 5.1. Vane shear tests were conducted at three different locations around the future scour hole after the soil

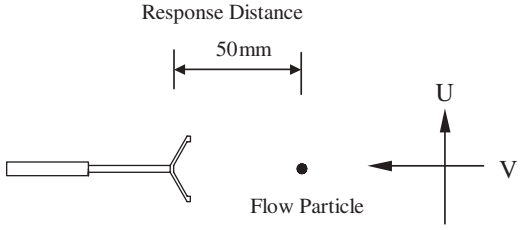

Figure 5.5. Diagram of the ADV.

TABLE 5.1 Geotechnical properties of the Porcelain clay

	Property	Test 1	Test 2
1	Liquid Limit, %	40.23	37.7
2	Plastic Limit, %	19.17	14.4
3	Plastic Index (PI), %	21.06	23.3
4	Bulk Unit Weight (KN/m^3)	19.65	24.99
5	Water Content, %	27.35	30.5
6	Shear Strength, *KPa*	10.7	18.1

bed was prepared, but before the experiment started; the average value is shown in the Table. The erosion properties of the Porcelain were tested by Cao (2001) in the EFA. Two samples were tested separately using tap water. The erosion rate versus shear stress curve is shown in Figure 5.6.

Gudavalli (1997) used three types of clays for his experiments: Porcelain, Armstone, and Bentonite. The properties of these clays are presented here because Gudavalli's tests were the basis of the original SRICOS Method and because these tests are used in this study as well. The geotechnical properties of these soils were measured according to ASTM standards and are given in Table 5.2. The erosion properties of the Porcelain clay were measured in the 0.45-m-wide flume. The bed shear stress was varied from 0.118 Pa to 7.92 Pa by changing the flow velocity. The water depth was maintained constant during the experiments. Each test was conducted for a few hours. The bed shear stress was computed by Prandtl's equation for the velocity versus depth profile obtained by ADV measurements very close to the soil bed. These experiments amounted to running a large-scale EFA test. The relationship between erosion rate and shear stress is shown in Figure 5.7.

The Porcelain clay was delivered in blocks of 250 mm × 180 mm × 180 mm. Each block was in a sealed bag. The clay was installed block by block in the soil tank, as shown in Figure 5.8. After the completion of one layer, kneading with a 20-lb concrete block was used to minimize the voids and holes between blocks. The next layer was placed on top of the first one, and so on. Once the soil tank was full, the soil surface was leveled by using a straight-edged spatula.

After each test, the excess water was pumped out, a zone of clay was removed around the scour hole until undisturbed clay was reached, and fresh Porcelain clay was placed in the excavated portion. It was critical to remove all the soft film and any excess water on the old soil surface; otherwise, the old soil and new soil would not stick tightly together and the new soil could be flushed away in lumps. This requirement was particularly important for the contraction scour tests.

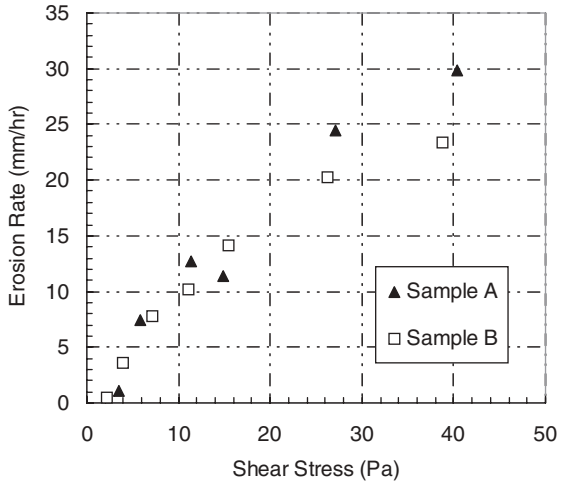

Figure 5.6. Erosion function for the Porcelain clay.

5.6 FLUME TESTS: PROCEDURE AND MEASUREMENT

Complex pier scour tests were conducted in the 1.5-m-wide flume and all of the tests were done according to the following procedure:

1. Prepare soil bed and pier installation;
2. Perform vane shear measurements;
3. Take initial readings of the soil surface elevation around the piers;
4. Install the ADV;
5. Perform calculations of water volume in the flume and pump rate to get the expected water depth and velocity;
6. Take measurements of the velocity profile and water surface elevation;

TABLE 5.2 Properties of the soils used in Gudavalli's research (Gudavalli, 1997)

S. No.	Property	Porcelain	Armstone	Bentonite
1	Liquid Limit, %	34.40	44.20	67.00
2	Plastic Limit, %	20.25	18.39	27.22
3	Plastic Index (PI), %	14.15	25.81	39.78
4	Specific Gravity	2.61	2.59	2.55
5	Water Content, %	28.51	26.18	39.28
6	Sand Content, %	------	25(grog)	------
7	Clay Content, %	100	75	100
8	Shear Strength, *KPa*	12.51	16.57	39.56
9	CEC, (meg/100g)	8.3	10.0	16.1
10	SAR	5.0	2.0	21.0
11	PH	6.0	5.2	8.5
12	Electrical Conductivity (mmhos/cm)	1.2	1.1	1.1
13	Bulk Unit Weight (KN/m^3)	18.0	17.89	17.45

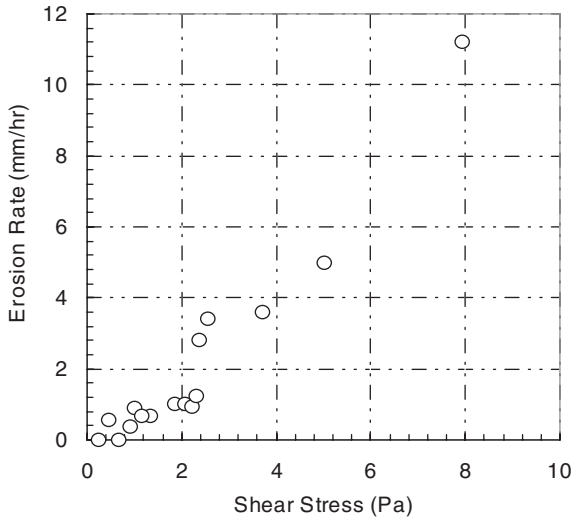

Figure 5.7. Erosion function for Gudavalli's Porcelain clay.

7. Take measurements of the scour depth at regular time intervals; and
8. Empty water, record shape of scour hole, and finish the test.

For each test, the primary measurements were flow velocity, water depth, scour depth, and time. Water depth and flow velocity were determined in the middle of the channel, 1.5 m upstream of the piers. The depth average velocity was calculated from the measured vertical velocity profile and was used as one of the major parameters in the data analysis. The flow velocity was kept constant throughout the experiment. For the measurements of scour depth increment, the point gage was moved around the pier to find the location of maximum scour.

Figure 5.8. Placement of the clay in the soil tank.

5.7 SHALLOW WATER EFFECT: FLUME TEST RESULTS

It appears that when the water depth exceeds about two times the pier width, the maximum scour depth is practically independent of the water depth. When the water depth becomes shallower than that, there is a reduction in the maximum scour depth. This is attributed to the fact that as the depth of the scour hole increases, the water loses its eroding energy faster in shallow waters than in deep waters. While extensive studies have been carried out on shallow water effects in sands, corresponding studies in clays are nonexistent. Gudavalli's flume tests indicate that in cohesive soils the flow depth has no clear influence on the scour depth when $H/B \geq 1.6$ where H is the water depth and B the pier diameter. In this study, a series of pier scour tests with water depths ranging from $H/B = 0.2$ to $H/B = 2.5$ were conducted. The cylindrical piers had diameters equal to 273 mm and 160 mm and were installed in one of the 1.2 m × 1.5 m × 0.3 m soil tanks filled with Porcelain clay.

The test parameters are presented in Table 5.3 and the measured curves of scour depth $z(t)$ versus time t are plotted in Figure 5.9 for the two different pier sizes. The flume tests were stopped after a time averaging about 5 days, and then a hyperbola was fitted to the scour depth versus time curve (Briaud et al., 1999, 2001). This technique gave an initial scour rate, $\dot{z}_i$, (initial slope of the hyperbola) and a maximum scour depth, Z_{max}, (asymptotic value). The values of the maximum scour depth, Z_{max}, and initial scour rate, $\dot{z}_i$, are shown in Table 5.3.

In the case of very shallow water tests, it was observed that noticeable surface rolling, formed due to the roughness of the streambed, would probably affect the scour depth, as mentioned by Ettema (1980). In addition, the velocity in this case becomes more difficult to measure and control due to the limitation of the response distance of the ADV.

5.8 SHALLOW WATER EFFECT ON MAXIMUM PIER SCOUR DEPTH

One way to present the data is to plot the relative scour depth Z_{max}/B versus relative flow depth H/B (Figure 5.10). Figure 5.10 indicates that in clay, much like in sand, the relative scour depth, Z_{max}/B, increases with the relative water depth, H/B, until a limiting H/B value is reached. The shallow water correction factor, K_w, is defined as the ratio of the maximum scour depth under shallow water flow to the maximum scour depth under a reference condition where the water depth has no noticeable influence on the maximum scour depth. In this study, the scour depth under the deepest relative water depth, $H/B = 2.5$, was selected as the reference. Therefore, the average value of Z_{max} for Tests Sh-1 and Sh-8 in Table 5.3 was called Z_{max}(deep) and was used to normalize the values of Z_{max}. Figure 5.11 shows the values of $K_w = Z_{max}/Z_{max}$(deep) as a function of H/B.

TABLE 5.3 Parameters and results for shallow water cases of pier scour

Test No.	H (mm)	B (mm)	V (m/s)	H/B	Exp. Duration (h)	$\dot{z}_i$ (mm/hr)	Z_{max} (mm)
Sh-1*	683.00	273.00	0.30	2.502	-----	----	112.94
Sh-2	546.00	273.00	0.30	2.000	515.75	1.06	129.62
Sh-3	258.00	273.00	0.30	0.945	262.33	1.57	79.37
Sh-4	137.00	273.00	0.30	0.502	237.42	1.39	57.80
Sh-5	60.00	273.00	0.30	0.220	164.08	1.71	81.30
Sh-6	60.00	273.00	0.30	0.220	111.03	4.49	61.35
Sh-7	25.80	273.00	0.30	0.095	30.50	38.91	35.59
Sh-8	400.00	160.00	0.40	2.500	191.33	1.50	76.92
Sh-9	320.00	160.00	0.40	2.000	129.67	1.82	109.67
Sh-10	170.00	160.00	0.40	1.063	117.17	1.98	77.73
Sh-11	85.00	160.00	0.40	0.531	64.50	2.62	53.48

*: The measured data for test Sh-1 is lost due to the malfunction of computer and Z_{max} is saved in previous summaries.

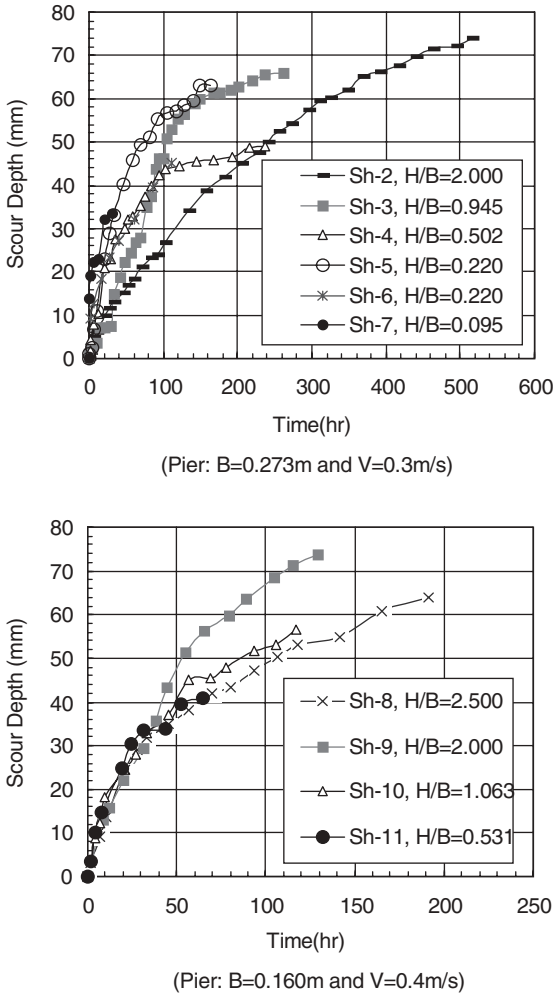

Figure 5.9. Flume test results for the shallow water cases.

In Figure 5.11, the correction factor K_w obtained in the current study on clay is compared to the correction factors recommended for cohesionless soils by Melville and Coleman (1999) and Johnson (1999). Johnson's correction factor depends on both pier size and velocity, so the label "Johnson 0.273/0.3, Equ(3.6A)" in the figure represents the correction factor for the condition of $B = 0.273$ m and $V = 0.3$ m/s following Johnson's equation. Because Johnson did not provide an equation for very shallow flow, a straight line is used to connect the origin to the shallowest end of the Johnson curves in Figure 5.11. Note also that Johnson's K_w factor is a correction factor for the HEC-18 equation while that equation already includes a water depth influence so a combined

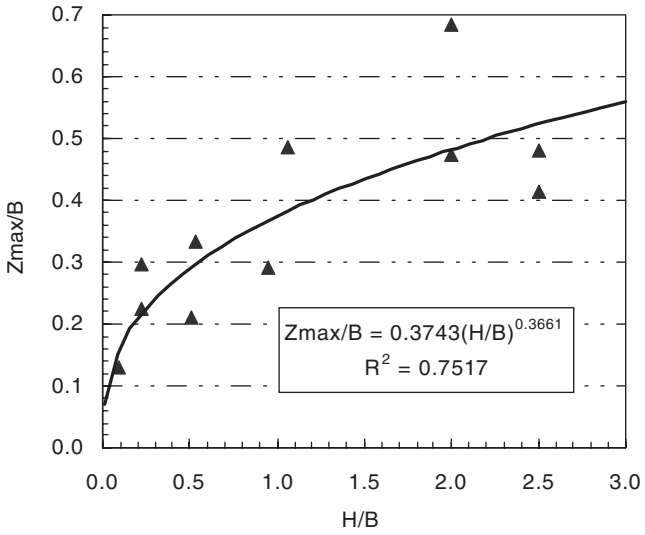

Figure 5.10. Influence of shallow water depth on maximum pier scour depth.

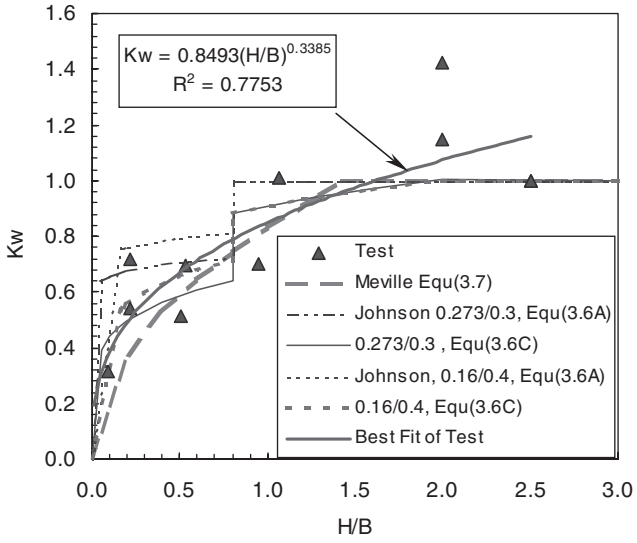

Figure 5.11. Correction factor for shallow water effect on maximum pier scour depth.

correction factor can be derived. These values correspond to the curves labeled "0.273/0.3, Equ(3.6C)" and "0.160/0.4, Equ(3.6C)" with $H/B = 2.5$ as the reference cases for $B = 0.273$ m, $V = 0.3$ m/s and $B = 0.160$, $V = 0.4$ m/s, respectively. Figure 5.11 shows that the shallow water effect factor obtained in this study is close to the correction factors for cohesionless soils.

By regression, the expression for the proposed cohesive soil correction factor K_w is

$$K_w = \begin{cases} 0.85\left(\dfrac{H}{B}\right)^{0.34} & H/B < 1.62 \\ 1 & H/B < 1.62 \end{cases} \tag{5.2}$$

5.9 SHALLOW WATER EFFECT ON INITIAL SHEAR STRESS

For a given scour depth versus time curve, the initial scour rate is the initial slope of that curve. It can be obtained by fitting a hyperbola to the data. These are the rates shown in Table 5.3. The two groups of initial scour rates are plotted in Figure 5.12. Test Sh-8 gave a much higher initial scour rate than the other tests (11 mm/hr), so the large picture does not show its value, but the inset one does. The inset indicates that the initial scour rate tends to increase as the water depth decreases and that the increase becomes particularly significant when $H/B < 0.5$. The figure also shows that the scour rates for the larger pier ($B = 0.273$ m) are smaller than the rates for the smaller pier ($B = 0.160$ m). Since the initial scour rate is directly tied to the initial shear stress through the erosion function, it can be stated that the initial shear stress increases when the water depth decreases and decreases when the pier diameter increases. These trends are the opposite of the trends for the maximum scour depth. This means that a pier in shallow water subjected to a constant velocity will scour faster at the beginning but will end up scouring to a shallower maximum depth than the same pier in deep water (Figure 5.13).

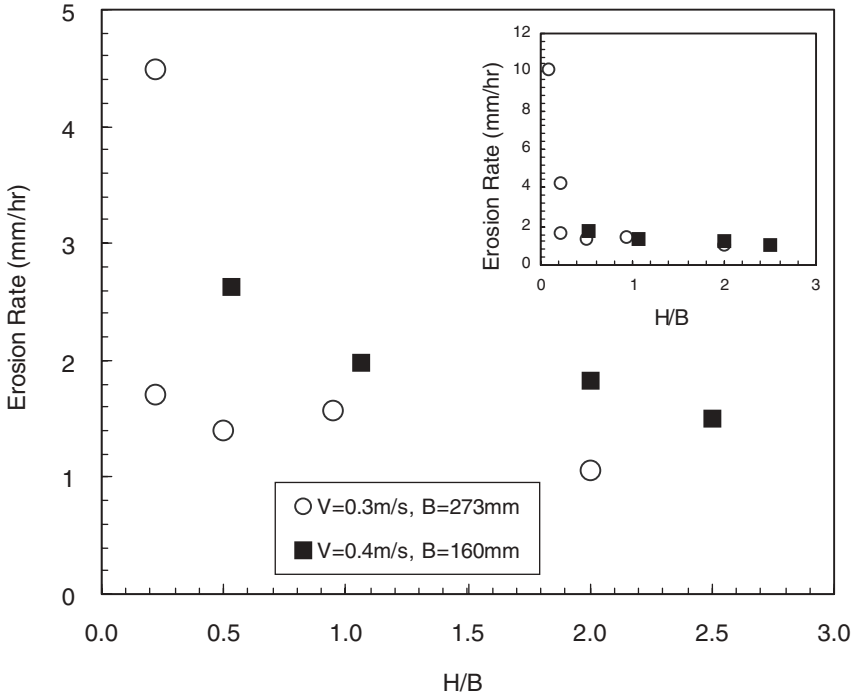

Figure 5.12. Initial scour rate as a function of water depth.

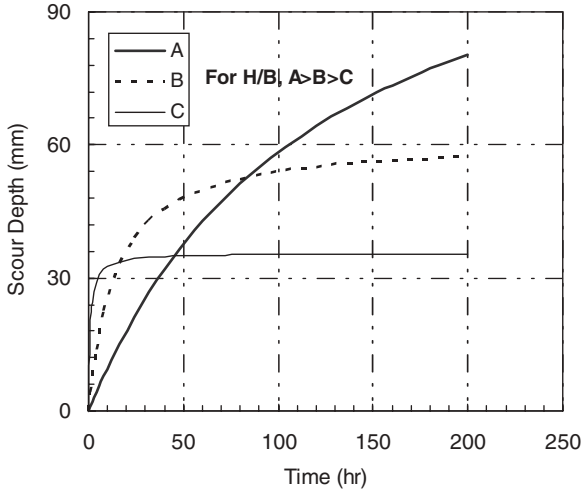

Figure 5.13. Comparison between scour in shallow and deep waters.

5.10 PIER SPACING EFFECT: FLUME TEST RESULTS

The pier spacing effect refers to the interaction between piers when they are closely spaced. In this case, the pier scour depth could be increased due to two reasons: (1) the interaction and enhancement of horseshoe vortices at the base of the pier, or (2) the acceleration of the flow due to the contraction caused by the piers. The pier spacing effect can be examined for two types of pier installation: (1) in a matrix and (2) in a line. The current study dealt with the effect of pier spacing when cylindrical piers are uniformly spaced and installed in a single row perpendicular to the flow.

For these flume tests, the piers were 0.160 m in diameter. The center-to-center distance, *C*, was called the pier spacing. A distance equal to the space of one pier was kept between the outmost pier and the wall of the flume. Due to the flume width, the maximum number of piers that could be installed was four and the corresponding minimum spacing ratio was $C/B = 1.88$. The maximum pier spacing ratio was $C/B = 4.69$ for a single pier. Raudkivi (1991) commented that when the pier spacing is larger than four, the group pier effect is negligible.

The parameters and results for the four pier spacing tests are summarized in Table 5.4. The initial scour rate and maximum scour depth were calculated in the same way as the shallow water cases. The measured scour curves are plotted in Figure 5.14. The maximum scour depth may happen either around the pier or at some intermediate location; its location was determined with the point gage system.

TABLE 5.4 Parameters and results for pier spacing flume tests

Test No.	H (mm)	B (mm)	V (m/s)	C/B	Time Lasting (h)	$\dot{z}_i$ (mm/hr)	Z_{max} (mm)
Gr-1	375.00	160.00	0.33	(1-pier) 4.69	165.00	2.33	165.56
Gr-2	375.00	160.00	0.33	(2-pier) 3.13	122.50	2.83	175.44
Gr-3	375.00	160.00	0.33	(3-pier) 2.34	144.08	5.24	204.08
Gr-4	375.00	160.00	0.33	(4-pier) 1.88	129.83	4.76	250.00

5.11 PIER SPACING EFFECT ON MAXIMUM SCOUR DEPTH

The pier spacing effect on the maximum pier scour depth can be incorporated in the general equation by using a correction factor, K_{sp}, equal to the ratio of the maximum scour depth of the line of piers over the maximum scour depth of the isolated pier. In this study, the single-pier case was the case of the single pier in the 1.5-m-wide flume. This case corresponds to a *C*/*B* ratio of 4.69 as mentioned previously. Figure 5.15 shows the correction factor. The difference of maximum scour depth between the single pier and a line of two piers was observed to be quite small, which gives some confidence in the use of the *C*/*B* ratio of 4.69 as the single-pier case.

In Figure 5.15, the pier spacing effect obtained in this study for a Porcelain clay is compared with existing recommendations for cohesionless soils. Elliot and Baker (1985) used oblong piers (46 mm wide and 150 mm long) in their tests on groups of piers. Their pier spacing effect was more severe than the others, possibly due to the aspect ratio of the piers used. Salim and Jones (1998) conducted flume tests on cylindrical and square piers installed in a matrix in the middle of a channel. Each pier in this group configuration was more affected by other piers than in the case of a single line of piers. This may be the reason why Jones' correction factor is more severe than the one found in this study. The test conditions for Raudkivi's experiments (1991) are very similar to the current study, with the following exceptions: only two cylindrical piers were installed in the middle of the flume and the soil was sand. In Raudkivi's tests, the pier spacing effect was examined by varying the distance between the two piers.

Several attempts were made to find a prediction equation. First, the single equivalent pier concept proposed by Salim and

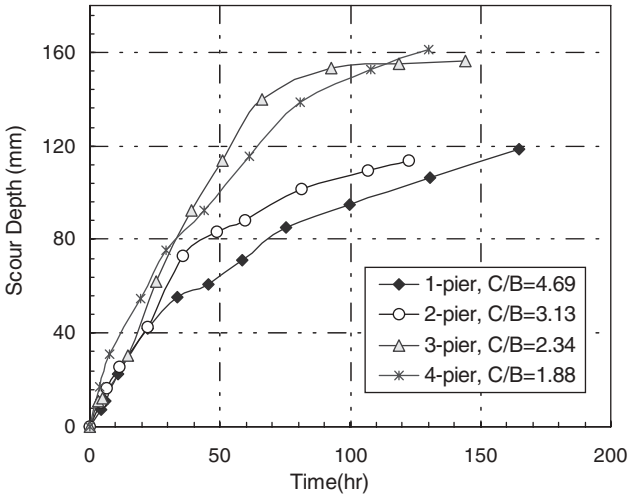

Figure 5.14. Scour depth versus time for the pier spacing cases.

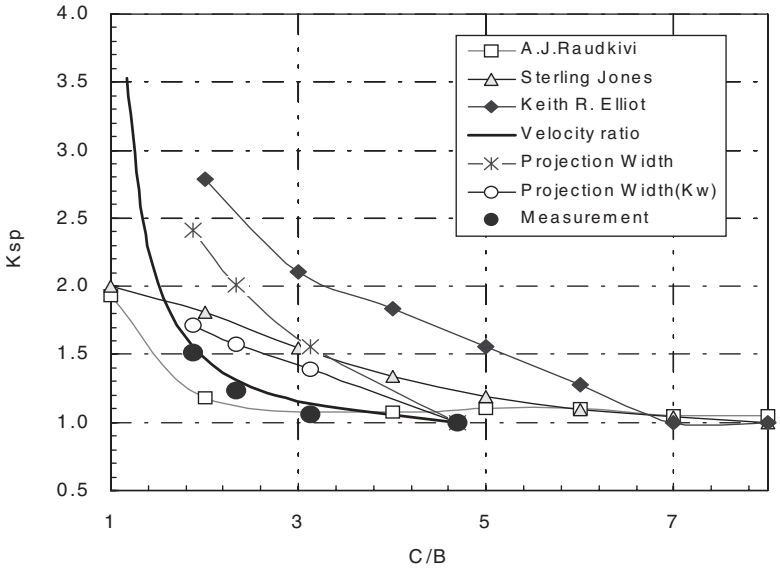

Figure 5.15. Correction factor for pier spacing effect.

Jones (1998) was used by adding the widths of all of the piers in the row. This was done by using Equation 5.1 with the equivalent width. The K_{sp} curve obtained in such a way is shown under the label "Projection Width" in Figure 5.15. That curve does not fit the measured data well (too conservative). Even after accounting for the water depth effect, the K_{sp} curve is still too high as shown under the label "Projection Width (K_w)" in Figure 5.15. This indicates that the single equivalent pier model would overestimate the pier spacing effect at least for piers installed in a row. It was found that the ratio of the width of the channel without the piers over the unobstructed width of the channel with the piers fit the data quite well. This equation is shown in Figure 5.15 under the label "Velocity Ratio" because the velocity also can be estimated through that ratio. For example, if the flume width is $B1$, the approaching velocity V_1, and there are n piers installed in a row with same diameter B, then the velocity with n piers can be estimated by: $V_n = (V1B1)/(B1 - nB)$, and the velocity ratio is: $Vn/V1 = B1/(B1 - nB)$. The equation proposed for K_{sp} is:

$$K_{sp} = \frac{B1}{(B1 - nB)} \tag{5.3}$$

5.12 PIER SPACING EFFECT ON INITIAL SCOUR RATE

The initial scour rate for the pier spacing flume tests is presented in Table 5.4 and plotted in Figure 5.16 where C is the center-to-center distance and B the pier width. It shows that the initial scour rate tends to increase as the piers become more closely spaced. In summary, both the maximum pier scour depth and the initial scour rate will increase as the piers become more closely spaced. This means that curves such as those presented in Figure 5.17 can be expected.

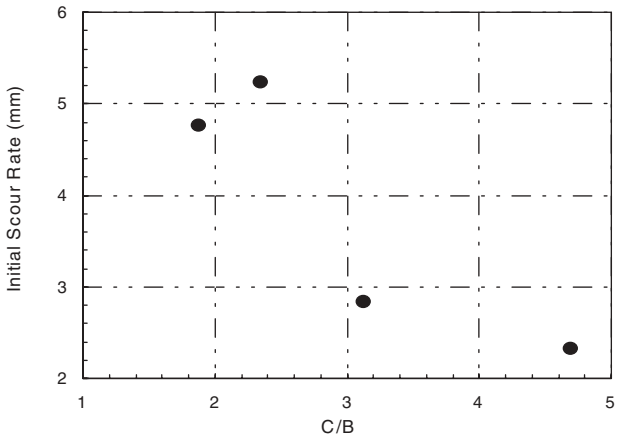

Figure 5.16. Initial scour rate for the group pier tests.

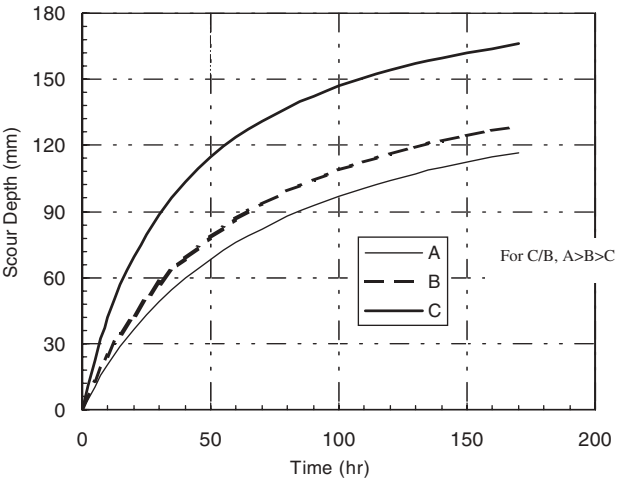

Figure 5.17. Scour curves for groups of piers in a line.

5.13 PIER SHAPE EFFECT: FLUME TEST RESULTS

The shape of a bridge pier can strongly affect the flow pattern around it. In this study, only rectangular piers were considered. Bridge piers are most often installed with the longer side parallel to the major flow direction; therefore, the length over width ratio, *L*/*B*, is kept greater than one for all piers in this study. The rectangular pier was installed with a 0-degree attack angle in the middle of the soil tank. Major scour always occurred around the four corners of the rectangular pier but only the time history of the maximum scour depth was used in the analysis. The shapes of the scour holes for different rectangular piers were recorded and compared. In addition, cylindrical piers with a diameter equal to the width of the rectangular pier were used as the reference case. Parameters and major results for the flume tests for pier shape effect are summarized in Table 5.5. Again, the maximum scour depth and the initial scour rate were calculated in the same way as in the case of the other flume tests. The scour depth development curves are plotted in Figure 5.18.

5.14 PIER SHAPE EFFECT ON MAXIMUM SCOUR DEPTH

The cylindrical pier test, SP-1, was chosen as the reference case. The correction factor, K_{sp}, is the ratio of the maximum scour depth for a given shape over the maximum scour depth for the cylinder (Figure 5.19). The results on Figure 5.19 indicate that there is no noticeable effect on scour depth due to the pier shape. Indeed, the correction factor varies from 1:1 to 1:12. This conclusion is consistent with the correction factor for sand listed in HEC-18. Therefore, it is concluded that a pier shape correction factor of 1.1 is a good approximation for the maximum scour depth around rectangular piers in both clay and sand as long as the *L*/*B* ratio is larger than 1. The case of the *L*/*B* ratio smaller than 1 was not covered in this research project.

5.15 PIER SHAPE EFFECT ON INITIAL SCOUR RATE

The initial scour rate for the flume tests on the rectangular piers having the same width but different lengths are compared in Figure 5.20. As can be seen, the rectangular piers

TABLE 5.5 Parameters and results for pier shape effect flume tests

Test No.	H (mm)	B (mm)	V (m/s)	L/B	Time Lasting (h)	$\dot{z}_i$ (mm/hr)	Zmax (mm)
Sp-1	375.00	61.00	0.33	Circular	151.92	1.45	68.03
Sp-2	375.00	61.00	0.33	1:1	129.50	5.00	73.53
Sp-3	375.00	61.00	0.33	4:1	124.42	2.05	72.99
Sp-4	375.00	61.00	0.33	8:1	131.58	1.93	74.63
Sp-5	375.00	61.00	0.33	12:1	131.50	1.84	75.19

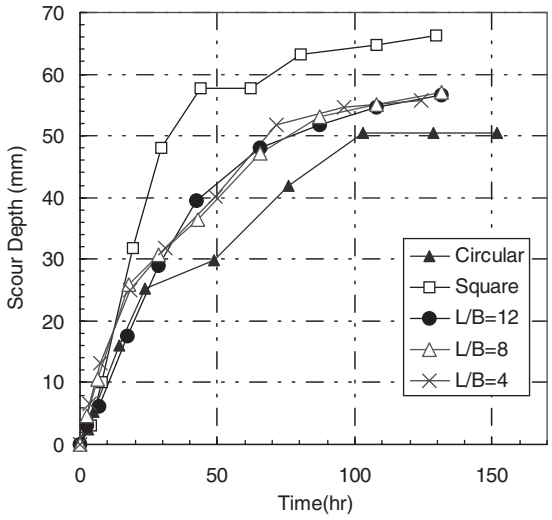

Figure 5.18. Scour depth versus time curves for pier shape effect tests.

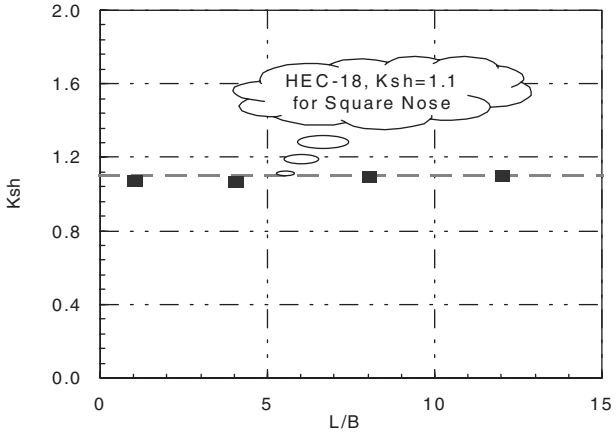

Figure 5.19. Correction factor for pier shape effect.

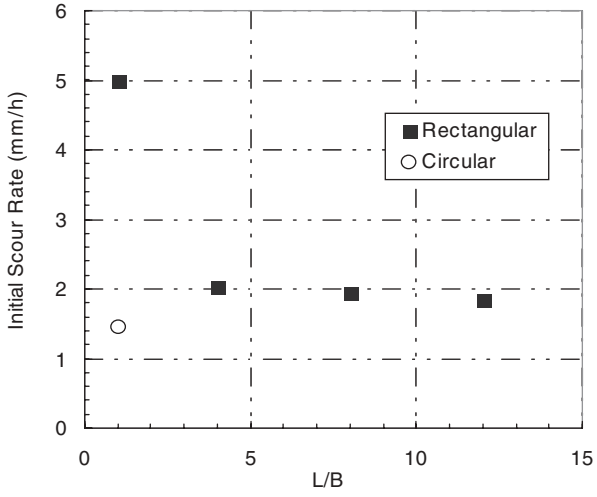

Figure 5.20. Initial scour rates for the shape effect flume tests.

consistently have larger initial scour rates than the cylindrical pier. The maximum value occurs for the square pier and the difference in rate decreases with the aspect ratio. Dietz (1972) found that the correction factor K_{sh} decreased from 1.5 to 1.1 when the *L*/*B* ratio increased from 1:1 to 5.

5.16 PIER SHAPE EFFECT ON PIER HOLE SHAPES

The shape of the scour holes in Tests Sh-2, Sh-4, and Sh-5 are roughly reproduced in Figure 5.21. In that figure, the shaded areas indicate the contours of the hole and the darker areas represent the deeper scour zones. The relative size of the scour hole produced by the square pier was observed to be much larger than in the other cases. Also, in the case of the square pier, the scour hole surrounds the entire pier. For piers with aspect ratios *L*/*B* greater than 4, the scour hole forms around the front face and the scour hole and scour behind the pier is negligible. Figure 5.22 summarizes these observations.

5.17 ATTACK ANGLE EFFECT: FLUME TEST RESULTS

The attack angle α is the angle between the direction of the bridge pier and the direction of the flow. The attack angle effect for pier scour is actually a composite effect and several influencing factors are involved. For a given rectangular pier, both the pier shape confronted to the flow and the pier projection width will change with the angle of attack. In addition, due to the change of pier projection width with the attack angle, the water depth effect and pier spacing effect will be influenced. To obtain the "pure" attack angle effect, a filtration process is necessary to eliminate the additional influences.

When the attack angle effect is examined through rectangular piers, there are two influencing parameters for the pier: one is the attack angle α, the other is the aspect ratio *L*/*B*. These two independent parameters form a parameter matrix

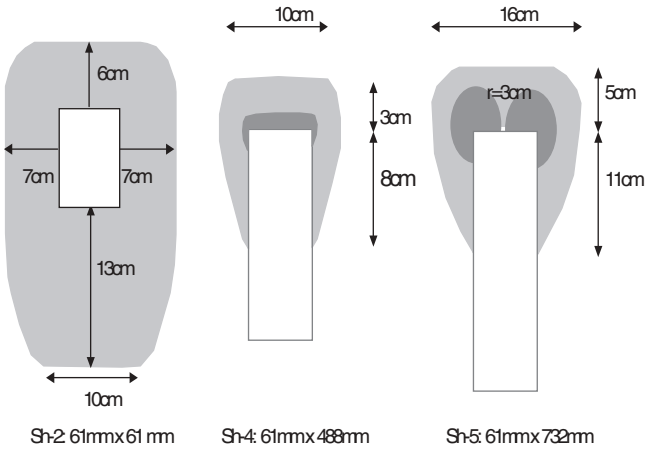

Figure 5.21. Shape of the scour hole for different aspect ratios.

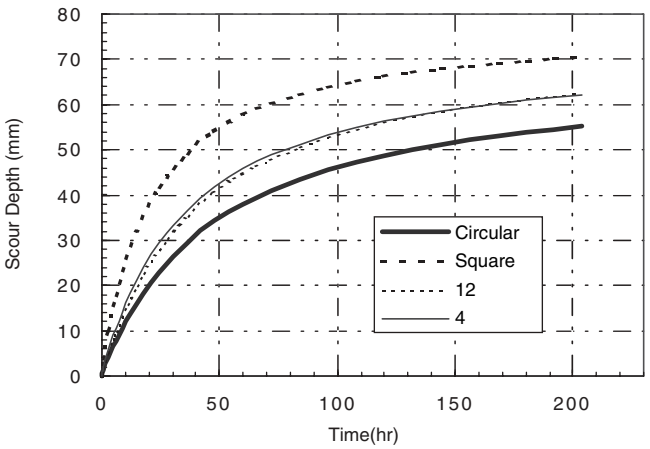

Figure 5.22. Scour curves for piers of different shapes.

of tests that need to be performed to find the general correction factor. Two perpendicular directions were selected to represent the whole matrix. In the transverse direction, the rectangular pier is kept at *L*/*B* = 4 and α is changed from 0 degrees to 90 degrees; in the longitudinal direction, α is kept constant at 45 degrees and the aspect ratio of the pier changes. During the experiments, the scour depths around the four corners of the rectangular pier were measured to find the maximum scour depth. The scour hole shapes for all of the cases also were recorded.

Parameters and major results for the flume tests for the attack angle effect are summarized in Table 5.6. The scour depth versus time curves are plotted in Figure 5.23. The maximum scour depth and initial scour rate were obtained in the same way as previously, by using the hyperbola model.

5.18 ATTACK ANGLE EFFECT ON MAXIMUM SCOUR DEPTH

The correction factor K_a, used to account for the attack angle effect on maximum pier scour depth, is calculated as the ratio of the maximum scour depth for a given pier and a given attack angle over the maximum scour depth for the same pier and an attack angle equal to zero (reference case). For example, the reference case of Test At-2 is Sp-3. If the reference case were not available, such as for Tests At-7 and

TABLE 5.6 Parameters and results for the attack angle effect

Test No.	H (mm)	B (mm)	α (°)	V (m/s)	L/B	Time Lasting (h)	$\dot{z}_i$ (mm/hr)	Zmax (mm)
At-1	375.00	61.00	15	0.33	4:1	186.00	1.49	103.09
At-2	375.00	61.00	30	0.33	4:1	211.08	2.37	117.65
At-3	375.00	61.00	45	0.33	4:1	115.17	2.07	151.50
At-4	375.00	61.00	60	0.33	4:1	117.25	2.02	196.08
At-5	375.00	61.00	90	0.33	4:1	117.08	1.88	208.77
At-6	375.00	61.00	45	0.33	1:1	112.67	1.88	147.06
At-7	375.00	61.00	45	0.33	2:1	115.08	2.79	161.29
At-8	375.00	61.00	45	0.33	6:1	115.08	2.28	185.19

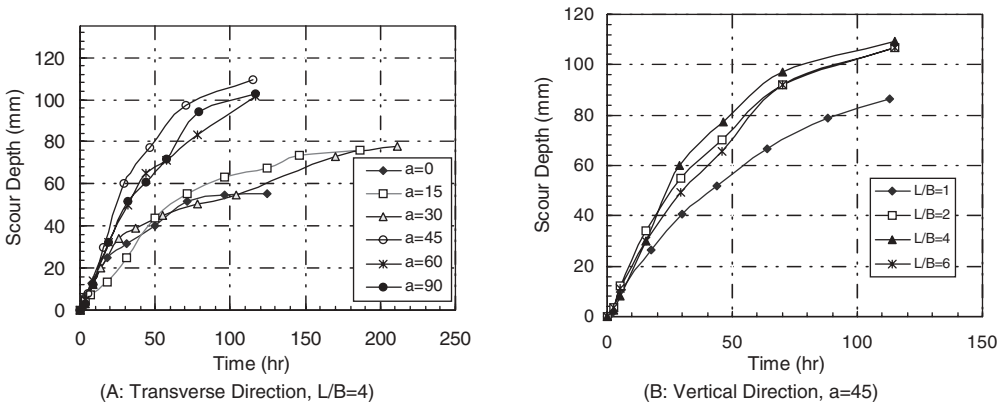

Figure 5.23. Scour depth versus time curves for attack angle tests.

At-8, interpolation between existing reference cases would be used to calculate the maximum scour depth of the required reference case. The pier projection width, B', as shown in Figure 5.24, is a widely accepted concept to evaluate the effect of the attack angle:

$$B' = L\sin\alpha + B\cos\alpha = B\left(\frac{L}{B}\sin\alpha + \cos\alpha\right) \qquad (5.4)$$

Common scour depth equations for 0-degree attack angle are of the form: $Z_{max} = f\,B^n$, where n is a constant. If the projection width is equivalent to the pier width, then the correction factor K_a can be calculated as

$$K_a = \frac{Z_{max}(\alpha)}{Z_{max}(0)} = \left(\frac{L}{B}\sin\alpha + \cos\alpha\right)^n \qquad (5.5)$$

The value of n generally varies from 0.6 to 0.9 and is equal to 0.635 in the SRICOS Method for scour depth prediction in cohesive soils.

In Figure 5.25, the correction factor obtained in the flume tests is shown together with other solutions using the projec-

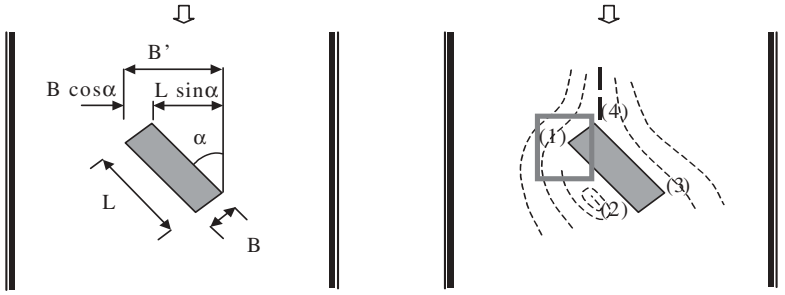

Figure 5.24. Skewed pier definitions.

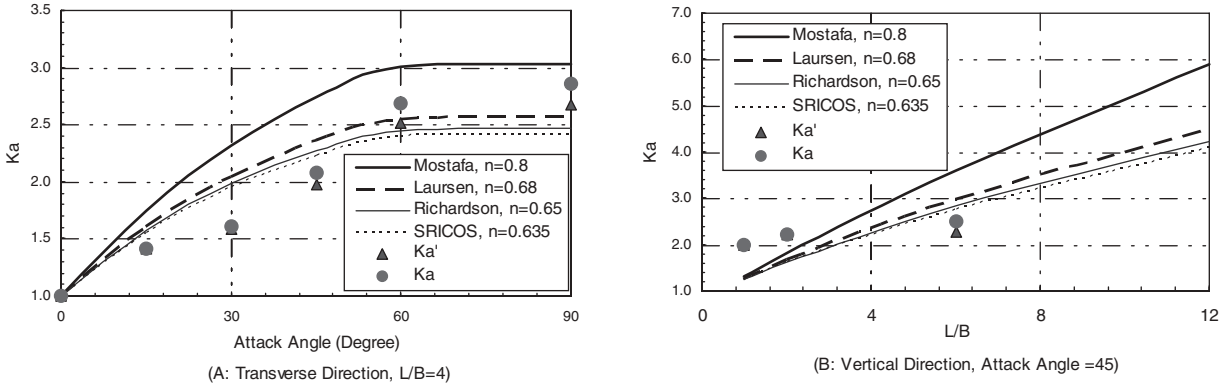

Figure 5.25. Attack angle effect on maximum scour depth.

TABLE 5.7 Calculations for isolating the attack angle effect in pier scour depth

α (°)	L/B	B′ (mm)	B′/B	Z_{max} (mm)	$Z_{max}(0)$ (mm)	H/B′	K_w	K_{sp}	K_a	K_a'
15	4:1	61.00	1.00	72.99	72.99	6.15	1.00	1.00	1.00	1.00
30	4:1	122.07	2.00	103.09	72.99	3.07	1.00	1.00	1.41	1.41
45	4:1	174.83	2.87	117.65	72.99	2.14	1.00	1.02	1.61	1.59
60	4:1	215.67	3.54	151.50	72.99	1.74	1.00	1.05	2.08	1.98
90	4:1	241.81	3.96	196.08	72.99	1.55	0.99	1.08	2.69	2.51
45	1:1	86.27	4.00	208.77	72.99	1.54	0.98	1.09	2.86	2.67
45	2:1	129.40	1.41	147.06	73.53	4.35	1.00	1.00	2.00	2.00
45	6:1	301.93	2.12	161.29	73.20	2.90	1.00	1.00	2.20	2.20

tion width and Equation 5.5 in both the transverse and the longitudinal direction. The difference between K_a and K_a' is linked to the influence of the water depth and pier spacing effect that occur when the angle of attack becomes more severe. In order to examine the pure attack angle effect, the shallow water effect and pier spacing effect need to be eliminated. The proposed equations for shallow water depth and pier spacing are used to isolate the angle of attack effect. The results of the calculations are shown in Table 5.7. The correction factor, K_a', for pure attack angle effect on scour depth is obtained based on the following relationship:

$$K_a = K_w \cdot K_{sp} \cdot K_a' \tag{5.6}$$

Figure 5.25 shows that when the attack angle is less than 30 degrees, the correction is not significant and that for angles of attack larger than 30 degrees, the correction factor would be overestimated if the correction was not done. Figure 5.25 also shows that using the projection width with the SRICOS exponent of 0.635 leads to a reasonable and often conservative prediction of the correction factor K_a'. Therefore, this approach is adopted for the proposed method.

5.19 ATTACK ANGLE EFFECT ON INITIAL SCOUR RATE

The initial scour rates for the attack angle flume tests are plotted in Figure 5.26 for both the transverse and vertical direction. In this case, the scour rates show a large scatter pattern. This is because several opposing factors are involved in the initial shear stress or the initial scour rate under a given attack angle condition. Based on the observations in previous sections, the scour rate will decrease with an increase in pier width and flow depth, but increase with an increase in pier contraction and the sharpness of pier corners. Therefore, the relative magnitude of the scour rate under a given attack angle depends on the balance between these influencing factors.

5.20 ATTACK ANGLE EFFECT ON SCOUR HOLE SHAPE

The attack angle also strongly affects the shape of the scour hole. If the four corners of the rectangular pier are numbered as in Figure 5.24, test observations indicate that

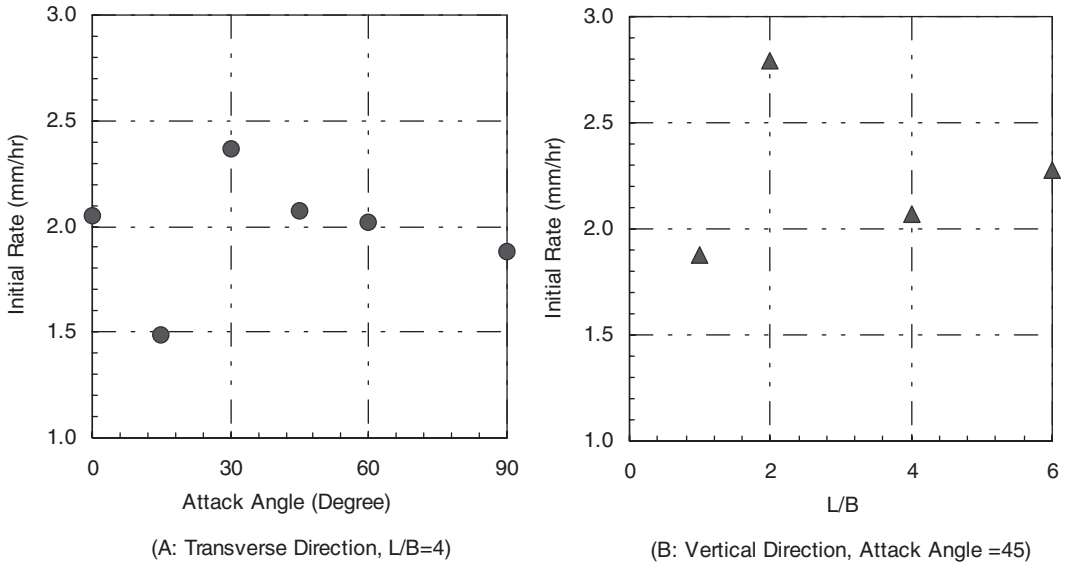

Figure 5.26. Initial scour rates for the attack angle flume tests.

TABLE 5.8 Transition of the location of maximum scour depth

Attack Angle (°)	Location of the maximum scour depth
0	(1), (4)
0<α<45	(1)
45	(1), (3)
45<α<90	(3)
90	(1), (2), (3), (4)

the location of the maximum scour depth will either happen at Corner 1 or Corner 3. When the attack angle increases, the location of the maximum scour depth gradually moves from Corner 1 to Corner 3, and this transition is documented in Table 5.8. It also was noted that the scour hole in the tested cohesive soil (Figure 5.27) was much smaller than the scour hole in sands sketched by Raudkivi (1991).

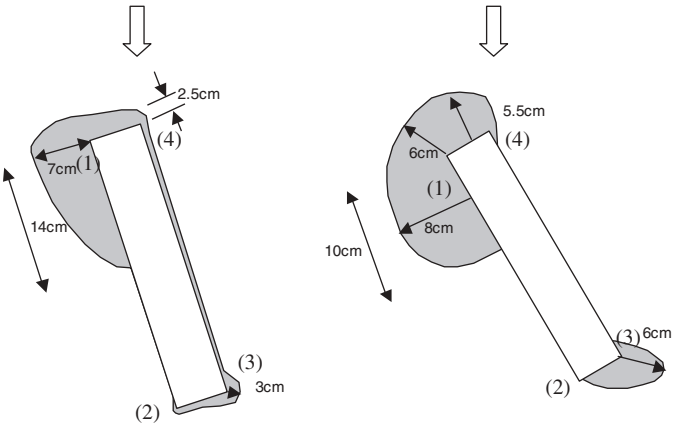

Figure 5.27. Shape of scour around a skewed pier in a cohesive soil (left: attack angle = 15 degrees, right: attack angle = 30 degrees).

5.21 MAXIMUM SCOUR DEPTH EQUATION FOR COMPLEX PIER SCOUR

In the previous sections, individual effects on the maximum pier scour depth were studied by flume testing. A series of figures and equations are given to quantify the corresponding correction factors. However, bridge piers are likely to exhibit a combination of these effects and recommendations are needed to combine these effects in the calculations. It is recommended that the correction factors be multiplied in order to represent the combined effect:

$$Z_{\max}(\text{mm}) = 0.18 \cdot K_w \cdot K_{sp} \cdot K_{sh} \cdot \left(\frac{B'V}{v}\right)^{0.635} \tag{5.7}$$

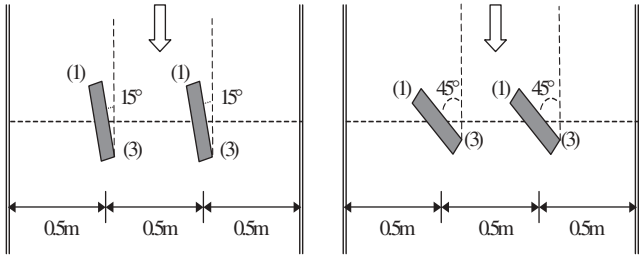

Figure 5.28. Configuration of the flume tests to verify the superposition rule.

where Z_{max} is the maximum depth of scour (mm); V is depth average velocity at the location of the pier if the pier or bridge was not there (m/s); B' is the projection width of the pier (m); v is the kinematic viscosity of water (10E-6 (m^2/s) at 20°C); K_w is the correction factor for shallow water effect (Equation 5.2), K_{sp} for pier spacing effect (Equation 5.3), and K_{sh} for pier shape effect (1.1 for rectangular piers); and B' is the pier projection width (Equation 5.4 for rectangular pier). This is a common approach that implies that the effects are independent and has been used in many instances before (HEC-18, Melville [1997]).

Two complex pier flume tests were conducted with the configuration shown in Figure 5.28 where all of the individual effects described in previous sections were expected to happen simultaneously. The main parameters and results are summarized in Table 5.9, and the time history of the scour development is plotted in Figure 5.29. The final maximum scour depth was obtained by using the hyperbola model.

The maximum scour depths for the two tests were calculated according to Equation 5.7. The calculations are detailed in Table 5.10, and the measured results also are listed at the bottom of that table which shows that the difference between the predictions and measurements is remarkably small (less than 5%). This tends to indicate that the chosen superposition law works well for complex pier scour predictions.

TABLE 5.9 Parameters and results for the complex pier flume tests

Test No.	H (mm)	V (mm/s)	L (mm)	B (mm)	C (mm)	g (°)	Time (h)	Z_{max} (mm)
Cp-1	375	330	244	61	500	15	115.32	175.4
Cp-2	375	330	244	61	500	45	150.67	285.7

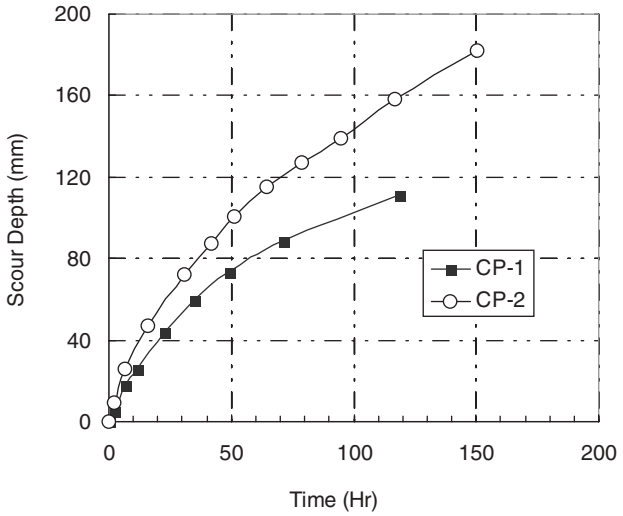

Figure 5.29. Scour development curves for the complex pier flume tests.

TABLE 5.10 Comparison of calculated and measured maximum pier scour depths

PARAMETERS	Cp - 1	Cp - 2	CALCULATION NOTE
Primary Inputs			
B (mm)	61	61	Pier width
L (mm)	244	244	Pier length
H (mm)	375	375	Water depth
α (˚)	15	45	Attack angle
V (mm/s)	330	330	Mean approaching velocity
C (mm)	500	500	Center to center pier spacing
Attack Angle Effect			
B' (mm)	122.07	215.67	Projection width following Eq. (5.4)
Basic Scour Depth			
Z1 (mm)	151.19	217.01	SRICOS: simple pier Eq. (5.6)
Water Depth			
H/B'	3.07	1.74	
Kw	1.00	1.00	Shallow water effect, Eq. (5.1)
Contraction Effect			
C/B'	4.10	2.32	
Ksp	1.0	1.233	Interpolated from Fig. 5.7
Pier Shape Effect			
Ksh	1.1	1.1	Calculated from Fig. 5.11
Composite Effect			
K	1.16	1.36	K= Kw·Ksp·Ksh
Final Scour Depth			
Zcal(mm)	174.63	294.33	Zcal=K·Z1
Comparison			
Ztest (mm)	175.44	285.71	
(Zcal-Ztest)/Ztest (%)	- 0.46	3.02	

CHAPTER **6**

THE SRICOS-EFA METHOD FOR INITIAL SCOUR RATE AT COMPLEX PIERS

6.1 GENERAL

The initial scour rate is an integral part of the SRICOS Method because it is one of the two fundamental parameters used to describe the scour depth versus time curve. The other fundamental parameter is the maximum depth of scour, which was studied in Chapter 5. The initial rate of scour for a given complex pier scour problem is obtained by first calculating the maximum shear stress τ_{max} existing around the pier before the scour hole develops (flat river bottom) and then reading the initial scour rate on the erosion function obtained in the EFA test. Therefore, the problem of obtaining the initial rate of scour is brought back to the problem of obtaining the maximum shear stress around the pier before scour starts. This problem was solved by using numerical simulations. The simulations performed and the associated results are described in this chapter. The goal was to develop correction factors for giving τ_{max} for a cylindrical pier in deep water (Equation 6.1):

$$\tau_{max} = 0.094\,\rho v^2\left(\frac{1}{\log R_e} - \frac{1}{10}\right) \tag{6.1}$$

These factors include the effects of shallow water depth, pier shape, pier spacing, and angle of attack.

6.2 EXISTING KNOWLEDGE ON NUMERICAL SIMULATIONS FOR SCOUR

Hoffman and Booij (1993) applied the Duct Model and the Sustra Model to simulate the development of local scour holes behind the structure. The flow model upon which Duct is based is a parabolic boundary-layer technique using the finite element method. The Sustra Model is used to compute the concentration field following the approach used by Van Rijn and Meijer (1986). The computational model results were compared with experimental data. The results (i.e., flow velocities, sediment concentration, and bed configurations as a function of time) showed an agreement between the experimental data and the computational model.

Olsen and Melaaen (1993) simulated scour around a cylinder by using SSIIM, a three-dimensional free-surface flow and transport model. The SSIIM Model solves Reynold stresses by the $k-\epsilon$ turbulence model. The authors observed and reported that there is agreement between the pattern of the vortices in front of the cylinder and the model. The application of the SSIIM Model can be found at http://www.sintef.no/nhl/vass/vassdrag.html.

Wei et al. (1997) performed a numerical simulation of the scour process in cohesive soils around cylindrical bridge piers. A multiblock chimera Reynolds-averaged Navier Stokes (RANS) method was incorporated with a scour rate equation to simulate the scour processes. The scour rate equation linked the scour rate to the streambed shear stress through a linear function. The simulation captured the important flow features such as the horseshoe vortex ahead of the pier and the flow recirculation behind the pier. A reasonable agreement was found between the progress of the scour depth obtained in the flume experiments and predicted by the numerical simulation. Wei et al. found that the value of the critical shear stress has a significant influence on the scour process around a cylinder in cohesive soils. The final scour depth and the time necessary to reach it increase with decreasing critical shear stress. Based on a number of parametric runs, they also presented an empirical formula for the maximum streambed shear stress for a cylindrical pier in deep water.

Dou (1997) simulated the development of scour holes around piers and abutments at bridge crossings. A stochastic turbulence closure model (Dou, 1980), which includes an isotropic turbulence, was incorporated into a three-dimensional flow model, CCHE3D, developed by the Center for Computational Hydroscience and Engineering at the University of Mississippi. The factors that reflect the secondary flow motion generated by the three-dimensional flow are adopted to modify the sediment transport capacity formula originally developed for estimating general scour. Dou's study also includes some investigations on sediment incipient movement in local scour and includes some laboratory experiments.

Roulund (2000) presents a comprehensive description on the flow around a circular pier and the development of the scour hole by numerical and experimental study. The numerical model solves the three-dimensional RANS equations with use of the $k-\epsilon$ (SST) turbulence closure model. The method is based on a full three-dimensional bed load formulation, including the effect of gravity. Based on the bed load calculation, the change in bed level with time is calculated from the equation of continuity for the sediments. For the experiments, the scour development from a flat bed to the equilibrium of the scour hole was videotaped and this visual record was used to

observe the scour development. The evolution of the three-dimensional scour hole with time was obtained by combining the scour profiles from all angles around the pier.

6.3 NUMERICAL METHOD USED IN THIS STUDY

In the present study, the three-dimensional flow chimera RANS Method of Chen et al. (1993, 1995a, 1995b, 1997) was used. First, the computational domain was divided into a number of smaller grid blocks to allow complex configurations and flow conditions to be modeled efficiently through the judicious selection of different block topology, flow solvers, and boundary conditions. The chimera domain decomposition technique was used to connect the overlapped grids together by interpolating information across the block boundaries. The Reynolds stresses were evaluated using the two-layer turbulence model of Chen and Patel (1988). The mean flow and turbulence quantities were calculated using the finite-analytical method of Chen, Patel, and Ju (1990). The SIMPLER/PISO pressure-velocity coupling approach of Chen and Patel (1989) and Chen and Korpus (1993) was used to solve for the pressure field. A detailed description of the multiblock and chimera RANS methods is given in Chen and Korpus (1993) and Chen, Chen, and Davis (1997). A useful summary of that method can be found in Nurtjahyo (2002). This summary discusses the governing equations, turbulence modeling (RANS or RANS equations), the boundary conditions on the pier surface, the river bottom, the outer boundaries, and the free water surface.

The computer code has the ability to simulate the development of the scour hole around the pier as a function of time. This is done by including an erosion function linking the vertical erosion rate to the shear stress at the interface between the water and the soil. The program then steps into time by adjusting the mesh in the vertical direction after each time step as the scour hole develops. This option is not necessary to obtain the maximum shear stress before scour starts, since in this case the bottom of the river is kept flat.

A typical run consists of the following steps:

1. Obtain the information for the problem: water depth, mean depth velocity at the inlet, pier size, and pier shape.
2. Calculate the Reynolds Number and Froude Number because they influence the size and distribution of the grid elements.
3. Generate the grid using a program called GRIDGEN (about 4 days' worth of work).
4. The input consists of the Reynolds Number, the Froude Number, and the boundary conditions on all surfaces. The initial condition consists of the velocity profile at the inlet and is automatically generated by the program on the basis of the inlet mean depth velocity and the geometry.
5. Typical runs last 5 hours of CPU time on the Texas A&M University SGI supercomputer when only the bed shear stress is required. The CPU time increases to 20 hours when the scour hole development needs to be simulated.
6. The output consists of the following parameters in three dimensions: velocity vectors, pressure, bed shear stress, and turbulent kinetic energy.

6.4 VERIFICATION OF THE NUMERICAL METHOD

This verification was achieved by comparing the shear stresses predicted by the numerical method to those measured experimentally. The measurements were performed by Hjorth (1975) who investigated the distribution of shear stresses around a circular pier. The experiment was conducted in a rigid boundary flume. Two circular piers were used (diameter 0.05 m and 0.075 m). The study focused on two different velocities (0.15 m/s and 0.20 m/s) and two different depths of approach flow (0.1 m and 0.2 m). The shear stress was measured by using a stationary hot film probe through the bottom of the flume flush with the bottom, then moving the position of the cylinder around the fixed probe. In that fashion, Hjorth obtained the shear stress at 35 different locations around the cylinder and created isostress lines by interpolation between the measurements. The numerical method was used to simulate the experiments performed by Hjorth. The output was the distribution of the shear stresses on the flume bottom around the cylinder. The result of the experiment and the numerical simulation for the 0.075-m-diameter cylinder are compared on Figures 6.1 and 6.2. The very favorable comparison gave confidence in the validity of the numerical results.

6.5 SHALLOW WATER EFFECT: NUMERICAL SIMULATION RESULTS

The objective of this parametric study was to obtain the relationship between the maximum bed shear stress τ_{max} and water depth (Figure 6.3).

One of the flume experiments was chosen to perform the simulation. The cylindrical pier with a diameter equal to 0.273 m was placed vertically in a 1.5-m-wide flume. The velocity was constant at 0.3 m/s and four different water depths were simulated: $H = 0.546$ m (or $H/B = 2$), $H = 0.258$ m (or $H/B = 0.95$), $H = 0.137$ m (or $H/B = 0.5$), and $H = 0.060$ m (or $H/B = 0.22$). The value of the Reynolds Number based on the diameter was $R_e = 81900$ and the Froude Number based on the diameter was $F_r = 0.1833$. In order to reduce the amount of CPU time, one-half of the symmetric domain was chosen. The grid was divided into four blocks as shown in Figure 6.4.

The grid was very fine near the pier and riverbed in order to apply the two-layer approach of the turbulence model. A few grid layers were placed within the viscous sublayer. The first step was to verify that the inlet velocity profile for the numerical simulation matched the experiment. The result was

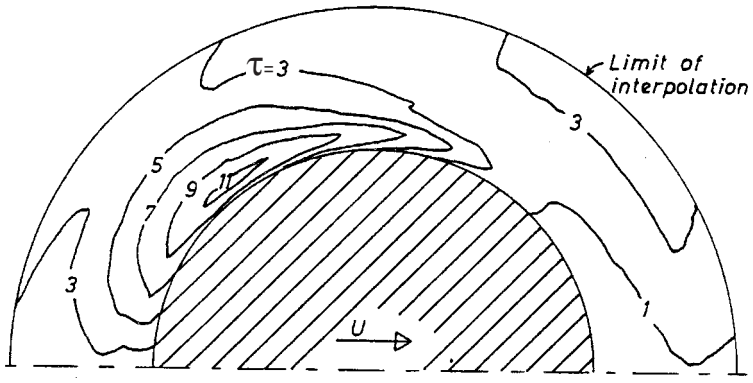

(a) Experiment (Hjorth, 1975)

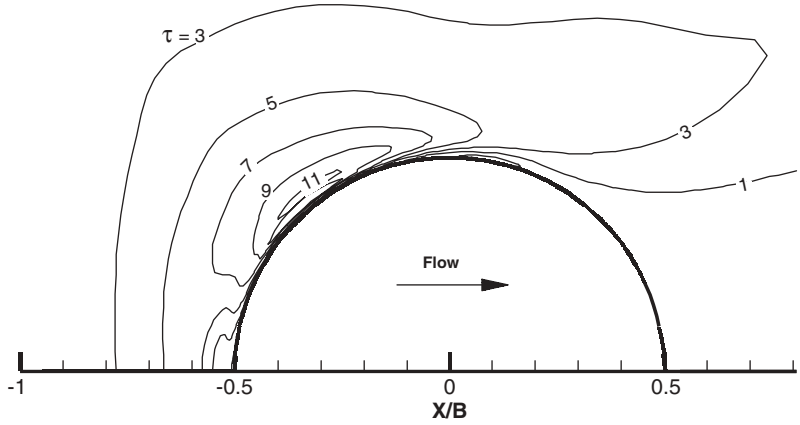

(b) Numerical

Figure 6.1. Comparison of bed shear stress (N/m^2) distribution around a circular pier as calculated from an experiment by Hjorth (1975) and numerical computations (B = 0.075 m, V = 0.15 m/s, H = 0.1 m).

shown in Figure 6.5. In the experiment, the thickness of the boundary layer was about 0.06 m for all cases. This observation was also found in Gudavalli's experiments (1997). The velocity vector around the pier is shown in Figure 6.6 for a shallow water case and a deep water case. The difference in velocity field can be observed on the figure, especially near the base of the pier where the horseshoe vortex is much stronger in the shallow water case.

Figures 6.7 and 6.8 show the distribution of shear stress around the pier for different relative water depths of $H/B = 0.2$ and $H/B = 2$. As can be seen in the figures, the shear stress is higher in the case of the shallow water depth. This is explained as follows. When the water is deep, the velocity profile has the conventional shape shown in Figure 6.5. When the water depth becomes shallow, and if the mean depth velocity is kept constant, the velocity profile must curve faster towards the bottom of the profile because of the lack in vertical distance forced by the shallow water condition. This leads to a higher gradient of velocity near the bottom and, therefore, to a higher shear stress τ since τ is proportional to the velocity gradient. Johnson and Jones (1992) made similar observations on the influence of the pier diameter on the bed shear stress; these observations were based on experiments.

Figure 6.9 shows the pressure field induced by the pier. If the pressure field is sufficiently strong, it causes a three-dimensional separation of the boundary layer, which in turn rolls up ahead of the pier to form the horseshoe vortex system. A blunt-nosed pier, for example, is a pier for which the induced pressure field is sufficiently strong to form the horseshoe vortex system.

6.6 SHALLOW WATER EFFECT ON MAXIMUM SHEAR STRESS

The maximum shear stress τ_{max} is the maximum shear stress that exists on the riverbed just before the scour hole starts to develop. One way to present the data is to plot $\tau_{max}/\tau_{max(deep)}$ as a function of H/B (Figure 6.10). The parameter $\tau_{max(deep)}$ is the value of τ_{max} for the deep water case and is given by Equation 6.1. The shallow water correction factor, k_w, is the ratio $\tau_{max}/\tau_{max(deep)}$. The data points on Figure 6.10 correspond to the results of the four numerical simulations.

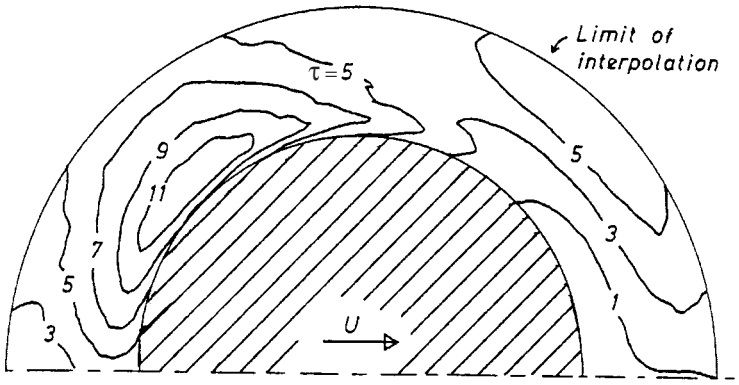

(a) Experiment (Hjorth,1975)

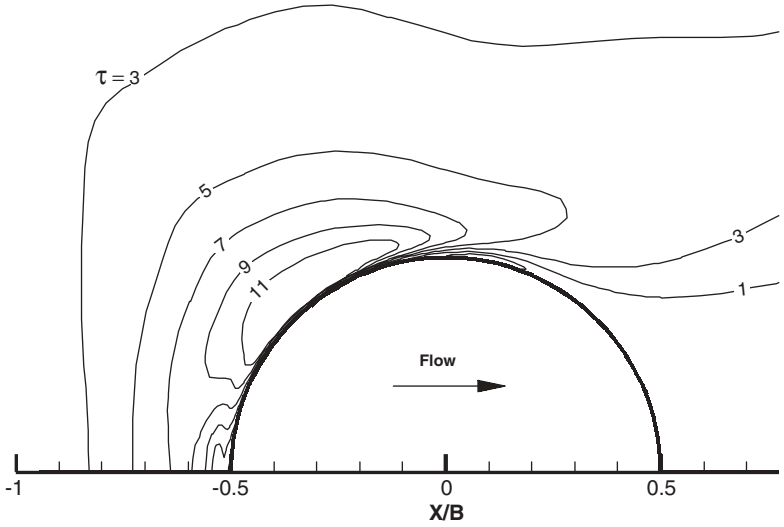

(b) Numerical

Figure 6.2. Comparison of bed shear stress distribution (N/m^2) around a circular pier as calculated from an experiment by Hjorth (1975) and numerical computations (B = 0.075 m, V = 0.30 m/s, H = 0.2 m).

By regression, the equation proposed for the correction factor k_w giving the influence of the water depth on the maximum shear stress is

$$k_w = \frac{\tau_{max}}{\tau_{max}(\text{deep})} = 1 + 16e^{-\frac{4H}{B}} \tag{6.2}$$

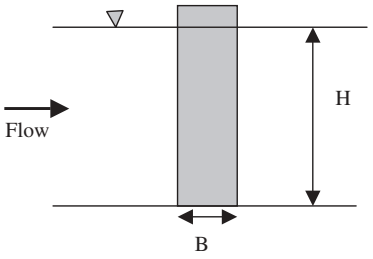

Figure 6.3. Problem definition for water depth effect.

6.7 PIER SPACING EFFECT: NUMERICAL SIMULATION RESULTS

The objective of this parametric study is to obtain the relationship between the maximum bed shear stress τ_{max} and pier spacing (Figure 6.11).

One of the flume experiments was chosen to perform the numerical simulation. The cylindrical pier had a diameter of 0.16 m and was placed vertically in a 1.5-m-wide flume. The mean depth approach velocity was 0.33 m/s and the water depth is 0.375 m. Four different pier spacings were simulated: S/B = 6 (in the case of one pile in the flume), S/B = 3.12 (in the case of two piles), S/B = 2.34 (in the case of three piles), and S/B = 1.88 (in the case of four piles). The Reynolds Number based on diameter was R_e = 52800 and the Froude Number based on diameter was F_r = 0.2634. The velocity between the piles became higher due to the decreased spacing and the corresponding shear stress increases.

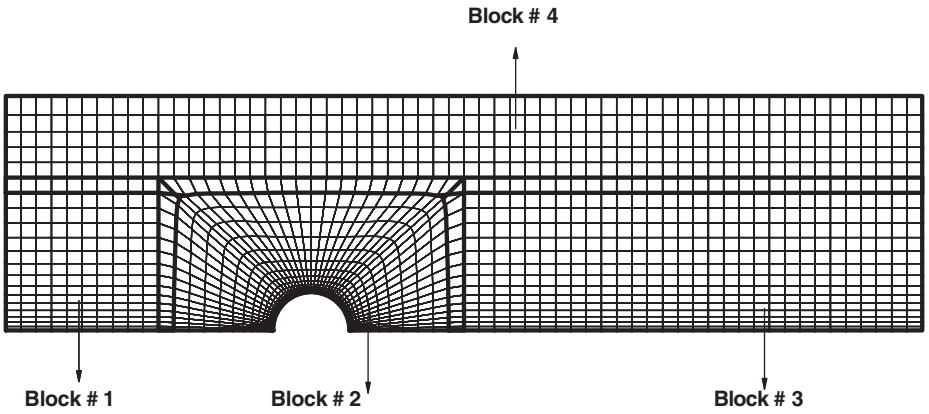

Figure 6.4. Grid system for the numerical simulation.

Figures 6.12 and 6.13 show the shear stress distribution for $S/B = 1.88$ and $S/B = 6$.

6.8 PIER SPACING EFFECT ON MAXIMUM SHEAR STRESS

The maximum shear stress τ_{max} is the maximum shear stress that exists on the riverbed just before the scour hole starts to develop. One way to present the data is to plot $\tau_{max}/\tau_{max(single)}$ as a function of S/B (Figure 6.10). The parameter $\tau_{max(single)}$ is the value of τ_{max} for the case of a single pier in deep water and is given by Equation 6.1. The pier spacing correction factor, k_{sp}, is the ratio $\tau_{max}/\tau_{max(single)}$. The data points on Figure 6.14 correspond to the results of the four numerical simulations.

By regression, the equation proposed for the correction factor k_{sp} giving the influence of the pier spacing on the maximum shear stress is

$$k_{sp} = \frac{\tau_{max}}{\tau_{max}(\text{single})} = 1 + 5e^{-1.1\frac{S}{B}}. \quad (6.3)$$

6.9 PIER SHAPE EFFECT: NUMERICAL SIMULATION RESULTS

The objective of this parametric study was to obtain the relationship between the maximum bed shear stress τ_{max} and the shape of rectangular piers (Figure 6.15). One of the flume experiments was chosen to perform the numerical

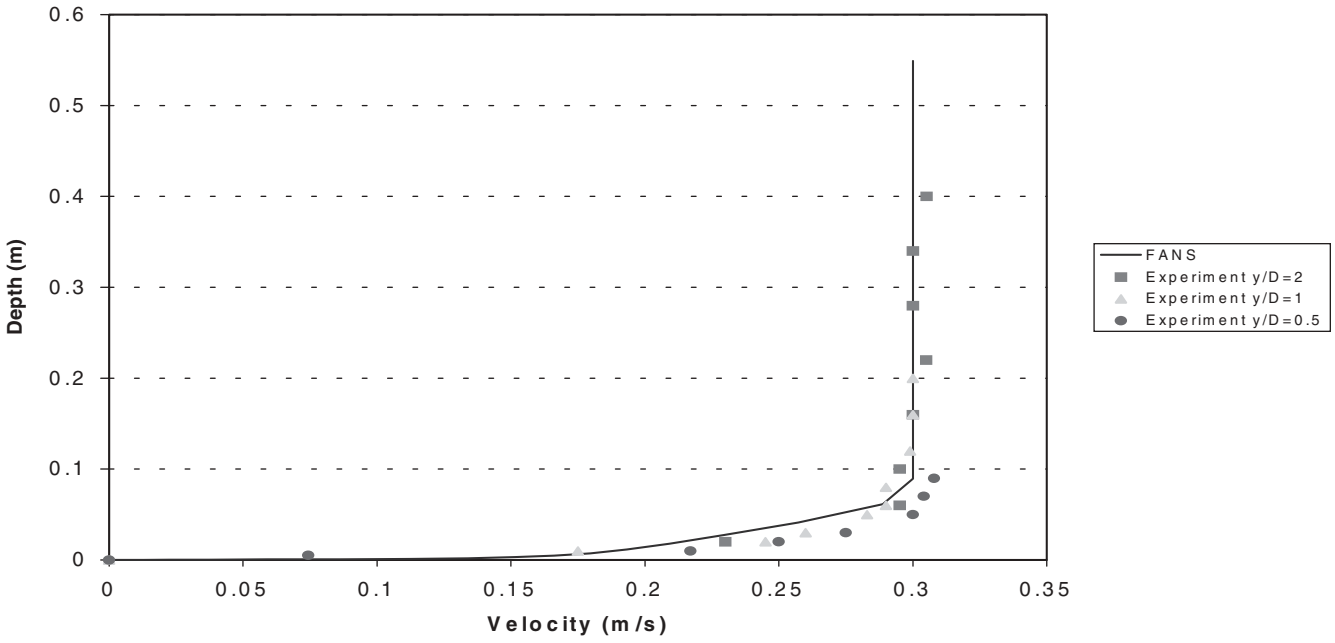

Figure 6.5. Velocity profile comparison between experiment and numerical simulation at the inlet.

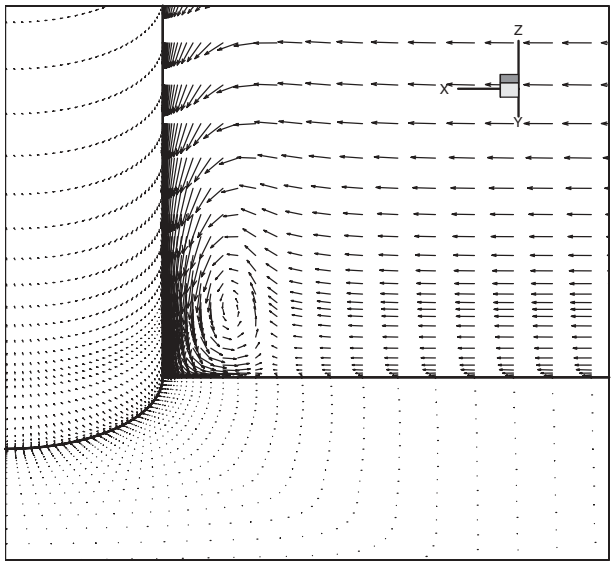

(a). H/B=0.2

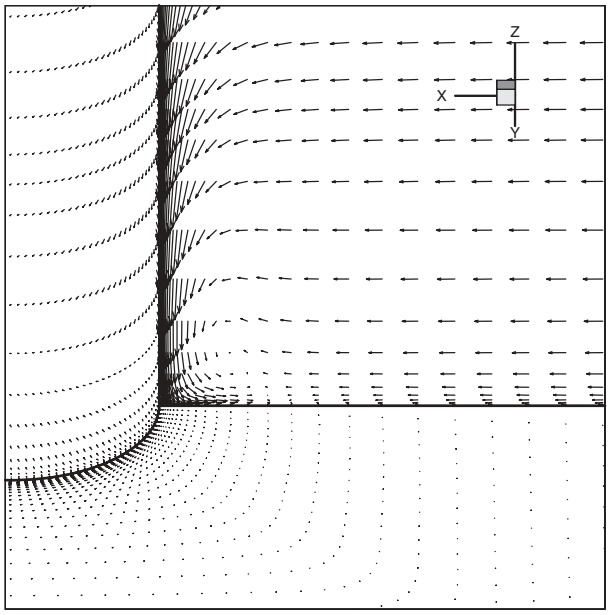

(b). H/B=2

Figure 6.6. Velocity vector around pier for (a) H/B = 0.2 and (b) H/B = 2.

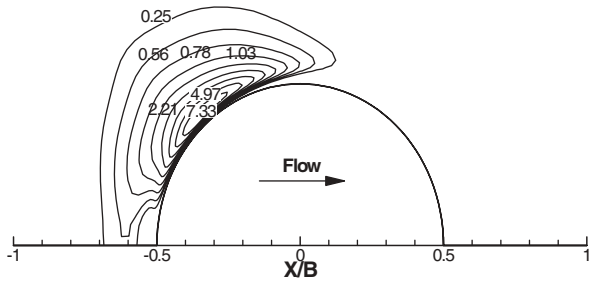

Figure 6.7. Initial bed shear stress distribution (N/m^2) around the pier (H/B = 0.2, V = 0.3m/s).

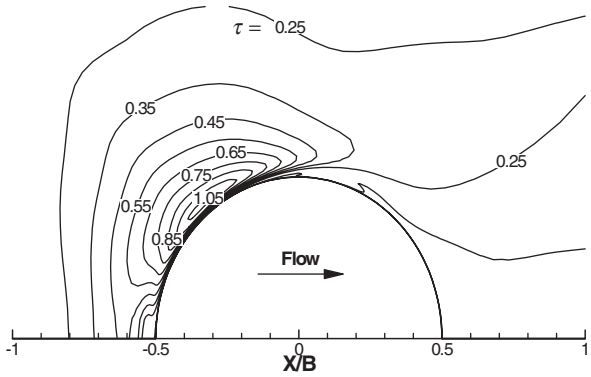

Figure 6.8. Initial bed shear stress distribution (N/m^2) around the pier (H/B = 2, V = 0.3m/s).

simulation. A rectangular pier with a width of 0.061 m was placed vertically in the 1.5-m-wide flume. The velocity was constant and equal to 0.33 m/s and the water depth was 0.375 m. Four different pier aspect ratios were simulated: *L*/*B* = 1, 4, 8, and 12. The value of the Reynolds Number based on the width of the rectangular pier was R_e = 20130 and the Froude Number based on the width of the rectangular pier was F_r = 0.4267.

Examples of velocity fields are presented in Figures 6.16 and 6.17 for rectangular piers with aspect ratios equal to 0.25 and 4. Figures 6.18 to 6.20 show the maximum bed shear stress contours around rectangular piers with different aspect ratios: *L*/*B* = 0.25, 1, and 4. The location of the maximum bed shear stress was at the front corner of the rectangle. It was found that the maximum bed shear stress, τ_{max}, was nearly constant for any aspect ratio above one. The value of τ_{max}

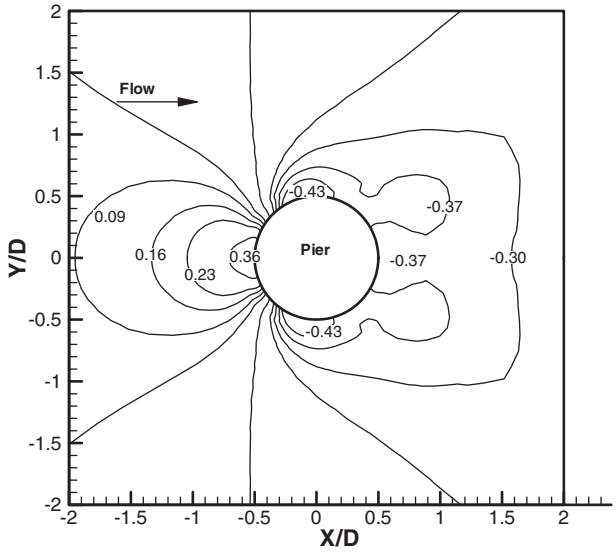

Figure 6.9. Normalized pressure (p/ρu^2) contours for H/B = 2 on the riverbed.

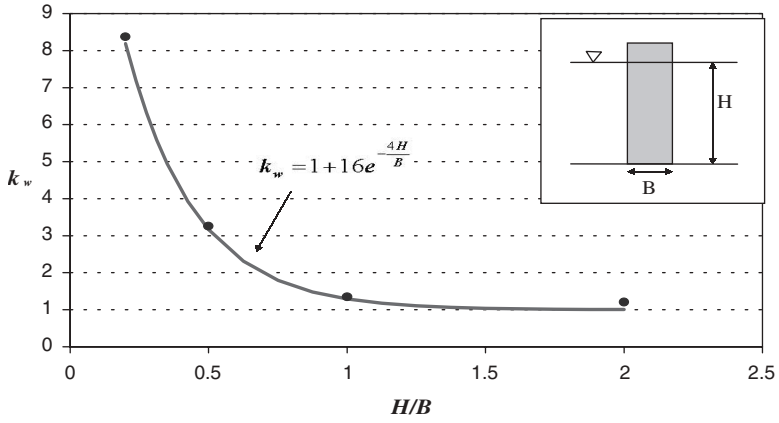

Figure 6.10. Relationship between k_w (= $\tau_{max}/\tau_{max(deep)}$) and H/B.

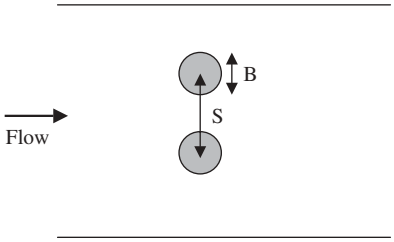

Figure 6.11. Problem definition of pier spacing effect.

increased, however, when *L*/*B* became less than one. Figures 6.16 and 6.17 indicate that the flow pattern around the rectangular pier for *L*/*B* = 0.25 is quite different from the pattern for *L*/*B* = 4 where the flow is separating at the sharp corner. For *L*/*B* = 0.25 the flow is allowed to go behind the pier while the flow for *L*/*B* = 4 follows the side of the pier. In the case of *L*/*B* = 4, the length of the flow separation is about 1 *B* from the corner; this may explain that τ_{max} is independent of the pier length for *L*/*B* > 1. On the contrary, for *L*/*B* < 1, there is no region of separated flow and the decreasing pressure behind the pile may increase the velocity around the corner.

6.10 PIER SHAPE EFFECT ON MAXIMUM SHEAR STRESS

The maximum shear stress τ_{max} is the maximum shear stress that exists on the riverbed just before the scour hole starts to develop. One way to present the data is to plot k_{sh} = $\tau_{max}/\tau_{max(circle)}$ as a function of *L*/*B* (Figure 6.21). The parameter $\tau_{max(circle)}$ is the value of τ_{max} for the case of a circular pier in deep water and is given by Equation 6.1. The pier spacing correction factor k_{sh} is the ratio $\tau_{max}/\tau_{max(circle)}$. The data points

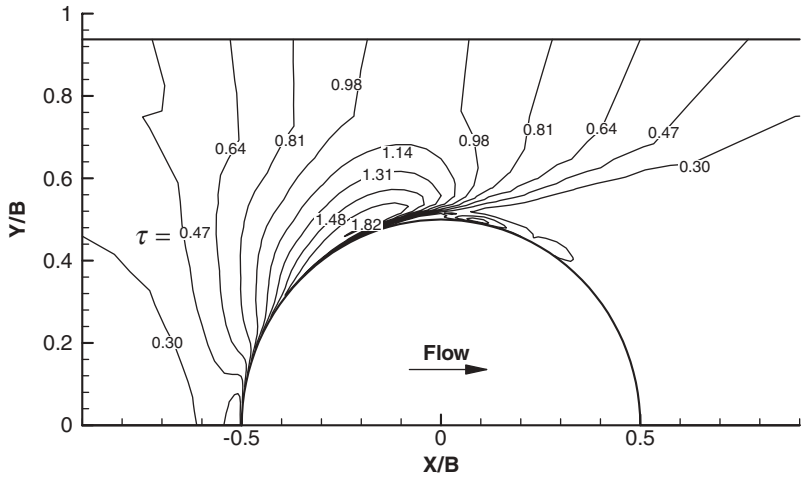

Figure 6.12. Initial bed shear stress distribution (N/m^2) around the pier (S/B = 1.88, H = 0.38m, V = 0.33m/s).

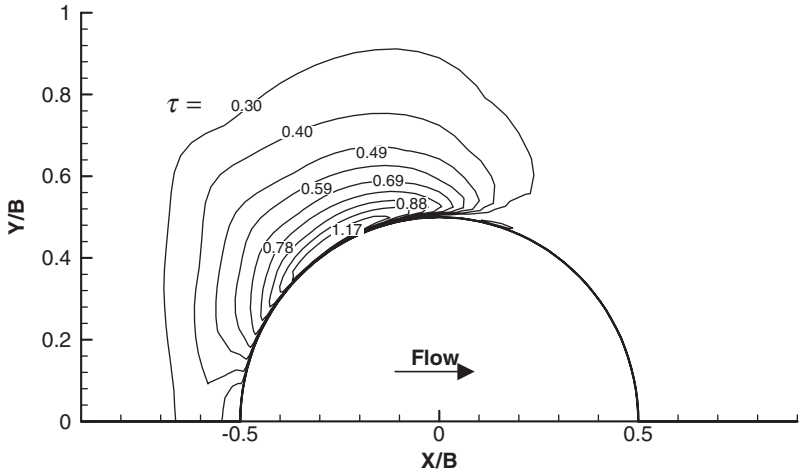

Figure 6.13. Initial bed shear stress distribution (N/m^2) around the pier (S/B = 6, H = 0.38m, V = 0.33m/s).

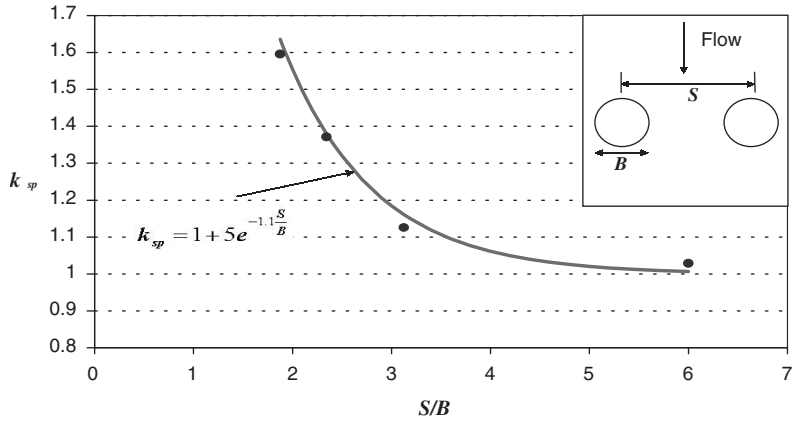

Figure 6.14. Relationship between k_{sp} (= $\tau_{max}/\tau_{max(single)}$) and S/B for deep water H/B > 2).

on Figure 6.21 correspond to the results of the seven numerical simulations.

The correction factor for shape effect k_{sh} is given by the following equation, which was obtained by regression of the data points on Figure 6.21:

$$k_{sh} = 1.15 + 7e^{-4\frac{L}{B}} \quad (6.4)$$

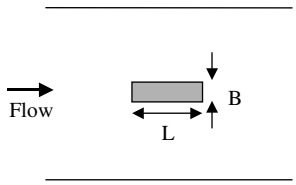

Figure 6.15. Problem definition for the shape effect.

6.11 ATTACK ANGLE EFFECT: NUMERICAL SIMULATION RESULTS

The objective of this parametric study was to obtain the relationship between the maximum bed shear stress τ_{max} and the angle of attack α defined as the angle between the flow direction and the pier direction (Figure 6.22). One of the flume experiments was chosen to perform the numerical simulation. A rectangular pier with a width of 0.061 m was placed vertically in a 1.5-m-wide flume. The velocity was 0.33 m/s, the aspect ratio of the pier was $L/B = 4$, and the water depth was 0.375 m. Four different attack angles were investigated: α = 15, 30, 45, and 90 degrees. Based on this data, the value of the Reynolds Number based on the width of the rectangular pier was $R_e = 20130$ and the Froude Number based on the width of the rectangular pier was $F_r = 0.4267$.

The bed shear stress distributions for attack angles of 15, 30, and 45 degrees are shown in Figures 6.23 to 6.25. These figures indicate that the value of the maximum bed shear

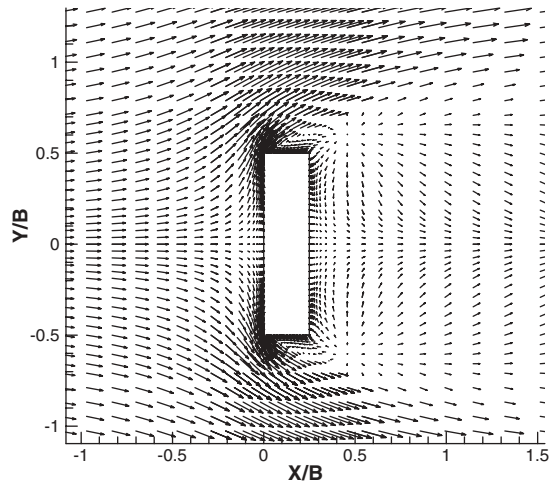

Figure 6.16. Velocity field around a rectangular pier with L/B = 0.25.

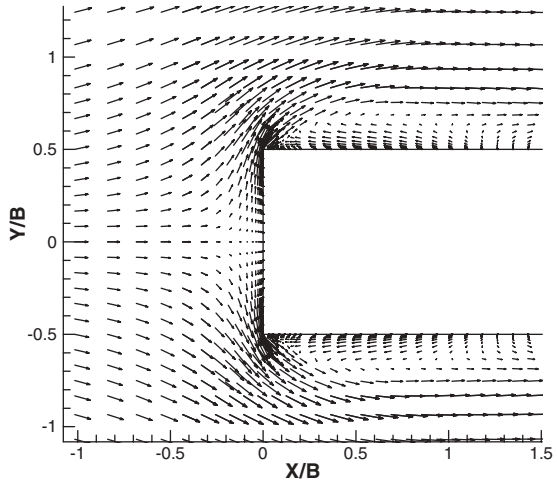

Figure 6.17. Velocity field around a rectangular pier with L/B = 4.

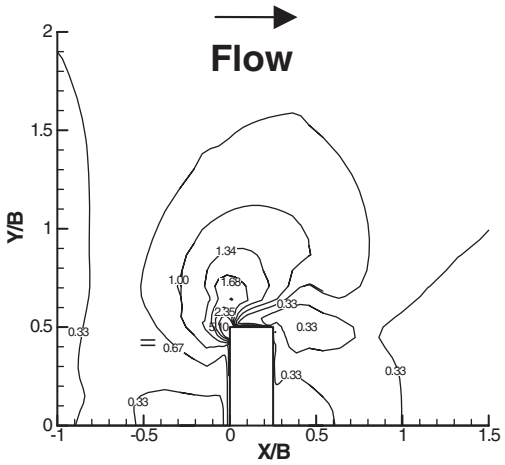

Figure 6.18. Bed shear stress contours (N/m^2) around a rectangular pier (L/B = 0.25).

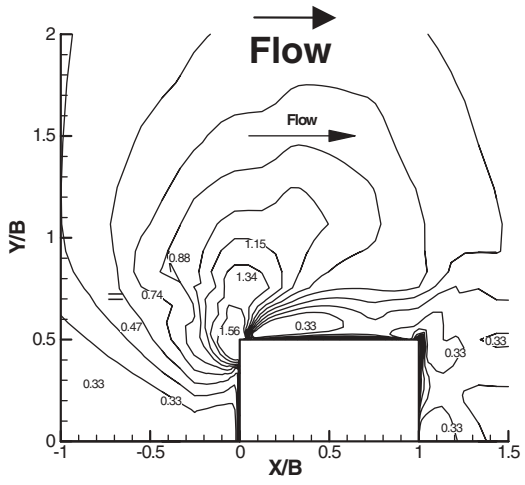

Figure 6.19. Bed shear stress contours (N/m^2) around a rectangular pier (L/B = 1).

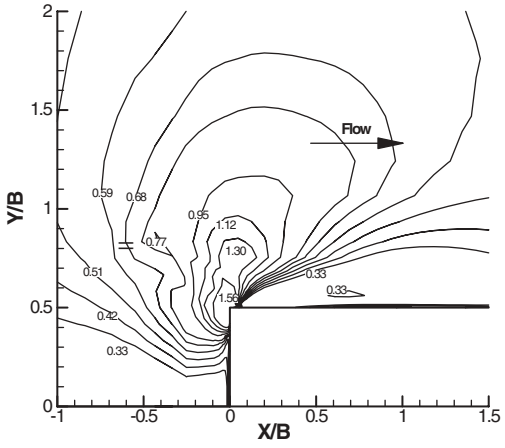

Figure 6.20. Bed shear stress contours (N/m^2) around a rectangular pier (L/B = 4).

stress tends to increase with the attack angle. They also show that the location of the maximum shear stress moves backward along the side of the pier as the attack angle increases.

6.12 ATTACK ANGLE EFFECT ON MAXIMUM SHEAR STRESS

The maximum shear stress τ_{max} is the maximum shear stress that exists on the riverbed just before the scour hole starts to develop. One way to present the data is to plot $\tau_{max}/\tau_{max(0\ degree)}$ as a function of α (Figure 6.26). The parameter $\tau_{max(0\ degree)}$ is the value of τ_{max} for the case of a pier in line with the flow in deep water and is given by Equation 6.1. The attack angle correction factor, k_{sh}, is the ratio $\tau_{max}/\tau_{max(0\ degree)}$. The data points on Figure 6.21 correspond to the results of the five numerical simulations. By regression, the equation

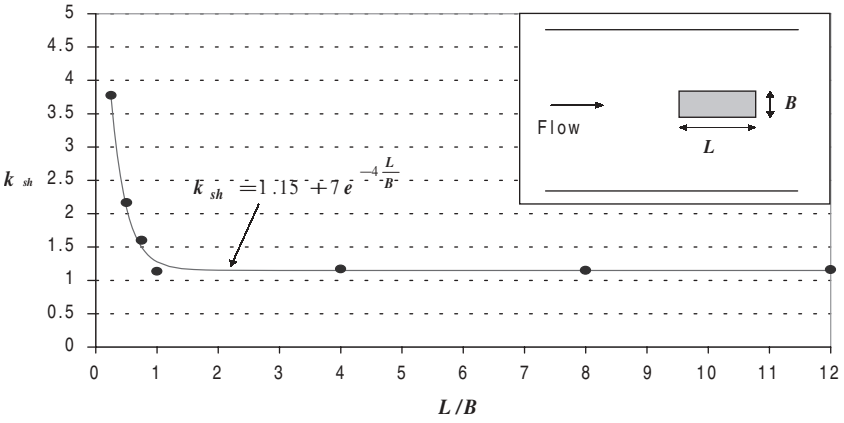

Figure 6.21. Relationship between k_{sh} ($= \tau_{max}/\tau_{max(circle)}$) and L/B for deep water (H/B > 2).

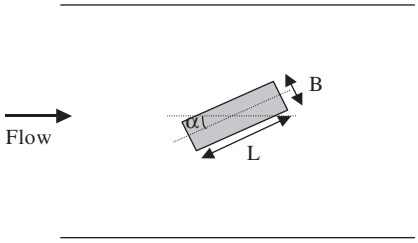

Figure 6.22. Definition of the angle of attack problem.

proposed for the correction factor k_a giving the influence of the attack angle on the maximum bed shear stress is

$$k_a = \frac{\tau_{\max}}{\tau_{\max}(0\ \text{deg})} = 1 + 1.5\left(\frac{\alpha}{90}\right)^{0.57} \tag{6.5}$$

6.13 MAXIMUM SHEAR STRESS EQUATION FOR COMPLEX PIER SCOUR

In the previous sections, individual effects on the maximum shear stress are studied by numerical simulations. A series of figures and equations are given to quantify the corresponding correction factors. However, bridge piers are likely to exhibit a combination of these effects and recommendations are needed to combine these effects in the calculations. It is recommended that the correction factors be multiplied in order to represent the combined effect. This common approach implies that the effects are independent and has been used in many instances.

The proposed equation for calculating the maximum shear stress for a complex pier before the scour process starts is

$$\tau_{\max} = k_w k_{sp} k_{sh} k_a \times 0.094 \rho V^2 \left[\frac{1}{\log \mathrm{Re}} - \frac{1}{10}\right] \tag{6.6}$$

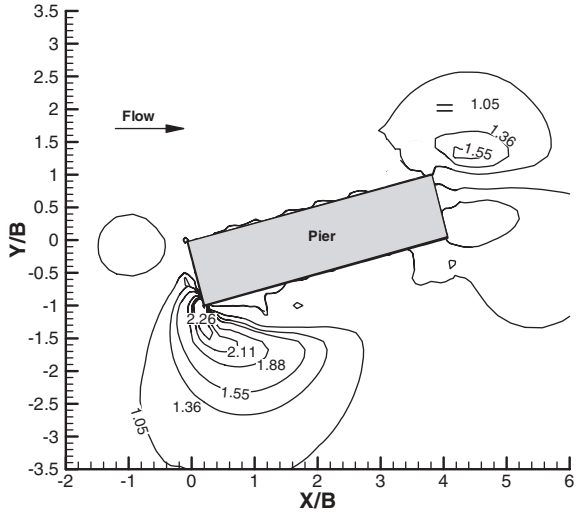

Figure 6.23. Bed shear stress (N/m^2) contours for an attack angle equal to 15 degrees.

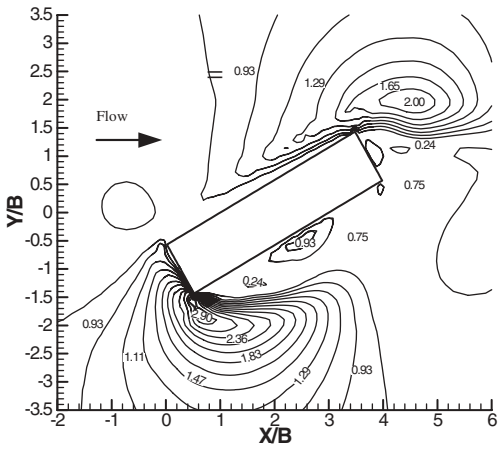

Figure 6.24. Bed shear stress (N/m^2) contours for an attack angle equal to 30 degrees.

where

- B is the pier width (m);
- H is the water depth (m);
- V is the upstream velocity (m/s);
- ρ is the density of water (kg/m^3);
- α is the attack angle (in degrees);
- R_e is the Reynolds Number, defined as $R_e = \frac{VB}{v}$;
- v is the kinematic viscosity (m^2/s);
- k_w is the correction factor for the effect of water depth, defined as $k_w = \frac{\tau_{max}}{\tau_{max}(deep)}$ and the equation is $k_w = 1 + 16e^{-\frac{4H}{B}}$;
- k_{sp} is the correction factor for the effect of pier spacing, defined as $k_{sp} = \frac{\tau_{max}}{\tau_{max}(\text{single})}$ and the equation is $k_{sp} = 1 + 5e^{-1.1\frac{S}{B}}$;
- k_{sh} is the correction factor for the effect of pier shape, defined as $k_{sh} = \frac{\tau_{max}}{\tau_{max}(circle)}$ and the equation is $k_{sh} = 1.15 + 7e^{-4\frac{L}{B}}$;
- $k_{sh} = 1$ for circular shape; and
- k_a is the correction factor for the effect of attack angle, defined as $k_a = \frac{\tau_{max}}{\tau_{max}(0\ \text{deg})}$ and the equation is $k_a = 1 + 1.5\left(\frac{\alpha}{90}\right)^{0.57}$

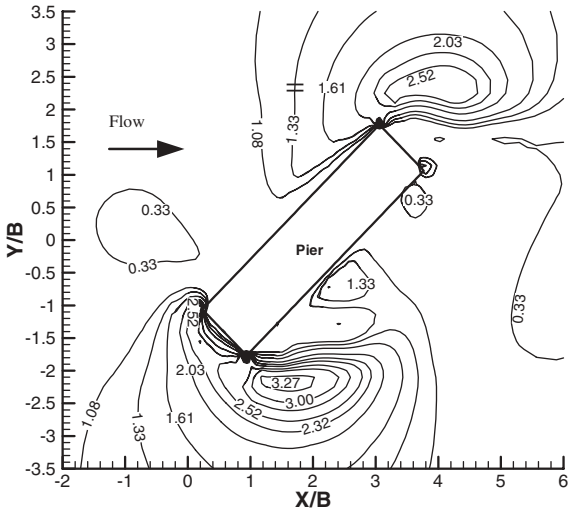

Figure 6.25. Bed shear stress (N/m^2) contours for an attack angle equal to 45 degrees.

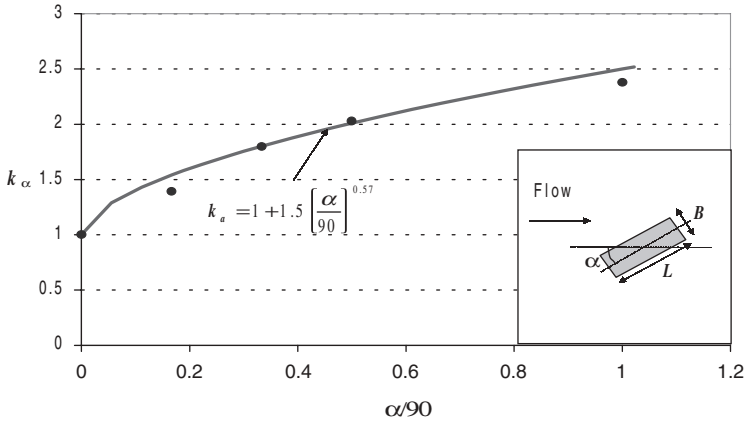

Figure 6.26. Relationship between k_a ($= \tau_{max}/\tau_{max(0\ degree)}$) and α for deep water ($H/B > 2$).

CHAPTER 7

THE SRICOS-EFA METHOD FOR MAXIMUM CONTRACTION SCOUR DEPTH

7.1 EXISTING KNOWLEDGE

Contraction scour refers to the lowering of the river bottom due to the narrowing of the flow opening between two abutments or between two bridge piers. In cohesionless soils equations are recommended by HEC-18 (1995) for live bed and clear water contraction scour depths. These equations involve one soil parameter: the mean grain size. The studies on cohesionless soils include those of Straub (1934), Laursen (1960, 1963), Komura (1966), Gill (1981), Lim (1998), Chang (1998), and Smith (1967).

For cohesive soils, two methods were found in the literature: Chang and Davis, and Ivarson. Both methods are empirically based and have neither a time nor stratigraphy component. The studies on contraction scour in cohesive soils are even fewer in number than the studies on pier scour in cohesive soils.

Chang and Davis (1998) proposed a method to predict clear water contraction scour at bridges. They assumed that the maximum scour depth is reached when the critical flow velocity for the bed material is equal to the average velocity of the flow. The critical velocity is defined as the velocity that causes the incipient motion of the bed particles. The method makes use of Neill's (1973) competent velocity concept, which is tied to the mean grain size D_{50}. A series of equations to predict the total depth of flow, including the maximum contraction scour depths, is proposed. The equations involve two parameters: the unit discharge at the contraction and the mean grain size.

Ivarson et al. (1996) (cited from Ivarson, 1998) developed an equation to predict contraction scour for cohesive soils based on Laursen's non-cohesive soils contraction scour equation. Ivarson et al. set the shear stress in the contracted section equal to the critical shear stress at incipient motion. For cohesive soils, they use the relationship between critical shear stress and unconfined compressive strength (Flaxman, 1963). Ivarson et al. propose an equation that includes the following parameters: the undrained shear strength of the soil, the water depth in the approach uncontracted channel, the discharge per unit width in the contracted channel, and Manning's Coefficient in the contracted channel.

7.2 GENERAL

This chapter addresses the problem of contraction scour (Figure 7.1). When contraction of the flow occurs and if the bed shear stress exceeds the critical shear stress of the cohesive soils, contraction scour develops and the contraction scour profile looks like that shown in Figure 7.1. This profile identifies two separate scour depths: the maximum contraction scour depth z_{max}, which occurs x_{max} after the beginning of the start of the contracted channel, and the uniform scour depth z_{unif}, which occurs after that.

As described in this chapter, a series of flume tests were performed to develop equations to predict the values of z_{max}, x_{max}, and z_{unif} in cohesive soils. One of the inputs was the mean depth velocity of the water. The velocity that controls the contraction scour was the velocity V_2 in the contracted channel; this velocity can be estimated by using the velocity in the uncontracted channel and the contraction ratio B_2/B_1 or by using a program such as HEC-RAS to obtain V_2 directly. These two approaches were developed in the analysis of the flume tests. In Chapter 8, the contraction scour rate issue is addressed through numerical simulation to obtain the initial shear stress before scour starts.

7.3 FLUME TESTS AND MEASUREMENTS

The flume used for the contraction tests was the 0.45-m-wide flume because initial tests in the 1.5-m-wide flume led to very large amounts of soil loss. The budget and the schedule did not allow the use of such large quantities of soil. The parameters influencing the contraction scour were the mean depth approach velocity V_1, the contraction ratio B_2/B_1, the approach water depth H_1, the contraction or abutment transition angle θ, the contraction length L, and the soil properties. In this research, a Porcelain clay, as described in Chapter 4, was used for all flume tests. The erosion function of the clay has been described previously in Section 5.5 and Figure 5.6.

The most important parameters were considered to be V_1, B_2/B_1, and H_1 and led to the main part of the equation. The influence of the transition angle θ and the contraction length L were incorporated through the correction factors. Therefore, the tentative form of the equation to predict the contraction depth Z (Z_{max} or Z_{unif}) is

$$Z = K_\theta K_L f\left(V_1, \frac{B_2}{B_1}, H_1\right) \tag{7.1}$$

Where, K_θ and K_L are the correction factors for transition angle and contraction length, respectively.

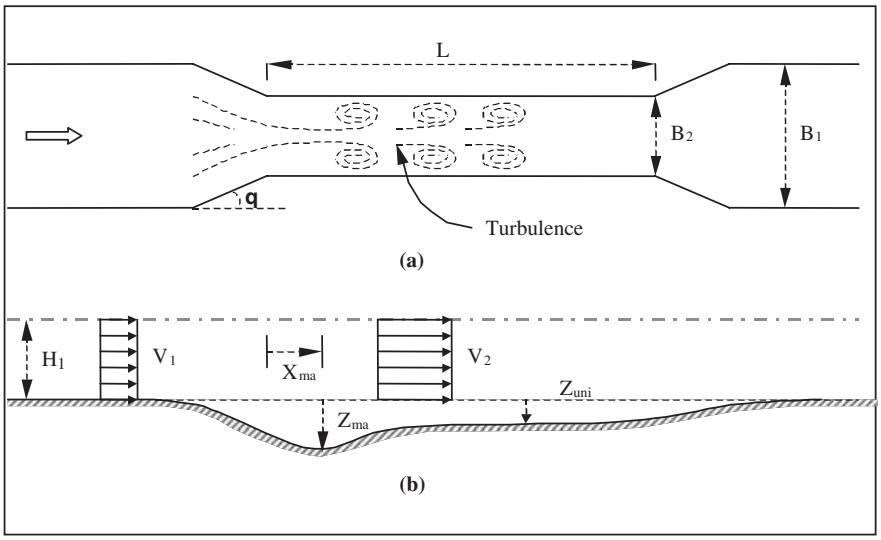

Figure 7.1. Concepts and definitions in contraction scour.

Based on the above analysis, the flume tests were divided into two parts: the tests run to obtain the function $f(V_1, B_2/B_1, H_1)$, called primary tests, and the tests run for the correction factors K_θ and K_L, called secondary tests The contraction geometries were shown in Section 5.3 and in Figure 5.4. The parameters for the tests performed are listed in Table 7.1 (primary tests) and Table 7.2 (secondary tests). There were seven primary tests where the contraction scour was generated in a long, contracted channel with a 90-degree transition angle. Among them, the contraction ratio was varied in Tests 1, 2, and 3; the water depth was varied in Tests 4, 5, and 6; and the velocity was varied in Tests 2, 6, and 7. There were two groups of secondary tests: Tests 2, 9, 10, and 11 were for the transition angle effect on contraction scour, and Tests 2, 12, 13, and 14 were for the contraction length effect on contraction scour.

The following measurements were carried out for each flume test:

1. Initial velocity distribution by ADV: vertical velocity profile in the middle of the channel at a location of 1.2 m upstream of the contraction and the longitudinal profile along the centerline of the channel;
2. Initial water surface elevation along the centerline of the channel (measured using a point gage);
3. Contraction scour profile along the centerline of the bottom of the channel, as a function of time (measured using a point gage);
4. Two abutment scour measurements, as a function of time (measured using a point gage);
5. Final longitudinal velocity profile along the channel centerline (measured using the ADV);
6. Final water surface elevation along the channel centerline (measured using a point gage); and
7. Photos of the final scour hole shape (taken by a digital camera).

7.4 FLUME TESTS: FLOW OBSERVATIONS AND RESULTS

The water surface profiles along the channel centerline at the beginning and at the end of Test 2 are plotted in Figure 7.2. The approaching flow of Test 2 was in the subcritical flow regime (all tests were subcritical except Test 1, which was supercritical at the beginning of the test); as a result, there was a drop in water surface elevation in the contracted section. This

TABLE 7.1 Parameters and results for the primary contraction scour tests

Test No.	V_1 (before) (cm/s)	V_1 (after) (cm/s)	V (Hec) (cm/s)	B_2/B_1	H_1 (before) (mm)	H_1 (after) (mm)	H (Hec) (mm)	θ (°)	L/B_1	Z_{max} (mm)	Z_{unif} (mm)	X_{max} (mm)
1	13.8	34.1	103	0.25	297	164.77	170	90	2.932	357.143	227.273	80
2	29	31	67	0.5	171.15	162.03	150	90	3.868	116.279	70.423	285
3	45	45.9	79	0.75	121.6	106.4	100	90	3.38	72.993	47.847	620
4	20.5	20.5	53	0.5	108.2	108.22	100	90	3.38	28.653	11.862	210
5	20.5	20.7	41	0.5	251.4	251.4	240	90	3.38	37.736	19.881	210
6	20.5	20.5	46	0.5	171.76	171.76	160	90	3.38	36.101	13.021	210
7	39	39	84	0.5	174.19	174.19	160	90	3.38	142.857	142.857	210

TABLE 7.2 Parameters and results for the secondary contraction scour tests

Test No.	V_1 (before) (cm/s)	V_1 (after) (cm/s)	V (Hec) (cm/s)	B_2/B_1	H_1 (before) (mm)	H_1 (after) (mm)	H (Hec) (mm)	θ (°)	L/B_1	Z_{max} (mm)	Z_{unif} (mm)	X_{max} (mm)
2	29	31	67	0.5	171.15	162.03	150	90	3.868	116.279	70.423	285
9	30	30.2	68	0.5	161	160.21	150	15	3.868	90.909	-----	785
10	30	30.2	78	0.5	153.6	152	110	45	3.38	128.205	95.234	385
11	30	29.3	69	0.5	166.59	163.25	150	60	3.38	80	41.322	785
12	29	33	75	0.5	172.37	160.5	130	90	0.844	111.11	-----	85
13	29.2	33	72	0.5	170.54	162.34	140	90	0.25	128.21	-----	152
14	29.2	34.1	70	0.5	180	164.77	140	90	0.125	208.33	-----	385

difference decreased as contraction scour developed. When the equilibrium scour depth profile was reached, the water surface elevation in the contracted section could be considered as level with the water surface elevation in the approach channel. This observation is also mentioned by other researchers (Laursen 1960, Komura 1966). As a result, the contraction scour depth can be simply calculated by subtracting the upstream water depth H_1 from the total water depth in the contraction section H_2. At equilibrium contraction scour, the contraction scour depth is

$$Z_{\max} = H_2(\text{equi}) - H_1 \tag{7.2}$$

In the final profile of the water surface elevation, it was also noticed that the upstream water surface gradually lowered to the downstream water surface. In other words, the equilibrium water surface elevation was intermediate between the initial upstream and downstream elevations.

The longitudinal velocity profiles along the channel centerline at the beginning and at the end of Test 2 are presented in Figure 7.3. The velocity was measured at a depth of 0.4 H from the water surface with the ADV. As expected, the velocity increased in the contracted channel since the water elevation decreased. As contraction scour deepened, the difference decreased but did not become zero. Instead, it was observed that the final value of the velocity in the contracted channel reached the same approximate value for all flume tests on the Porcelain clay. This tends to indicate that contraction scour stops at the critical velocity in the contracted channel no matter what the contraction geometry is.

$$V_2(\text{equi}) = V_c \tag{7.3}$$

It also was observed that the highest velocity and the lowest water surface elevation in the contracted channel happened at the same approximate location behind the contraction inlet, but this location was different from the maximum contraction scour location as described later.

HEC-RAS (Hydraulic Engineering Center—River Analysis System, 1997) is a widely used program in open channel analysis. It was used with the flume cross-section profiles before scour started to predict the quantities measured during the tests. The HEC-RAS outputs are listed in Tables 7.1 and 7.2 and compared with the measured water surface elevation and velocity profiles in Figures 7.2 and 7.3. It is found that HEC-RAS leads to relatively constant values of the water surface elevation and velocity before and after the contraction, which is a significant simplification of the measured behavior.

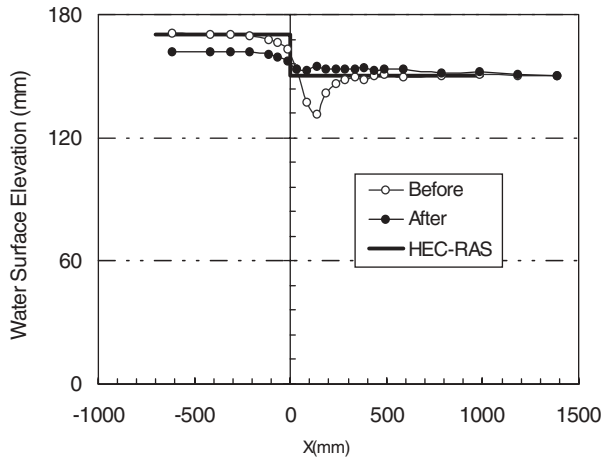

Figure 7.2. Water surface elevations along the channel centerline in Test 2.

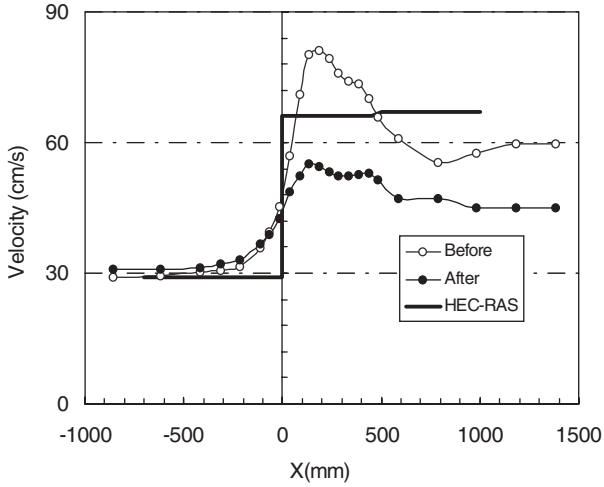

Figure 7.3. Velocity distribution along the channel centerline in Test 2.

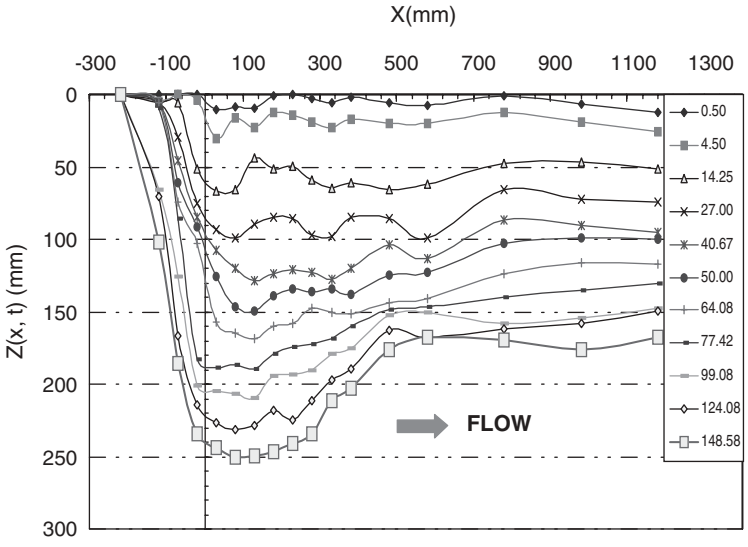

Figure 7.4. Contraction scour profiles along the channel centerline as a function of time for Test 1 (the numbers in the legend are the elapsed times in hours).

It is also noted that the maximum velocity predicted by HEC-RAS in the contracted channel is less than the measured value.

7.5 FLUME TESTS: SCOUR OBSERVATIONS AND RESULTS

An example of the measurement results is shown in Figure 7.4 for Test 1. Figure 7.5 shows a sketch of the contraction distribution in plan view. The measurement emphasis was placed on obtaining four parameters at the equilibrium contraction scour: the maximum contraction scour depth Z_{max}, the uniform contraction scour depth Z_{unif}, the location of the maximum contraction scour X_{max}, and the contraction profile along the channel centerline. The maximum and uniform contraction scour depths at equilibrium are listed in Tables 7.1 and 7.2. These values were obtained by fitting the scour depth versus time curve with a hyperbola and using the ordinate of the asymptote as the equilibrium value. The fit between the measured data and the hyperbola was very good for Z_{max} and Z_{unif} in Test 1, as is shown on Figures 7.6 and 7.7. The R^2 values were consistently higher than 0.99. The results of tests involving the transition angle and the length of the contraction are shown on Figures 7.8 and 7.9; Figure 7.10 regroups all of the measurements taken for the primary tests (Table 7.1).

For the uniform contraction scour depth, the average value of the last four points (over a 0.4-m span) in the contraction scour depth profile was used as the uniform scour value. In addition, it should be noted that for short contraction lengths (Tests 13 and 14), a fully developed uniform contraction did not exist. The location of the maximum contraction scour, X_{max}, is measured from the beginning of the fully contracted section. It can be seen that X_{max} oscillates at the beginning of the test but becomes fixed in the late stages. This value was chosen for X_{max} and is the one shown in Tables 7.1 and 7.2.

An important observation was noted during the tests: the abutment scour never added itself to the contraction scour. In fact, the abutment scour and the contraction scour were of the same order of magnitude. Figure 7.11 shows the different

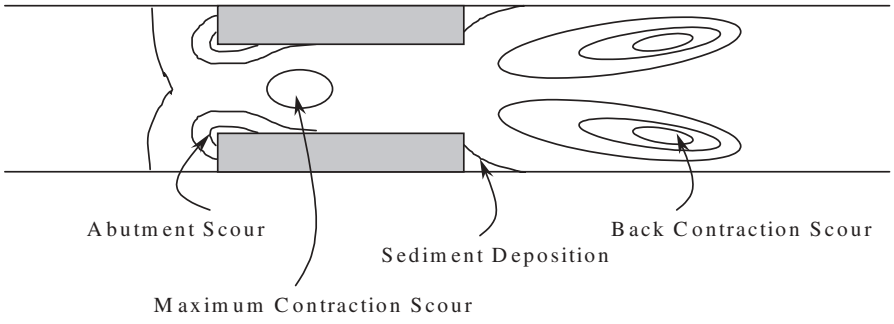

Figure 7.5. Plan view sketch of the contraction scour pattern.

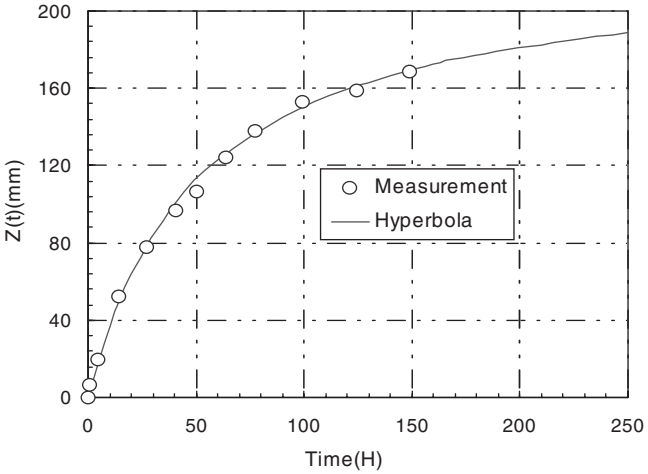

Figure 7.6. Maximum contraction scour and hyperbola model for Test 1.

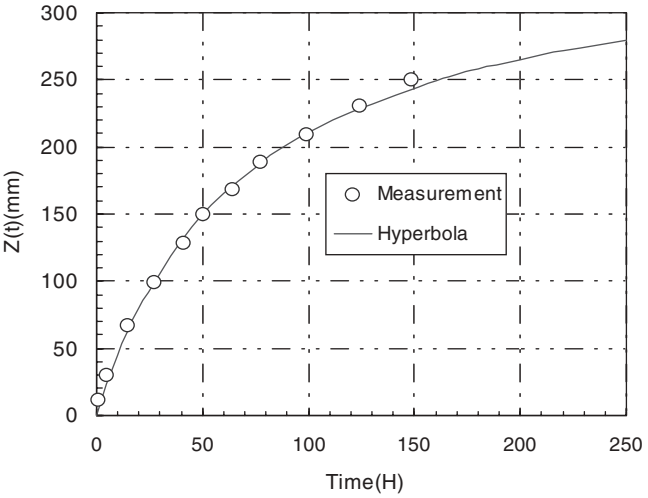

Figure 7.7. Uniform contraction scour and hyperbola model for Test 1.

configurations that occurred during the tests. If the combination of contraction ratio and transition angle is small, then the contraction scour is downstream from the contraction inlet and the abutment scour exists by itself at the contraction inlet. If the combination of contraction ratio and transition angle is medium, the abutment scour and the contraction scour occur within the same inlet cross section but do not overlap. If the combination of contraction ratio and transition angle is severe, the abutment scour and the contraction scour overlap but do not add to each other.

7.6 MAXIMUM AND UNIFORM CONTRACTION DEPTHS FOR THE REFERENCE CASES

The reference case for the development of the basic equation is the case of a 90-degree transition angle and a long contraction length ($L/B_2 > 2$, Figure 7.5). The maximum depth of contraction scour Z_{max} is the largest depth that occurs along the contraction scour profile in the center of the contracted channel. The uniform contraction scour depth Z_{unif} is the scour depth that develops in the contracted channel far from the transition zone (Figure 7.1).

The Reynolds Number (inertia force/gravity force) and the Froude Number (inertia force/viscous force) were used as basic correlation parameters. Both Z_{max} and Z_{unif} were normalized with respect to H_1, the upstream water depth. Figure 7.12 shows the attempt to correlate the contraction scour depths to the Reynolds Number defined as V_1B_2/υ. As can be seen, the Reynolds Number is not a good predictor of the contraction scour depths. Figures 7.13 and 7.14 show the correlation with the Froude Number. Although there are only seven points for the correlation, the results are very good.

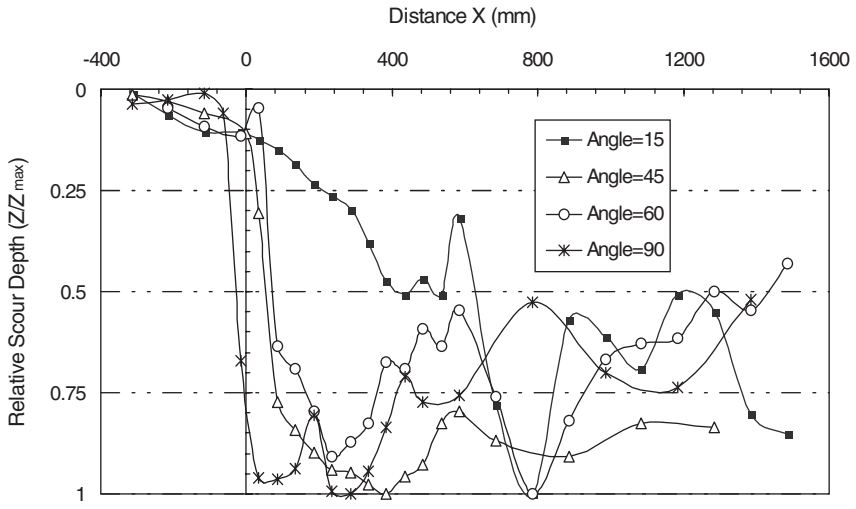

Figure 7.8. Contraction scour profile along the channel centerline for transition angle effect.

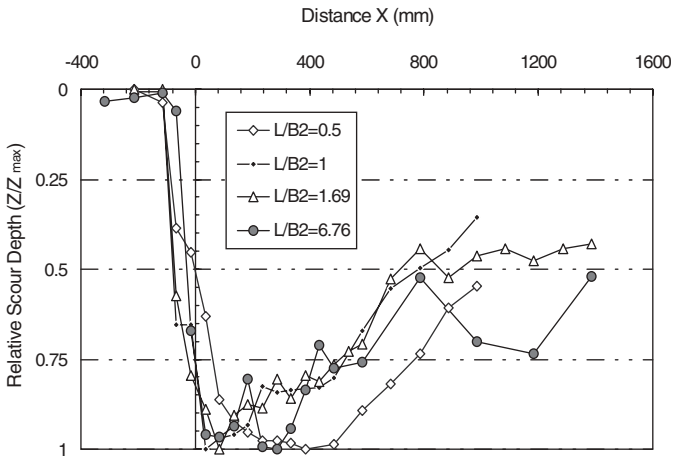

Figure 7.9. Contraction scour profile along the channel centerline for contraction length effect.

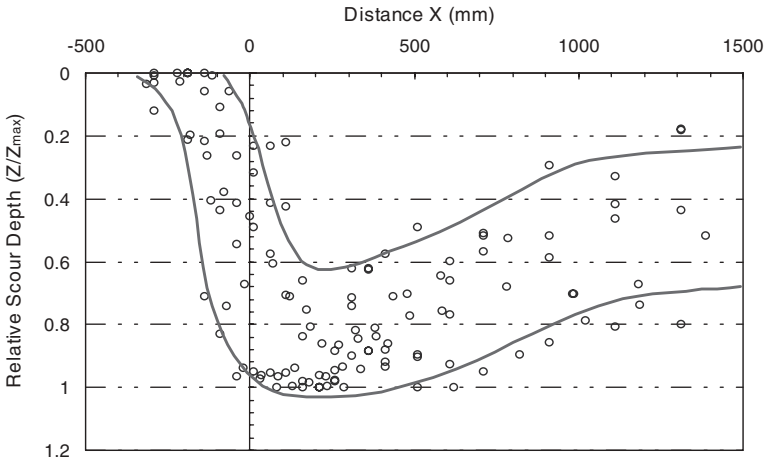

Figure 7.10. Contraction scour profiles along the channel centerline for standard tests.

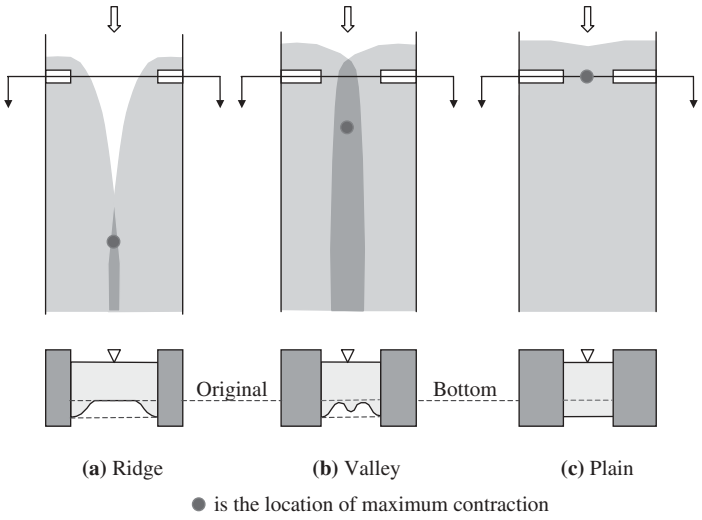

Figure 7.11. Overlapping of scour for contraction scour and abutment scour.

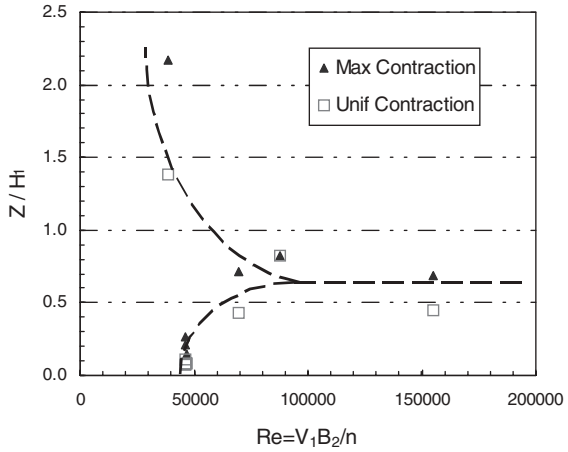

Figure 7.12. Correlation attempt between contraction scour depth and Reynolds Number.

The Froude Number was calculated as follows. From simple conservation, we have $V_1B_1H_1 = V_2B_2H_2$. Because the water depth H_2 may not be known for design purposes and because other factors may influence V_2, the velocity used for correlation purposes was simply V_1B_1/B_2. As will be seen later, a factor will be needed in front of V_1B_1/B_2 for optimum fit.

$$V^* = V_1B_1/B_2 \tag{7.4}$$

Then the Froude Number was calculated as

$$\mathrm{Fr}^* = (V_1B_1/B_2)/(gH_1)^{0.5} \tag{7.5}$$

The relationship between the critical shear stress and the critical velocity for an open channel was established (Richardson et al., 1995).

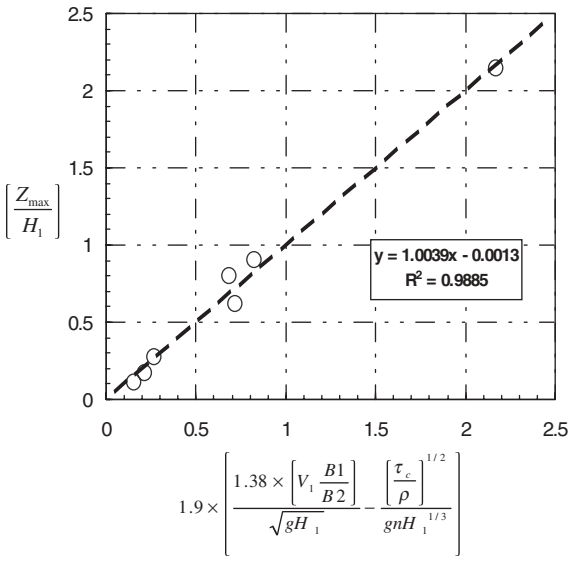

Figure 7.13. Normalized maximum contraction scour depth versus Froude Number.

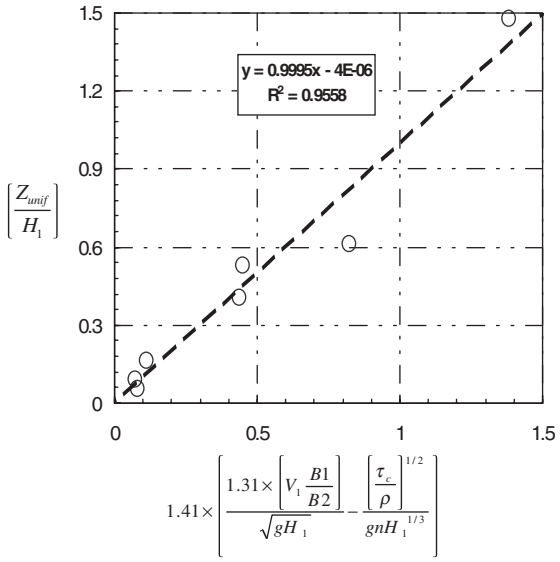

Figure 7.14. Normalized uniform contraction scour depth versus Froude Number.

$$\tau_c = (\rho g n^2 V_c^2)/(H_1)^{0.33} \tag{7.6}$$

So the critical Froude Number can be written as

$$\mathrm{Fr}_c = V_c/(gH1)^{0.5} = (\tau_c/\rho)^{0.5}/(gnH1)^{0.33} \tag{7.7}$$

The contraction scour depths are likely to be proportional to the difference (Fr-Fr$_c$). However, as mentioned before, the velocity used to calculate Fr may require a factor β. The final form of the equation sought was

$$Z/H_1 = \alpha(\beta \mathrm{Fr}^* - \mathrm{Fr}_c) \tag{7.8}$$

The factors α and β were obtained by optimizing the R^2 value in the regression on Figures 7.13 and 7.14. The proposed equations are

$$\frac{Z_{\max}}{H_1} = 1.90\left(\frac{1.38\left(V_1\frac{B_1}{B_2}\right)}{\sqrt{gH_1}} - \frac{\left(\frac{\tau_c}{\rho}\right)^{1/2}}{gnH_1^{1/3}}\right) \tag{7.9}$$

$$\frac{Z_{\mathrm{unif}}}{H_1} = 1.41\left(\frac{1.31\left(V_1\frac{B_1}{B_2}\right)}{\sqrt{gH_1}} - \frac{\left(\frac{\tau_c}{\rho}\right)^{1\,2}}{gnH_1^{1/3}}\right) \tag{7.10}$$

where $Z_{\max}$ is the maximum depth of contraction scour; H_1 is the upstream water depth after scour has occurred; V_1 is the mean depth upstream velocity after the contraction scour has occurred; B_1 is the upstream channel width; B_2 is the contracted channel width; g is the acceleration due to gravity; τ_c is the critical shear stress of the soil (obtained from an EFA test); ρ is the mass density of water; and n is the Mannings Coefficient. Note that V_1 and H_1 are the upstream velocity

and water depth after contraction scour has occurred. The difference between the V_1 and H_1 values before and after contraction scour is small in most cases and, except for in Test 1, the correlations were good when using the values of V_1 and H_1 before the contraction scour occurred. Test 1 had a very small contraction ratio (B_2/B_1 = 0.25) and an initial supercritical flow, whereas all other tests had larger contraction ratios and an initial subcritical flow. In the case of Test 1, Equations 7.9 and 7.10 worked only when using the values of V_1 and H_1 after contraction scour had occurred. This use of values after scour occurs is consistent with the approach taken by other researchers (Laursen, 1960,1963; Komura, 1966; Gill, 1981; and Lim 1998).

The value of the β factor is shown as a function of the contraction ratio for all of the flume contraction tests on Figure 7.15. An average value of 1.38 was chosen for Z_{max} and 1.31 for Z_{unif}. Since β should be equal to 1 when B_2/B_1 is equal to 1 (no contraction), the best-fit line on Figure 7.15 should go through that point. It was decided to achieve that result as shown on Figure 5.15.

An attempt was made to find a relationship between Z_{unif} and Z_{max}. The following equation gave a high R^2 value:

$$Z_{unif}/Z_{max} = 4\,\mathrm{Fr} \qquad \text{where } \mathrm{Fr} = V_1/(gB_1)^{0.5} \tag{7.11}$$

7.7 LOCATION OF MAXIMUM CONTRACTION DEPTH FOR THE REFERENCE CASES

Knowledge of the location of the maximum contraction scour depth is very important for the design of a bridge. Indeed, the bridge is usually a fairly narrow contraction and the maximum contraction scour depth in this case can be downstream from the bridge site. Based on the flume test observations, the maximum contraction scour generally occurs close to and behind the opening of the contraction. For the primary tests, the data listed in Tables 7.1 and 7.2 indicate that X_{max} is mostly controlled by the contracted channel width B_2 and the contraction ratio B_2/B_1. The wider the contraction opening is, the bigger the X_{max} is (Figure 7.16). Figure 7.17 shows the relationship between X_{max}/B_2 versus B_2/B_1. By regression, the best-fit equation for X_{max} is

$$\frac{X_{max}}{B_2} = 2.25\,\frac{B_2}{B_1} + 0.15 \tag{7.12}$$

Equation 7.12 indicates that the location of the maximum depth of contraction scour is independent of the velocity and, therefore, remains constant during the period associated with a hydrograph. This means that an accumulation method such as the SRICOS Method can be used to predict the maximum

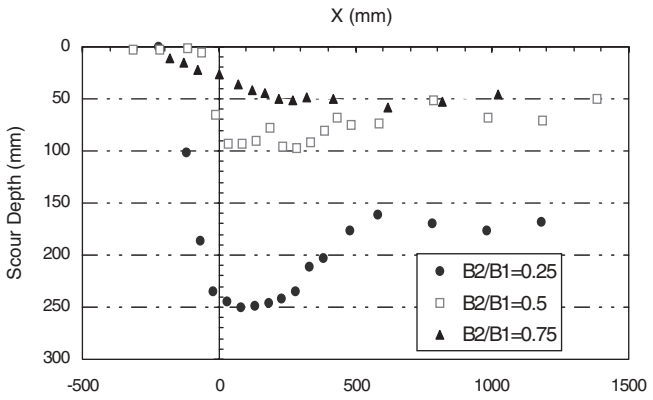

Figure 7.16. Influence of the contraction ratio on the longitudinal scour profile.

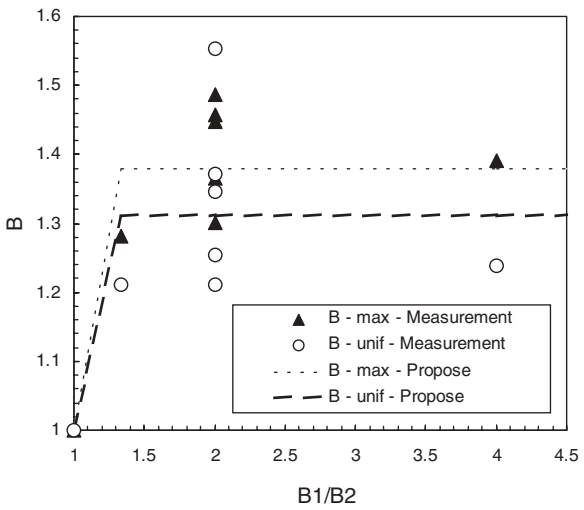

Figure 7.15. The factor β as a function of the contraction ratio.

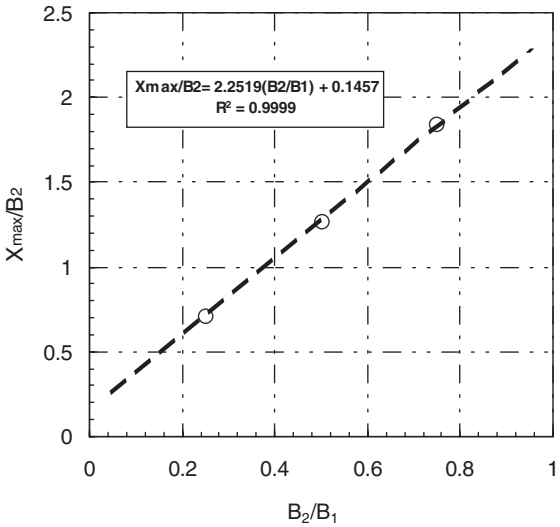

Figure 7.17. Relationship between X_{max} and the contraction geometry.

depth of contraction scour after the bridge site has been subjected to a long-term hydrograph.

7.8 CORRECTION FACTORS FOR TRANSITION ANGLE AND CONTRACTION LENGTH

There are seven secondary tests listed in Table 7.2. Tests 2, 9,10, and 11 are for the transition angle effect, and Tests 2, 12, 13, and 14 are for the contraction length effect. Test 2 is the reference case for both groups and comparisons to Test 2 are used to derive the correction factors for the equations that give Z_{max}, Z_{unif}, and X_{max}.

A smooth transition angle is generally built to ease the effect of the approaching flow (Figure 7.18). As can be seen, the approaching flow runs against the abutments and then is guided toward the contracted channel at an angle related to the transition angle θ. The location of the maximum contraction scour depth will be pushed further back from the contraction inlet when the transition angle becomes smoother. Even though the transition angle can change the local flow pattern around the contraction inlet, this influence decreases into the contraction channel where a uniform flow develops. This indicates that the transition angle may affect the maximum contraction scour but not the uniform contraction scour.

Figure 7.19 shows the influence of the transition angle θ on the maximum contraction scour depth Z_{max}. It can be seen that θ does not have a clear impact on Z_{max}. This observation is consistent with Komura's (1977) observation on sands where he stated that a smooth transition angle was not helpful in reducing the scour depth around the abutment inlets. If Test 10 is ignored due to its odd scour profile, the uniform contraction scour depth Z_{unif} is practically independent of the transition angle θ (Figure 7.20), as expected. However, the transition angle has a significant impact on the location of the maximum contraction scour X_{max}, as shown in Figure 7.21. Regression analysis of the data leads to the following relationship between the X_{max} and θ:

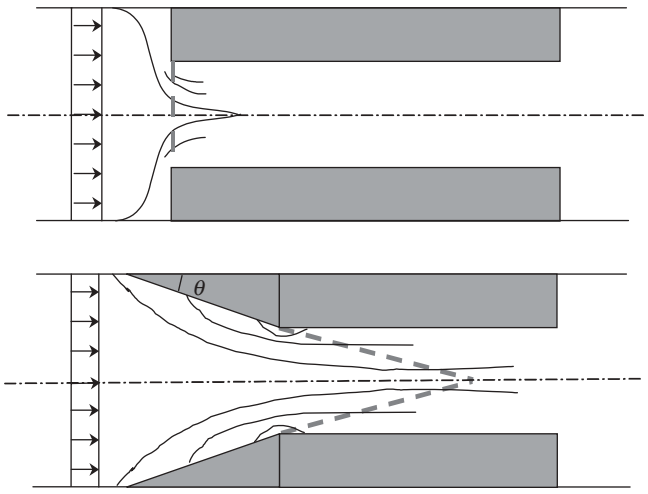

Figure 7.18. Flow around contraction inlets.

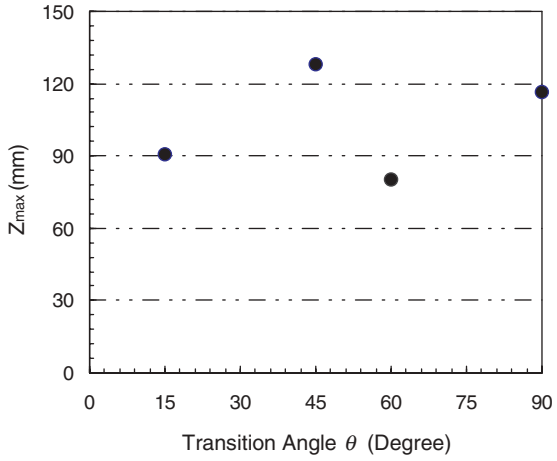

Figure 7.19. Transition angle effect on maximum contraction scour depth.

$$\frac{X_{max}(\theta)}{X_{max}(90°)} = 0.4793/\tan\theta + 0.9475 \tag{7.13}$$

Figure 7.18 indicates that X_{max} is at $(B_2/2)/\tan\theta$ if the flow follows the prolongation of the transition sides, but Equation 7.13 shows that the real location of the maximum contraction scour is farther downstream of this estimated point.

In summary, if Test 2, the test with the 90-degree transition angle, is selected as the reference case for the transition angle effect, and the correction factors are calculated as the ratios between the value for θ over the value for 90 degrees, the transition angle effect for contraction scour, in three aspects of Z_{max}, Z_{unif}, and X_{max}, is

$$\begin{cases} K_{\theta/Z_{max}} = 1.0 \\ K_{\theta/Z_{unif}} = 1.0 \\ K_{\theta/X_{max}} = 0.48/\tan\theta + 0.95 \end{cases} \tag{7.14}$$

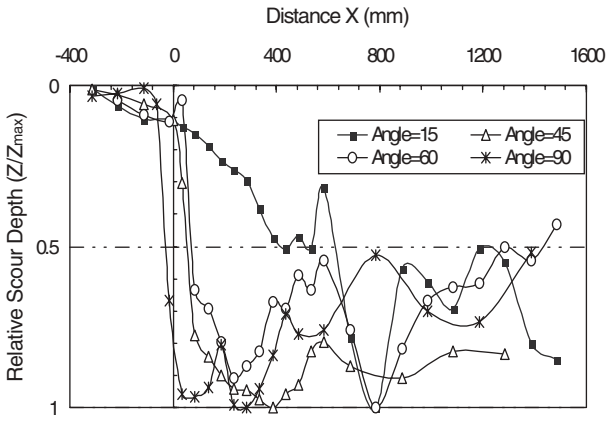

Figure 7.20. Transition angle effect on scour profile and uniform contraction scour.

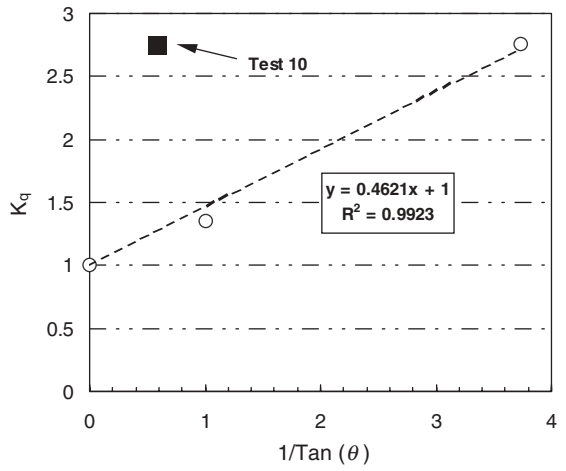

Figure 7.21. Transition angle effect on the location of the maximum scour depth.

Bridge contractions are often short, and the abutments work like a thin wall blocking the flow. The uniform contraction scour depth cannot develop under these conditions. Instead, two back contraction scour holes behind the contracted section can develop (Figure 7.5). Further, as shown in Figure 7.9, when the contraction length is between $6.76B_2$ and $0.5B_2$, the maximum depth of contraction scour Z_{max} and the location of that depth X_{max} are unaffected by the length of the contracted channel. If the long contraction channel of Test 2 is chosen as the reference case, the correction factors K_L for contraction length are

$$\begin{cases} K_{L/Z_{max}} = 1.0 \\ K_{L/Z_{unif}} = void \\ K_{L/X_{max}} = 1.0 \end{cases} \tag{7.15}$$

Test 14 has the shortest contraction length with L/B_1 = 0.125. The maximum scour depth is 1.79 times the scour depth in Test 2, and X_{max} is also multiplied at the same time. This situation is very like the "thin wall" pier scour. Therefore, when L/B_2 is smaller than 0.25, it is necessary to increase the predicted Z_{max} and X_{max} values. This case has not been evaluated in this research.

7.9 SRICOS-EFA METHOD USING HEC-RAS GENERATED VELOCITY

Equations 7.9 and 7.10, which have been proposed to calculate contraction scour depths, have a shortcoming: they are developed from tests in rectangular channels. For channels with irregular cross sections, which is the case in most real situations, some researchers have recommended the use of the flow rate ratio Q_1/Q_2 instead of the contraction ratio B_1/B_2 to account for the flow contraction (e.g., Sturm et al., 1997). Here, Q_1 is the total flow rate in the approach channel and Q_2 is the flow rate in the part of the approach channel limited by two lines representing the extensions of the banks of the contracted channel.

The approach recommended here, however, is to replace the nominal velocity V_1B_1/B_2 used in Equations 7.9 and 7.10 by the velocity V_{Hec} obtained by using a program like HEC-RAS. With this approach, the complex geometry of the approach channel can be handled by the program, and a more representative velocity can be used. The problem is to find the proper relationship between the HEC-RAS calculated velocity, V_{Hec}, and the nominal velocity V_1B_1/B_2. This was done by conducting a series of HEC-RAS analyses to simulate the flow condition in the flume tests, obtaining the resulting velocity V_{Hec}, and correlating it to V_1B_1/B_2. The velocities are listed in Tables 7.1 and 7.2 and the correlation graph is shown in Figure 7.22. Regression analysis gave the following relationship between the two variables:

$$V_{Hec} = 1.14 \cdot V_1 \cdot \frac{B_1}{B_2} \tag{7.16}$$

In this figure, the point for Test 1 is still outstanding because of the severe backwater effect during that test, which exhibited an extreme contraction case ($(B_2/B_1) = 0.25$).

Now, it is possible to rewrite Equations 7.9 and 7.10 using V_{Hec}.

For maximum contraction scour

$$\frac{Z_{max}}{H_1} = 1.9\left(\frac{1.49V_{Hec}}{\sqrt{gH_1}} - \frac{\left(\frac{\tau_c}{\rho}\right)^{1/2}}{gnH_1^{1/3}}\right) \tag{7.17}$$

For uniform contraction scour

$$\frac{Z_{unif}}{H_1} = 1.41\left(\frac{1.57V_{Hec}}{\sqrt{gH_1}} - \frac{\left(\frac{\tau_c}{\rho}\right)^{1/2}}{gnH_1^{1/3}}\right) \tag{7.18}$$

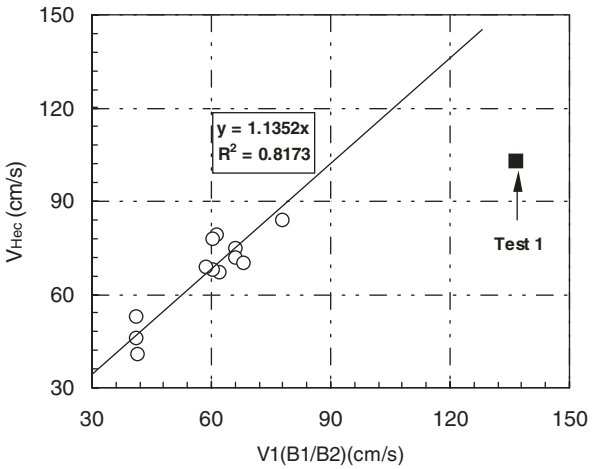

Figure 7.22. Relationship between the nominal velocity and the HEC-RAS calculated velocity.

Users of Equations 7.17 and 7.18 should be aware that the velocity V_{Hec} also has its limitations. These limitations are tied to the ability of the program HEC-RAS to simulate the flow at the contraction. As an illustration, the water surfaces and velocity distributions measured and predicted by different means along the centerline of the channel are compared for Test 2 in Figure 7.23. As can be seen, the HEC-RAS generated velocity profile cannot give the peak velocity value in the contracted channel. Instead, HEC-RAS gives a step function that parallels the bank contraction profile.

7.10 CONSTRUCTING THE COMPLETE CONTRACTION SCOUR PROFILE

Three characteristic dimensions of the contraction scour profile have been determined by the flume tests Z_{max}, Z_{unif}, and X_{max}. Additional information was obtained from the tests in order to develop a procedure to draw the complete contraction scour profile. It was found that the contraction scour hole, much like the pier scour hole, is determined by both the flow and soil strength. In the front part of the scour hole, the flow vortex can generate a steep slope that stresses the soil beyond its shear strength. Therefore, it is the soil strength that controls the front slope of the scour. At the back of the scour hole, the slope is usually gentle and slope stability is not a problem. Based on these and other observations, the following steps are recommended to draw the full contraction scour profile (Figure 7.24):

1. Plot the position of the bridge contraction, especially the start point of the full contraction;
2. Calculate X_{max} by Equations 7.13, 7.14, and 7.15, and mark the position where the maximum contraction scour happens in the figure;
3. Calculate Z_{max} by Equations 7.10, 7.14, and 7.15, draw a horizontal line at this depth and extend it 0.5 Z_{max} on both sides of the location of Z_{max} (B and C on Figure 106);
4. Plot A, the starting point of the contraction scour profile at a distance equal to Z_{max} from the starting point of the full contraction;
5. Connect A and B as the slope of the contraction scour profile before the maximum scour;
6. Calculate Z_{unif} by Equations 7.11, 7.14, and 7.15, and draw a line with an upward slope of 1 to 3 from Point C to a depth equal to Z_{unif} (D on Figure 106); Line CD is the transition from the maximum contraction scour depth to the uniform contraction scour depth.
7. Draw a horizontal line downstream from Point D to represent the uniform contraction scour.

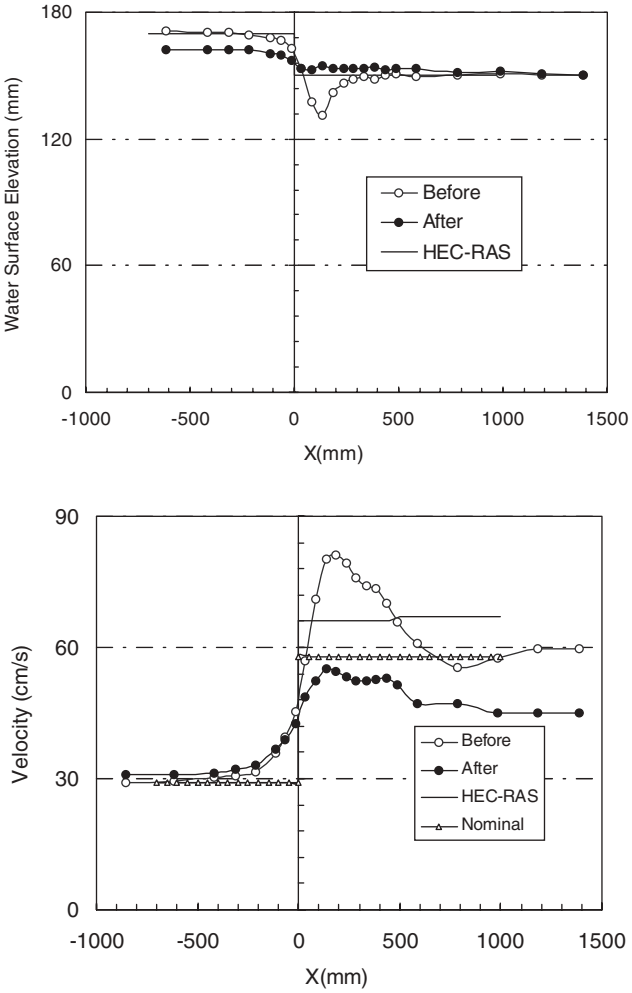

Figure 7.23. Comparison of water depth and velocity between HEC-RAS simulations and measurements for contraction Test 2.

7.11 SCOUR DEPTH EQUATIONS FOR CONTRACTION SCOUR

The following equations summarize the results obtained in this chapter.

$$Z_{max}(\text{Cont}) = K_\theta K_L \times 1.90 \left(\frac{1.38\left(V_1 \frac{B_1}{B_2}\right)}{\sqrt{gH_1}} - \frac{\left(\frac{\tau_c}{\rho}\right)^{0.5}}{gnH_1^{1/3}} \right) H_1 \geq 0 \qquad (7.19)$$

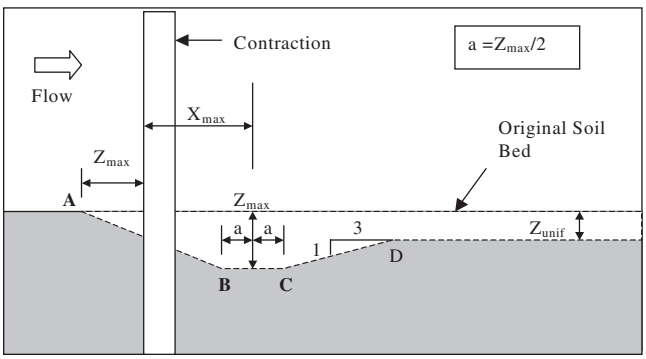

Figure 7.24. Generating the complete contraction scour profile.

$$Z_{max}(\text{Cont}) = K_\theta K_L \times 1.90 \left(\frac{1.49 V_{Hec}}{\sqrt{g H_1}} - \frac{\left(\frac{\tau_c}{\rho}\right)^{0.5}}{g n H_1^{1/3}} \right) H_1 \geq 0 \quad (7.20)$$

$$Z_{unif}(\text{Cont}) = K_\theta K_L \times 1.41 \left(\frac{1.31\left(V_1 \frac{B_1}{B_2}\right)}{\sqrt{g H_1}} - \frac{\left(\frac{\tau_c}{\rho}\right)^{0.5}}{g n H_1^{1\,3}} \right) H_1 \geq 0 \quad (7.21)$$

$$Z_{unif}(\text{Cont}) = K_\theta K_L \times 1.41 \left(\frac{1.57_{Hec}}{\sqrt{g H_1}} - \frac{\left(\frac{\tau_c}{\rho}\right)^{0.5}}{g n H_1^{1/3}} \right) H_1 \geq 0 \quad (7.22)$$

$$\frac{X_{max}}{B_2} = K_\theta K_L \times \left(2.25 \frac{B_2}{B_1} + 0.15 \right) \quad (7.23)$$

where Z_{max}(Cont) is the maximum depth of scour along the centerline of the contracted channel, Z_{unif}(Cont) is the uniform depth of scour along the centerline of the contracted channel, X_{max} is the distance from the beginning of the fully contracted section to the location of Z_{max}, V_1 is the mean velocity in the approach channel, V_{Hec} is the velocity in the contracted channel given by HEC-RAS, B_1 is the width of the approach channel, B_2 is the width of the contracted channel, τ_c is the critical shear stress as given by the EFA, ρ is the mass density of water, n is Manning's Coefficient, H_1 is the water depth in the approach channel, K_θ is the correction factor for the influence of the transition angle as given by Equation 7.24 below, and K_L is the correction factor for the influence of the contraction length as given by Equation 7.25 below.

$$\begin{cases} K_{\theta/Z_{max}} = 1.0 \\ K_{\theta/Z_{unif}} = 1.0 \\ K_{\theta/X_{max}} = 0.48/\tan\theta + 0.95 \end{cases} \quad (7.24)$$

$$\begin{cases} K_{L/Z_{max}} = 1.0 \\ K_{L/Z_{unif}} = \textit{void} \\ K_{L/X_{max}} = 1.0 \end{cases} \quad (7.25)$$

CHAPTER **8**

THE SRICOS-EFA METHOD FOR INITIAL SCOUR RATE AT CONTRACTED CHANNELS

8.1 BACKGROUND

The existing knowledge on numerical methods for scour studies was presented at the beginning of Chapter 6 (Section 6.2) and the existing knowledge on contraction scour in cohesive soils was presented at the beginning of Chapter 7 (Section 7.1).

The initial scour rate is an integral part of the SRICOS Method to predict contraction scour as a function of time because it is one of the two fundamental parameters used to describe the scour depth versus time curve. The other fundamental parameter is the maximum depth of contraction scour that was studied in Chapter 7. The initial rate of scour for a given contraction scour problem is obtained by first calculating the maximum shear stress τ_{max} existing in the contracted channel before the scour starts (flat river bottom) and then reading the initial scour rate on the erosion function obtained in the EFA test. Therefore, the problem of obtaining the initial rate of contraction scour is brought back to the problem of obtaining the maximum shear stress in the contracted channel before scour starts. This problem was solved by numerical simulations that use the chimera RANS method. This method was described in Section 6.3 and a verification of its reliability was presented in Section 6.4. This chapter describes the simulations performed and the associated results. The goal was to develop an equation for the maximum shear stress τ_{max} existing in the contraction zone.

The equation for the maximum shear stress τ_{max} at the bottom of an open channel without contraction is given by (Munson et al., 1990) as

$$\tau_{max} = \gamma n^2 V^2 R_h^{-\frac{1}{3}} \tag{8.1}$$

where γ is the unit weight of water, n is Manning's roughness coefficient, V is the mean depth velocity, and R_h is the hydraulic radius defined as the cross-section area of the flow divided by the wetted perimeter. The equation obtained for the contracted channel case should collapse to the open channel case when the contraction ratio B_2/B_1 becomes equal to 1. The objective of the numerical simulations was to obtain correction factors that would introduce the effect of the contraction ratio, the transition angle, and the length of the contracted zone.

8.2 CONTRACTION RATIO EFFECT: NUMERICAL SIMULATION RESULTS

One of the flume experiments was chosen to perform the numerical simulation. The width of the flume used was 0.45 m. The upstream flow was a steady flow with a velocity V_1 of 0.45 m/s and the upstream water depth H was 0.12 m. Three different contraction ratios were chosen: $B_2/B_1 = 0.25$, 0.5, and 0.75. In order to reduce the CPU time, a half domain was used based on the symmetry of the problem. For numerical purposes, the characteristic length B was defined as half of the flume width. Based on this definition, the value of the Reynolds Number ($R_e = VB/\nu$) was 101250 and the Froude Number $\left(Fr = V/\sqrt{gB}\right)$ was 0.303. The grid was made of four blocks as shown in Figure 8.1.

The bed shear stress contours around the abutment and in the contracted zone are shown in Figures 8.2 to 8.4. The maximum bed shear stress is found around the abutment but the maximum contraction bed shear stress τ_{max} is found along the centerline of the channel in the contracted section. As expected, it is found that the magnitude of τ_{max} increases when the contraction ratio (B_2/B_1) decreases. It is also observed that the distance X_{max} between the beginning of the fully contracted section and the location of τ_{max} increases when the contraction ratio (B_2/B_1) increases.

8.3 TRANSITION ANGLE EFFECT: NUMERICAL SIMULATION RESULTS

Again, one of the flume experiments was chosen to perform the numerical simulation. The width of the flume used was 0.45 m. The upstream flow was a steady flow with a velocity of 0.45 m/s, the contracted length L was such that $L/(B_1 - B_2) = 6.76$ and the water depth was 0.12 m. Four different transition angles were chosen for the simulations: $\alpha =$ 15, 30, 45, and 90 degrees. The width ($B_1 - B_2$) was chosen as the characteristic length B. The Reynolds Number was 101250 and the Froude Number was 0.303.

The bed shear stress contours around the abutment and in the contracted zone are shown in Figures 8.5 to 8.7. As can be seen, the magnitude of the maximum bed shear stress τ_{max} along the center of the channel in the contracted section increases when the transition angle θ increases. However the transition angle does not have a major influence on τ_{max}. It is

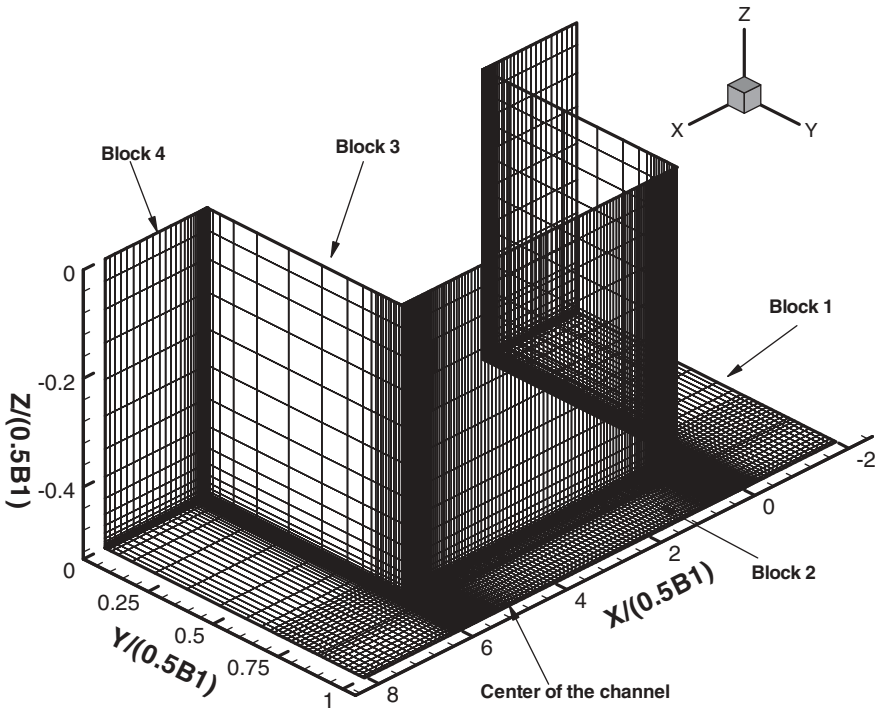

Figure 8.1. Grid system for the simulation in the case of $B_2/B_1 = 0.25$.

also observed that the distance x_{max} between the beginning of the fully contracted section and the location of τ_{max} increases when θ increases

8.4 CONTRACTED LENGTH EFFECT: NUMERICAL SIMULATION RESULTS

Again, one of the flume experiments was chosen to perform the numerical simulation. The width of the flume used was 0.45 m. The upstream flow was a steady flow with a velocity of 0.45 m/s, the contraction channel ratio ($B2/B1$) was equal to 0.5, the transition angle was 90 degrees, and the water depth was 0.12 m. Four different contraction lengths were simulated: $L/(B1 - B2) = 0.25$, 0.5, 1.0 and 6.76. The difference ($B1 - B2$) was chosen as the characteristic length B. The Reynolds Number was 101250 and the Froude Number was 0.303. The initial bed shear stress distribution around the contracted zone is shown in Figures 114 to 116 for various

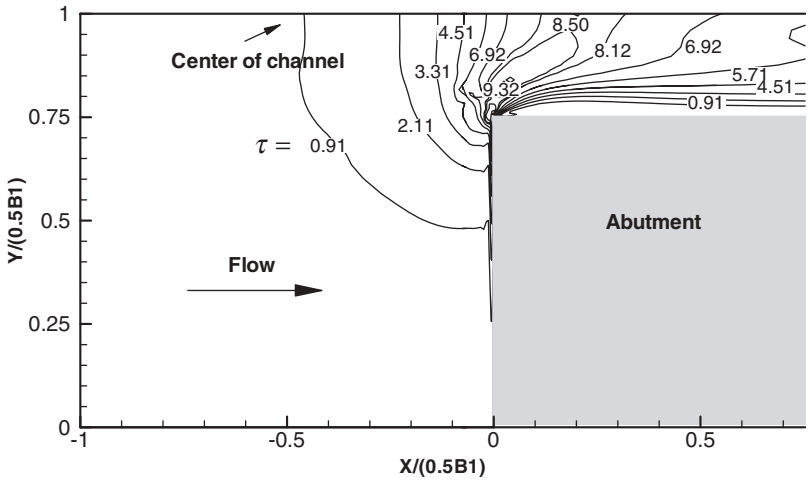

Figure 8.2. Initial bed shear stress distribution (N/m^2) for $B_2/B_1 = 0.25$ and $V = 0.45m/s$.

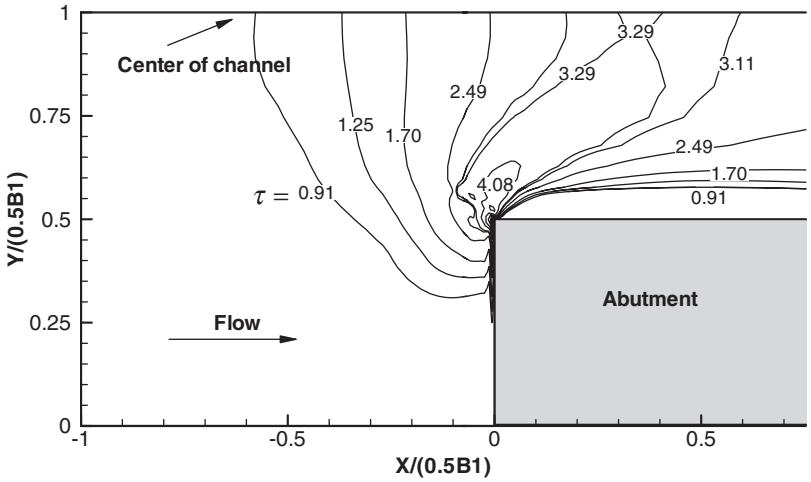

Figure 8.3. Initial bed shear stress distribution (N/m^2) for $B_1/B_2 = 0.50$ and V = 0.45m/s.

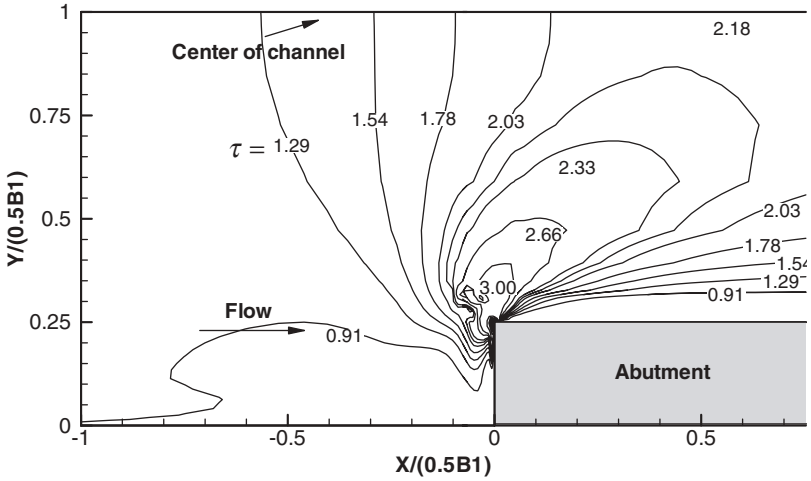

Figure 8.4. Initial bed shear stress distribution (N/m^2) for $B_2/B_1 = 0.75$, and V = 0.45m/s.

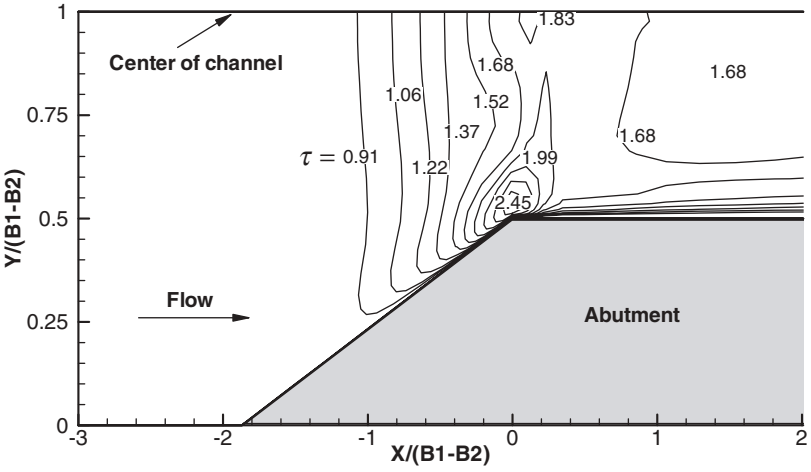

Figure 8.5. Initial bed shear stress distribution (N/m^2) for $B_2/B_1 = 0.5$, V = 0.45 m/s, $L/(B_1 - B_2) = 6.76$, and $\theta = 15$ degrees).

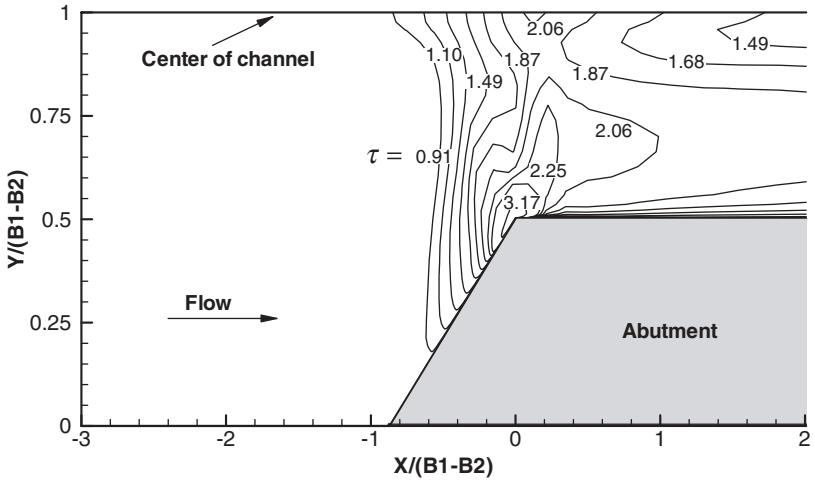

Figure 8.6. Initial bed shear stress distribution (N/m^2) for $B_2/B_1 = 0.5$, $V = 0.45$ m/s, $L/(B_1 - B_2) = 6.76$, and $\theta = 30$ degrees).

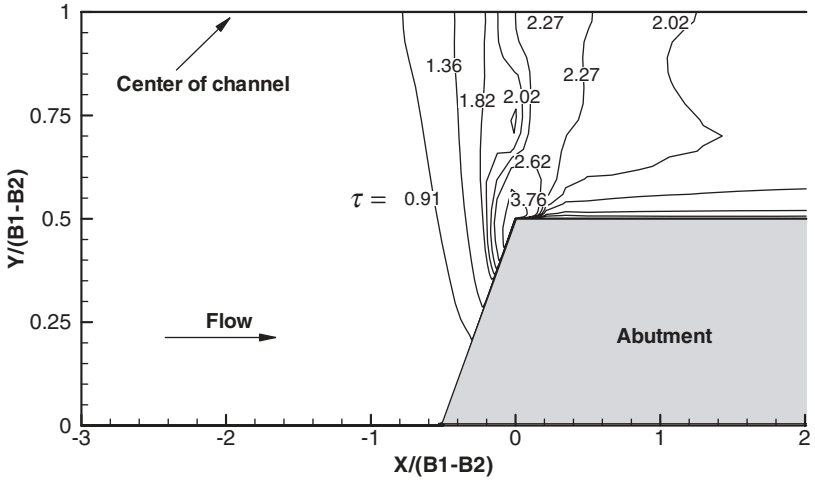

Figure 8.7. Initial bed shear stress distribution (N/m^2) for $B_2/B_1 = 0.5$, $V = 0.45$ m/s, $L/(B_1 - B_2) = 6.76$, and $\theta = 45$ degrees).

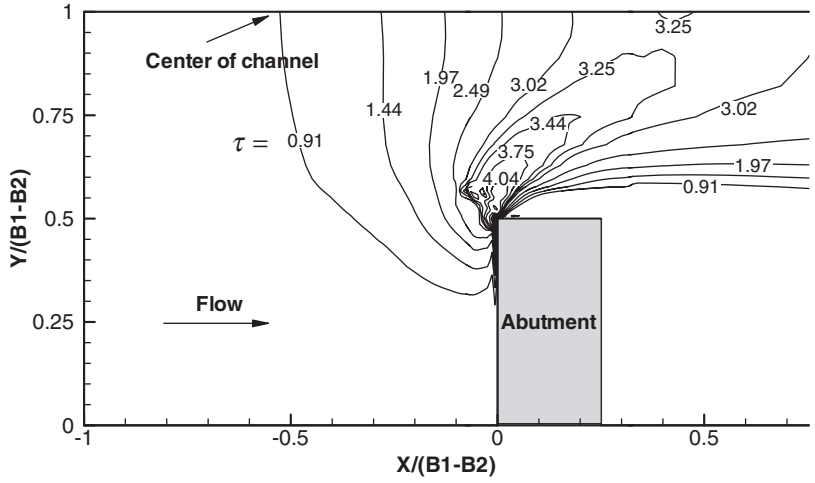

Figure 8.8. Initial bed shear stress distribution (N/m^2) for $B_2/B_1 = 0.5$, $V = 0.45$ m/s, and $L/(B_1 - B_2) = 0.25$).

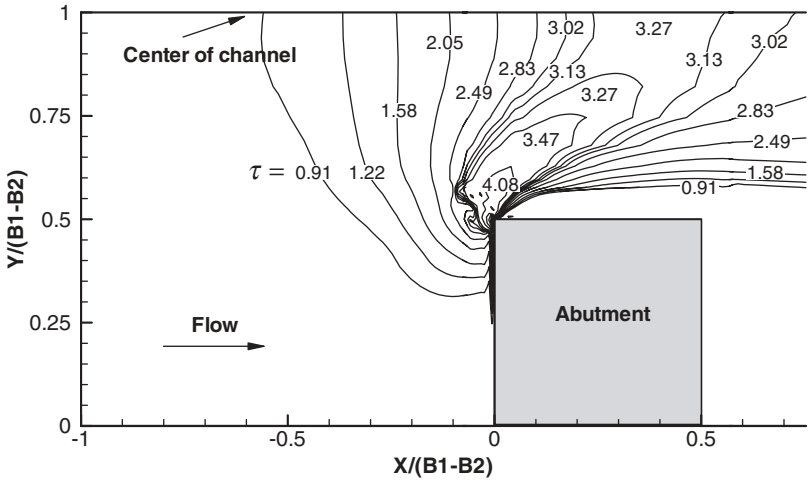

Figure 8.9. Initial bed shear stress distribution (N/m^2) for $B_2/B_1 = 0.5$, $V = 0.45$ m/s, and $L/(B_1 - B_2) = 0.5$).

contraction lengths. As can be seen, the maximum bed shear stress along the center of the channel in the contracted section is the same for all of the contraction lengths. At the same time, the location of the maximum bed shear stress is not influenced by the contraction length. Therefore, τ_{max} and x_{max} are independent of the contraction length, and there is no need for any correction factors for contraction length. It was discovered later that in the case of a very thin contraction length ($L/(B1 - B2) < 0.33$), the maximum shear stress within the contracted length is smaller than the maximum shear stress due to the contraction. The reason is that the maximum shear stress occurs downstream from the contraction. The correction factor will reflect this finding at very small values of the contracted length ($L/(B1/B2) < 0.33$) (Section 8.6).

8.5 WATER DEPTH EFFECT: NUMERICAL SIMULATION RESULTS

It was found that the water depth had no influence on the magnitude or the location of the maximum bed shear stress for the contraction problem. In fact, the water depth is already included in the equation through the hydraulic radius of Equation 8.1.

8.6 MAXIMUM SHEAR STRESS EQUATION FOR CONTRACTION SCOUR

The influence of four parameters on the maximum shear stress and its location near a channel contraction was investi-

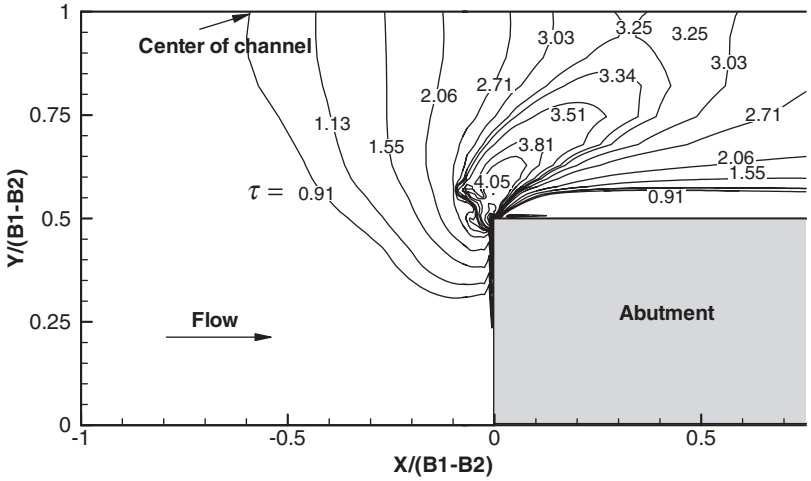

Figure 8.10. Initial bed shear stress distribution (N/m^2) for $B_2/B_1 = 0.5$, $V = 0.45$ m/s, and $L/(B_1 - B_2) = 1.0$).

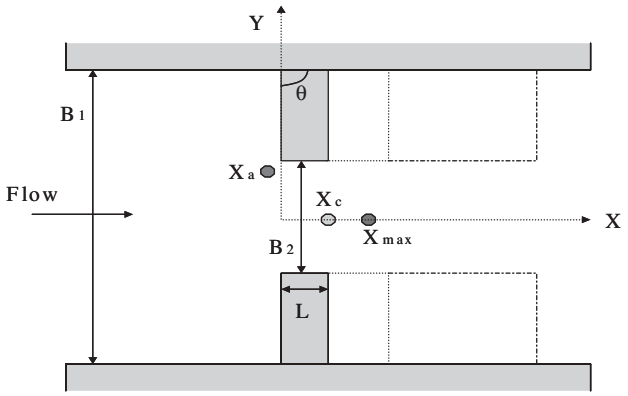

Figure 8.11. Definition of parameters for contraction scour.

gated by numerical simulation. These factors are the contraction ratio (B_2/B_1), the transition angle (θ), the length of contraction (L), and the water depth (H). Figure 8.11 describes the problem definition for abutment and contraction scour. In this figure, B_1 is the width of channel, B_2 is the width of the contracted section, L is the length of abutment, θ is the transition angle, X_a is the location of maximum bed shear stress due to the abutment, and X_{max} is a normalized distance that gives the location of the maximum bed shear stress along the centerline of the channel ($X_{max} = X/(B_1 - B_2)$) where X is the actual distance to τ_{max}.

It was found (for certain θ and B_1/B_2) that the influence of L on X_{max} and τ_{max} was negligible. In the case of $\theta = 90$ degrees and $B_1/B_2 = 2$, the value of X_{max} was about 0.35 for $L/(B_1 - B_2)$ varying from 0.25 to 6.76. For engineering design, what we are interested in is scouring around the pier or the abutment and along the contracted section. For small ratios of $L/(B1 - B2)$ (less than 0.33) the maximum shear stress τ_{max} is past the contracted location and the shear stress of interest is located at X_c from the beginning of the fully contracted channel.

The correction factor for a given influencing parameter is defined as the ratio of the τ_{max} value including that parameter to the τ_{max} value for the case of the open channel without any contraction. The results of the numerical simulations were used to plot the shear stress as a function of each influencing parameter. Regressions were then used to obtain the best-fit equation to describe the influence of each parameter. Figure 8.12 shows the variation of the correction factor k_{c-R} for the influence of the contraction ratio B_2/B_1. Figure 8.13 shows the correction factor $k_{c-\theta}$ for the influence of the transition angle θ. Figure 8.14 shows the correction factor k_{c-L} for the influence of the contracted length L. The correction factor k_{c-H} for the water depth influence was found to be equal to 1.

The proposed equation for calculating the maximum shear stress within the contracted length of a channel along its centerline is

$$\tau_{max} = k_{c-R} k_{c-\theta} k_{c-H} k_{c-L} \gamma n^2 V^2 R_h^{-\frac{1}{3}} \tag{8.2}$$

where

- γ is the unit weight of water (kN/m^3);
- n is Manning's roughness coefficient (s/m$^{1/3}$);
- V is the upstream mean depth velocity (m/s);

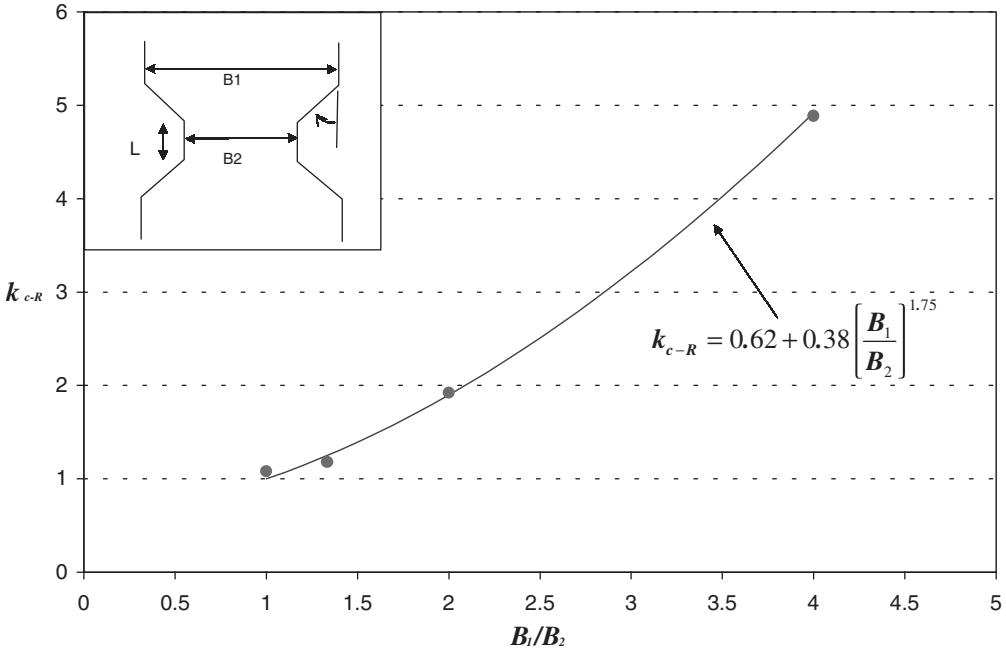

Figure 8.12. Relationship between k_{c-R} and B_1/B_2.

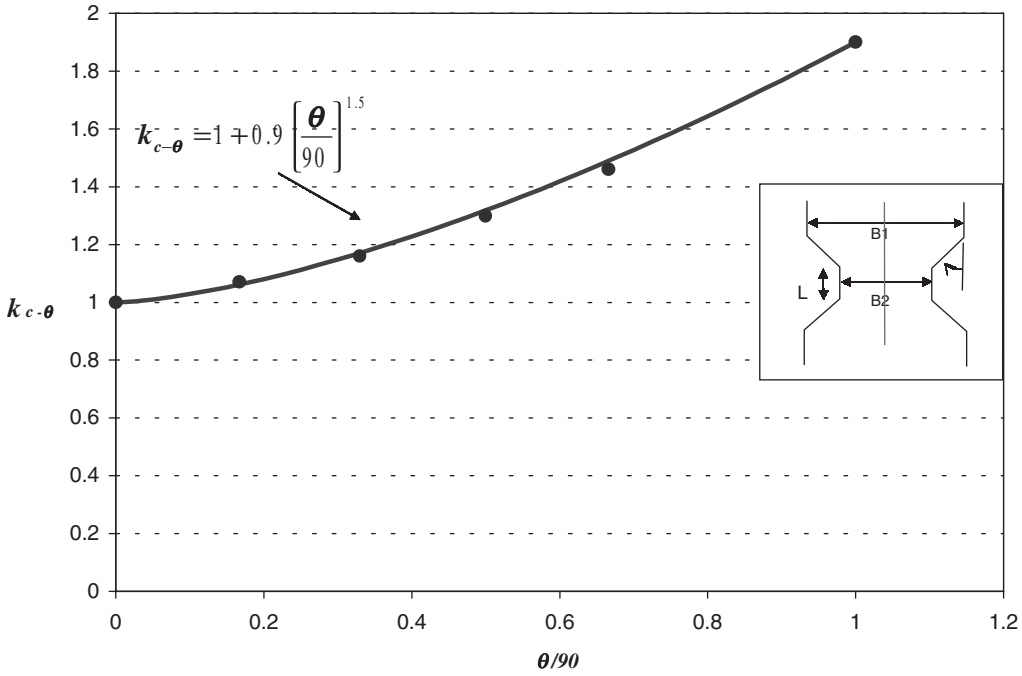

Figure 8.13. Relationship between $k_{c-\theta}$ and θ/90.

- θ is the contraction transition angle (in degrees) (Figure 8.13);
- R_h is the hydraulic radius defined as the cross-section area of the flow divided by the wetted perimeter (m);
- $k_{c\text{-}R}$ is the correction factor for the contraction ratio, given by
- $k_{c-R} = 0.62 + 0.38\left(\frac{B_1}{B_2}\right)^{1.75}$ (Figure 8.12);
- $k_{c-\theta}$ is the correction factor for the contraction transition angle, given by
- $k_{c-\theta} = 1 + 0.9\left(\frac{\theta}{90}\right)^{1.5}$ (Figure 8.13);

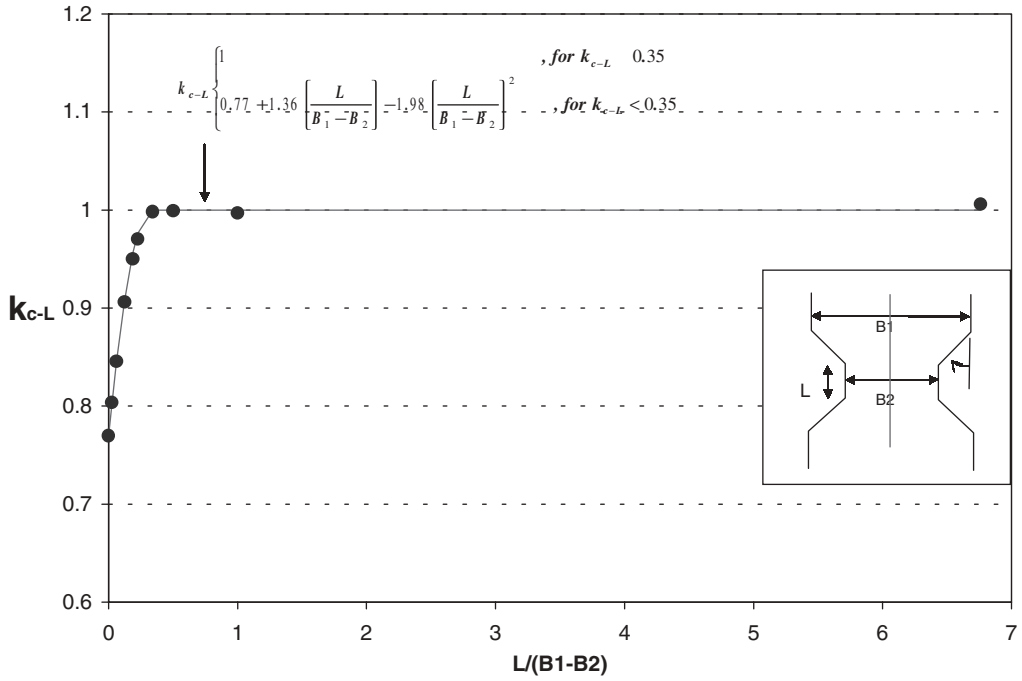

Figure 8.14. Relationship between k_{c-L} and $L/B_1 - B_2$.

- $k_{c\text{-}L}$ is the correction factor for the contraction length, given by

$$k_{c-L} = \begin{cases} 1 & , for \quad k_{c-L} \geq 0.35 \\ 0.77 + 1.36\left(\frac{L}{B_1 - B_2}\right) - 1.98\left(\frac{L}{B_1 - B_2}\right)^2, & \text{for} \end{cases}$$

- $k_{c\text{-}L} < 0.35$ (Figure 8.14); and
- $k_{c\text{-}H}$ is the correction factor for the contraction water depth.

Since the water depth has a negligible influence, then $k_{c\text{-}H} \approx 1$. The influence of the water depth H is in R_h.

Note that the last part of the equation ($\gamma n^2 V^2 R^{-0.33}_h$) is the formula for the bed shear stress in an open channel (Equation 8.2). Equation 8.2 is consistent with the open channel case since all correction factors collapse to 1 when the parameter corresponds to the open channel case. In other words when $\boldsymbol{B_1/B_2} = 1$, $\theta = 0$, and $(\boldsymbol{B_1 - B_2})/\boldsymbol{L} = 0$, then $\boldsymbol{k_{c-R}} = 1$, $\boldsymbol{k_{c-L}} = 1$, $\boldsymbol{k_{c-\theta}} = 1$.

Figures 8.15 and 8.16 give the location of the maximum shear stress along the centerline of the contracted channel. Figure 8.15 shows the influence of the transition angle, and Figure 8.16 shows the influence of the contraction ratio.

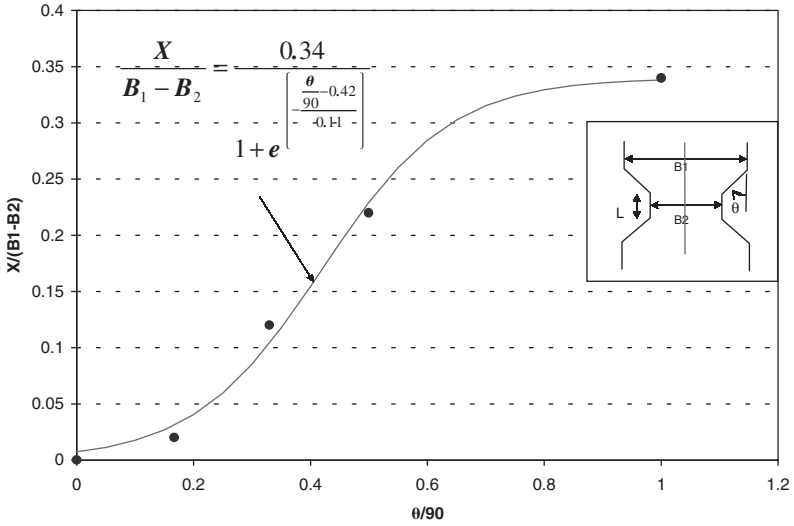

Figure 8.15. Distance from the beginning of the fully contracted section to the location of the maximum shear stress along the centerline of the channel X, as a function of the normalized transition angle θ/90.

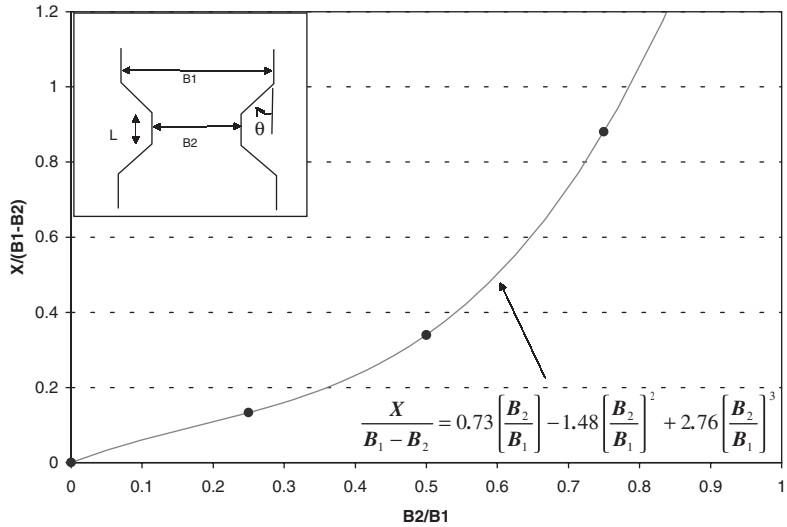

Figure 8.16. Distance from the beginning of the fully contracted section to the location of the maximum shear stress along the centerline of the channel X, as a function of the Contraction Ratio $\boldsymbol{B_2/B_1}$.

CHAPTER 9

THE SRICOS-EFA METHOD FOR COMPLEX PIER SCOUR AND CONTRACTION SCOUR IN COHESIVE SOILS

9.1 BACKGROUND

The SRICOS-EFA method for complex pier and contraction scour can be used to handle the complex pier problem alone or contraction scour alone. It also can handle the combined case of complex pier scour and contraction scour (integrated SRICOS-EFA Method). Abutment scour is not included in this project but will be added later. A method exists in HEC-18 to predict bridge scour under the combined influence of contraction scour, pier scour, and abutment scour. This method consists of calculating the individual scour depths independently and simply adding them up. Engineers have often stated that the results obtained in such a way are too conservative. The integrated SRICOS-EFA Method is not just adding the complex pier scour and the contraction scour. The method considers the time factor, soil properties and—most importantly—the interaction between the contraction scour and the pier scour. In the following sections, the principle, accumulation algorithm, and step-by-step procedure for the integrated SRICOS-EFA Method are presented.

9.2 THE INTEGRATED SRICOS-EFA METHOD: GENERAL PRINCIPLE

In the integrated SRICOS-EFA Method for calculating bridge scour, the scour process is separated into two steps: (1) calculation of the total contraction scour and (2) calculation of pier scour. The contraction scour is assumed to happen first and without considering pier scour. This does not mean that the piers are not influencing the contraction scour; indeed the piers are considered in the contraction scour calculations because their total projection width is added to the abutment projection width to calculate the total contraction ratio. The contraction scour is calculated in this fashion for a given hydrograph. Then, the pier scour is calculated. There are two options for the pier scour calculations as follows:

1. If the contraction scour calculations indicate that there is no contraction scour at the bridge site, then the pier scour is calculated by following the SRICOS-EFA complex pier scour calculation procedure. In this case, HEC-RAS, for example, can be used to calculate the water depth and the velocity in the contracted section after removing the piers obstructing the flow. The removal of the piers is necessary because the velocity used for pier scour calculations is the mean depth velocity at the location of the pier if the pier were not there.
2. If the calculations indicate that contraction scour occurs at the bridge site, then the pier scour calculations are made using the critical velocity, not the actual velocity, because when contraction scour has stopped (Z_{max}(Cont) is reached), the velocity in the contracted section is the critical velocity V_c. The value of V_c can be obtained from the EFA tests for cohesive soils or from the equations presented in HEC-18 for cohesionless soils. The water depth for the pier scour calculations is the water depth in the contracted section after the contraction scour has occurred. The bottom profile of the river after scour has occurred is obtained by adding the contraction scour and the pier scour.

This approach is valid for the maximum scour depth calculations. For the time stepping process, the maximum scour depth is not reached at each step but the maximum scour depth is calculated as part of each step and used to calculate the partial scour depth. Therefore, the above technique is included in each time step. The other parameter calculated at each time step is the initial maximum shear stress; this shear stress is used to read the initial scour rate on the erosion function obtained from the EFA tests. Both parameters, Z_{max} and $\dot{Z}_i$, are used to generate the scour depth versus time curve and the actual scour depth is read on that curve at the value equal to the time step. The details of that procedure are presented in the next section.

9.3 THE INTEGRATED SRICOS-EFA METHOD: STEP-BY-STEP PROCEDURE

Step I: Input Data Collection (Figure 9.1)

Water:	Flow (mean velocity V_1, and water depth H_1) upstream of the bridge where the flow is no noticeably influenced by the existence of bridge contraction and piers.
Geometry:	Bridge contraction parameters and pier geometry.
Total Contraction Ratio:	$B_2/B_1 = (w_1+w_2+w_3+w_4)/B_1$ (9.1)

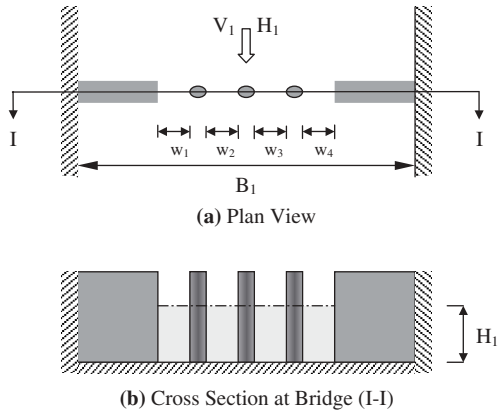

(a) Plan View

(b) Cross Section at Bridge (I-I)

Figure 9.1. Step I—bridge scour input data and primary calculation.

Soil: Critical shear stress and erosion function.

All of the parameters are shown in Figure 9.1.

Step II: Maximum Contraction Scour Calculation (Figure 9.2)

Based on the upstream flow conditions, soil properties, and total bridge contraction ratio calculated in Step I, the maximum contraction scour can be calculated directly by Equation 9.2 as follows:

$$Z_{\max}(\text{Cont}) = K_\theta K_L \times 1.90 \left(\frac{1.38\left(V_1 \frac{B_1}{B_2}\right)}{\sqrt{gH_1}} - \frac{\left(\frac{\tau_c}{\rho}\right)^{0.5}}{gnH_1^{1\,3}} \right) H_1 \quad \geq 0 \qquad (9.2)$$

where Z_{max}(Cont) (m) is the maximum contraction scour; K_θ is the factor for the influence of the transition angle (K_θ is equal to 1); K_L is the factor for the influence of the length of the contracted channel (K_L is equal to 1); V_1 (m/s) is the velocity in the uncontracted channel; B_1 (m) is the width of the uncontracted channel B_2 (m) is the width of the contracted channel as defined in Equation 9.1 and Figure 9.1; g (m/s^2) is the acceleration due to gravity; H_1 (m) is the water depth in the uncontracted channel; τ_c (kN/m^2) is the critical shear stress of the soil obtained in the EFA; ρ is the mass density of water (kg/m^3); and n is Manning's Coefficient (s/m$^{1/3}$).

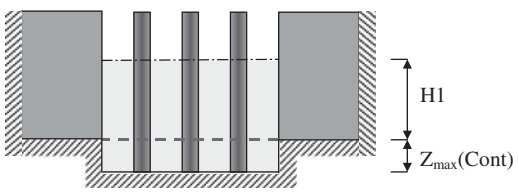

Figure 9.2. Step II—contraction scour calculation and distribution.

The engineers may prefer to calculate the velocity V_{hec} in the contracted channel with a width B_2 as calculated according to Equation 9.1 and Figure 9.1 by using a program like HEC-RAS. In this case, the engineer needs to use Equation 9.3:

$$Z_{\max}(\text{Cont}) = K_\theta K_L \times 1.90 \left(\frac{1.49 V_{\text{HEC}}}{\sqrt{gH_1}} - \frac{\left(\frac{\tau_c}{\rho}\right)^{0.5}}{gnH_1^{1/3}} \right) H_1 \quad \geq 0 \qquad (9.3)$$

where V_{Hec} is the maximum velocity in the middle of the contracted channel (m/s). If the value of the maximum contraction scour Z_{max}(Cont) is negative, the flow and contraction are not severe enough to cause any contraction scour and the maximum contraction scour is zero. If there is contraction scour, the shear stress reached on the river bottom at the time of maximum contraction scour Z_{max}(Cont) is the critical shear stress of the soil τ_c, and scour at the bridge site is as shown in Figure 9.2.

Step III: Pier Scour Calculation

1. If Step II leads to no contraction scour, the pier scour is calculated by using the velocity V and water depth H at the location of the pier in the contracted channel assuming that the bridge piers are not there. The velocity V_{hec} and water depth can be calculated directly by using a program like HEC-RAS.
2. If Step II leads to a maximum contraction scour depth Z_{max}(Cont), then the maximum pier scour depth is calculated by using the critical velocity V_c for the soil and the water depth H_2, including the contraction scour depth. These are

$$H_2 = H_1 + Z_{\max}(\text{Cont}) \qquad (9.4)$$

$$V = \begin{cases} V_c = \sqrt{\frac{\tau_c H_2^{\frac{1}{3}}}{\rho g n^2}} & Z_{\max}(\text{Cont}) > 0 \\ V_{\text{HEC}} & Z_{\max}(\text{Cont}) = 0 \end{cases} \qquad (9.5)$$

where H_1 is the water depth in the contracted channel before contraction scour starts (m).

Then, the maximum pier scour depth Z_{max}(pier) can be calculated by using Equation 9.6:

$$Z_{\max}(\text{Pier}) = 0.18 K_w K_{sp} K_{sh} R_e^{0.635} \qquad (9.6)$$

where K_w is the correction factor for pier scour water depth, given by

$$\text{For } H/B \leq 1.6 \quad K_w = 0.85(H/B)^{0.34}$$

$$\text{For } H/B > 1.6 \quad K_w = 1 \qquad (9.7)$$

K_{sp} is the correction factor for the pier spacing effect on the pier scour depth, when n piers of diameter B are installed in a row, given by

$$K_{sp} = \frac{B_1}{(B_1 - nB)} \tag{9.8}$$

K_{sh} is the correction factor for pier shape effect on pier scour. K_{sh} is equal to 1.1 for rectangular piers with length to width ratios larger than 1. R_e is the Reynolds Number:

$$R_e = VB'/v \tag{9.9}$$

where V is the mean depth average velocity at the location of the pier if the pier is not there when there is no contraction scour, or the critical velocity V_c (Equation 9.5) of the bed material if contraction scour occurs; B' is the pier diameter or projected width ($L\sin\alpha + B\cos\alpha$); B and L are the pier width and length respectively; α is the attack angle; and v is the kinematic viscosity of water.

Step IV: Total Maximum Bridge Scour Calculation

The maximum bridge scour is (Figure 9.3):

$$Z_{max} = Z_{max}(\text{Cont}) + Z_{max}(\text{Pier}) \tag{9.10}$$

Step V: Maximum Shear Stress around the Bridge Pier (Figure 9.4)

In the calculations of the initial development of the scour depth, the maximum shear stress τ_{max} is needed. This maximum shear stress is the one that exists around the bridge pier since the pier is the design concern. This step describes how to obtain τ_{max}. Figure 9.4 shows the parameters.

In the case of an uncontracted channel (no abutments), the maximum bed shear stress τ_{max} around the pier is given by

$$\tau_{max} = k_w k_{sh} k_{sp} k_\alpha \cdot 0.094 \rho V_1^2 \left[\frac{1}{\log R_e} - \frac{1}{10}\right] \tag{9.11}$$

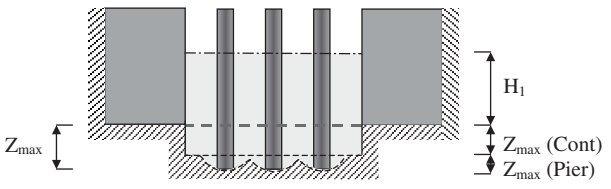

Figure 9.3. Steps III and IV—calculations of pier scour and superposition.

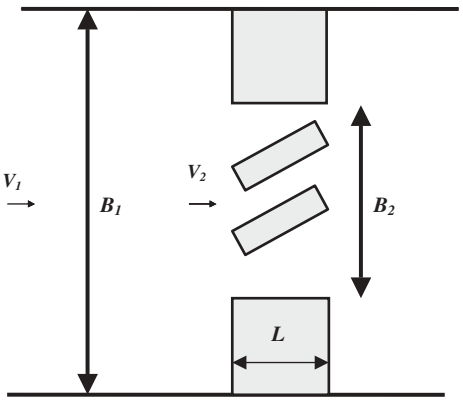

Figure 9.4. Plan view of complex pier scour and contraction scour.

where ρ is the water mass density (kg/m^3); V_1 is the mean depth velocity in the approach uncontracted channel (m/sec); R_e is the Reynolds Number based (V_1B/v) where B (m) is the pier diameter or pier projected width; v is the kinematic viscosity of the water (m^2/s); and k_w, k_{sh}, k_{sp}, k_α are the correction factors for water depth, shape, pier spacing, and attack angle, respectively.

$$k_w = \frac{\tau_{max}}{\tau_{max}(\text{deep})} = 1 + 16e^{-\frac{4H}{B}} \tag{9.12}$$

$$k_{sp} = \frac{\tau_{max}}{\tau_{max}(\text{single})} = 1 + 5e^{-1.1\frac{S}{B}} \tag{9.13}$$

$$k_{sh} = \frac{\tau_{max}}{\tau_{max}(\text{circle})} = 1.15 + 7e^{-4\frac{L}{B}} \tag{9.14}$$

$k_{sh} = 1$ for circular shape

$$k_\alpha = \frac{\tau_{max}}{\tau_{max}(0\,\text{deg})} = 1 + 1.5\left(\frac{\alpha}{90}\right)^{0.57} \tag{9.15}$$

where H is the water depth, B is the pier diameter or projected width, S is the pier center-to-center spacing, L is the pier length, and α is the angle between the direction of the flow and the main direction of the pier.

In the case of a contracted channel (Figure 9.4), the maximum bed shear stress around the pier is given by Equation (9.11), except that the velocity in the contracted section V_2 is used instead of the approach velocity V_1. The equation is

$$\tau_{max} = k_w k_{sh} k_{sp} k_\alpha 0.094 \rho V_2^2 \left[\frac{1}{\log \text{Re}} - \frac{1}{10}\right] \tag{9.16}$$

where V_2 (m/s) is the mean depth velocity in the contracted channel at the location of the pier without the presence of the pier. The velocity V_2 can be obtained from HEC-RAS or from mass conservation for a rectangular channel

$$V_2 = 1.14V_1\left(\frac{B_1}{B_2}\right) \tag{9.17}$$

Step VI: Time History of the Bridge Scour

This part of the method proceeds like the original SRICOS-EFA Method, which has been described in Step III. The initial shear stress τ_{max} around the pier is calculated from Equation 9.16 and the corresponding initial erosion rate $\dot{Z}_i$ is obtained from the erosion function (measured in the EFA), the maximum scour depth due to contraction scour and pier scour is calculated from Equation 9.10. With these two quantities defining the tangent to the origin and the asymptotic value of the scour depth versus time curve, a hyperbola is defined to describe the entire curve:

$$Z(t) = \frac{t}{\frac{1}{\dot{Z}_i} + \frac{t}{Z_{max}}} \tag{9.18}$$

where $Z(t)$ is the scour depth due to a flood; t is the flood duration; $\dot{Z}_i$ is the initial erosion rate; and Z_{max} is the maximum scour depth due to the flood (Equation 9.10). In the case of a complete hydrograph and of a multilayer soil system, the accumulation algorithms are as follows.

Multiflood System The hydrograph of a river indicates how the velocity varies with time. The fundamental basis of the accumulation algorithms is that the velocity histogram is a step function with a constant velocity value for each time step. When this time step is taken as 1 day, the gage station value is constant for that day because only daily records are kept. The case of a sequence of two different constant velocity floods scouring a uniform soil is considered (Figure 9.5). Flood 1 has velocity V_1 and lasts time t_1 while Flood 2 has a velocity V_2 and lasts time t_2. After Flood 1, a scour depth Z_1 is reached at time t_1 (Point A on Figure 9.5b) and can be calculated as follows:

$$Z_1 = \frac{t_1}{\frac{1}{\dot{Z}_{i1}} + \frac{t_1}{Z_{max\,1}}} \tag{9.19}$$

For Flood 2, the scour depth will be

$$Z_2 = \frac{t_2}{\frac{1}{\dot{Z}_{i2}} + \frac{t_2}{Z_{max\,2}}} \tag{9.20}$$

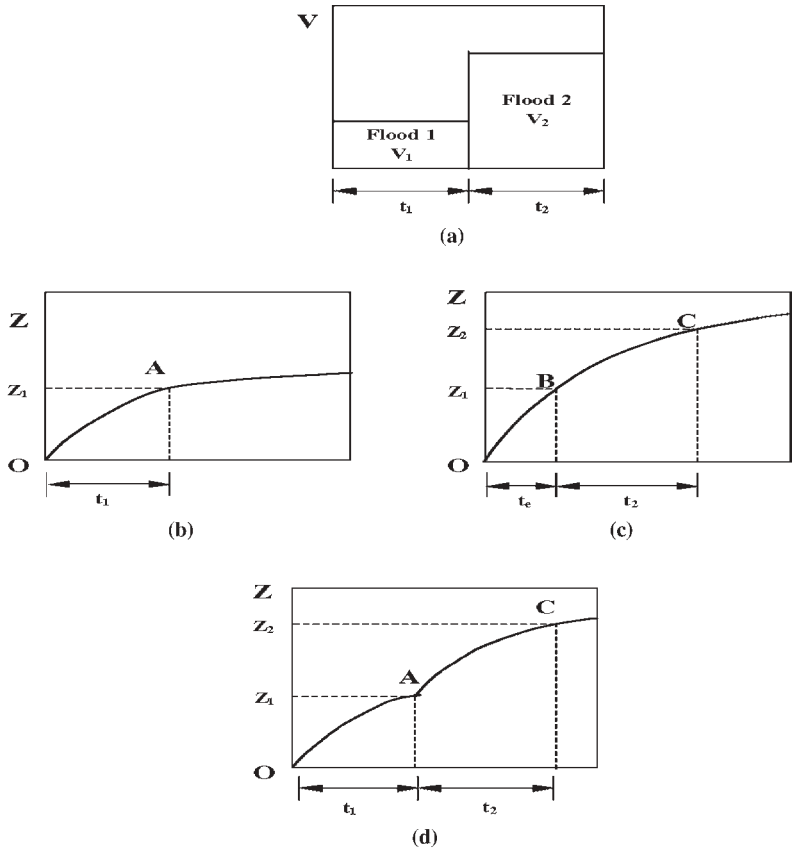

Figure 9.5. Scour due to a sequence of two flood events.

The scour depth Z_1 also could have been created by Flood 2 in time t_e (Point B on Figure 9.5c). The time t_e is called the equivalent time. The time t_e can be obtained by using Equations 9.19 and 9.20 with $Z_2 = Z_1$ and $t_2 = t_e$.

$$t_e = \frac{t_1}{\frac{\dot{Z}_{i2}}{\dot{Z}_{i1}} + t_1 \dot{Z}_{i2}\left(\frac{1}{Z_{max1}} - \frac{1}{Z_{max2}}\right)} \tag{9.21}$$

When Flood 2 starts, even though the scour depth Z_1 was due to Flood 1 over time t_1, the situation is equivalent to having had Flood 2 for time t_e. Therefore, when Flood 2 starts, the scour depth versus time curve proceeds from Point *B* on Figure 9.5c until Point C after time t_2. The *Z* versus *t* curve for the sequence of Floods 1 and 2 follows the path OA on the curve for Flood 1 then switches to BC on the curve for Flood 2. This is shown as the curve OAC on Figure 9.5d.

The procedure described above is for the case of velocity V_1 followed by velocity V_2 higher than V_1. In the opposite case, where V_2 is less than V_1, Flood 1 creates scour depth Z_1 after time t_1. This depth is compared with Z_{max2} due to Flood 2. If Z_1 is larger than Z_{max2}, it means that, when Flood 2 starts, the scour hole is already deeper than the maximum scour depth that Flood 2 can create. Hence, Flood 2 cannot create any additional scour and the scour depth versus time curve remains flat during Flood 2. If Z_1 is less than Z_{max2}, the procedure of Figure 9.5d should be followed.

In the general case, the complete velocity hydrograph is divided into a series of partial flood events, each lasting Δt. The scour depth due to Floods 1 and 2 in the hydrograph will be handled by following the procedure of Figure 9.5d. At this point the situation is reduced to a single Flood 2 that lasts t_e. Then the process will consider Flood 3 as a "new Flood 2" and will repeat the procedure of Figure 9.5d applied to Flood 2 lasting t_{e2} and Flood 3. Therefore, the process advances with only two floods to be considered: the previous flood with its equivalent time and the "new Flood 2." The time step Δt is typically 1 day and the velocity hydrograph can be 70 years long.

Multilayer System In the multiflood system analysis, the soil is assumed to be uniform. In reality, the soil involves different layers and the layer characteristics can vary significantly with depth. It is necessary to have an accumulation process that can handle the case of a multilayer system. Consider the case of a first layer with a thickness equal to ΔZ_1 and a second layer with a thickness equal to ΔZ_2. The riverbed is subjected to constant velocity V (Figure 9.6a). The scour depth *Z* versus time *t* curves for Layer 1 and Layer 2 are given by Equations 9.19 and 9.20 (Figure 9.6b, Figure 9.6c). If the thickness of Layer 1 ΔZ_1 is larger than the maximum scour depth Z_{max1}, given by Equation 9.10, then the scour process only involves Layer 1. This case is the case of a uniform soil. On the other hand, if the maximum scour depth Z_{max1} exceeds the thickness ΔZ_1, then Layer 2 will also be

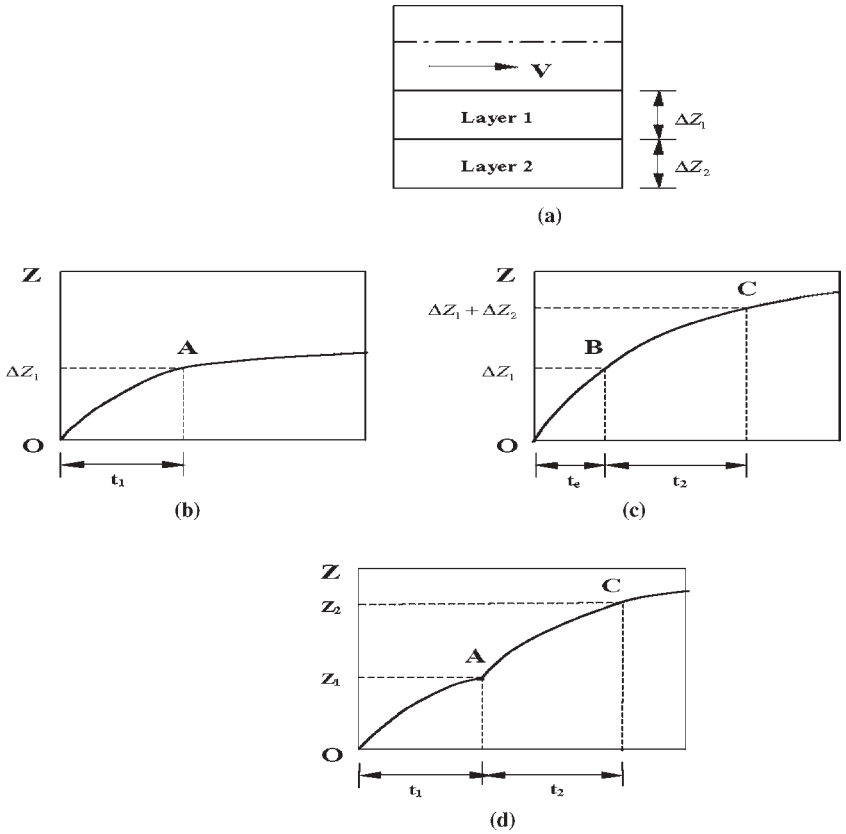

Figure 9.6. Scour of a two-layer soil system.

involved in the scour process. In this case, the scour depth ΔZ_1 (Point A on Figure 9.6b) in Layer 1 is reached after time t_1; at that time, the situation is equivalent to having had Layer 2 scoured over an equivalent time t_e (Point B on Figure 9.6c). Therefore, when Layer 2 starts to be eroded, the scour depth versus time curve proceeds from Point B to Point C on Figure 9.6c. The combined scour process for the two-layer system corresponds to the path OAC on Figure 9.6d.

In reality, there may be a series of soil layers with different erosion functions. The computations proceed by stepping forward in time. The time steps are Δt long, the velocity is the one for the corresponding flood event, and the erosion function ($\dot{z}$ versus τ) is the one for the soil layer corresponding to the current scour depth (bottom of the scour hole). When Δt is such that the scour depth enters a new soil layer, the computations follow the process described in Figure 9.6d.

9.4 INPUT FOR THE SRICOS-EFA PROGRAM

The input includes parameters for the soil, water, and geometry of the problem.

Soil Properties

In the SRICOS-EFA Method, the soil properties at the bridge site are represented by the soil erosion function, which is a measure of the erodibility of the soil. The soil erosion function is the relationship between the erosion rate $\dot{z}$ of the soil and the hydraulic shear stress τ applied on the bottom of riverbed. It is obtained by performing an EFA test on the soil sample (Briaud et al., 2002). The erosion function (Figure 9.7) is needed for each layer within the potential scour depth at the bridge site.

Hydrologic Data

The water flow is represented by the velocity hydrograph. This hydrograph can be obtained from a nearby gage station. The hydrograph should last as long as the required period of prediction. Furthermore, if the hydrograph obtained from the gage station does not contain a 100-year flood, it can be spiked artificially to include such a large event if required by design. The hydrograph is typically in the form of discharge as a function of time. Because the input for scour calculations is the velocity and not the discharge, it is necessary to transform the discharge data at the gage station into velocity data at the bridge site. This can be done by using a program such as HEC-RAS (Hydrologic Engineering Center—River Analysis System, HEC-RAS, 1997), which was developed by the U.S. Army Corps of Engineers. In order to run HEC-RAS, several geographic features are necessary, such as the average slope of the channel bed, the channel cross section, and the roughness coefficient of the riverbed. Figure 9.8 shows the discharge hydrograph, the discharge versus velocity curve (HEC-RAS results), and the mean depth velocity at one of the piers versus time (velocity hydrograph) for the Woodrow Wilson Bridge on the Potomac River in Washington D.C. between 1960 and 1998.

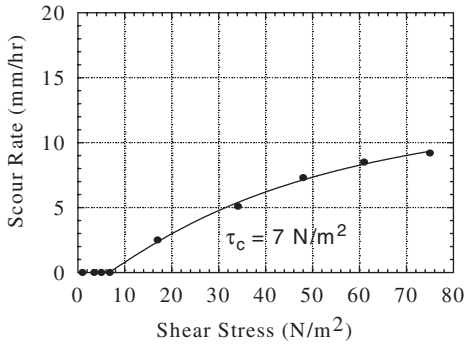

Figure 9.7. Typical EFA test result.

Geometry

The geometry includes channel geometry and bridge geometry. The channel and bridge geometry are used for contraction scour evaluation, including the determination of the contraction ratio. The pier's size, shape, spacing, and angle of attack are used for pier scour calculations. Table 9.1 elaborates on aspects of geometry.

9.5 THE SRICOS-EFA PROGRAM

The SRICOS-EFA program automates the SRICOS-EFA Method. The first version of the program was solving the problem of a cylindrical pier in deep water (Kwak, 1999; Kwak et al., 2001). In this study the program was extended to predict complex pier scour and contraction including the superposition of both scour modes. Using the input described in the previous section, the program automates the calculations of all of the parameters: transformation of discharge into velocities, maximum shear stress, initial slope of the scour rate versus shear stress curve, maximum scour depth, and so on. Then, it proceeds with the techniques described to handle multiflood and multilayer systems.

The program was written in FORTRAN by using Visual FORTRAN 5.0. The flow chart of the program in Figure 9.9 gives an overall view of the SRICOS-EFA Method, including all of the equations. As can be seen, there is one branch to handle complex pier scour alone, one branch to handle contraction scour alone, and one branch to handle the concurrent occurrence of complex pier scour and contraction scour. The SRICOS-EFA program is a user-friendly, interactive code that guides the user through a step-by-step data input procedure except for velocity or discharge data. This program, however, is not in the Windows™ environment and needs to be implemented in such an environment for easier use. For the hydrograph, the number of velocity or discharge data points can be at least several tens of thousands for the time duration corresponding to the design life of bridges and if the velocity data is given on a daily basis. The velocity or discharge data should be prepared in the format of an ASCII file or a text document before running the program. The input

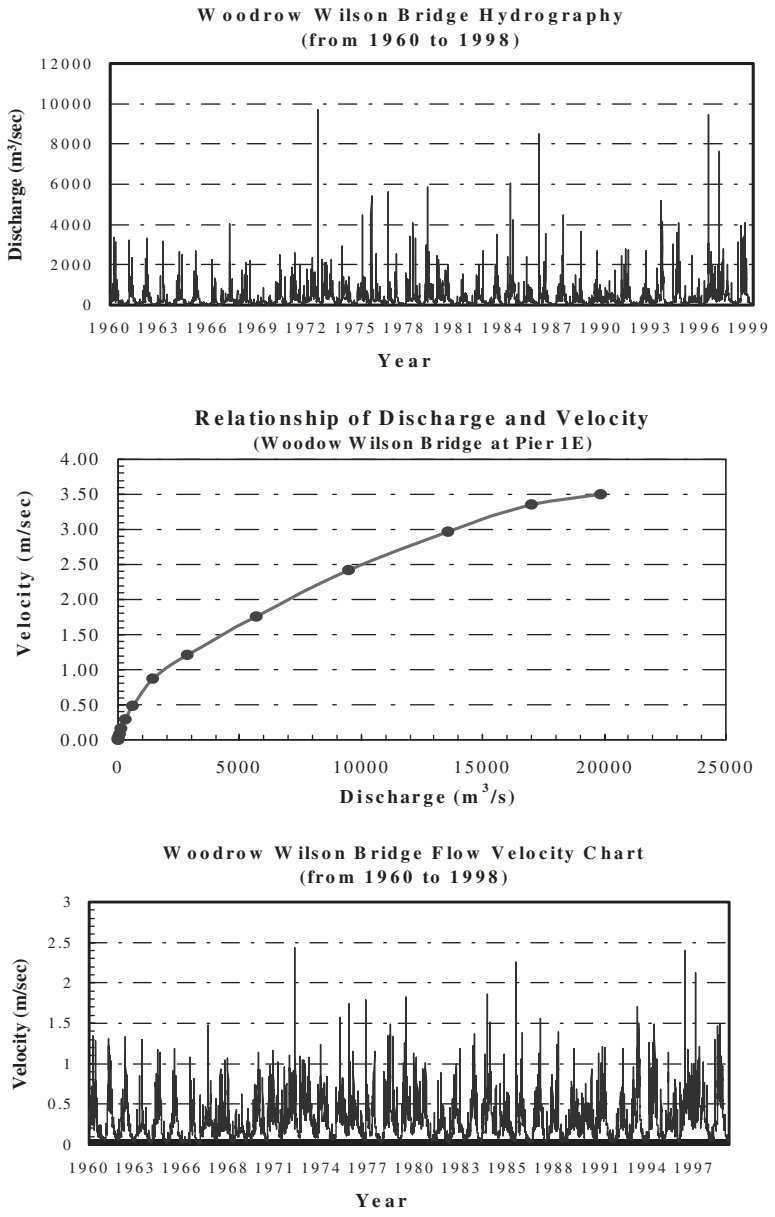

Figure 9.8. Example of hydrograph transformation for Pier 1E of the Woodrow Wilson Bridge on the Potomac River in Washington, D.C.

TABLE 9.1 Summary of geometry factors

Bridge Geometric Factors		**Channel Geometric Factors**	
Bridge opening	Bridge contraction ratio	Channel characteristics	Channel contraction ratio
	Bridge contraction length		Channel contraction length
Bridge piers	Type, shape		Channel water depth
	Attack angle		
	Size, length, width (diameter)		Manning coefficient
	Pier spacing		Channel hydraulic radius
	Number of piers		Soil stratigraphy

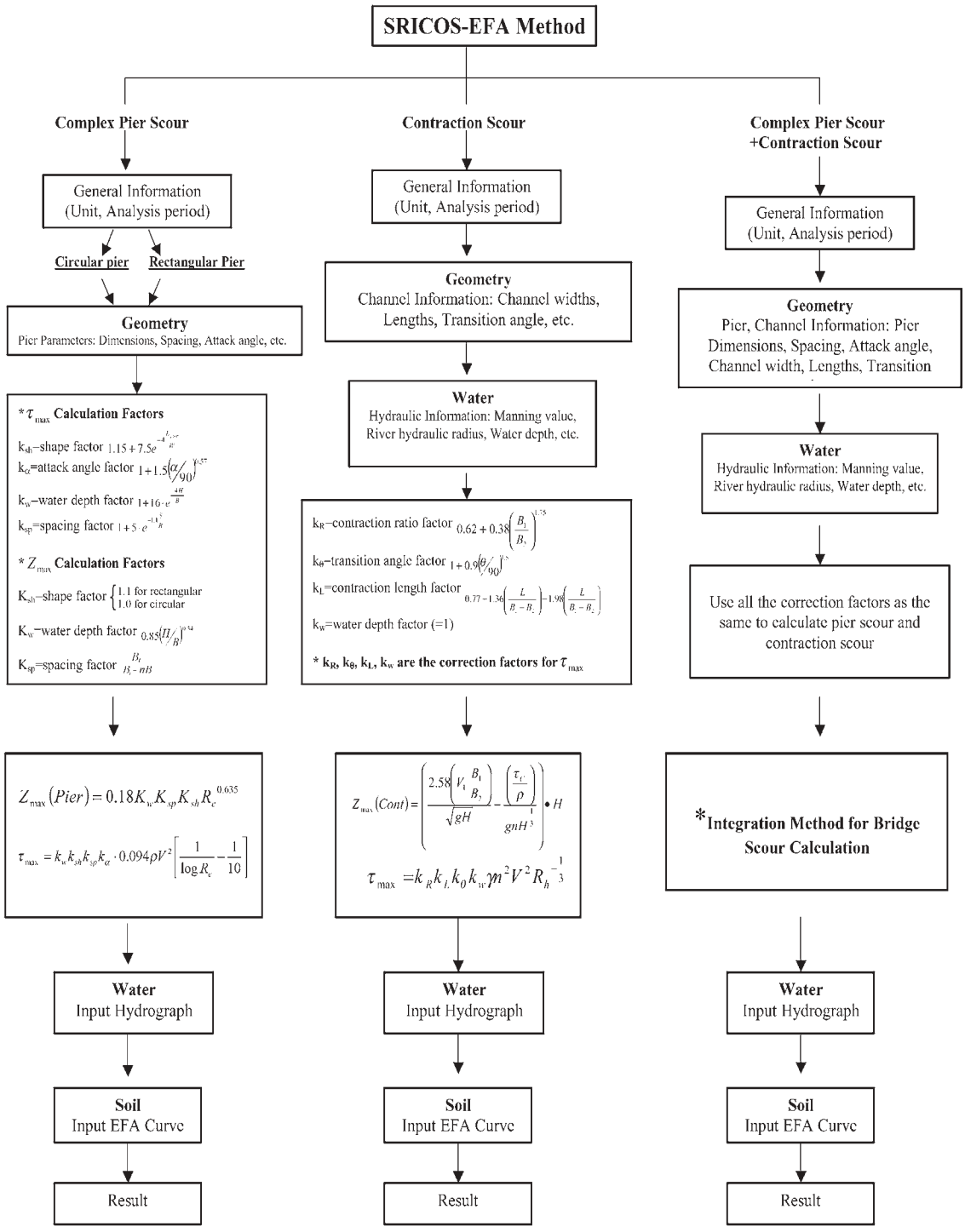

*Integration Method for Bridge Scour Calculation will be presented in detail in following section.

Notes:

L_{pier}: Length of rectangular pier	S: Spacing of group piers	V_1: Approaching velocity	ρ: unit mass of water at 20°C
W: Width of rectangular pier	B_1: Width of un-contracted channel	n: Manning's value	g: acceleration of gravity
B: Diameter of pier	B_2: Width of contracted channel	R_e: Reynolds number	τ_c: Critical shear stress of riverbed
H: Approaching water depth	L: Length of contracted channel	R_h: Hydraulic radius	

Figure 9.9. Flow chart of the SRICOS-EFA Program.

TABLE 9.2 Example of SRICOS-EFA Program output file

NO.	TIME (DAYS)	VELOCITY (m/s)	WATER DEPTH (m)	SHEAR STRESS (N/m2)	MAXIMUM SCOUR DEPTH (mm)	LOCAL SCOUR DEPTH (mm)
1	1.0	0.3403	5.68	1.7079	1838.485	0.0
2	2.0	0.3239	5.62	1.5835	1770.571	0.0
3	3.0	0.3259	5.63	1.5989	1779.206	0.0
4	4.0	0.3649	5.76	1.8986	1935.717	0.0
5	5.0	0.3649	5.76	1.8986	1935.517	0.0
6	6.0	0.4141	5.93	2.2926	2137.200	0.0
7	7.0	0.4203	5.95	2.3430	2260.586	0.0
8	8.0	0.3752	5.80	1.9793	2006.358	0.0
9	9.0	0.3403	5.68	1.7079	1838.485	0.0
10	10.0	0.3095	5.58	1.4766	1572.614	0.0
11	11.0	0.6732	6.98	4.3798	4320.126	15.5
12	12.0	0.7187	7.17	4.7433	5622.733	33.6
13	13.0	0.5554	6.95	1.4065	1489.698	33.6

data can be either in the metric system or U.S. customary system; the output also can be in either system. The User's Manual for SRICOS-EFA is presented in Appendix D of the research team's final report, which is available from NCHRP.

9.6 OUTPUT OF THE SRICOS-EFA PROGRAM

Once the program finishes all of the computations successfully, the output file is created automatically. The output file includes the following columns: time, flow velocity, water depth, shear stress, maximum scour depth (pier, contraction, or total), and instantaneous scour depth (pier, contraction, or total). The first few days of a typical output file of the program are shown in Table 9.2. For this example, the critical shear stress was 4 N/m^2; as can be seen, no scour occurred until the velocity was high enough to overcome the critical shear stress on day 11. The format of the output file is a text file. This file can be used to plot a number of figures (Figure 9.10). The most commonly plotted curves are water velocity versus time, water depth versus time, shear stress versus time, and scour depth versus time. The scour depth versus time curve indicates whether the final scour depth Z_{final} (scour depth at the end of the hydrograph) is close to the maximum scour depth for the biggest flood in the hydrograph Z_{max} or not. Typically, in sand the answer is yes, but in low erodibility clays the difference is significant enough to warrant the analysis in the first place. Kwak et al. (2001) showed the results of a parametric analysis indicating the most important parameters in the prediction process.

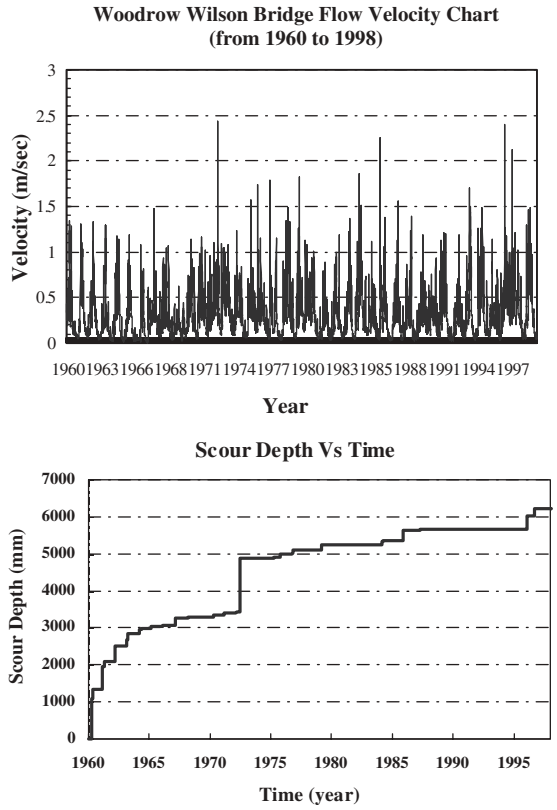

Figure 9.10. Example of plots generated from SRICOS-EFA output.

CHAPTER **10**

VERIFICATION OF THE SRICOS-EFA METHOD

10.1 BACKGROUND

The SRICOS-EFA Method for complex pier and contraction scour in cohesive soils was developed on the basis of flume tests for the maximum scour depth equations and numerical simulations for the maximum initial shear stress equations. As with any new method, there is a need to verify the method against other measurements. These measurements should preferably be full-scale case histories. For this project, the case histories had to satisfy the following site requirements:

1. Channel contraction exists;
2. A bridge with piers in the water exists;
3. A gage station exists giving the hydrograph over a period of time *t*;
4. The soil is cohesive;
5. The site can be accessed with a drill rig; and
6. The riverbed cross section was documented at the beginning and at the end of the same period of time *t* as the hydrograph.

A survey of U.S. DOTs was conducted and many sites were collected. Upon further review, it was found that none of the sites had the requirements necessary for evaluating the method. Since this avenue could not be pursued, it was decided to look in the literature for existing data associated with the topic of complex pier and contraction scour. The following databases were found:

1. Mueller (1996) for complex pier scour,
2. Froehlich (1988) for complex pier scour, and
3. Gill (1981) for contraction scour.

These databases were created primarily for cohesionless soils, but it was felt that it would be useful to compare the SRICOS-EFA Method to cohesionless soils measurements. The following gives a brief description of the databases and shows the comparisons between measured and predicted scour depth. Note that since the data pertains to cohesionless soils, the comparison is limited to evaluating the equations for the maximum scour depth Z_{max}(complex pier and contraction).

10.2 MUELLER (1996) DATABASE: PIER SCOUR

The Mueller Database was obtained from report FHWARD-95-184, "Channel Scour at Bridges in the United States." More than 380 pier scour measurements were collected at 56 bridge sites in Alaska, Arkansas, Colorado, Delaware, Georgia, Illinois, Indiana, Louisiana, Maryland, Mississippi, Montana, New York, Ohio, and Virginia. Figure 10.1 shows the comparison between the complex pier scour depth calculated by the SRICOS-EFA Method and the measurements in the database. The equation used was the SRICOS equation for the maximum pier scour depth. Figure 10.2 shows the predictions by the HEC-18 equation compared to the measurements for the same database. Both SRICOS and HEC 18 appear to be conservative; there is less scatter in the SRICOS predictions.

In order to investigate the influence of D_{50} on the match between SRICOS-EFA predictions and measurements, the database was divided in three D_{50} categories. Figures 10.3 and 10.4 show the results. No obvious trends are evident.

10.3 FROEHLICH (1988) DATABASE: PIER SCOUR

The Froehlich Database was obtained from an ASCE report, "Analysis of Onsite Measurements of Scour at Piers." In the Froehlich Database, there are 79 pier scour measurement points, 50 cases for round-nosed pier, 9 cases for square-nosed pier, and 20 cases for sharp-nosed pier. Figure 10.5 shows the comparison between the complex pier scour depth calculated by the SRICOS-EFA Method and the measurements in the database. The equation used was the SRICOS equation for the maximum pier scour depth. Figure 10.6 shows the HEC-18 equation compared with the same database. With this database, HEC-18 appears to be more conservative than SRICOS.

10.4 GILL (1981) DATABASE: CONTRACTION SCOUR

The Gill Database was obtained from the *Journal of the Hydraulic Division* of the American Society of Civil Engineers (ASCE) in an article entitled "Bed Erosion in Rectangu-

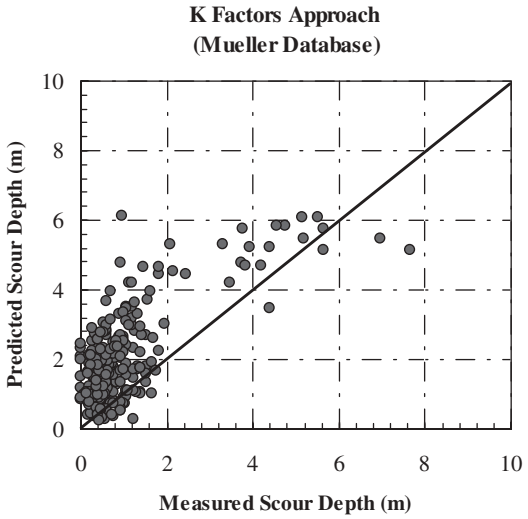

Figure 10.1. SRICOS-EFA predictions against Mueller (1996) Database.

lar Long Contraction." Gill (1981) ran some contraction tests on sand in the laboratory. The experiments were conducted in a rectangular steel channel that was 11.4 m in length, 0.76 m in width and 0.46 m in depth. There were two sizes of contracted sections in the channel. In the first series of experiments, the effective length of the contraction was 1.83 m, excluding the upstream (inlet) and downstream (outlet) transitions, each 0.46 m long. In the second series of experiments, the effective length of the contraction was 2.44 m with transitions each 0.46 m long. The width of the contracted section was 0.5 m. Two types of nearly uniform sand were used in the experiments. The average size of the coarse sand, D_{50}, was

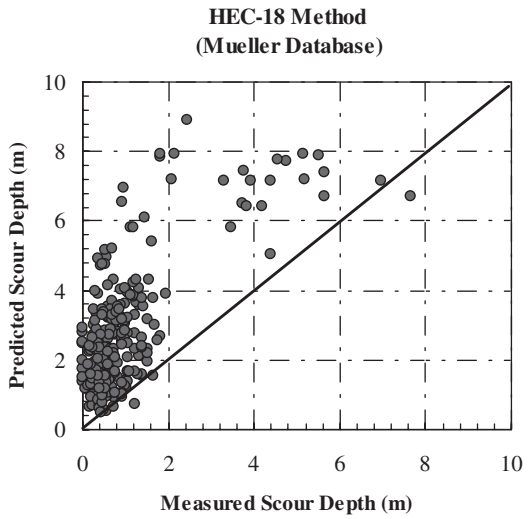

Figure 10.2. HEC-18 predictions against Mueller (1996) Database.

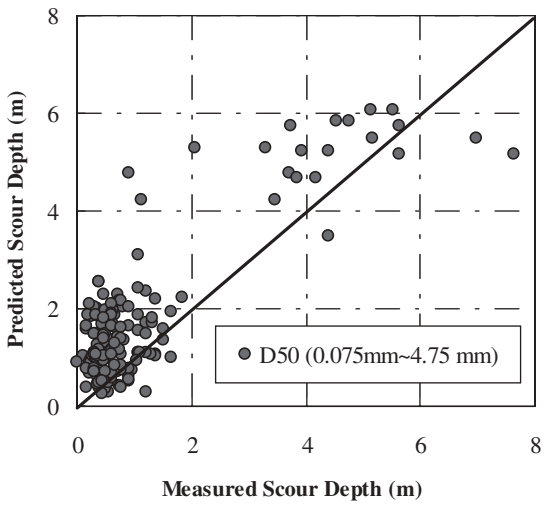

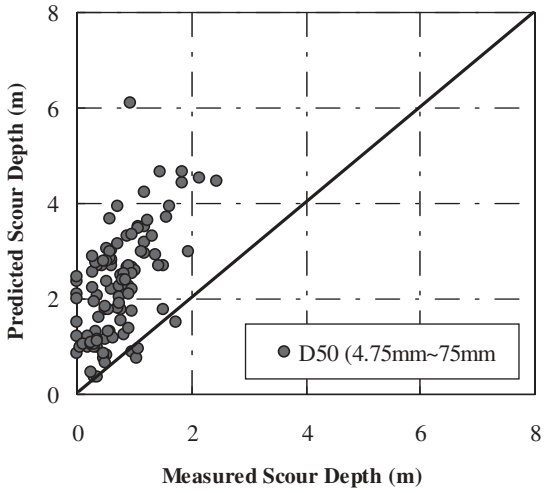

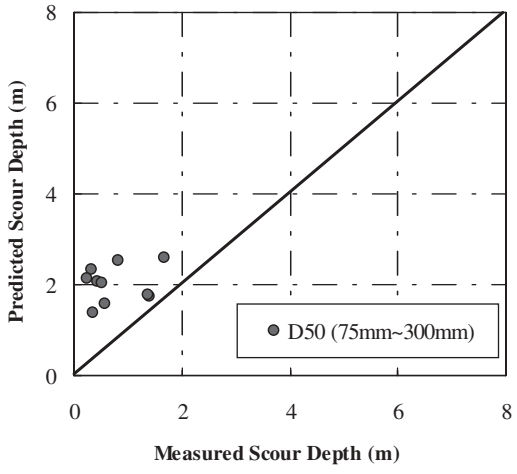

Figure 10.3. SRICOS-EFA predictions versus Mueller Database for various ranges of D_{50}.

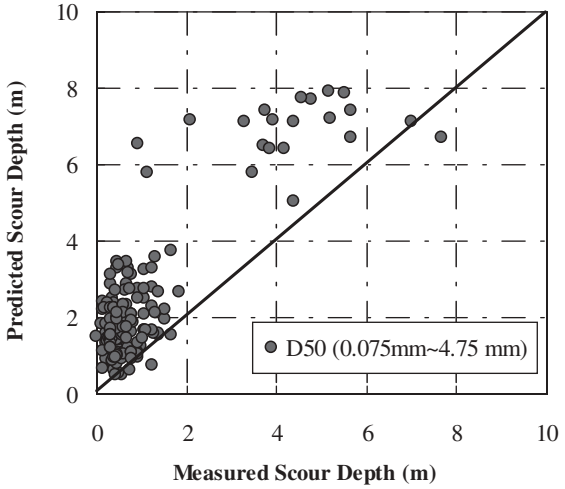

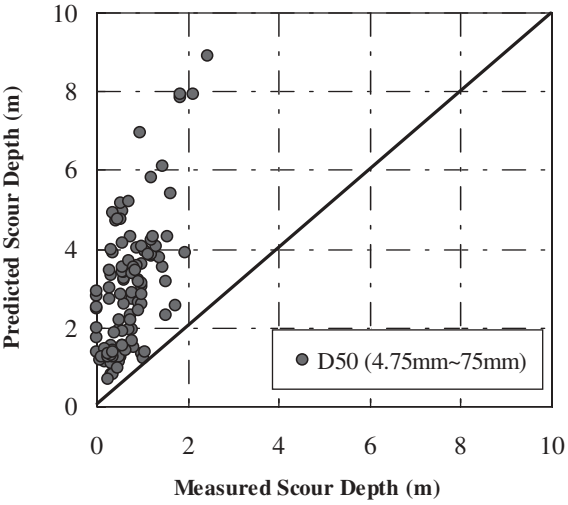

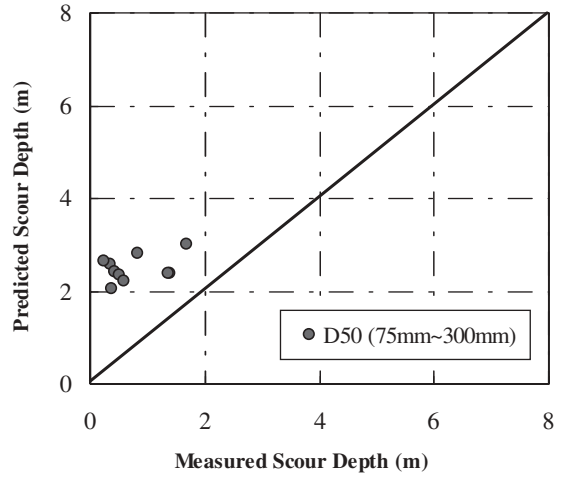

Figure 10.4. HEC-18 predictions versus Mueller Database for various ranges of D_{50}.

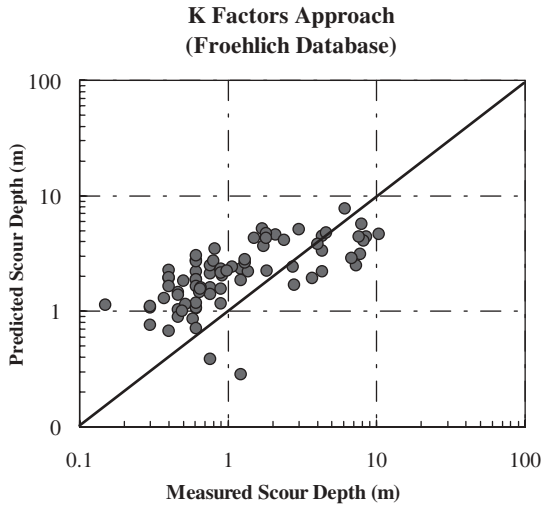

Figure 10.5. SRICOS-EFA predictions against Froehlich (1988) Database.

1.53 mm; D_{50} of the fine sand was 0.92 mm. The angle of transition at the contraction was approximately 15 degrees.

The scour depth was obtained by averaging several depth readings taken along the centerline of the channel. According to the location of the measurements, the scour depth measured by Gill was the uniform scour depth in this study. Therefore, the Gill (1981) Database was used to verify the uniform contraction scour equation Z_{unif}, not Z_{max}. The SRICOS-EFA Method calls for a value of the critical velocity V_c measured in the EFA. Since this data was not available in Gill's database, the expression recommended in HEC-18 was used.

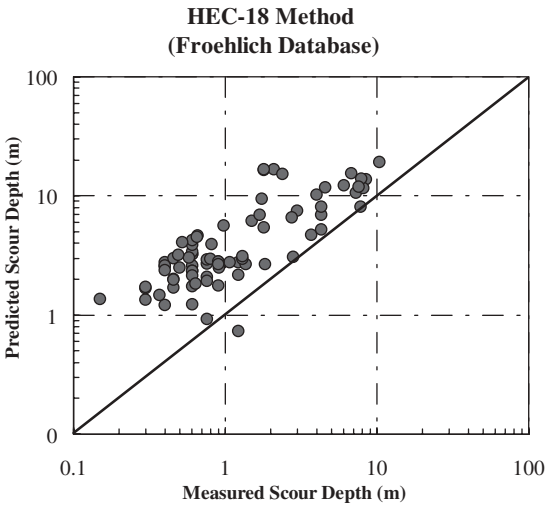

Figure 10.6. HEC-18 predictions against Froehlich (1988) Database.

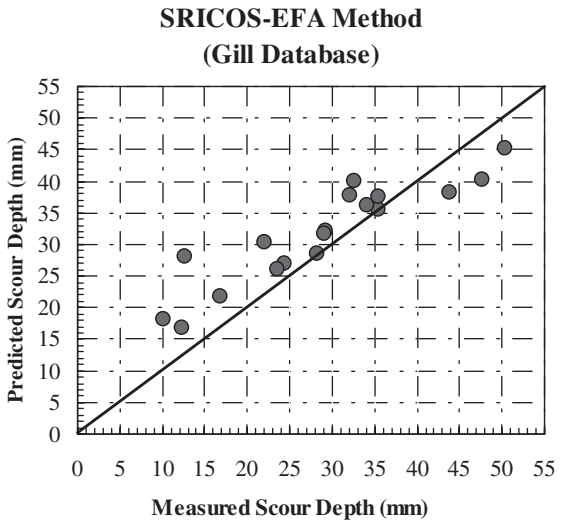

Figure 10.7. SRICOS-EFA Method against Gill (1981) Database.

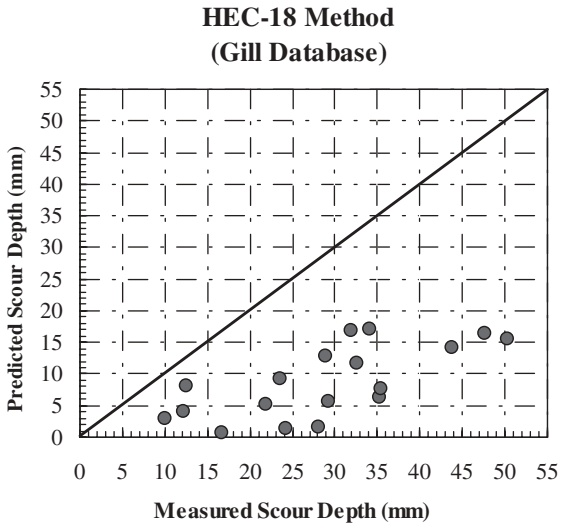

Figure 10.8. HEC-18 Method against Gill (1981) Database.

$$V_c = 6.19 y^{\frac{1}{6}} D_{50}^{\frac{1}{3}} \quad (10.1)$$

where V_c is the critical velocity of the bed material, m/s; y is the water depth in the upstream flow, m; and D_{50} is the particle corresponding to 50% passing by weight, m. Figure 10.7 shows the comparison between the uniform contraction scour depth calculated by the SRICOS-EFA Method and the measurements in the database. Figure 10.8 shows the HEC-18 equation compared with the same database. As shown, the SRICOS Method is reasonably good, but the HEC-18 Method is severely under predicting.

10.5 REMARKS

While it would have been preferable to find a number of full-scale case histories, at least the comparison to databases obtained primarily on cohesionless soils gave an idea of how the SRICOS-EFA Method compares to the HEC-18 Method. Note that the comparison is only based on the maximum depth of scour values and does not involve the scour rate, which is the major difference between the current HEC-18 Method and the SRICOS-EFA Method. Overall, it was found that the performance of the SRICOS-EFA Method is similar to the HEC-18 Method except for the contraction scour depth where the SRICOS-EFA Method is much closer to the measurements.

CHAPTER **11**

FUTURE HYDROGRAPHS AND SCOUR RISK ANALYSIS

11.1 BACKGROUND

Since the SRICOS-EFA Method predicts the scour depth as a function of time, one of the inputs is the velocity versus time curve, or hydrograph, at the foundation location. This hydrograph should cover the period over which the scour depth must be predicted. A typical bridge is designed for 75 years. Therefore, the design for a new bridge requires the knowledge of the hydrograph from the year of construction until 75 years later. The question is: how can one obtain the future hydrograph covering that long period of time? This requires predicting the future over a 75-year period.

One solution is to use a hydrograph recorded at a nearby gage station over the last 75 years and assume that the future hydrograph will be equal to the past hydrograph. If the gage is not at the future bridge location, the discharge can be multiplied by the ratio of the drainage area at the bridge site over the drainage area at the gage site. If the record at the gage station is not 75 years long, one can simply repeat the recorded hydrograph until it covers the 75-year period. If the recorded hydrograph does not include the design flood (100-year flood or 500-year flood), one can spike the hydrograph with one or more of those floods before running the SRICOS program (Figure 11.1).

Another solution is to use the new technique that is presented here. This technique consists of using a past hydrograph, preparing the frequency distribution plot for the floods within that hydrograph, sampling the distribution randomly and preparing a future hydrograph for the required period that has the same mean and standard deviation as the measured hydrograph. This process is repeated 10,000 times and, for each hydrograph, a final scour depth (the depth reached after 75 years of flow) is generated. These 10,000 final depths of scour are organized in a frequency distribution plot with a mean and standard deviation. That plot can be used to quote a scour depth with a corresponding probability of occurrence, or better, to choose a risk level and quote the corresponding final depth of scour.

11.2 PREPARATION OF THE FUTURE HYDROGRAPHS

The SRICOS-EFA Method determines the scour depth at the end of the bridge life as a progressive process driven by a given sequence of daily stream-flow values throughout the life, L_t, of the structure. The randomness of the hydrologic forcing suggests combining the scour model with some hydrological and statistical analyses. If the stream-flow sequence (or hydrograph) is modeled as a stochastic process, it is possible to set up a Monte Carlo procedure that samples different realizations of the hydrograph (of length L_t) from that process and estimates (using the SRICOS-EFA Method) the scour depth, *d,* at the end of the bridge life for each of them. Thus, *d* is regarded as a random variable and its statistics can be studied in detail to determine the risk of failure associated with different choices of the design value of the scour depth.

The modeling of daily stream-flow, *Q,* can be tackled using different approaches (e.g., Bras and Rodriguez-Iturbe, 1986; Montanari et al., 1997; 2000) corresponding to different levels of complexity. A first simple analysis suggested here considers *Q* as a random, uncorrelated variable. A suitable distribution is fit to the data and the hydrographs are then generated as a series of values sampled from such a distribution. Ongoing research also is applying other stochastic models to account for both the autocorrelation and the memory of the process and is assessing whether the temporal structure (i.e., both autocorrelation and memory) of the stream-flow sequences is able to affect the statistical properties of the scour-depth probability distribution.

The theoretical distribution used to model daily stream-flow observations needs to be defined only for positive values of *Q,* to have a positive skew, and to be able to provide an accurate representation of the extreme values (i.e., good fit at the upper tail of the distribution). As expected, the extreme values are found to greatly affect the scour depth estimates and an imprecise modeling of stream-flow maxima could easily lead to unrealistic estimations of the scour depth statistics. Logarithmic transformations are frequently used to study stream-flow extremes (e.g., Chow et al., 1988; Benjamin and Cornell, 1970); therefore, a log-normal distribution can be a good candidate for modeling the daily stream-flows. The method of moments is used to determine the parameters of the distribution. As such, *Q* is expressed as the exponential of a normally distributed random variable, *y,* with mean

$$\mu_y = \frac{1}{2}\mathrm{Log}\left[\frac{\mu_Q{}^2}{1+\left(\frac{\sigma_Q}{\mu_Q}\right)^2}\right] \tag{11.1}$$

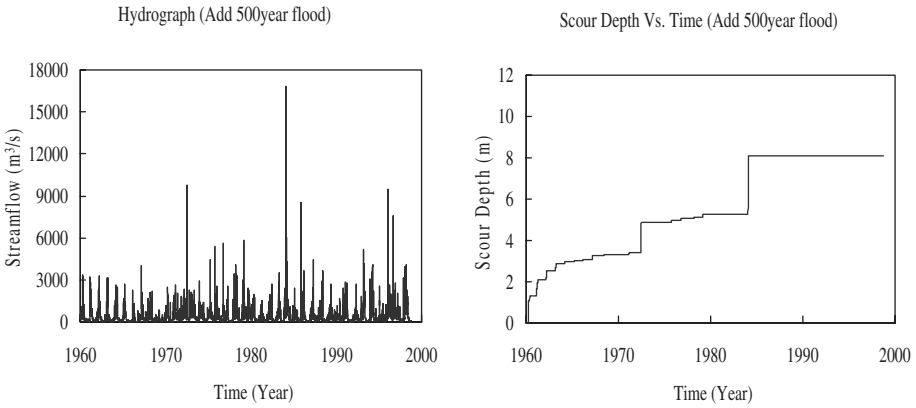

(a) Hydrograph **(b)** Scour Depth Vs. Time Curve

Figure 11.1. Woodrow Wilson measured hydrograph spiked with a 500-year flood.

and standard deviation

$$\sigma_y = \sqrt{\mathrm{Log}\left[1+\left(\frac{\sigma_Q}{\mu_Q}\right)^2\right]} \qquad (11.2)$$

with μ_Q and σ_Q being the mean and the standard deviation of daily stream-flow, respectively.

In the case of the Woodrow Wilson Bridge, stream-flow data is available at the Little Falls Station (USGS #01646500) on the Potomac River, approximately 13 km upstream from the bridge. Correction of the measured stream flow is applied by multiplying the values by the drainage area ratio. The correction is on the order of 3%. Figure 11.2 shows the original hydrograph and the corresponding prediction of scour depth history using the SRICOS-EFA Method. The mean and standard deviation of Q in the period of record 1931–2000 are μ_Q=327 m^3s^{-1}, and σ_Q=467 m^3s^{-1}, respectively, while the maximum discharge in the 70-year-long record was 12,056 m^3s^{-1}. Synthetic hydrographs of the same length generated by sampling from a log-normal distribution of mean μ_Q and standard deviation σ_Q have, on average, a maximum value of about 12,000 m^3s^{-1}, which suggests that such a distribution gives an adequate representation of the extrema. Figure 11.3 shows an example of a generated future hydrograph and the associated scour depth history as predicted by the SRICOS-EFA Method.

11.3 RISK APPROACH TO SCOUR PREDICTIONS

Many equally possible future hydrographs such as the one in Figure 11.3 are generated by the random sampling process. For each hydrograph, the SRICOS program generates a scour depth history, including a final depth of scour, d, at the end of the project life. These values of the final depth of scour can be organized in a frequency distribution. Figure 11.4 shows the probability distributions obtained for the example of the Woodrow Wilson Bridge at the end of a chosen bridge life, L_t.

This analysis can be used to estimate the level of risk, R, associated with the choice of different design values of scour depth and project lives. By definition, the risk level is the prob-

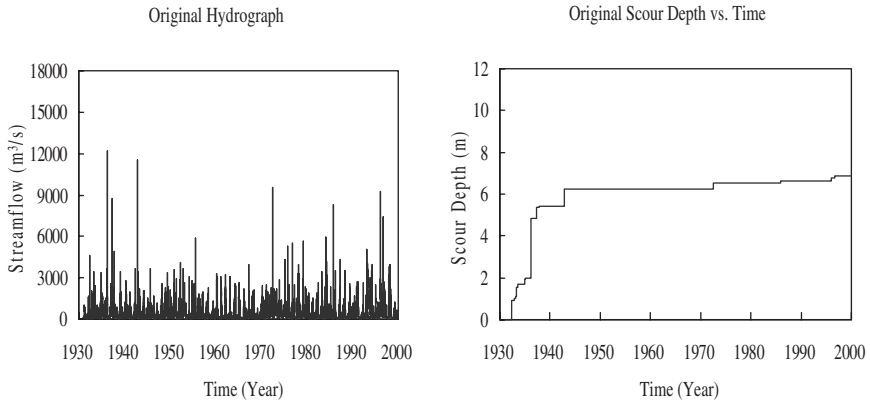

(a) Hydrograph **(b)** Scour Depth vs. Time

Figure 11.2. Original hydrograph and scour depth versus time near Woodrow Wilson Bridge site.

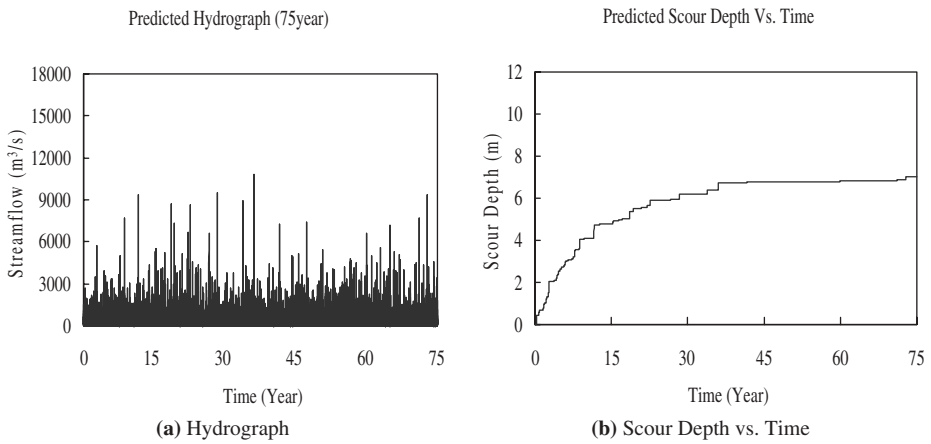

(a) Hydrograph **(b)** Scour Depth vs. Time

Figure 11.3. Predicted hydrograph and scour depth versus time curve near Woodrow Wilson Bridge site (Project time = 75 years).

ability that the design conditions are exceeded in the course of the life of the structure. Thus, from the probability distribution of d (Figure 11.4) it is possible to determine the cumulative distribution function (CDF) of d (Figure 11.5). The risk is then estimated as the probability of exceedance (Figure 11.5). Table 11.1 reports the risk level associated with different project lives and design values of d. It is observed that R is a nonlinear function of d and L_t. This analysis provides a statistical framework that can be used in a cost–benefit study of bridge foundation design.

Commonly accepted methods of scour analysis in cohesionless soils refer to a single peak-flow value selected on the basis of its return period, T_r, as well as to the associated level of risk. Such an approach does not account for the contribution to bridge scour due to smaller (and more frequent) floods. The SRICOS-EFA Method can be used to include the effect of the entire hydrograph. The Monte Carlo procedure outlined in this section represents a possible new probabilistic approach to scour analysis. Ongoing research is developing an extended version of this approach using different stochastic hydrologic models able to account for the daily flow distribution and for the autocorrelation of the stream-flow series. This study will show whether the scour depth is sensitive to the temporal structure of stream-flow sequences and will indicate the level of detail that is necessary to include in the hydrologic stochastic model.

11.4 OBSERVATIONS ON CURRENT RISK LEVELS

A direct comparison between the risk results obtained here with the SRICOS Method (Table 11.1) and traditional approaches based on single peak-flow values is not easy. Nevertheless, an example is provided here. The peak-flow value associated with a given return period can be determined through a flood-frequency analysis (e.g., Chow et al., 1988; pp. 375–378). Figure 11.6 shows the result of such an analysis for the Woodrow Wilson Bridge measured hydrograph. As can be seen on that figure, the 100-year flood has a discharge of 12,600 m^3/s and the 500-year flood has a value of 16,600 m^3/s. If the design life of the bridge is L_t, the

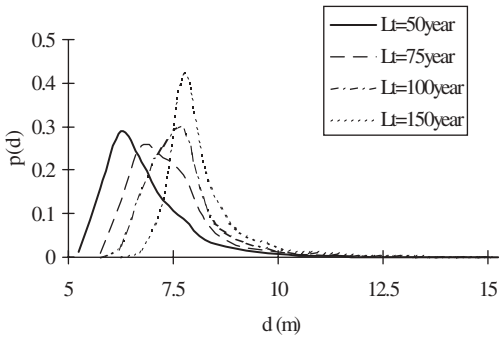

Figure 11.4. Probability distribution of scour depth, d, for different lengths of the project life, L_t.

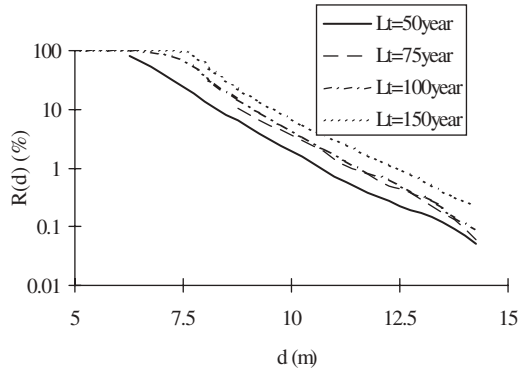

Figure 11.5. Risk associated with different design values of the final scour depth, d, and different lengths of the project life, L_t.

TABLE 11.1 Risk of failure associated with different design values of scour depth and project lives

Design value of	Project Life			
Scour depth (m)	50 yrs	75 yrs	100 yrs	150 yrs
6.5	42%	74%	91%	99.8%
7.0	25%	48%	70%	93%
7.5	14%	27%	40%	65%

probability of exceedance or risk R for a flood having a return period T_r is given by the following:

$$R = 1 - (1 - 1/T_r)^{Lt} \tag{11.3}$$

If the design life of the bridge is 75 years, the probability that the flood with a return period of 100 years will be exceeded during the 75-year design life is 53% (or about one chance out of two) according to Equation 11.3. For the 500-year flood and for the same 75-year design life, the risk is 14% (or about one chance in seven).

Even if a bridge designed for a 100- or 500-year flood experiences a 1,000-year flood, this bridge may not collapse. Indeed, collapse of the bridge is based on a different criterion than just exceedance of the design flood. There are numerous inherent redundancies in the design of a bridge and many design parameters have to be exceeded before collapse occurs. Nevertheless, the risk level associated with the floods used in everyday design appears very high compared to risk levels in other disciplines within civil engineering. For example, structural engineers have based their codes on a risk level of about 0.1%. Geotechnical engineers probably operate at about 1%. Scour engineers seem to operate at a much higher risk level. This is particularly worrisome since there is no safety factor on the depth of scour passed on from the scour engineer to the geotechnical engineer from which the pile length is calculated.

One useful approach in this respect is to conduct a sensitivity analysis by varying the input parameters and monitoring the impact of the parameter variation on the final scour depth. This would help in realizing how important each parameter is and give a range of scour depth values. Note that the proposed method is a prediction method, not a design method. Indeed, the equations were derived from a number of best-fit regressions against the experimental data. The proposed method becomes a design method when a factor of safety is added. The recommended factor of safety is 1.5. In other words, the predicted final depth of scour should be multiplied by 1.5 before it becomes a design scour depth.

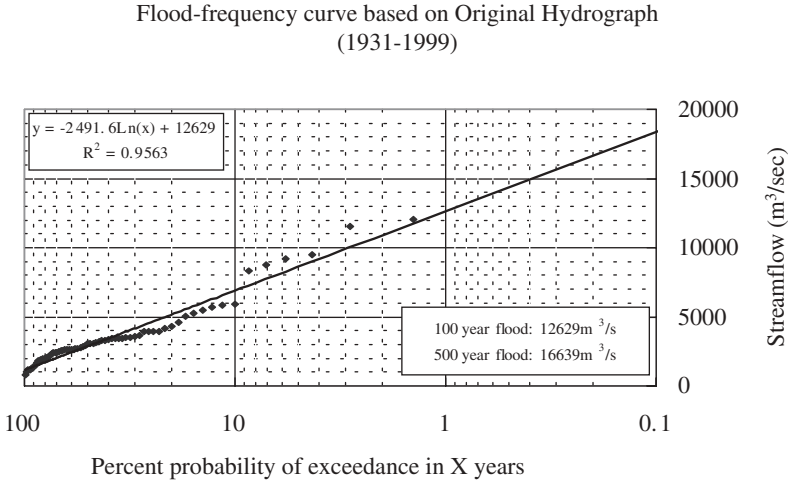

Figure 11.6. Flood-frequency curve for the Potomac River at the Woodrow Wilson Bridge.

CHAPTER **12**

SCOUR EXAMPLE PROBLEMS

12.1 EXAMPLE 1: SINGLE CIRCULAR PIER WITH APPROACHING CONSTANT VELOCITY

Given:

Pier geometry:	Pier diameter $B = 2.5$ m, circular pier
Channel geometry:	Channel upstream width $B_1 = 50$ m
Flow parameters:	Water depth $H = 3.12$ m, Approaching constant velocity $V = 3.36$ m/sec Angle of attack: 0 degrees
EFA result:	Layer 1: Thickness 10 m; critical shear stress 2 N/m^2 Layer 2: Thickness 20 m; critical shear stress 4 N/m^2
Flood period:	2 days for hand calculation 2 years for computer calculation
Determine:	The magnitude of maximum pier scour depth

12.1.1 SRICOS-EFA Method: Hand Calculation

(1) Calculate the K factors for τ_{max} and Z_{max}:

$$k_w = 1 + 16 \cdot e^{-4\frac{H}{B}} = 1 + 16 \cdot e^{-4\times\frac{3.12}{2.5}} = 1.109$$

$$K_w = 0.85\left(H/B\right)^{0.34} = 0.85 \times \left(\frac{3.12}{2.5}\right)^{0.34} = 0.916$$

Since the pier in this case is a circular pier, $k_{sh} = 1$ and $K_{sh} = 1$.
It is a single pier, so $k_{sp} = 1$ and $K_{sp} = 1$.
There is no attack angle of the flow, so $k_\alpha = 1$.

(2) Calculate Reynolds Number as

$$R_e = \frac{Vd}{v} = \frac{3.36 \times 2.5}{10^{-6}} = 8.4 \times 10^6$$

(3) Maximum hydraulic shear stress around the pier is

$$\tau_{max} = k_w k_{sh} k_{sp} k_\alpha \cdot 0.094 \rho V^2 \left[\frac{1}{\log R_e} - \frac{1}{10}\right] = 1.109$$

$$\times 0.094 \times 1000 \times 3.36^2 \left[\frac{1}{\log\left(8.4 \times 10^6\right)} - \frac{1}{10}\right]$$

$$= 52.28\ N/m^2$$

(4) The initial rate of scour $\dot{Z}$ is read on the EFA curve (Layer 1) at $\tau = \tau_{max}$

$\dot{Z} = 8.6$ mm/hr

(5) The maximum depth of scour Z_{max} is

Z_{max} (Pier) $= 0.18 K_w K_{sp} K_{sh} R_e^{0.635} = 0.18 \times 0.916 \times (8.4 \times 10^6)^{0.635} = 4112.3$mm

(6) The equation for $z\ (t)$ is

$$z = \frac{t}{\frac{1}{\dot{Z}} + \frac{t}{Z_{max}}} = \frac{t(\text{hrs})}{\frac{1}{8.6} + \frac{t(\text{hrs})}{4112.3}}$$

(7) The flood lasts 2 days (48 hours), therefore

$Z = 375$ mm or 9.1% of Z_{max}

12.1.2 SRICOS-EFA Method: Computer Calculation

Use SRICOS-EFA program Option 1: Complex Pier Scour

Results:
After a 2-year period of the flood having 3.36 m/s velocity, the final pier scour is

$Z = 4$ m

Table 12.1 and Figures 12.1 through 12.3 provide further information. Figure 12.4 illustrates the scour depth development with time.

12.2 EXAMPLE 2: SINGLE RECTANGULAR PIER WITH ATTACK ANGLE AND APPROACHING HYDROGRAPH

Given:

Pier geometry:	Pier width $B = 1.22$ m, pier length $L_{pier} = 18$ m, rectangular pier

TABLE 12.1 Summary of data input (Example 1)

Input Unit **Output Unit**		SI SI	1 1
First Date of Analysis **Last Date of Analysis**			01-01-2003 01-01-2005
No. Of Input Data			730
Upstream Channel Width **Type of Pier** **Pier Diameter**		Circular Pier	50 1 2.5
Time Step		Hours	24
Type of Hydrologic Input **Number of Regression Points** **Values of Regression Points**		Velocity Velocity vs. Water Depth Velocity, Water Depth	2 1 3.36, 3.12
No. Of Layers			2
Properties of 1st Layer		Thickness Critical Shear Stress	10 2
Estimate Initial Scour Rate	**Number of Regression Points**	Shear Stress vs. Scour Rate	8
	Value of Regression Points	Shear Stress, Scour Rate	1, 0 2, 0.1 4,1 6,2 9, 3 20, 6 40, 8 60, 8.9
Properties of 2nd Layer		Thickness Critical Shear Stress	20 4
Estimate Initial Scour Rate	**Number of Regression Points**	Shear Stress vs. Scour Rate	8
	Value of Regression Points	Shear Stress, Scour Rate	3, 0 4, 0.1 6,1 9,2 18.5, 4 27, 5 40, 6 60, 6.9

Scour rate (mm/hr)	Shear stress (N/m^2)
0	1
0.1	2
1	4
2	6
3	9
6	20
8	40
8.9	60

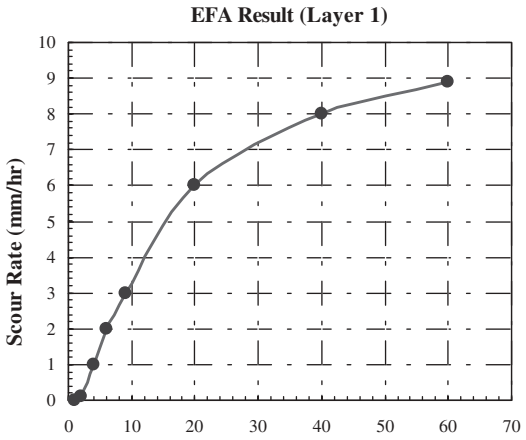

Figure 12.1. EFA Results for Soil Layer 1 (Example 1).

Scour rate (mm/hr)	Shear stress (N/m^2)
0	3
0.1	4
1	6
2	9
4	18.5
5	27
6	40
6.9	60

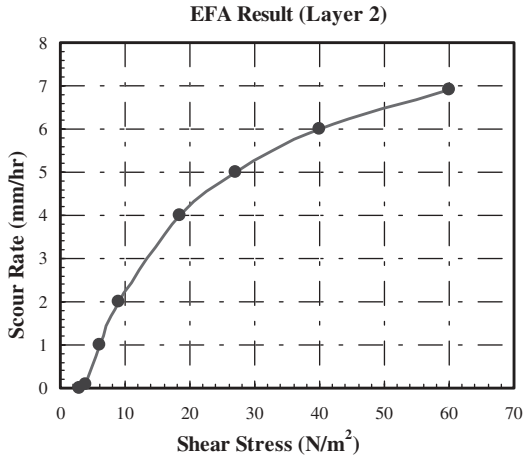

Figure 12.2. EFA Results for Soil Layer 2 (Example 1).

Channel geometry: Channel upstream width $B_1 = 50$ m
Flow parameters: Angle of attack: 20 degrees
70 years predicted hydrograph
EFA result: Layer 1: Thickness 10 m; critical shear stress 2 N/m^2
Layer 2: Thickness 20 m; critical shear stress 4 N/m^2
Time duration: 70 years
Determine: The magnitude of maximum pier scour depth

12.2.1 SRICOS-EFA Method: Computer Calculation

Since the hydrograph is used in this case as hydrologic data input, the relationship between discharge and velocity and the relationship between discharge and water depth need to be defined. The HEC-RAS program can be a good tool to define these relationships. The following charts present the results obtained from HEC-RAS for this case.

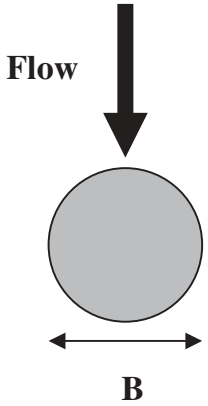

Figure 12.3. Plan view of single circular pier scour case (Example 1).

Use SRICOS-EFA program Option 1: Complex Pier Scour.

Results:
After a 70-year period of flood, the final pier scour is

$Z = 4.7$ m

Table 12.2 lists data input for this example. Figure 12.5 illustrates the scour depth development with time. Figures 12.6 through 12.8 provide further information.

12.3 EXAMPLE 3: GROUP RECTANGULAR PIERS WITH ATTACK ANGLE AND APPROACHING CONSTANT VELOCITY

Given:
Pier geometry: Pier width $B = 1.22$ m, pier length $L_{pier} = 18$ m, rectangular pier, number of piers, N = 3, spacing, $S = 18$ m
Channel geometry: Channel upstream width $B_1 = 150$ m
Flow parameters: Water depth $H = 3.12$ m,
Angle of attack: 20 degrees

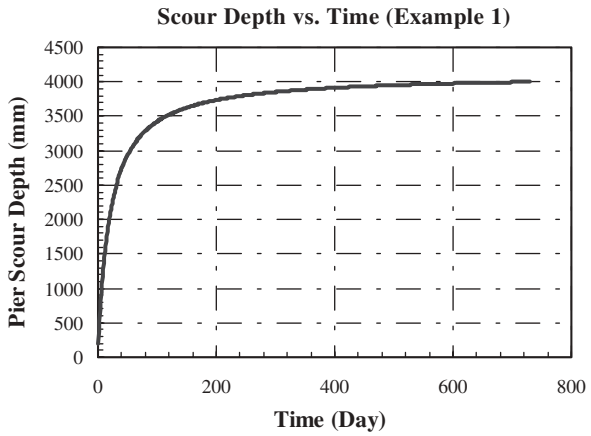

Figure 12.4. Scour depth versus time (Example 1).

TABLE 12.2 Summary of data input (Example 2)

Input Unit **Output Unit**		SI SI	1 1
First Date of Analysis **Last Date of Analysis**			01-01-2003 01-01-2073
No. Of Input Data			25569
Upstream Channel Width			50
Type of Pier **Pier Width** **Pier Length** **Attack Angle** **Number of Piers**		Rectangular Pier	2 1.22 18 20 1
Time Step		Hours	24
Input Hydrologic Data	**Type of Hydrologic Input**	Discharge	1
	Number of Regression Points	Discharge vs. Velocity	8
	Values of Regression Points	Discharge, Velocity	1.42, 0 14, 0.02 141, 0.16 566, 0.49 1415, 0.87 5663, 1.75 13592, 2.97 19821, 3.56
	Number of Regression Points	Discharge vs. Water Depth	8
	Values of Regression Points	Discharge, Water Depth	1.42, 3.86 14, 4.18 141, 5.02 566, 6.18 1415, 7.83 5663, 11.33 13592, 13.15 19821, 14.19
No. Of Layers			2
Properties of 1st Layer		Thickness Critical Shear Stress	10 2
Estimate Initial Scour Rate	**Number of Regression Points**	Shear Stress vs. Scour Rate	8
	Value of Regression Points	Shear Stress, Scour Rate	1, 0 2, 0.1 4,1 6,2 9, 3 20, 6 40, 8 60, 8.9
Properties of 2nd Layer		Thickness Critical Shear Stress	20 4
Estimate Initial Scour Rate	**Number of Regression Points**	Shear Stress vs. Scour Rate	8
	Value of Regression Points	Shear Stress, Scour Rate	3, 0 4, 0.1 6,1 9,2 18.5, 4 27, 5 40, 6 60, 6.9

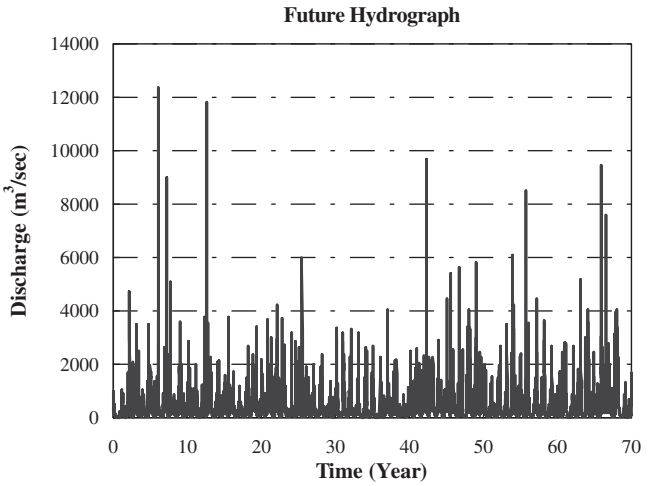

Figure 12.5. Seventy years future approaching hydrograph (Example 2).

Approaching constant velocity V = 3.36 m/sec

EFA result: Layer 1: Thickness 10 m; critical shear stress 2 N/m^2

Layer 2: Thickness 20 m; critical shear stress 4 N/m^2

Flood period: 2 days for hand calculation
2 years for computer calculation

Determine: The magnitude of maximum pier scour depth

12.3.1 SRICOS-EFA Method: Hand Calculation

(1) Calculate the K factors for τ_{max} and Z_{max} as follows:

$$k_w = 1 + 16 \cdot e^{-4\frac{H}{B}} = 1 + 16 \cdot e^{-4\times\frac{3.12}{7.3}} = 3.9$$

$$K_w = 0.85\left(H/B\right)^{0.34} = 0.85 \times \left(\frac{3.12}{7.3}\right)^{0.34} = 0.637$$

Here, B is the projected width of pier.

$B = L_{pier} \sin\alpha + W \cos\alpha = 18 \times \sin 20° + 1.22 \times \cos 20° = 7.3$ m

Scour rate (mm/hr)	Shear stress (N/m^2)
0	1
0.1	2
1	4
2	6
3	9
6	20
8	40
8.9	60

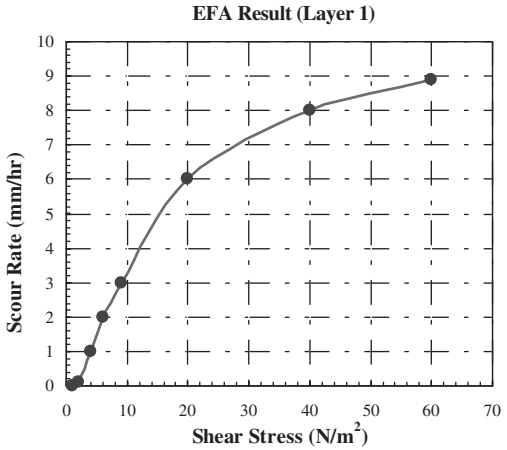

Figure 12.6. EFA results for Soil Layer 1 (Example 2).

Scour rate (mm/hr)	Shear stress (N/m^2)
0	3
0.1	4
1	6
2	9
4	18.5
5	27
6	40
6.9	60

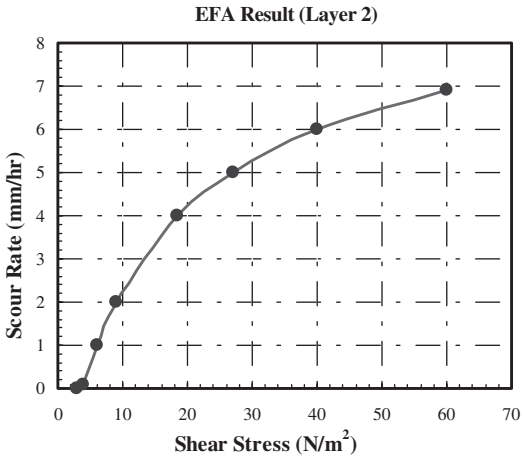

Figure 12.7. EFA results for Soil Layer 2 (Example 2).

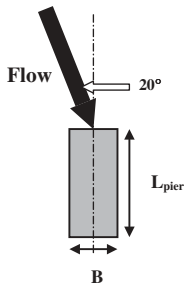

Figure 12.8. Plan view of single rectangular pier scour case (Example 2).

Since in this case, the pier is a rectangular pier, so

$$k_{sh} = 1.15 + 7 \times e^{-4\frac{18}{1.22}} = 1.15$$

Since there are three piers in this case, the effect of a group pier exists.

$$k_{sp} = 1 + 5e^{\left(-1.1\frac{S}{D}\right)} = 1 + 5e^{\left(-1.1\frac{18}{7.3}\right)} = 1.33$$

$$K_{sp} = \frac{B_1}{B_1 - nB} = \frac{150}{150 - 3*7.3} = 1.17$$

There is attack angle of the flow, so

$$k_{\alpha} = 1 + 1.5\left(\frac{\alpha}{90}\right)^{0.57} = 1 + 1.5\left(\frac{20}{90}\right)^{0.57} = 1.636$$

TABLE 12.3 Summary of data input (Example 3)

Input Unit		SI	1
Output Unit		SI	1
First Date of Analysis			01-01-1998
Last Date of Analysis			01-01-2000
No. Of Input Data			730
Upstream Channel Width		Rectangular Pier	150
Type of Pier			2
Pier Width			1.22
Pier Length			18
Attack angle			20
Number of piers			3
Pier spacing			18
Time Step		Hours	24
Type of Hydrologic Input		Velocity	2
Number of Regression Points		Velocity vs. Water Depth	1
Values of Regression Points		Velocity, Water Depth	3.36, 3.12
No. Of Layers			2
Properties of 1st Layer		Thickness	10
		Critical Shear Stress	2
Estimate Initial Scour Rate	**Number of Regression Points**	Shear Stress vs. Scour Rate	8
	Value of Regression Points	Shear Stress, Scour Rate	1, 0 4, 1 6,2 9,3 6, 30 100, 10 200, 12.5 400, 16
Properties of 2nd Layer		Thickness	20
		Critical Shear Stress	4
Estimate Initial Scour Rate	**Number of Regression Points**	Shear Stress vs. Scour Rate	8
	Value of Regression Points	Shear Stress, Scour Rate	3, 0 4, 0.1 6,1 9,2 18.5, 4 27, 5 40, 6 60, 6.9

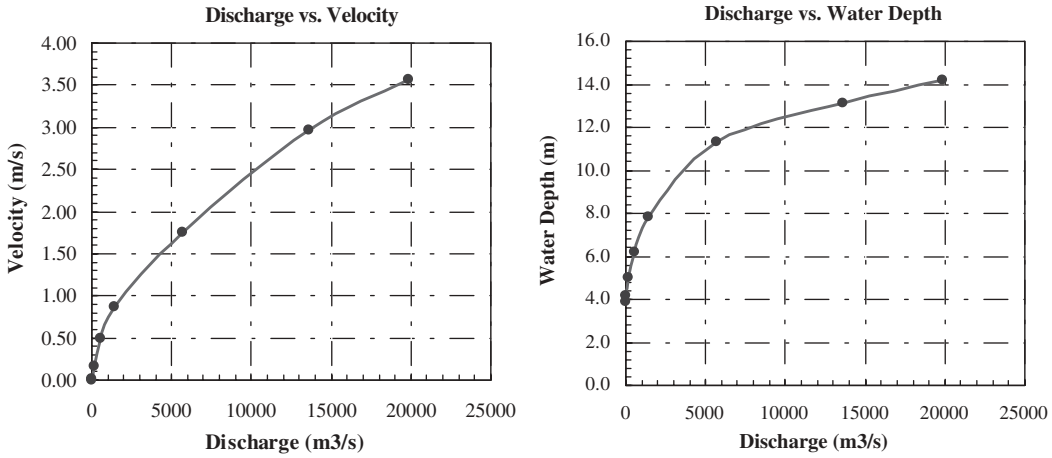

Figure 12.9. Relationship of discharge versus velocity and discharge versus water depth (Example 2).

(2) Calculate Reynolds Number

$$R_e = \frac{VD}{v} = \frac{3.36 \times 7.3}{10^{-6}} = 2.45 \times 10^7$$

(3) Maximum hydraulic shear stress around the pier is

$$\tau_{max} = k_w k_{sh} k_{sp} k_\alpha \cdot 0.094 \rho V^2 \left[\frac{1}{\log R_e} - \frac{1}{10}\right]$$

$$\tau_{max} = 3.9 \times 1.15 \times 1.33 \times 1.636 \times 0.094 \times 1000 \times 3.36^2 \left[\frac{1}{\log(2.45 \times 10^7)} - \frac{1}{10}\right]$$

$$= 365.8 \, N/m^2$$

(4) The initial rate of scour $\dot{Z}$ is read on the EFA curve (Layer 1) at $\tau = \tau_{max}$

$\dot{Z} = 15.3$ mm/hr

(5) The maximum depth of scour Z_{max} is

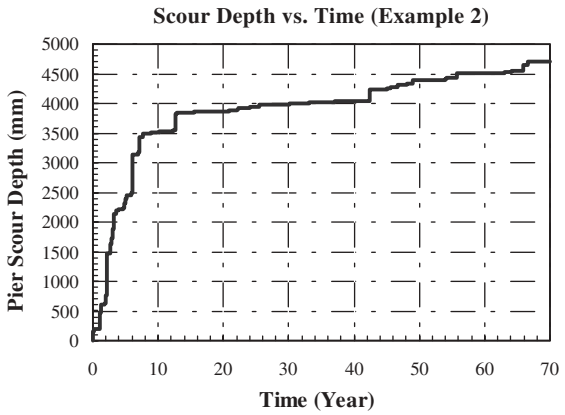

Figure 12.10. Scour depth versus time (Example 2).

$$Z_{max}(Pier) = 0.18 K_w K_{sp} K_{sh} R_e^{0.635}$$

$$Z_{max} = 0.18 \times 0.64 \times 1.17 \times 1.1 \times (2.45 \times 10^7)^{0.635} = 7297 \text{ mm}$$

(6) The equation for z (t) is

$$z = \frac{t}{\frac{1}{\dot{Z}} + \frac{t}{Z_{max}}} = \frac{t(\text{hrs})}{\frac{1}{15.3} + \frac{t(\text{hrs})}{7297}}$$

(7) The flood lasts 2 days (48 hours), therefore

$Z = 667$ mm or 9.1% of Z_{max}

12.3.2 SRICOS-EFA Method: Computer Calculation

Use SRICOS-EFA program Option 1: Complex Pier Scour

Results:
After a 2-year period of flood having 3.36 m/sec velocity, the final pier scour is

$Z = 7.1$ m

Table 12.3 provides a summary of input data. Figure 12.11 illustrates the scour depth development with time. Figures 12.12 through 12.14 provide further information.

12.4 EXAMPLE 4: CONTRACTED CHANNEL WITH 90-DEGREE TRANSITION ANGLE AND APPROACHING CONSTANT VELOCITY

Given:

Channel geometry: Upstream uncontracted channel width $B_1 = 150$ m, contracted channel width due to bridge abutment $B_2 = 50$ m, contraction length of channel L: = 30 m

Scour rate (mm/hr)	Shear stress (N/m^2)
0	1
1	4
2	6
3	9
6	30
10	100
12.5	200
16	400

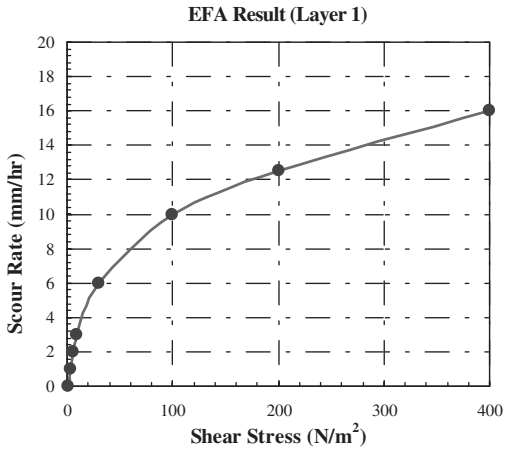

Figure 12.11. EFA results for Soil Layer 1 (Example 3).

Scour rate (mm/hr)	Shear stress (N/m^2)
0	3
0.1	4
1	6
2	9
4	18.5
5	27
6	40
6.9	60

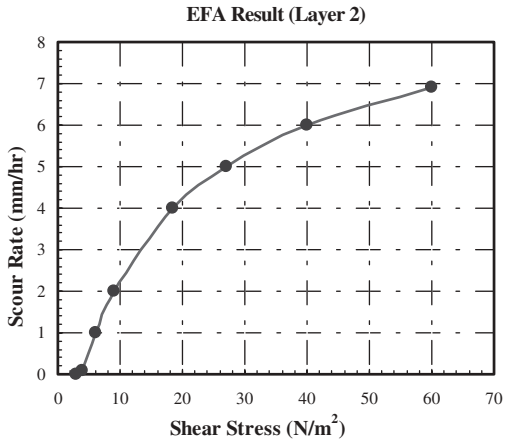

Figure 12.12. EFA results for Soil Layer 2 (Example 3).

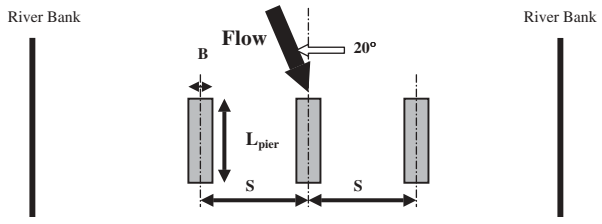

Figure 12.13. Plan view of rectangular piers group scour case (Example 3).

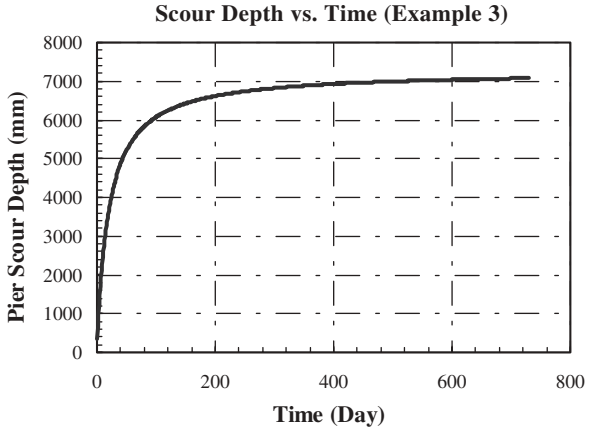

Figure 12.14. Scour depth versus time (Example 3).

TABLE 12.4 Summary of data input (Example 4)

Input Unit **Output Unit**		SI SI	1 1
First Date of Analysis **Last Date of Analysis**			01-01-2003 01-01-2005
No. Of Input Data			730
Upstream Uncontracted Channel Width **Contracted Channel Width** **Contraction Length of Channel** **Transition Angle of Channel** **Manning's Coefficient** **Average Hydraulic Radius**			150 50 30 90 0.02 2.77
Time Step		Hours	24
Type of Hydrologic Input **Number of Regression Points** **Values of Regression Points**		Velocity Velocity vs. Water Depth Velocity, Water Depth	2 1 3.36, 3.12
No. of Layers			2
Properties of 1st Layer		Thickness Critical Shear Stress	15 2
Estimate Initial Scour Rate	**Number of Regression Points**	Shear Stress vs. Scour Rate	8
	Value of Regression Points	Shear Stress, Scour Rate	1, 0 4, 1 6,2 9,3 6, 30 100, 10 200, 12.5 400, 16
Properties of 2nd Layer		Thickness Critical Shear Stress	20 4
Estimate Initial Scour Rate	**Number of Regression Points**	Shear Stress vs. Scour Rate	8
	Value of Regression Points	Shear Stress, Scour Rate	3, 0 4, 0.1 6,1 9,2 18.5, 4 27, 5 40, 6 60, 6.9

Abutment transition angle: 90 degrees
Flow parameters: Water depth $H = 3.12$ m, Approaching constant velocity $V = 3.36$ m/sec
Manning Coefficient: 0.02
EFA result: Layer 1: Thickness 15 m; critical shear stress 2 N/m^2
Layer 2: Thickness 20 m; critical shear stress 4 N/m^2
Flood period: 2 days for hand calculation
2 years for computer calculation
Determine: The magnitude of maximum contraction scour depth

12.4.1 SRICOS-EFA Method: Hand Calculation

(1) Calculate the K factors for τ_{max}:

$$k_w \approx 1$$

$$k_R = 0.62 + 0.38\left(\frac{B_1}{B_2}\right)^{1.75} = 0.62 + 0.38\left(\frac{150}{50}\right)^{1.75} = 3.2$$

$$k_\theta = 1 + 0.9\left(\frac{\theta}{90}\right)^{1.5} = 1 + 0.9\left(\frac{90}{90}\right)^{1.5} = 1.9$$

$$\text{Since } \frac{L}{(B_1 - B_2)} = \frac{30}{100} = 0.3 < 0.35, \text{so}$$

$$k_L = 0.77 + 1.36\left(\frac{L}{B_1 - B_2}\right) - 1.98\left(\frac{L}{B_1 - B_2}\right)^2 \approx 1$$

Scour rate (mm/hr)	Shear stress (N/m^2)
0	1
1	4
2	6
3	9
6	30
10	100
12.5	200
16	400

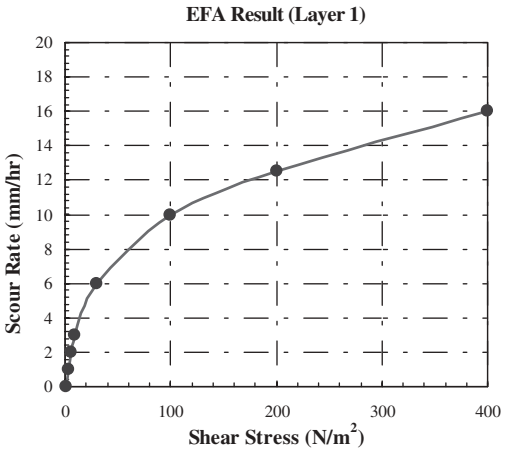

Figure 12.15. EFA results for Soil Layer 1 (Example 4).

(2) Calculate hydraulic radius of contracted section

$$R_h = \frac{A}{P} = \frac{3.12 \times 50}{2 \times 3.12 + 50} = 2.77\,\text{m}$$

(3) Maximum hydraulic shear stress in contraction channel is

$$\tau_{max} = k_R k_L k_w k_\theta \cdot \gamma n^2 V^2 R_h^{-\frac{1}{3}} = 3.2 \times 1.9 \times 9810$$

$$\times 0.02^2 \times 3.36^2 \times 2.77^{-\frac{1}{3}} = 191.8\,N/m^2$$

(4) The initial rate of scour $\dot{Z}$ is read on the EFA curve at $\tau = \tau_{max}$

$$\dot{Z} = 12.2 \text{ mm/hr}$$

(5) The maximum depth of scour Z_{max} is

$$Z_{max}(\text{Cont}) = 1.9\left(\frac{1.38\left[V_1 \frac{B_1}{B_2}\right]}{\sqrt{gH}} - \frac{\left[\frac{\tau_C}{\rho}\right]^{0.5}}{gnH^{\frac{1}{3}}}\right)$$

$$\cdot H = 13.98\,m$$

$$Z_{max}(\text{Unif}) = 1.41\left(\frac{1.31\left[V_1 \frac{B_1}{B_2}\right]}{\sqrt{gH}} - \frac{\left[\frac{\tau_C}{\rho}\right]^{0.5}}{gnH^{\frac{1}{3}}}\right)$$

$$\cdot H = 9.81\,m$$

(6) The equation for $z\,(t)$ is

$$z = \frac{t}{\frac{1}{\dot{Z}} + \frac{t}{Z_{max}}} = \frac{t(\text{hrs})}{\frac{1}{12.2} + \frac{t(\text{hrs})}{13980}}$$

$$z = \frac{t}{\frac{1}{\dot{Z}} + \frac{t}{Z_{max}}} = \frac{t(\text{hrs})}{\frac{1}{12.2} + \frac{t(\text{hrs})}{9810}}$$

Scour rate (mm/hr)	Shear stress (N/m^2)
0	3
0.1	4
1	6
2	9
4	18.5
5	27
6	40
6.9	60

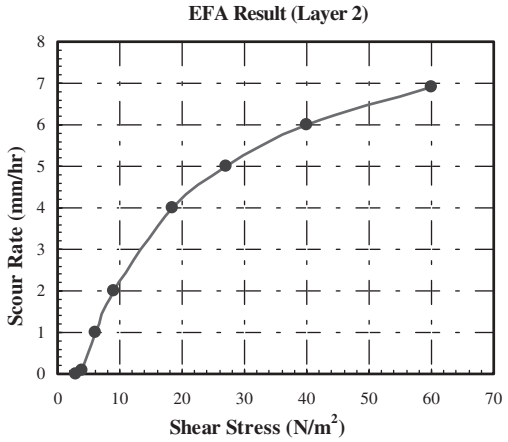

Figure 12.16. EFA results for Soil Layer 2 (Example 4).

(7) The flood lasts 2 days (48 hours), therefore

$Z_{(Cont)}$ = 562 mm or 4% of $Z_{max(Cont)}$

$Z_{(Unif)}$ = 553 mm or 5.6% of $Z_{max(Cont)}$

12.4.2 SRICOS-EFA Method: Computer Calculation

Use SRICOS-EFA program Option 2: Contraction Scour.

Results:
After a 2-year period of flood having 3.36 m/sec velocity, the final contraction scours are

$Z_{(Cont)}$ = *13.14 m*

$Z_{(Unif)}$ = 9.39 m

Table 12.4 and Figures 12.15 through 12.19 provide a summary of input data and illustrate the results.

12.5 EXAMPLE 5: CONTRACTED CHANNEL WITH 60-DEGREE TRANSITION ANGLE AND APPROACHING HYDROGRAPH

Given:

Channel geometry:	Upstream uncontracted channel width B_1 = 150, contracted channel width due to bridge abutment B_2 = 50 m, contraction length of channel L: = 30 m
Abutment transition angle:	60 degrees
Flow parameters:	70 years predicted hygrograph
Manning Coefficient:	0.02
Hydraulic Radius:	2.72 m
EFA result:	Layer 1: Thickness 10 m; critical shear stress 2 N/m^2 Layer 2: Thickness 20 m; critical shear stress 4 N/m^2

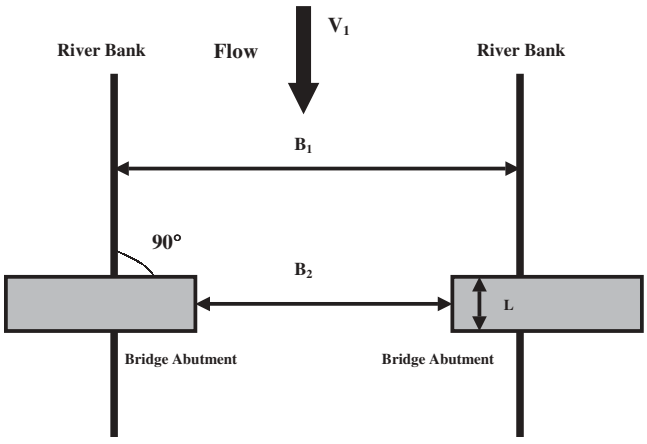

Figure 12.17. Plan view of contracted channel scour case (Example 4).

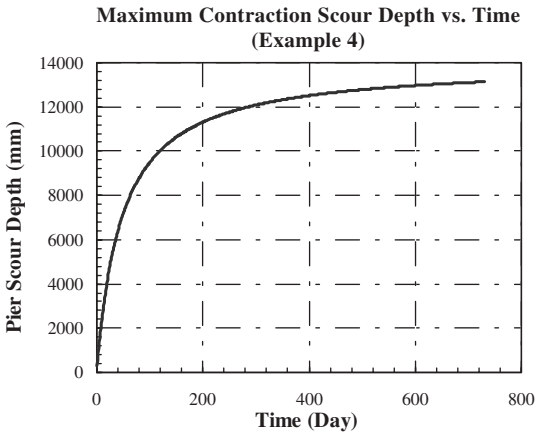

Figure 12.18. Maximum contraction scour depth versus time (Example 4).

Flood period:	70 years
Determine:	The magnitude of maximum contraction scour depth

12.5.1 SRICOS-EFA Method: Computer Calculation

Since the hydrograph is used in this case as hydrologic data input, the relationship between the discharge and velocity and the relationship between discharge and water depth need to be defined. The HEC-RAS program can be a good tool to define these relationships. The following charts present the results obtained from HEC-RAS for this case.

Use SRICOS-EFA program Option 2: Contraction Scour.

Results:
After a 70-year period of flood, the final contraction scours are

$Z_{(Cont)}$ = *8.8* m

$Z_{(Unif)}$ = 6.6 m

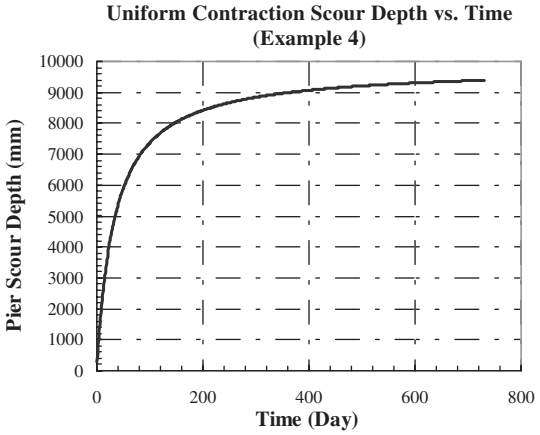

Figure 12.19. Uniform contraction scour depth versus time (Example 4).

TABLE 12.5 Summary of data input (Example 5)

Input Unit **Output Unit**		SI SI	1 1
First Date of Analysis **Last Date of Analysis**			01-01-2003 01-01-2073
No. Of Input Data			25569
Upstream Uncontracted Channel Width **Contracted Channel Width** **Contraction Length of Channel** **Transition Angle of Channel** **Manning's Coefficient** **Average Hydraulic Radius**			150 50 30 60 0.02 2.77
Time Step		Hours	24
Input Hydrologic Data	**Type of Hydrologic Input**	Discharge	1
	Number of Regression Points	Discharge vs. Velocity	8
	Values of Regression Points	Discharge, Velocity	1.42, 0 14, 0.02 141, 0.16 566, 0.49 1415, 0.87 5663, 1.75 13592, 2.97 19821, 3.56
	Number of Regression Points	Discharge vs. Water Depth	8
	Values of Regression Points	Discharge, Water Depth	1.42, 3.86 14, 4.18 141, 5.02 566, 6.18 1415, 7.83 5663, 11.33 13592, 13.15 19821, 14.19
No. Of Layers			2
Properties of 1st Layer		Thickness Critical Shear Stress	10 2
Estimate Initial Scour Rate	**Number of Regression Points**	Shear Stress vs. Scour Rate	8
	Value of Regression Points	Shear Stress, Scour Rate	1, 0 4, 1 6,2 9,3 6, 30 100, 10 200, 12.5 400, 16
Properties of 2nd Layer		Thickness Critical Shear Stress	20 4
Estimate Initial Scour Rate	**Number of Regression Points**	Shear Stress vs. Scour Rate	8
	Value of Regression Points	Shear Stress, Scour Rate	3, 0 4, 0.1 6,1 9,2 18.5, 4 27, 5 40, 6 60, 6.9

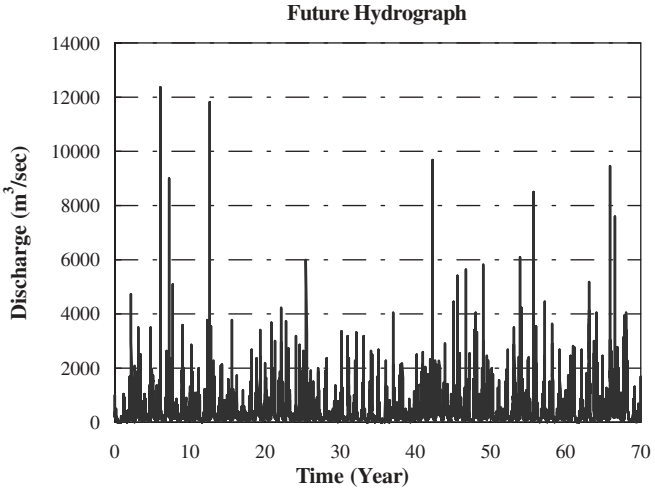

Figure 12.20. Seventy years future approaching hydrograph (Example 5).

Table 12.5 and Figures 12.20 through 12.26 provide a summary of input data and illustrate the results.

12.6 EXAMPLE 6: BRIDGE WITH GROUP PIERS AND CONTRACTED CHANNEL WITH HYDROGRAPH IN CONTRACTED SECTION

Given:

Pier geometry: Pier width B = 1.52 m, pier length L_{pier} = 12.19 m, rectangular pier, number of piers, N = 6, spacing, S = 30 m

Channel geometry: Upstream uncontracted channel width B_1 = 725 m, contracted channel width due to bridge abutment B_2 = 122 m, Contraction length of channel L: = 40 m

Scour rate (mm/hr)	Shear stress (N/m^2)
0	1
1	4
2	6
3	9
6	30
10	100
12.5	200
16	400

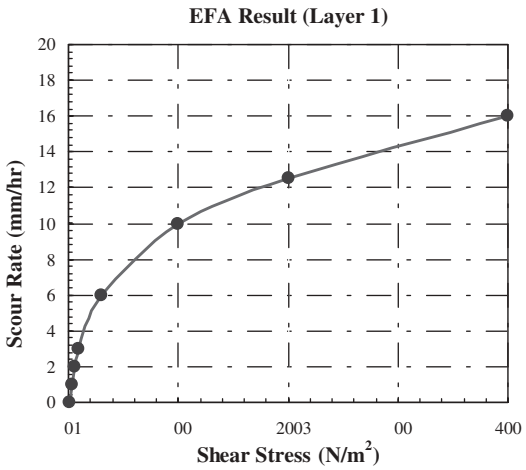

Figure 12.21. EFA results for Soil Layer 1 (Example 5).

Scour rate (mm/hr)	Shear stress (N/m^2)
0	3
0.1	4
1	6
2	9
4	18.5
5	27
6	40
6.9	60

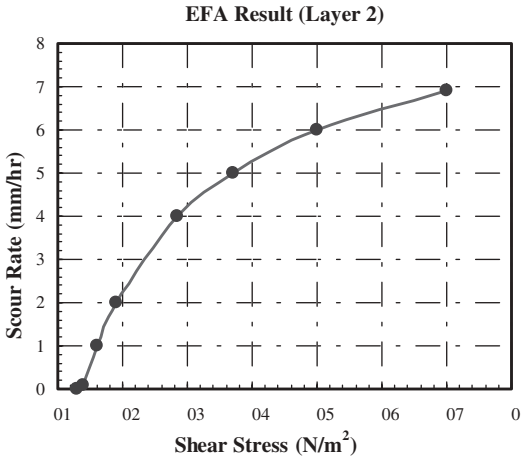

Figure 12.22. EFA results for Soil Layer 2 (Example 5).

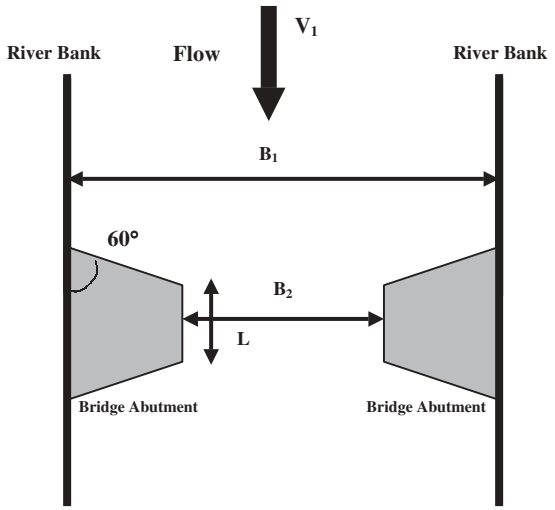

Figure 12.23. Plan view of contracted channel scour case (Example 5).

Abutment transition angle:	90 degrees
Flow parameters:	70 years predicted hydrograph
Manning Coefficient:	0.0146
Hydraulic radius:	2.62 m
EFA result:	Layer 1: Thickness 15 m; critical shear stress 2 N/m^2 Layer 2: Thickness 20 m; critical shear stress 4 N/m^2
Flood period:	70 years
Determine:	The magnitude of maximum bridge scour depth

12.6.1 SRICOS-EFA Method: Computer Calculation

Since the hydrograph is used in this case as hydrologic data input, the relationship between the discharge and

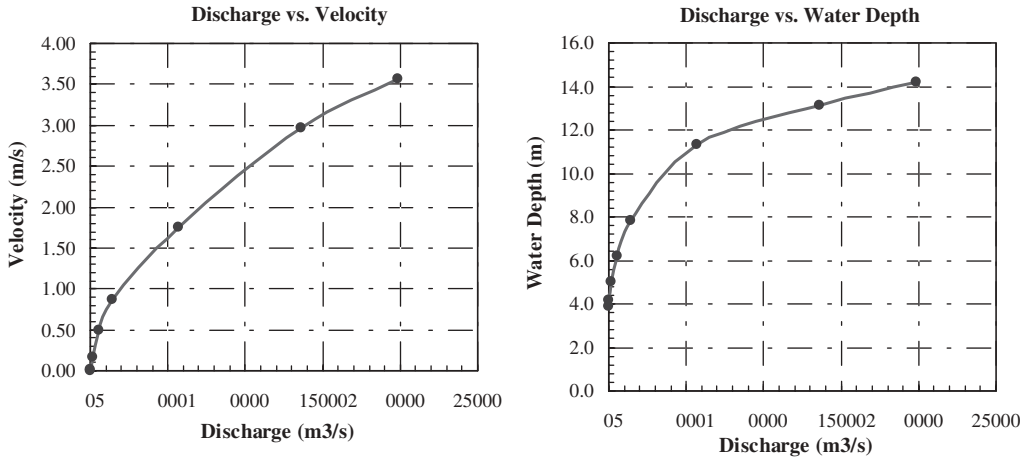

Figure 12.24. Relationship of discharge versus velocity and discharge versus water depth (Example 5).

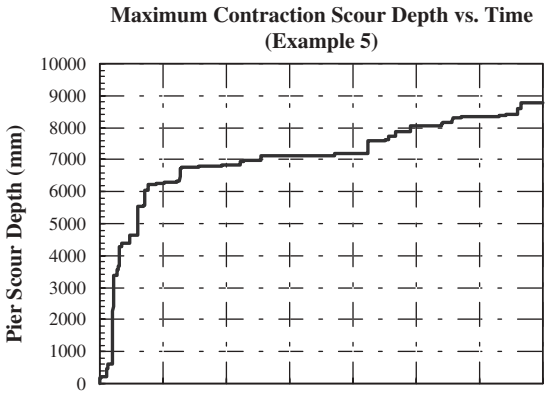

Figure 12.25. Maximum contraction scour depth versus time (Example 5).

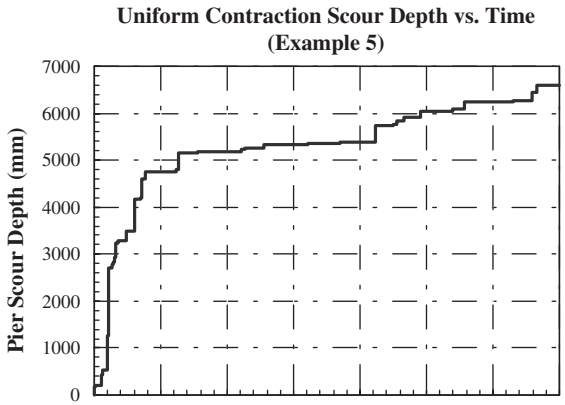

Figure 12.26. Uniform contraction scour depth versus time (Example 5).

TABLE 12.6 Summary of data input (Example 6)

Input Unit **Output Unit**		SI SI	1 1
First Date of Analysis **Last Date of Analysis**			01-01-2003 01-01-2073
No. Of Input Data			25569
Type of Pier **Pier Width** **Pier Length** **Attack angle** **Number of piers** **Pier spacing**		Rectangular Pier	2 1.52 12.19 0 6 30
Upstreamed Uncontracted Channel Width **Contracted Channel Width** **Contraction Length of Channel** **Transition Angle of Channel** **Manning's Coefficient** **Average Hydraulic Radius**			725 122 40 90 0.0146 2.62
Time Step		Hours	24
Input Hydrologic Data	**Type of Hydrologic Input**	Discharge	1
	Type of Velocity	Velocity in contracted section	2
	Number of Regression Points	Discharge vs. Velocity	8
	Values of Regression Points	Discharge, Velocity	1.42, 0 14, 0.02 141, 0.16 566, 0.49 1415, 0.90 5663, 2.50 12375, 4.20 19821, 5.60
	Number of Regression Points	Discharge vs. Water Depth	8
	Values of Regression Points	Discharge, Water Depth	1.42, 3.86 14, 4.18 141, 5.02 566, 6.18 1415, 7.83 5663, 11.33 13592, 13.15 19821, 14.19
No. Of Layers			2
Properties of 1st Layer		Thickness Critical Shear Stress	15 2
Estimate Initial Scour Rate	**Number of Regression Points**	Shear Stress vs. Scour Rate	8
	Value of Regression Points	Shear Stress, Scour Rate	1, 0 4, 1 6,2 9,3 6, 30 100, 10 200, 12.5 400, 16
Properties of 2nd Layer		Thickness Critical Shear Stress	20 4
Estimate Initial Scour Rate	**Number of Regression Points**	Shear Stress vs. Scour Rate	8
	Value of Regression Points	Shear Stress, Scour Rate	3, 0 4, 0.1 6,1 9,2 18.5, 4 27, 5 40, 6 60, 6.9

velocity and the relationship between discharge and water depth need to be defined. The HEC-RAS program can be a good tool to define these relationships. The following charts present the results obtained from HEC-RAS for this case.

Use SRICOS-EFA program Option 3: Bridge Scour.

Results:
After a 70-year period of flood, in this case the maximum final bridge scour is

Z = 6.2 m

Table 12.6 and Figures 12.27 through 12.33 provide a summary of input data and illustrate the results.

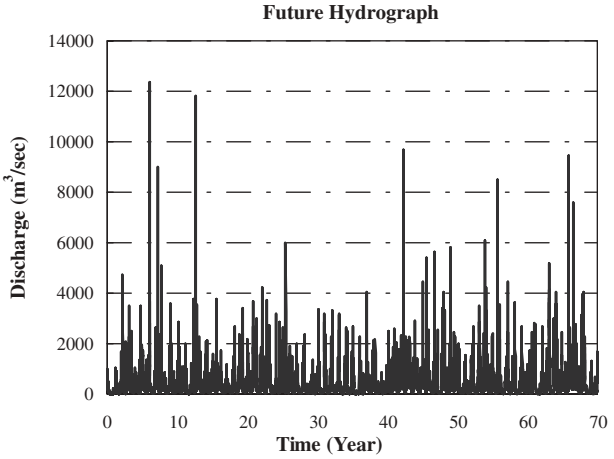

Figure 12.27. Seventy years future hydrograph (Example 6).

Scour rate (mm/hr)	Shear stress (N/m^2)
0	1
1	4
2	6
3	9
6	30
10	100
12.5	200
16	400

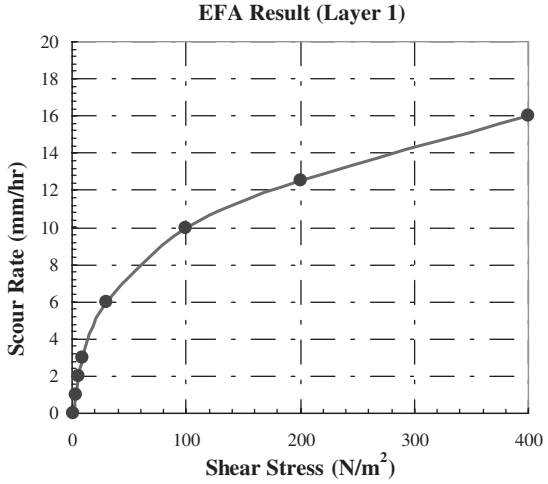

Figure 12.28. EFA results for Soil Layer 1 (Example 6).

Scour rate (mm/hr)	Shear stress (N/m^2)
0	3
0.1	4
1	6
2	9
4	18.5
5	27
6	40
6.9	60

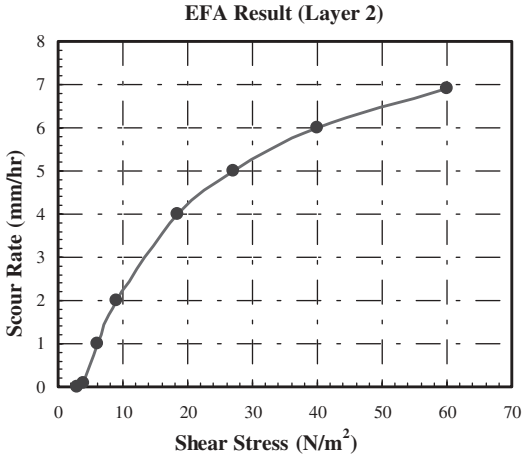

Figure 12.29. EFA results for Soil Layer 2 (Example 6).

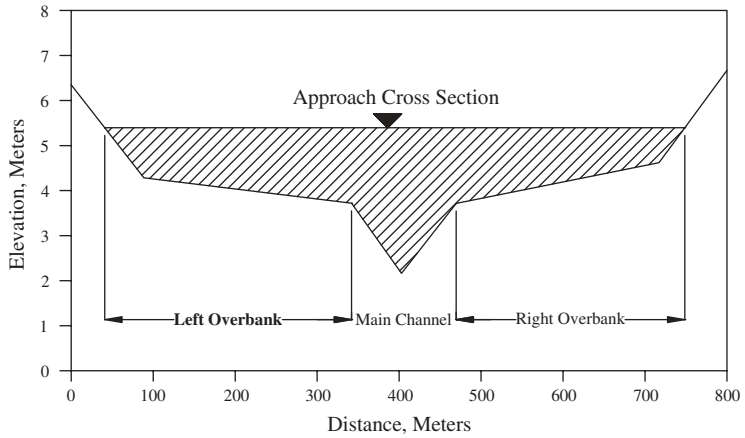

Figure 12.30. Cross-section view of approaching channel (Example 6).

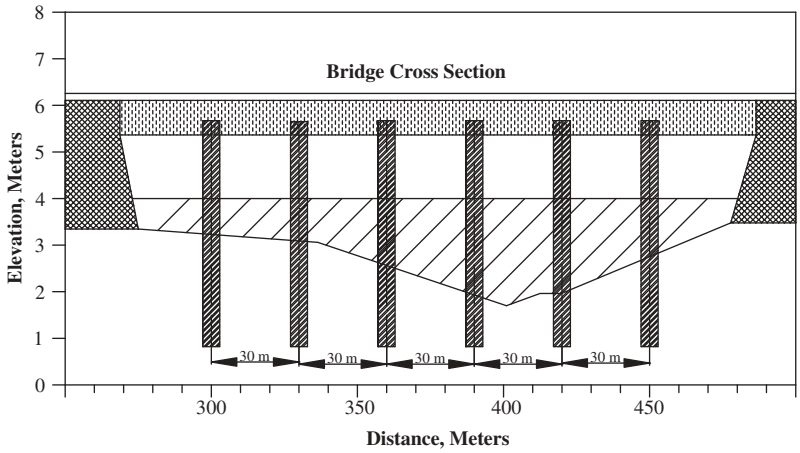

Figure 12.31. Cross-section view of bridge (Example 6).

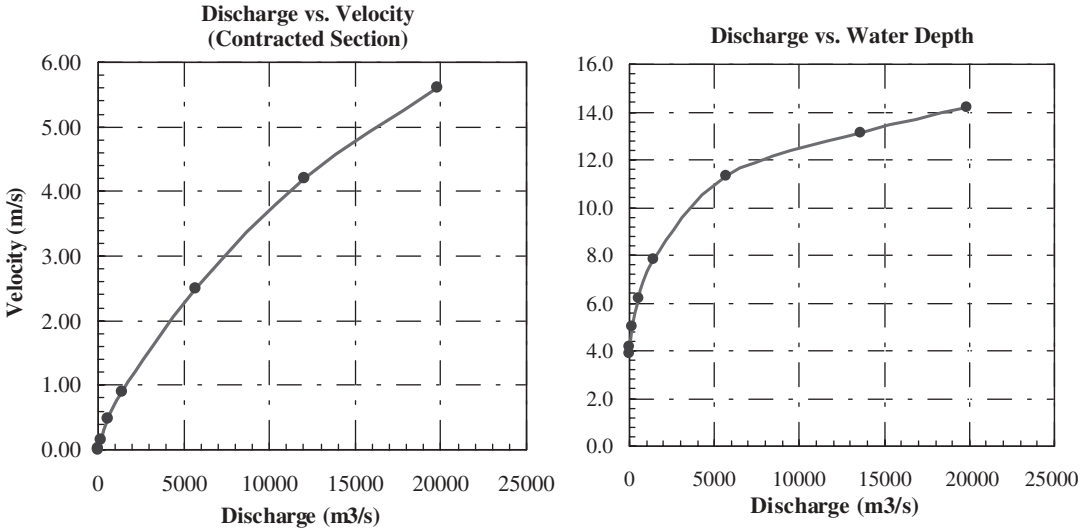

Figure 12.32. Relationship of discharge versus velocity and discharge versus water depth (Example 6).

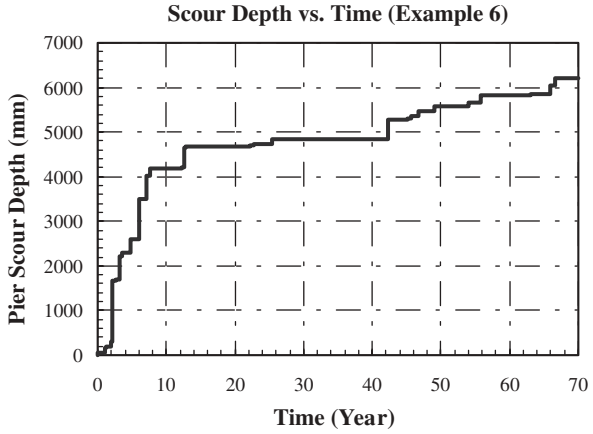

Figure 12.33. Bridge scour depth versus time (Example 6).

CHAPTER 13

CONCLUSIONS AND RECOMMENDATIONS

13.1 CONCLUSIONS

13.1.1 General

The topic addressed is the prediction of the scour depth around a bridge pier founded in cohesive soils and subjected to water flow. The scour components considered are complex pier scour and contraction scour. The proposed method, which is based on 42 useful flume tests and 49 useful numerical simulations, is a further development of the method formulated earlier for simple pier scour (cylindrical pier in deep water).

13.1.2 Erodibility of Cohesive Soils

It is emphasized that erodibility is not an index but a relationship or function between the water velocity (or, better, the shear stress at the water-soil interface) and the erosion rate of the soil. Erodibility is represented by the erosion function. Two important parameters help describe the erosion function: the critical shear stress and the initial slope of the erosion function. It is found that, although the critical shear stress of a cohesive soil is not related to its mean grain size, the common range of critical shear stress values for cohesive soils (0.5 N/m2 to 5 N/m2) is comparable to the range obtained in sands. This explains why the maximum scour depth in cohesive soils is comparable to the one obtained in sands. The initial slope of the erosion function can be many times less than the one in sand (e.g., 1,000 times less) and, therefore, the scour depth can develop very slowly in some cohesive soils. There lies the advantage of developing a method that can predict scour depth as a function of time for a given hydrograph (cohesive soil) rather than a maximum depth of scour for a design flood (sands). This was the goal of this project. It also was found that the critical shear stress and the initial slope were not related to soil properties because the R2 of the regressions were all very low. To obtain the erosion function this study recommends using the Erosion Function Apparatus (EFA).

13.1.3 EFA

This EFA was developed in the early 1990s to obtain the erosion function. A soil sample is retrieved from a bridge site using an ASTM standard, thin-wall steel tube (i.e., a Shelby tube); placing it through a tight-fitting opening in the bottom of a rectangular cross-section conduit; pushing a small protrusion of soil into the conduit; sending flowing water over the top of the sample at a chosen velocity; and recording the corresponding erosion rate. This is repeated for several velocities and the erosion function for each is obtained in that fashion.

13.1.4 SRICOS-EFA Method for Cylindrical Piers in Deep Water

SRICOS stands for Scour Rate In COhesive Soils. Since the method makes use of the erosion function measured in the EFA, the method is referred to as the SRICOS-EFA Method. The SRICOS-EFA Method (program) gives the scour depth as a function of time for the period covered by the hydrograph for a given velocity hydrograph at a bridge, a given multilayered soil stratigraphy with an erosion function defined for each layer, and a given cylindrical pier in deep water (water depth larger than 1.6 times the pier diameter).

The method is based on the calculation of two basic parameters: the maximum depth of pier scour and the initial rate of scour. The maximum depth of scour is based on an equation obtained from flume tests and the initial rate is based on an equation giving the initial shear stress obtained from numerical simulations. The initial rate of scour is read on the EFA erosion function at the corresponding value of the calculated shear stress. A hyperbola is used to connect the initial scour rate to the maximum or asymptotic scour depth and describes the complete scour depth versus time curve. Robust algorithms are used to incorporate the effect of varying velocities and multilayered soil systems. This earlier method was developed by the authors under TxDOT sponsorship and was verified by satisfactory comparison between predicted scour and measured scour at eight bridges in Texas.

13.1.5 SRICOS-EFA Method for Maximum Scour Depth at Complex Piers

A set of flume experiments was conducted to study the maximum depth of scour for a pier including the effect of shallow water depth, the effect of rectangular shapes, the effect of the angle of attack on rectangular shapes, and the

effect of spacing between piers positioned in a row perpendicularly to the flow. The proposed equation for the maximum depth of scour is in the form of the equation for the cylindrical pier in deep water with correction factors based on the results of the flume tests.

$$Z_{\max}(\text{Pier}) \text{ in mm} = K_w K_{sp} K_{sh}\left(0.18 R_e^{0.635}\right)$$

Where Z_{max}(Pier) is the maximum depth of pier scour in millimeters; Re is the Reynolds Number equal to VB'/v, V (m/s) being the mean depth velocity at the location of the pier if the bridge were not there; the K factors take into account the shallow water depth, spacing, shape, and angle of attack being considered through the use of the projected width B' (m) in the calculation of the Reynolds Number.

13.1.6 SRICOS-EFA Method for Initial Scour Rate at Complex Piers

A set of numerical simulations was performed to study the maximum shear stress around a pier including the effect of shallow water depth, rectangular shapes, angle of attack on rectangular shapes, and spacing between piers positioned in a row perpendicularly to the flow. The proposed equation for the maximum shear stress is in the form of the equation for the cylindrical pier in deep water with correction factors based on the results of the numerical simulations.

$$\tau_{\max}(\text{Pier}) = k_w k_{sh} k_{sp} k_\alpha \left(0.094 \rho V^2 \left[\frac{1}{\log R_e} - \frac{1}{10}\right]\right)$$

where τ_{max}(Pier) (kN/m^2) is the maximum shear stress around the pier; Re is the Reynolds Number equal to VB/v, V (m/s) being the mean depth velocity at the location of the pier if the bridge were not there; B (m) is the pier diameter or pier width; ρ (kg/m^3) is the mass density of water; the k factors take the shallow water depth, pier shape, pier spacing, and attack angle into account.

13.1.7 SRICOS-EFA Method for Maximum Contraction Scour Depth

A set of flume experiments was conducted to study the depth of scour associated with the contraction of a channel including the effects of the ratio of the contracted channel width over the approach channel width, the contracted channel length, and the transition angle. The proposed equation for the maximum depth of contraction scour is

$$Z_{\max}(\text{Cont}) = K_\theta K_L \times 1.90 H_1 \left(\frac{1.49 V_{HEC}}{\sqrt{g H_1}} - \frac{\left(\frac{\tau_c}{\rho}\right)^{0.5}}{g n H_1^{1/3}} \right) \geq 0$$

Where Z_{max}(Cont) (m) is the maximum depth of contraction scour; H_1 (m) is the water depth along the center line of the uncontracted channel after scour has occurred; V_{HEC} (m/s) is the mean depth water velocity at the location of the pier in the contracted channel; τ_c (N/m^2) is the critical shear stress of the soil; ρ (kg/m^3) is the mass density of water; g (m/s^2) is the acceleration due to gravity; n is the Manning's Coefficient (s/m$^{1/3}$); and the K factors take the transition and the contracted channel length into account. Note that the parenthesis in the equation is a factored difference between the Froude Number and the critical Froude Number. Equations also are proposed for the uniform contraction scour depth as well as the location of the scour depths.

13.1.8 SRICOS-EFA Method for Initial Contraction Scour Rate

A set of numerical simulations was performed to study the maximum shear stress around the contraction of a channel including the effects of the ratio of the contracted channel width over the approach channel width, the transition angle, the water depth, and the contracted channel length. The proposed equation for the maximum shear stress is in the form of the equation for the shear stress at the bottom of an open and uncontracted channel with correction factors based on the results of the numerical simulations.

$$\tau_{\max}(\text{Cont}) = k_{c-R} k_{c-\theta} k_{c-H} k_{c-L} \left(\gamma n^2 V^2 R_h^{-\frac{1}{3}}\right)$$

where τ_{max}(Cont) (N/m^2) is the maximum shear stress along the centerline of the contracted channel; γ is the unit weight of water (kN/m^3); n is the Manning's Coefficient (s/m$^{1/3}$); V (m/s) is the upstream mean depth velocity; R_h (m) is the hydraulic radius defined as the cross-section area of the flow divided by the wetted perimeter; and the k factors take the contraction ratio, the transition angle, the water depth effect, and the contracted length into account. Equations also are proposed for the location of the maximum shear stress.

13.1.9 SRICOS-EFA Method for Complex Pier Scour and Contraction Scour in Cohesive Soils

Once the equations were established, the SRICOS-EFA Method was assembled. Care was taken not to simply add complex pier scour and contraction scour to get total pier scour. Instead, advantage was taken of the fact that at the end of the maximum contraction scour, the velocity is at the critical velocity and the maximum pier scour should be calculated using the critical velocity of the soil and not the initial velocity in the contracted channel. In addition, the rules of accumulation due to the hydrograph and the multilayer system developed for the simple pier scour method were adapted for the complex pier and contraction scour method. The superposition and accumulation reasoning lead to the following steps for the SRICOS-EFA Method for predicting the

scour depth at a complex pier in a contracted channel. This step-by-step procedure has been automated in a computer program.

1. Collect the input data: velocity and water depth hydrograph, geometry of the pier and of the contracted channel, erosion functions of the soil layers.
2. Calculate the maximum contraction scour depth for the *i*th velocity in the hydrograph.
3. Calculate the maximum complex pier scour depth using the *i*th velocity in the hydrograph at the pier location if there is no contraction scour in Step 2, or the critical velocity for the soil if there is contraction scour in Step 2.
4. Calculate the total pier scour depth as the total of Step 2 and Step 3.
5. Calculate the initial maximum shear stress for pier scour using the *i*th velocity in the hydrograph.
6. Read the initial scour rate corresponding to the initial maximum shear stress of Step 5 on the erosion function of the soil layer corresponding to the current scour depth.
7. Use the results of Steps 4 and 6 to construct the hyperbola describing the scour depth versus time for the pier.
8. Calculate the equivalent time for the given curve of Step 7. The equivalent time is the time required for the *i*th velocity on the hydrograph to scour the soil to a depth equal to the depth scoured by all of the velocities occurring prior to the *i*th velocity.
9. Read the additional scour generated by the *i*th velocity starting at the equivalent time and ending at the equivalent time plus the time increment.
10. Repeat Steps 2 to 9 for the $(i + 1)^{th}$ velocity and so on until the entire hydrograph is consumed.

13.1.10 Verification of the SRICOS-EFA Method

Several full case histories were identified for verification but none could satisfy the requirements necessary to verify the method developed. Some did not have enough details on the observed scour depth, some turned out not to be made of cohesive soil after drilling, some did not have a gage station nearby. It was decided to compare the maximum scour depth for pier and contraction to existing databases. These databases were mostly in sand, however, and included those collected by Mueller (pier scour), Froehlich (pier scour), and Gill (contraction scour). The comparisons between the predicted and measured scour depths are very satisfactory although it is not clear whether they should be or not since the soils were not primarily cohesive. Nevertheless, these comparisons give an indication that the SRICOS-EFA Method may not be limited to cohesive soils. Indeed, the fact that the method is based on site-specific testing of the erosion function permits incorporating the soil behavior directly in the predictions.

13.1.11 Future Hydrographs and Scour Risk Analysis

A novel technique was presented on generating future hydrographs. Indeed, since the SRICOS-EFA Method predicts the scour depth as a function of time, it is necessary to input into the program the hydrograph over the design life of the bridge. The proposed technique consists of using a past hydrograph (from a gage station, for example), preparing the frequency distribution plot for the floods within that hydrograph, sampling the distribution randomly and preparing a future hydrograph for the required period that has the same mean and standard deviation as the measured hydrograph. This process is repeated 10,000 times and, for each hydrograph, a final scour depth (the depth reached at the end of the design life of the bridge) is generated. These 10,000 final depths of scour are organized in a frequency distribution plot with a mean and a standard deviation. That plot can be used to quote a scour depth with a corresponding probability of occurrence, or better, to choose a risk level and quote the corresponding final depth of scour.

13.1.12 Example Problems

A set of example problems was presented to help the reader become more familiar with the SRICOS-EFA Method. Some examples are performed by hand calculations; some use the SRICOS-EFA computer program.

13.2 RECOMMENDATIONS

It is recommended that

1. The proposed method be incorporated in the next version of HEC-18;
2. The SRICOS-EFA Method program be transferred to a Windows™ environment;
3. The project be continued to solve abutment scour, the last major unsolved scour problem in cohesive soils; and
4. A set of short courses be offered across the country to teach the new method and the corresponding program.

REFERENCES

ASTM D1587, American Society for Testing and Materials, Philadelphia, USA.

Benjamin, J.R., and Cornell, C., A., "Probability, Statistics, and Decisions for Civil Engineers", 1970, McGraw-Hill, New York, USA.

Bras, R. L., and Rodriguez-Iturbe, I., "Random Functions and Hydrology", 1986. Dover.

Briaud, J.-L., Ting, F., Chen, H.-C., Gudavalli, R., Kwak, K., Philogene, B., Han, S.-W., Perugu, S., Wei, G.S., Nurtjahyo, P., Cao, Y.W., Li, Y., "SRICOS: Prediction of Scour Rate at Bridge Piers, TTI Report no. 2937-1 to the Texas DOT, 1999, Texas A&M University, College Station, Texas, USA.

Briaud, J.-L., Ting, F., Chen, H.C., Gudavalli, S.R., Perugu, S., and Wei, G., "SRICOS: Prediction of Scour Rate in Cohesive Soils at Bridge Piers", ASCE Journal of Geotechnical Engineering, Vol. 125, 1999, pp. 237–246.

Briaud, J.-L., Ting, F., Chen, H.C., Cao, Y., Han, S.-W., Kwak, K., "Erosion Function Apparatus for Scour Rate Predictions". Journal of Geotechnical and Geoenvironmental Engineering, ASCE, Vol. 127, No. 2, 2001a, pp. 105–113.

Briaud, J.-L., Chen, H. C., Kwak, K., Han, S-W., Ting, F., "Multiflood and Multilayer Method for Scour Rate Prediction at Bridge Piers", Journal of Geotechnical and Geoenvironmental Engineering, ASCE, Vol. 127, No. 2, 2001b, pp. 105–113.

Cao, Y., "The Influence of Certain Factors on the Erosion Functions of Cohesive Soil", Master's Thesis, 2001, Texas A&M University, College Station, Texas, USA

Chang, F. and Davis, S., "Maryland SHA Procedure for Estimating Scour at Bridge Abutments: part 2-Clear Water Scour", ASCE Compendium of Conference Scour Papers (1991 to 1998), pp. 412–416, Reston, VA.

Chen, H. C., "Submarine Flows Studied by Second-Moment Closure", Journal of Engineering Mechanics, Vol. 121, 1995a, pp. 1136–1146.

Chen, H. C., "Assessment of a Reynolds Stress Closure Model for Appendage Hull Junction Flows", Journal of Fluids Engineering, Vol. 117, 1995b, pp. 557–563.

Chen, H. C., Chen, M., and Davis, D. A., "Numerical Simulation of Transient Flows Induced by a Berthing Ship", International Journal of Offshore and Polar Engineering, Vol. 7, 1997, pp. 277–284.

Chen, H. C. and Korpus, R. A., "A Multi-Block Finite-Analytic Reynolds-Average Navier-Stokes Method for 3D Incompressible Flow", Individual Papers in Fluids Engineering, *ASME*, Vol. 150, 1993, pp. 113–121.

Chen, H. C. and Patel, V. C., "Near-Wall Turbulence Models for Complex Flows Including Separation", AIAA Journal, Vol. 26, No. 6, 1988, pp. 641–648.

Chen, H. C. and Patel, V. C., "The Flow Around Wing-Body Junctions", in *Proceedings,* 4th Symposium on Numerical and Physical Aspects of Aerodynamic Flows, Long Beach, CA, January, 16–19, 1989.

Chen, H. C., Patel, V. C., and Ju, S., "Solutions of Reynolds-Averaged Navier-Stokes Equations for Three-dimensional Incompressible Flows", Journal of Computational Physics, Vol. 88, No. 2, 1990, pp. 305–336.

Chiew, Y.M., "Local Scour at Bridge Piers," University of Auckland, School of Engineering, Report No. 355, 1984.

Chow, V.T., Maidment, D.R., and Mays, L.W., Applied Hydrology, 1988, McGraw-Hill.

Das, B. M., *Principle of Geotechnical Engineering*, 4th edition, 1998, PWS Publishing Company, Boston, MA, 712 pages.

Dietz, J. W., "Ausbildung von Langen Pfeilern bei Schraganstromung am Beispiel der BAB-Mainbrucke Eddersheim," Mitteilungsblatt der BAW, 31: 79–94, 1972, Karlsruhe, Germany.

Dou, G.R., "The Stochastic Theory and the General Law of All Flow Regions for Turbulent Open Channel Flows", Proc. First International Symposium on River Sedimentation, Beijing, 1980, pp. 151–161.

Dou, X. "Numerical Simulation of Three-dimensional Flow Field and Local Scour at Bridge Crossings", Ph.D. Dissertation, 1997, The University of Mississippi.

Elliott, K. R. and Baker, C. J., "Effect of Pier Spacing on Scour around Bridge Piers", Journal of Hydraulic Engineering, Vol. 111, No. 7, July 1985, pp. 1105–1109

Ettema, R. "Scour at Bridge Piers," Report No. 216, 1980, Department of Civil Engineering, University of Auckland.

Flaxman, E. M., "Channel Stability in Undisturbed Cohesive Soils" Journal of the Hydraulic Division, Proceedings of the ASCE, Vol. 89, No. HY2, Proceeding Paper 3462, March 1963, pp. 87–96.

Froehlich, D. C., "Analysis of Onsite Measurements of Scour at Piers", Proceedings ASCE National Hydraulic Engineering Conference, 1988, Colorado Spring, Colorado.

Gill, M. A, "Bed Erosion in Rectangular Long Contraction," Journal of Hydraulic Division, ASCE, Vol. 107, No. 3, 1981, pp. 273–284.

Gudavalli, S. R., "Prediction Model for Scour Rate Around Bridge Piers in Cohesive Soils on the Basis of Flume Tests", 1997, PhD Dissertation, Civil Engineering, Texas A&M University, USA.

HEC-RAS River Analysis System, *User's Manual, Version 2.0*, Hydrologic Engineering Center, 1997, U.S. Army Corps of Engineering, Davis, CA

Hoffmans, G. J. C. M. and Booij, R., "Two-Dimensional Mathematical Modeling of Local Scour Holes", Journal of Hydraulic Research, Vol. 31, No.5, 1993.

Hosny, H.M., "Experimental Study of Local Scour Around Circular Bridge Piers in Cohesive Soils", Ph.D. Dissertation, Spring 1995, Civil Engineering Department, Colorado State University, Fort Collins, Colorado.

Hjorth, P., "Studies on Nature of Local Scour" Bulletin Series A. No. 46, Department of Water Resources Engineering, Lund Institute of Technology/University of Lund, 1975.

Ivarson, W. R. "Scour and Erosion in Clay Soils", ASCE Compendium of Conference Scour Papers (1991 to 1998), 1998, pp. 104–119, Reston, VA.

Johnson, P. A., "Scour at Wide Piers Relative to Flow Depth," ASCE Compendium of Conference Scour Papers (1991 to 1998), pp. 280–287, Reston, VA.

Johnson, P. A. and Jones, J. S., "Shear Stress at Base of Bridge Pier" Bridge and Hydrology Research, Transportation Research Board No 1350, 1992, pp. 14–18.

Kwak, K., Briaud, J.-L., Chen, H.-C., 2001, "SRICOS: Computer Program for Bridge Pier Scour", Proceedings of the 15th International Conference on Soil Mechanics and Geotechnical Engineering, Vol. 3, pp. 2235–2238, A.A. Balkema Publishers, Rotterdam, The Netherlands.

Kwak, K., Briaud, J.-L., Cao, Y., Chung M.-K., Hunt, B., and Davis, S., "Pier Scour at Woodrow Wilson Bridge and SRICOS Method", 2002, First International Conference on Scour of Foundations, Texas A&M University, Chen-Briaud (editors), College Station, Texas, USA.

Laursen, E. M., "Scour at Bridge Crossings," Journal of Hydraulic Division, ASCE, Vol. 86, No. HY2, May 1960, pp.93–118.

Laursen, E. M., "An Analysis of Relief Bridge Scour," Journal of Hydraulic Division, ASCE, Vol. 89, No. HY3, 1963.

Lim, S.-Y. and Cheng, N.-S. "Scouring in Long Contractions", Journal of Irrigation and Drainage Engineering, Vol. 124, No. 5, Sep–Oct 1998, pp. 258–261, Reston, VA.

Melville, B. W., "Pier and Abutment Scour: Integrated Approach," Journal Hydraulic Division, ASCE, Vol. 123, No. 2, 1997, pp. 125–136.

Melville, B. W. and Coleman, S.E., *Bridge Scour*, 1999, Water Resources Publications, LLC, pp. 173–186.

Molinas, A., Jones, S., and Hosny, M. " Effect of Cohesive Material Properties on Local Scour Around Piers", Transportation Research Board, 78th Annual Meeting, January 10–14, 1999, Washington, D. C.

Montanari, A., Rosso, R., Taqqu, M.S., 1997. "Fractionally Differenced ARIMA Models Applied to Hydrologic Time Series: Identification, Estimation and Simulation", Water Resour. Res., Vol. 33, No. 4, pp. 1035–1044, American Geophysical Union, Washington, D.C., USA.

Montanari, A., Rosso, R., Taqqu, M.S., 2000. "A Seasonal Fractional ARIMA Model Applied to the Nile River Monthly Flows at Aswan", Water Resour. Res., Vol. 36, No. 5, pp. 1249–1259, American Geophysical Union, Washington, D.C., USA.

Moody, L.F., "Friction Factors for Pipe Flow", Transactions of the American Society of Civil Engineers, 1944, Vol. 66, Reston, Virginia, USA.

Muller D.S. and Landers M., "Channel Scour at Bridges in the United States", FHWA-RD-95-184, 1996, Federal Highway Administration, VA, USA

Munson, B. R., Young, D. F., and Okiishi, T. H., *Fundamentals of Fluid Mechanics*, 1990, Wiley, New York.

Neill, C. R., *Guide to Bridge Hydraulic*, 1973, Roads and Transportation Association of Canada, University of Toronto Press.

Nurtjahyo, P. Y., " Numerical Simulation of Pier Scour and Contraction Scour," Ph.D. Dissertation, 2002, Department of Civil Engineering, Ocean Engineering Program, Texas A&M University, College Station, Texas.

Olsen, N. R. B. and Melaaen, M. C. "Three-Dimensional Calculation of Scour Around Cylinder", Journal of Hydraulic Engineering, Vol. 119, No. 9, 1993, pp. 1048–1054.

Raudkivi A.J., (1991), "Scour at bridge piers," Chapter 5; H. Breudsers and A.J. Raudkivi (ED.) IAHR, Hydraulic Structures Design Manual No 2; A.A Balkema, Rotterdam, NL.

Richardson, E. V. and Davis, S. M. "Evaluating Scour at Bridges", Publication No. FHWA-IP-90-017, HEC No.18, 1995, US Department of Transportation, Washington, D. C.

Roulund, A., Sumer, B. M., Fredsoe, J., and Michelsen, J., "3D Mathematical Modeling of Scour Around a Circular Pile", ISRS 98, December 16–18, 1998, Hong Kong.

Salim M., Jones J. S., "Scour Around Exposed Pile Foundations", ASCE Compendium of Conference Scour Papers (1991 to 1998), 1998, pp. 104–119, Reston, VA.

Shields, A., "Application of similarity principles, and turbulence research to bed-load movement," 1936, California Institute of Technology, Pasadena (translated from German).

Smith, C. D., "Simplified Design for Flume Inlets," Journal of Hydraulic Division, ASCE, Vol. 93, No. 6, 1967, pp. 25–34.

Straub, L. G., "Effect of Channel Contraction Works upon Regime of Movable Bed Streams," Trans. Am. Geophysical Union, Part II, 1934, pp. 454–463.

Vanoni, V. A., "Sedimentation Engineering", ASCE-Manuals and Reports on Engineering Practice no. 54, 1975, prepared by the ASCE task committee.

Van Rijn, L. C. and Meijer, K., "Three-dimensional modeling of suspended sediment transport for current and waves", Report No. Q250/Q432/H461, 1986, Delft Hydraulic, Delft, Netherlands.

Wei, G., Chen, H. C., Ting, F., Briaud, J.-L, Gudavalli, S. R., and Perugu, S., "Numerical Simulation to Study Scour Rate in Cohesive Soils" Research report to the Texas Department Transportation, 1997, Department of Civil Engineering, Texas A&M University, College Station, TX.

Young D.F., Munson B.R., Okiishi T.H., *A Brief Introduction to Fluid Mechanics*, 1997, John Wiley & Sons, New York, NY, USA.

NOMENCLATURE

α	Pier attack angle
θ	Transition angle for bridge contraction
ρ	Mass density of water
γ	Unit weight of water
ε	Roughness coefficient
μ_Q	Mean value of daily stream-flow
σ_Q	Standard deviation of daily stream-flow
#200	Percentage of soil passing No.200 sieve
a	Width of the cross section of the rectangular pipe in EFA
b	Length of the cross section of the rectangular pipe in EFA
B	Pier width
B′	Pier projection width
B_1	Channel upstream width
B_2	Contracted channel width
C	Pier center-center spacing
CEC	Cation exchange capacity
CSS	Critical shear stress of soil
d	Scour depth, a random variable and its statistics can be studied in detail to determine the risk of failure associated with difference choices of the design value of the scour depth
D_{50}	Particle size
f	Friction factor obtained from Moody Chart
Fr	Froude number
g	Acceleration due to gravity
h	Length of soil sample eroded in EFA test
H	Average water depth upstream bridge piers
H_1	Average water depth in approaching flow upstream contraction
H_2	Average water depth in contracted channel
H_{Hec}	Initial average water depth in contracted channel calculated by HEC-RAS
L	Length of contraction channel
L_{pier}	Length of rectangular pier
k_w	Correction factor of water depth for the initial shear stress of pier scour
k_{sh}	Correction factor of pier shape effect for the initial shear stress of pier scour
k_{sp}	Correction factor of pier spacing effect for the initial shear stress of pier scour
k_α	Correction factor of pier attack angle effect for the initial shear stress of pier scour
$k_{c\text{-}R}$	Correction factor of contraction ratio effect for the initial shear stress of contraction scour
$k_{c\text{-}L}$	Correction factor of contraction length effect for the initial shear stress of contraction scour
$k_{c\text{-}H}$	Correction factor of flow water depth effect for the initial shear stress of contraction scour
$k_{c\text{-}\theta}$	Correction factor of transition angle effect for the initial shear stress of contraction scour
K_w	Correction factor of water depth for pier scour depth
K_{sh}	Correction factor of pier shape effect for pier scour depth
K_{sp}	Correction factor of pier spacing effect for pier scour
K_α	Correction factor of pier attack angle effect for pier scour depth
K_L	Correction factor of contraction length effect for contraction scour depth
K_θ	Correction factor of transition angle effect for contraction scour depth
$K_{L/Zmax}$	Correction factor of contraction length effect for maximum contraction scour depth
$K_{L/unif}$	Correction factor of contraction length effect for uniform contraction scour depth
$K_{L/Xmax}$	Correction factor of contraction length effect for location of maximum contraction scour depth
$K_{\theta/Zmax}$	Correction factor of transition angle effect for maximum contraction scour depth
$K_{\theta/unif}$	Correction factor of transition angle effect for uniform contraction scour depth
$K_{\theta/Xmax}$	Correction factor of transition angle effect for location of maximum contraction scour
L_t	Life of structure
n	Manning's coefficient
pH	Log Scale Unit of Measure, and is used to express the degree of acidity of a substance.
PI	Plasticity index
Q	Daily stream-flow discharge

R	Level of risk associated with the choice of different design values of scour depth and project lives
Re	Reynolds number = VB/v
R_h	Hydraulic radius
S	Piers center-center spacing
SAR	Sodium adsorption ratio
Si	Initial erodibility
S_U	Undrained shear strength of soil
t	Time required for soil sample to be eroded in EFA test
t_e	Equilibrium time for multi-flood scour depth calculation
T_r	Return period in risk analysis
τ	Shear stress on the surface of soil sample
τ_c	Critical shear stress of soil
τ_{max}	Initial shear stress which also is the maximum value during shear stress history
$\tau_{max(Deep)}$	Initial shear stress which also is the maximum value during shear stress history for pier sour or contraction scour in deep water case
$\tau_{max(Circle)}$	Initial shear stress which also is the maximum value during shear stress history for pier sour or contraction scour in circular pier case
$\tau_{max(0\ degree)}$	Initial shear stress which also is the maximum value during shear stress history for pier sour or contraction scour in no attack angle case
$\tau_{max(Cont)}$	Initial shear stress which also is the maximum value during shear stress history for contraction scour
$\tau_{max(Single)}$	Initial shear stress which also is the maximum value during shear stress history for pier sour or contraction scour in single pier case
$\tau(z)$	Shear stress on the bottom of scour hole at depth z
ν	Kinematics viscosity of water
V	Approaching average velocity for pier scour
V_1	Approaching average velocity for contraction scour
V_2	Average velocity in the contracted channel
V_{HEC}	Calculated velocity in the contracted channel by HEC-RAS
X_a	Location of maximum bed shear stress due to abutment
X_c	Location of maximum bed shear stress around pier or the abutment (most interested)
X_{max}	Location of the maximum contraction scour
$\dot{Z}$	Erosion rate
$\dot{Z}_i$	Initial erosion rate
$Z_{max\ (Cont)}$	Equilibrium maximum contraction scour depth
$Z_{max\ (Deep)}$	Equilibrium pier scour depth or equilibrium maximum contraction scour depth in deep water case
$Z_{unif(Cont)}$	Equilibrium uniform contraction scour

UNIT CONVERSIONS

This report is in SI units. The following conversion table is provided for convenience.
The SRICOS-EFA program allows for the use of SI or American customary units.

Acceleration	9.81 m/s^2=386.22 $in./s^2$=32.185 ft/s^2, Paris: g=9.80665 m/s^2, London: g = 3.2174×10^1 ft/s^2
Area	1 m^2 = 1.5500×10^3 in^2 = 1.0764×10^1 ft^2 = 1.196 yd^2 = 10^6 mm^2 = 10^4 cm^2 = 2.471×10^{-4} acres = 3.861×10^{-7} mi^2 = 1.0000×10^{-4} hectares
Bending Stiffness	1 $kN.m^2$ = 10^3 $N.m^2$ =10^6 $kN.mm^2$ = 2.4198×10^3 $lb.ft^2$ =2.4198 $kip.ft^2$ =3.4845×10^2 $kip.in^2$ = 3.4845×10^5 $lb.in^2$
Coefficient of consolidation	1 m^2/s = 3.1557×10^7 m^2/yr = 10^4 cm^2/s =6x 10^5 cm^2/min = 3.6×10^7 cm^2/h = 8.64×10^8 cm^2/day = 2.628×10^{10} $cm^2/month$ = 3.1536×10^{11} $cm^2/year$ = 1.550×10^3 in^2/s = 4.0734×10^9 $in^2/month$ = 1.3392×10^8 in^2/day = 4.8881×10^{10} $in^2/year$ = 9.3000×10^5 ft^2/day = 2.8288×10^7 $ft^2/month$ = 3.3945×10^8 $ft^2/year$
Flow	1 m^3/s = 10^6 cm^3/s = 8.64×10^4 m^3/day = 8.64×10^{10} cm^3/day = 3.5314×10^1 ft^3/s = 3.0511×10^6 ft^3/day
Force	10 kN = 2.2481×10^3 lb = 2.2481 kip = 1.1240 t (short ton = 2000 lb) = 1.0197×10^3 kg = 1.0197×10^6 g = 1.0197 T (metric ton= 1000 kg) = 10^9 dynes = 3.5969×10^4 ounces = 1.022 tl (long ton = 2200 lb)
Force per unit length	1 kN/m = 6.8522×10^1 lb/ft = 6.8522×10^{-2} kip/ft = 3.4261×10^{-2} t/ft = 1.0197×10^2 kg/m = 1.0197×10^{-1} T/m
Length	1 m = 3.9370×10^1 in. = 3.2808 ft = 1.0936 yd = 10^{10} Angstrom = 10^6 microns = 10^3 mm = 10^2 cm = 10^{-3} km = 6.2137×10^{-4} mile = 5.3996×10^{-4} nautical mile
Moment or energy	1 kN.m = $7.3756 \times l0^2$ lb.ft = 7.3756×10^{-1} kip.ft = 3.6878×10^{-1} t.ft = 1.0197×10^3 g.cm = 1.0197×10^2 kg.m = 1.0197×10^{-1} T.m = 10^3 N.m = 10^3 Joule
Moment of inertia	1 m^4 = 2.4025×10^6 in^4 = 1.1586×10^2 ft^4 = 1.4304 yd^4 = 10^8 cm^4 = 10^{12} mm^4
Moment per unit length	1 kN.m/m = 2.2481×10^2 lb.ft/ft = 2.2481×10^{-1} kip.ft/ft = 1.1240×10^{-1} t.ft/ft = 1.0197×10^2 kg.m/m = 1.0197×10^{-1} T.m/m
Pressure	100 kPa = 10^2 kN/m^2 = 1.4504×10^1 $lb/in.^2$ = 2.0885×10^3 lb/ft^2 = 1.4504×10^{-2} $kip/in.^2$ = 2.0885 kip/ft^2 = 1.0443 t/ft^2 = 7.5006×10^1 cm of Hg (0 °C) = 1.0197 kg/cm^2 = 1.0197×10^1 T/m^2 = 9.8692×10^{-1} Atm = 3.3489×10^1 ft of H_2O (60 °F) = 1.0000 bar = 10^6 $dynes/cm^2$
Temperature	°C = 5/9 (°F – 32), °K =°C + 273.15
Time	1 yr. = 12 mo. = 365 day = 8760 hr = 5.256×10^5 min = 3.1536×10^7s
Unit weight, coefficient of subgrade reaction	10 kN/m^3 = 6.3659×10^1 lb/ft^3 = 3.6840×10^{-2} $lb/in.^3$ = 1.0197 g/cm^3 = 1.0197 T/m^3 = 1.0197×10^3 kg/m^3
Velocity or permeability	1 m/s = 3.6 km/h = 2.2369 mile/h = 6×10^1 m/min = 10^2 cm/s = 3.15×10^7 m/yr = 1.9685×10^2 ft/min = 3.2808 ft/s = 1.0346×10^8ft/year = 2.8346×10^5 ft/day
Volume	1 m^3 = 6.1024×10^4 $in.^3$ = 3.5315×10^1 ft^3 = 1.3080 yd^3 = 10^9 mm^3 = 10^6 cm^3 = 10^3 dm^3 = 33814.02 ounces = 2113.38 pints (US) = 10^3 liter = 2.1997×10^2 gallon (UK) = 2.6417×10^2 gallon (US)
Volume loss in a tubing	1 $cm^3/m/kPa$ = 8.91×10^{-4} $in.^3/ft/psf$

Reproduced from: Briaud, J.-L., 1992, “The Pressuremeter”, A.A. Balkema Publishers
(email: *info@ashgate.com*) (web - *http://balkema.ima.nl*)

APPENDIX A

PHOTOGRAPHS FROM THE FLUME TESTS

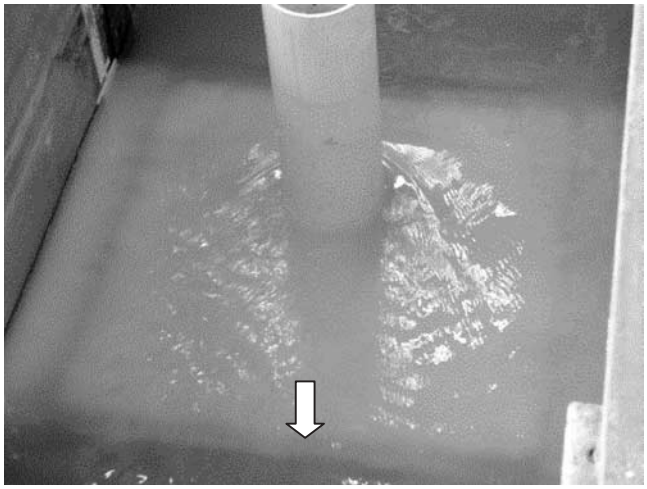

Figure A1 Flow Pattern around Pier under Shallow Water Condition.

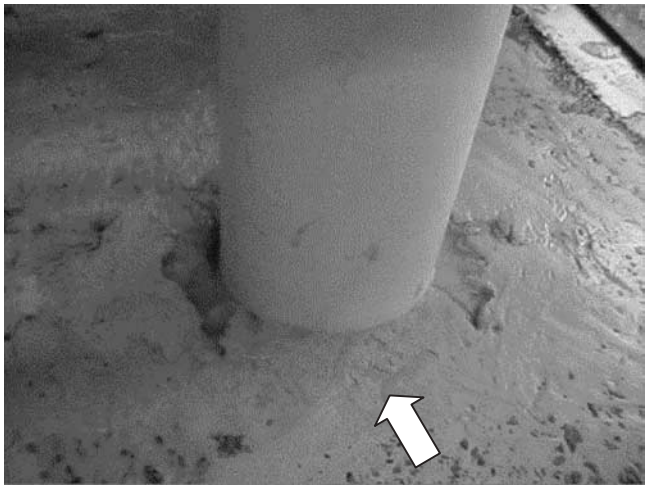

Figure A2 Pier Scour Hole under Shallow Water Condition—Front View.

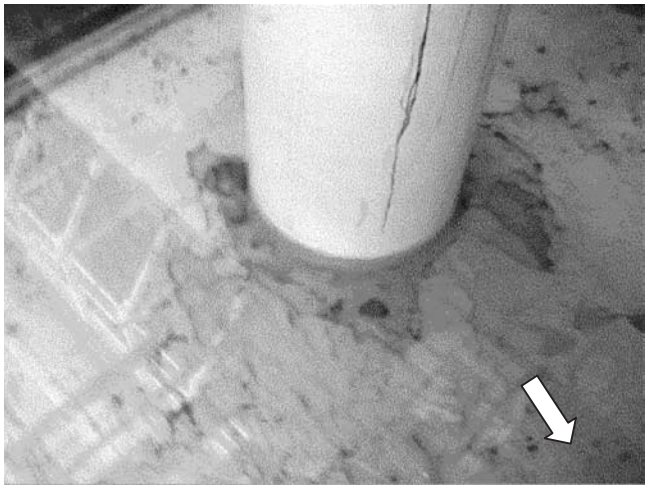

Figure A3 Pier Scour Hole under Shallow Water Condition—Back View.

Figure A4 Pier Scour Hole in Sand under Shallow Water Condition.

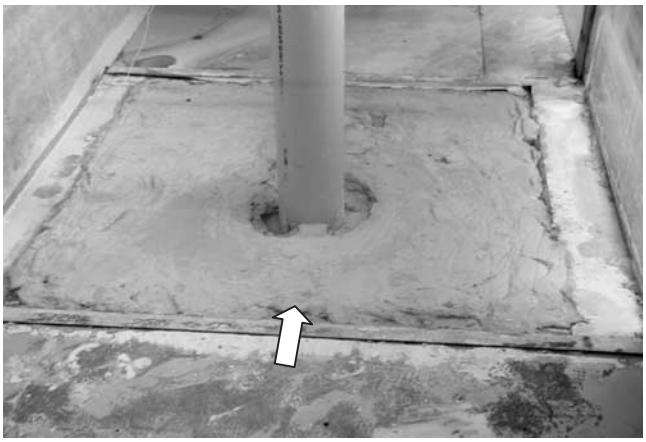

Figure A5 Scour Hole of Test Gr-1.

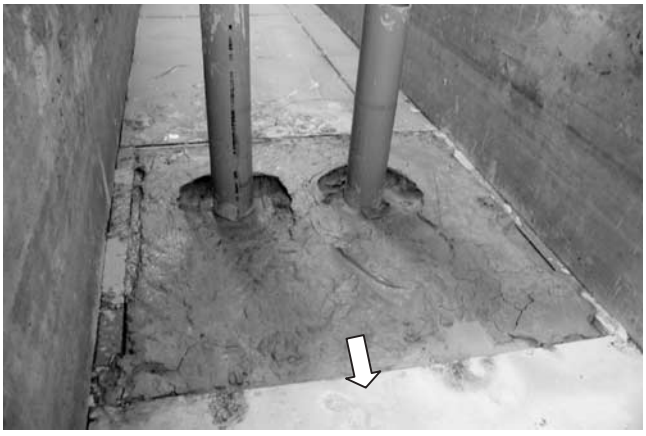

Figure A6 Scour Hole of Test Gr-2.

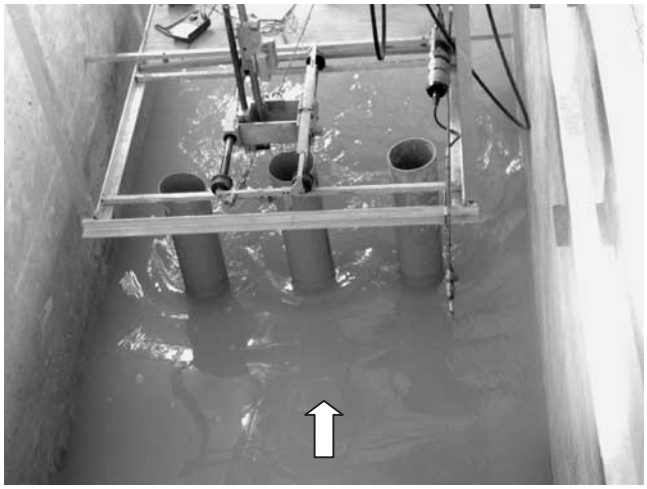

Figure A7 Flow Pattern around Pier Group in Test Gr-3.

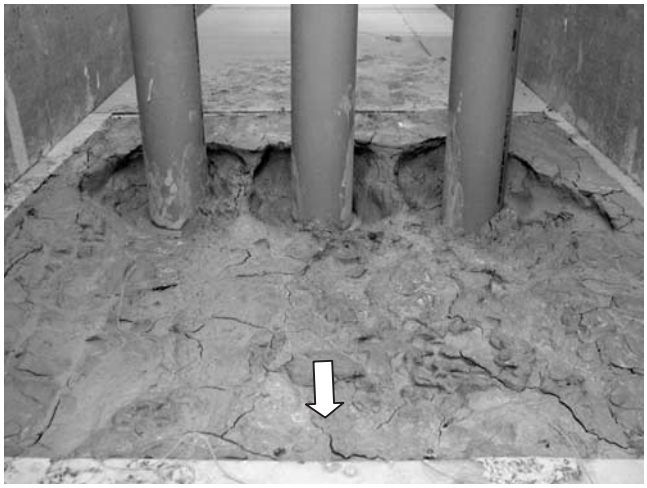

Figure A8 Scour Hole of Test Gr-3—Back View.

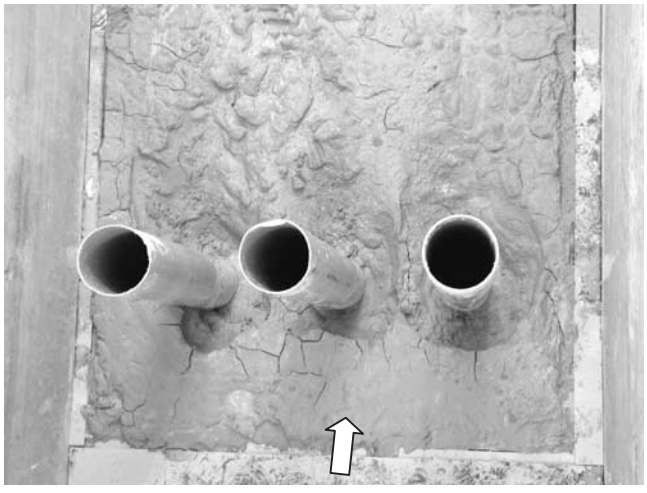

Figure A9 Scour Hole of Test Gr-3—Top View.

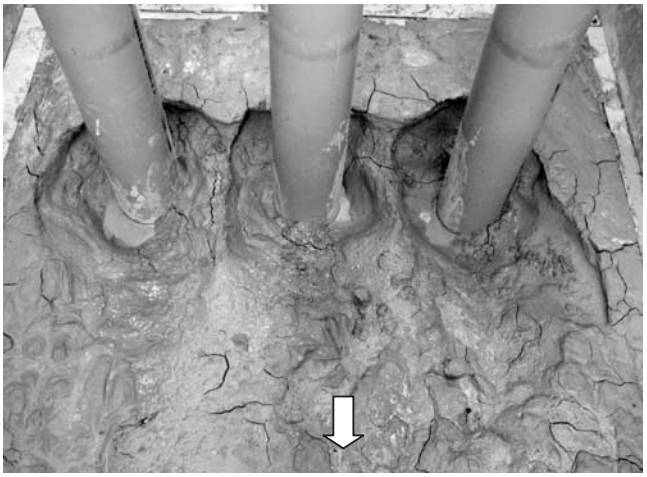

Figure A10 Scour Hole of Test Gr-3—Back View (Large Scale).

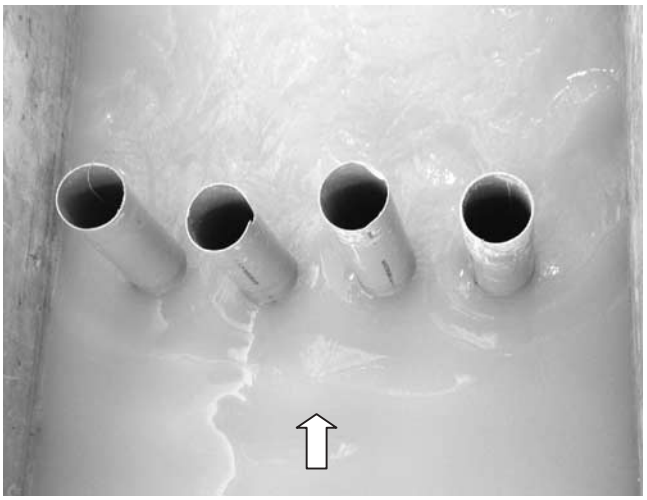

Figure A11 Flow Pattern around Pier Group in Test Gr-4.

Figure A12 Scour Hole in Test Sh-3.

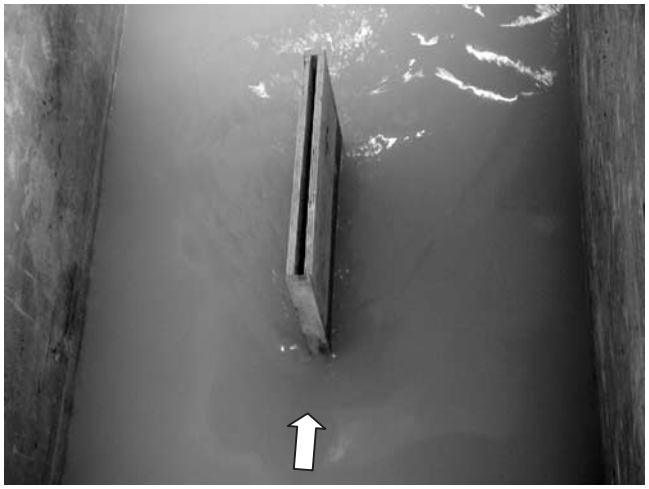

Figure A13 Flow Pattern around Rectangular Pier in Test Sh-5.

Figure A14 Scour Hole in Test At-1—Back View.

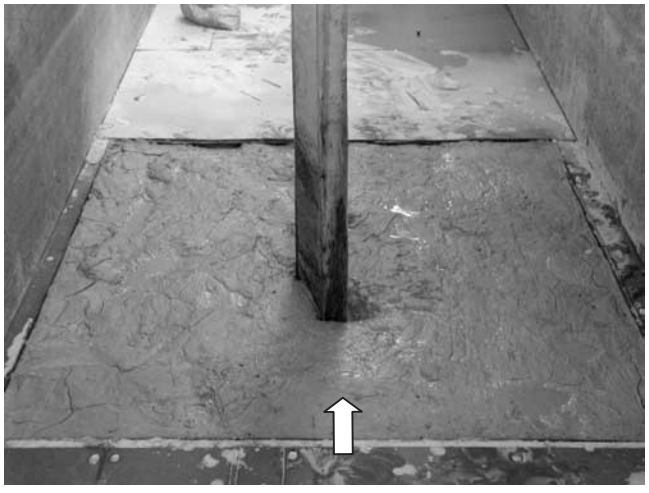

Figure A15 Scour Hole in Test At-1—Front View.

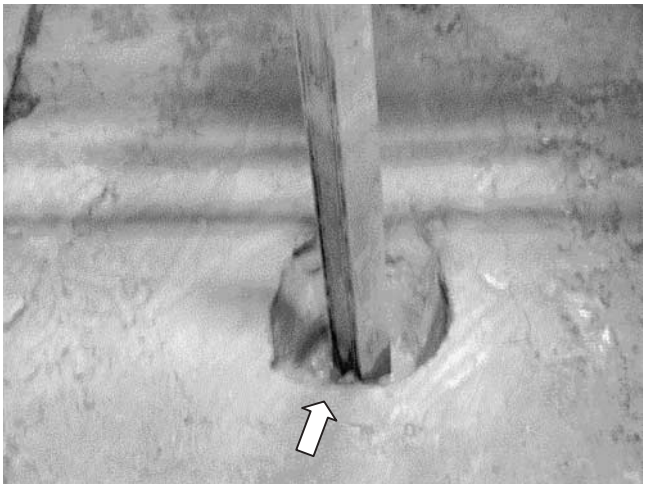

Figure A16 Scour Hole in Test At-6—Front View.

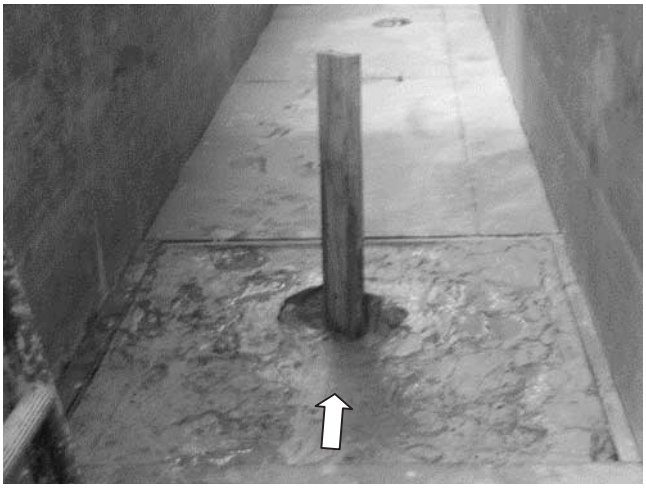

Figure A17 Scour Hole in Test At-6—Back View.

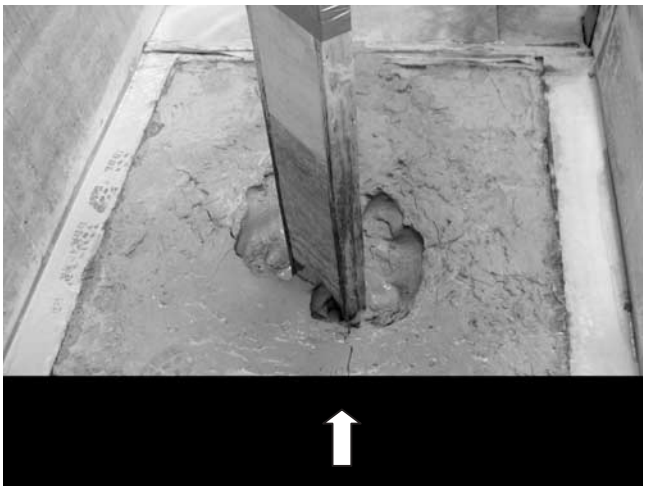

Figure A18 Scour Hole in Test At-3.

Figure A19 Scour Hole in Test At-8.

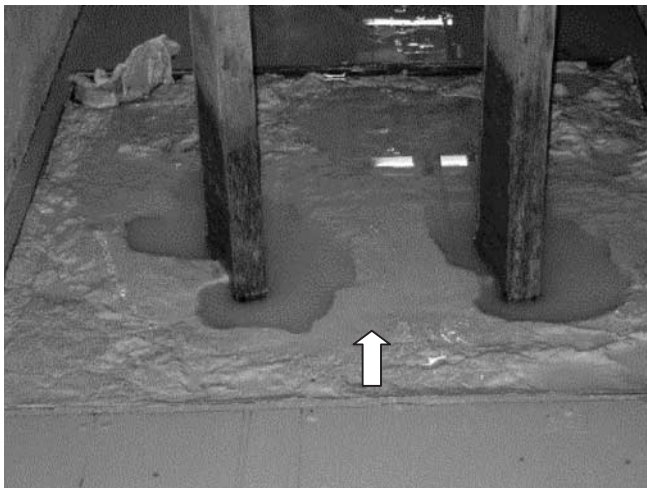

Figure A20 Scour Hole Contour in Test Cp-1.

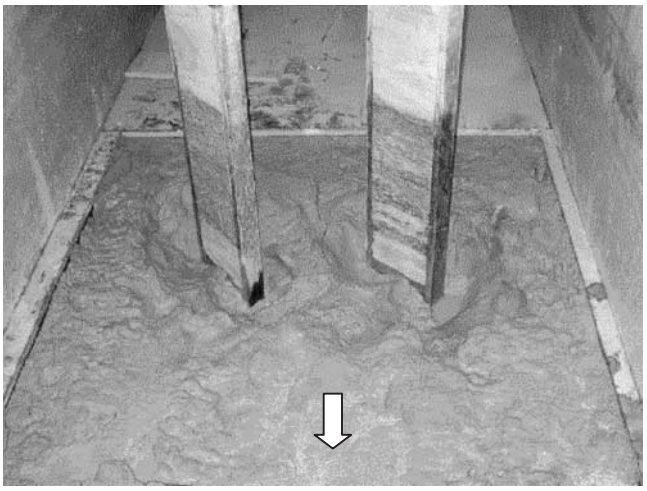

Figure A21 Scour Hole in Test Cp-2.

Figure A22 Scour Hole in Contraction Scour Test 1.

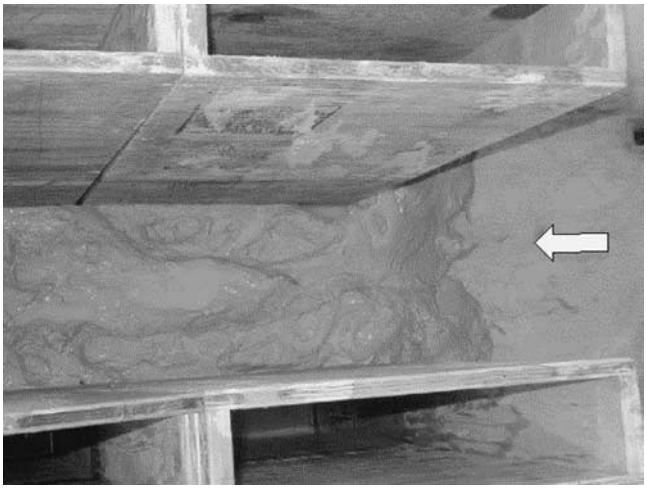

Figure A23 Scour Hole in Contraction Scour Test 2.

Figure A24 Scour Hole in Contraction Scour Test 2—Overview.

Figure A25 Flow Pattern in Contraction Scour Test 2.

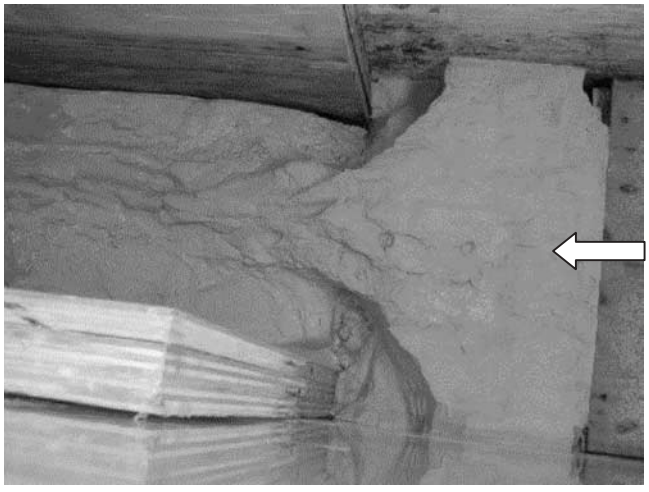

Figure A26 Scour Hole in Contraction Scour Test 3.

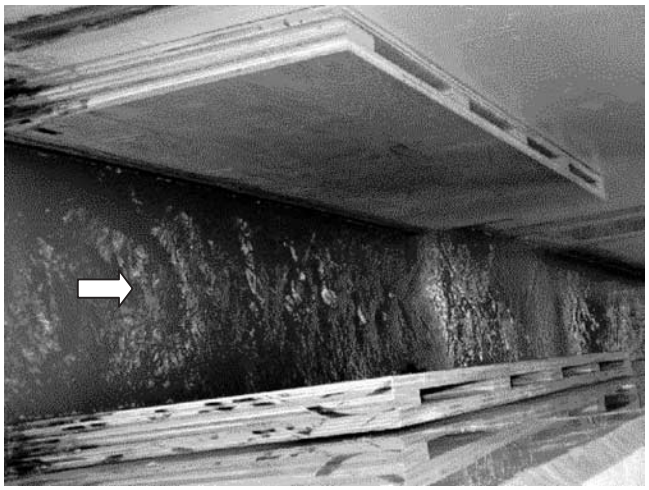

Figure A27 Flow Pattern in Contraction Scour Test 3.

Figure A28 Scour Hole in Contraction Scour Test 9.

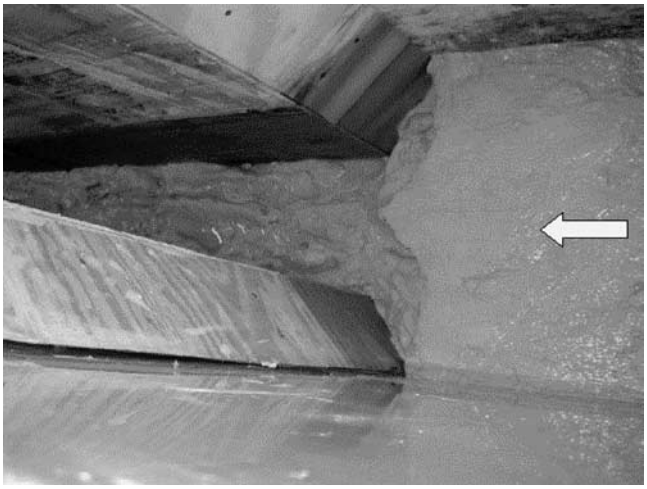

Figure A29 Scour Hole in Contraction Scour Test 10.

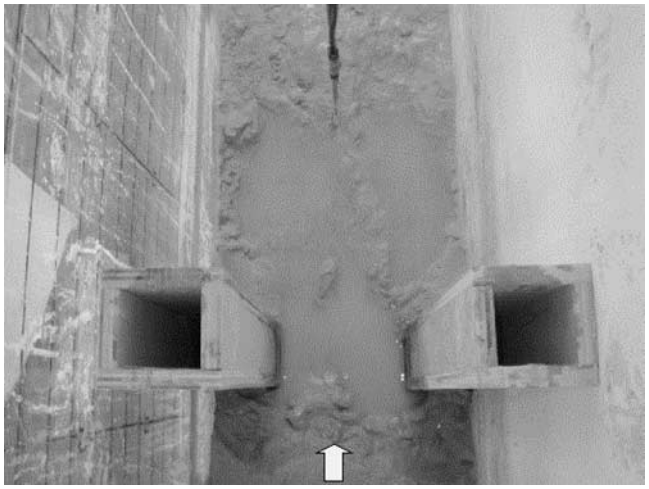

Figure A30 Scour Hole in Contraction Scour Test 13—Top View.

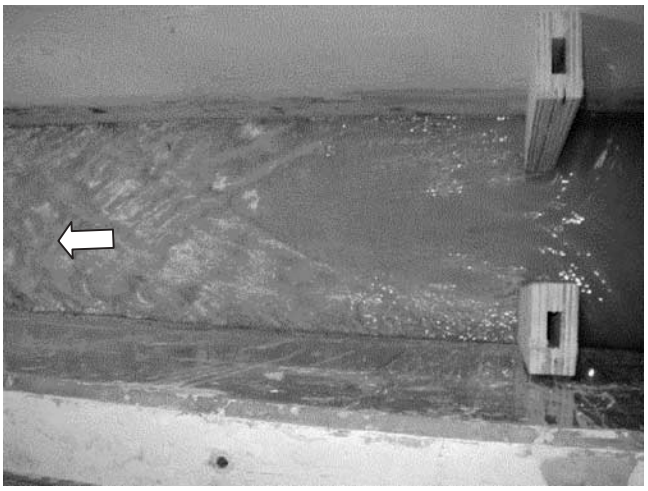

Figure A32 Flow Pattern in Contraction Scour Test 14.

Figure A31 Scour Hole in Contraction Scour Test 13—Back View.

Figure A33 Scour Hole in Contraction Scour Test 14.

Abbreviations used without definitions in TRB publications:

AASHO	American Association of State Highway Officials
AASHTO	American Association of State Highway and Transportation Officials
APTA	American Public Transportation Association
ASCE	American Society of Civil Engineers
ASME	American Society of Mechanical Engineers
ASTM	American Society for Testing and Materials
ATA	American Trucking Associations
CTAA	Community Transportation Association of America
CTBSSP	Commercial Truck and Bus Safety Synthesis Program
FAA	Federal Aviation Administration
FHWA	Federal Highway Administration
FMCSA	Federal Motor Carrier Safety Administration
FRA	Federal Railroad Administration
FTA	Federal Transit Administration
IEEE	Institute of Electrical and Electronics Engineers
ITE	Institute of Transportation Engineers
NCHRP	National Cooperative Highway Research Program
NCTRP	National Cooperative Transit Research and Development Program
NHTSA	National Highway Traffic Safety Administration
NTSB	National Transportation Safety Board
SAE	Society of Automotive Engineers
TCRP	Transit Cooperative Research Program
TRB	Transportation Research Board
U.S.DOT	United States Department of Transportation